SEPTEMBER 1961 VOLUME 13 (1961) No. 2

GREGG M. SINCLAIR LIBRARY
UNIVERSITY OF HAWAII
8-7-63

NUCLEAR INSTRUMENTS & METHODS

A JOURNAL ON ACCELERATORS, INSTRUMENTATION AND TECHNIQUES IN NUCLEAR PHYSICS

EDITOR: K. SIEGBAHN - UPPSALA

CONTENTS

H. G. BLOSSER and M. M. GORDON, Performance estimates for injector cyclotrons 101
B. B. CULWICK and S. J. GOLDSACK, Measuring machine for bubble chamber photographs . 118
G. A. DORAN and M. JOBES, An automatic track following device 124
W. P. DODD, G. A. DORAN, J. B. KINSON, L. RIDDIFORD and B. TALLINI, Operation of a 9-inch bubble chamber with deuterium 127
E. BRUNINX and G. RUDSTAM, Electro-spraying: A method of making samples for β counting allowing accurate correction for self–scattering and self-absorption 131
J. KANTELE and R. W. FINK, Coincidence summing and nonlinearity studies with a two-crystal scintillation gamma spectrometer 141
R. D. MCCORMICK and J. D. MCCORMACK, Hydrogen and carbon target preparation for a positive ion accelerator 147
L. J. DE VRIES and F. UDO, A fast pulse-shape discriminator with applications as a spectrometer and sensitive monitor for 1–30 MeV neutrons 153
D. BERÉNYI and GY. MÁTHÉ, Experiences in the use of scintillation detector in a β-spectrometer of toroid-sector type 161
IWAO OGAWA, TADAYOSHI DOKE and MASAHIRO TSUKUDA, The double-grid ionization chamber 169
GEORGES C. BRET and ERWIN F. SHRADER, Fast tunnel diode circuits for NaI(Tl) detectors 177
GÖSTA NILSSON, Improved fission counting method for uranium isotope analysis . . . 183
G. D. HICKMAN, A miniature fast fission counter 190
A. ADLER, M. PALMAI and V. PEREZ-MENDEZ, 100 Mc/s tunnel-diode discriminator and pulse-shaper 197
S. BERGLUND and S. SVENNERSTEDT, Some characteristics of a toroidal pinch with a reversed field 201
J. BOK et J. P. NOEL, Diode a barrière de surface pour la détection de particules nucléaires . 206
A. H. F. MUGGLETON and F. A. HOWE, The preparation of thin self supporting boron films . 211
W. M. CURRIE, R. E. AZUMA and G. M. LEWIS, Measurements of instrumental time delay and resolution in a fast coincidence system 215
HANS DECKERS, Calculation of recoil spectra induced by fast neutron spectra in nuclear emulsions 224
D. W. ANDERSON and J. MCKENZIE, A propane bubble chamber with mechanical expansion 231
CARL E. ANDERSON, D. A. BROMLEY and M. SACHS, Simultaneous nuclide identification and energy measurement of nuclear reaction products 238
T. K. ALEXANDER and F. S. GOULDING, An amplitude-insensitive system that distinguishes pulses of different shapes 244
R. J. LAMDEN, A random pulse generator with provision for excursions 247
K. GOPALAN and E. S. RAJAGOPAL, An instantaneous pulse frequency meter for random pulses 253
S. L. GUPTA and N. K. SAHA, Spark counter as a fast pulse generator 258
C. NOACK und W. ROETHER, Ein Kabelverstärker für Impulse grosser Amplitude 261

Letters to the Editor

G. R. MARTIN, The estimation of the resolving time of a counting apparatus 263
C. INFANTE, A constant input impedance plug-in for the Tektronix 581 oscilloscope . . . 264
News Items 265
Book Reviews 266

NUCLEAR INSTRUMENTS AND METHODS

A journal on accelerators, instrumentation and techniques in nuclear physics

EDITOR: K. SIEGBAHN, UPPSALA

EDITORIAL BOARD:

J. B. ADAMS (CERN)
F. A. ALSINA (Buenos Aires)
E. AMALDI (Rome)
H. L. ANDERSON (Chicago)
K. T. BAINBRIDGE (Cambridge Mass.)
P. R. BELL (Oak Ridge)
R. E. BELL (Montreal)
A. BERTHELOT (Saclay)
H. BRINKMAN (Groningen)
E. H. COOKE-YARBOROUGH (Harwell)
S. DE BENEDETTI (Pittsburgh)
M. DE HEMPTINNE (Louvain)
A. DE-SHALIT (Rehovoth)
M. DEUTSCH (Cambridge Mass.)
S. DU TOIT (Pretoria)
B. S. DŽELEPOV (Leningrad)
W. GENTNER (Heidelberg)
P. C. GUGELOT (Amsterdam)
H. HALBAN (Paris)
O. HAXEL (Heidelberg)
P. HUBER (Basel)
S. KIKUCHI (Tokyo)
J. KOCH (Copenhagen)
M. S. KOZODAEV (Moscow)
S. LIVINGSTON (Cambridge Mass.)
E. M. MCMILLAN (Berkeley)
M. G. MEŠČERJAKOW (Moscow)
P. B. MOON (Birmingham)
M. L. OLIPHANT (Canberra)
W. PAUL (Bonn)
A. S. RAO (Bombay)
G. SALVINI (Rome)
P. SAVIĆ (Belgrade)
P. SCHERRER (Zürich)
CH. SCHMELZER (CERN)
R. TANGEN (Oslo)
D. TAYLOR (Northampton)
V. I. VEKSLER (Moscow)
G. VON DARDEL (CERN)
O. WERNHOLM (Stockholm)
R. R. WILSON (Cornell)
S. D. WINTER (Saclay)

INSTRUCTIONS FOR CONTRIBUTORS

Contributions may be sent to the Editor, Professor K. Siegbahn, Institute of Physics, University of Uppsala, Sweden, either directly or through the intermediation of one of the members of the Editorial Board. Contributions may be written in English, French or German but should always, except for very short papers, be supplied with a brief abstract in English. Figures should be in inked original drawings or glossy prints and they should be sufficiently large. Contributors should make sure that important details in drawings and photographs will show up clearly in the diminished copy used by the publisher.

Books for review should be sent to Professor Siegbahn.

Objective and descriptive material on endeavours and product developments from the industry for the section "Spotlight on Industry" should be sent directly to the publishers, North-Holland Publishing Company, P.O. Box 103, Amsterdam.

Nuclear Instruments and Methods is published monthly. The subscription price of a volume of 360 pages is $ 17.00 (130s), postage free.

Subscriptions should be sent to the publishers, North-Holland Publishing Company, P.O. Box 103, Amsterdam, or to any subscription-agent.

No part of this issue may be reproduced in any form, by print, photoprint, microfilm or any other means without written permission from the publisher.

NUCLEAR INSTRUMENTS AND METHODS **13** (1961) 101–117; NORTH-HOLLAND PUBLISHING CO.

PERFORMANCE ESTIMATES FOR INJECTOR CYCLOTRONS†*

H. G. BLOSSER and M. M. GORDON

Michigan State University, East Lansing, Michigan

Received 23 May 1961

Available evidence on performance to be expected from injector cyclotrons is collected and reviewed. On the basis of this information, estimates are made of current, spot size, angular divergence, energy spread and duty cycle for the extracted beam of possible 40 MeV and 200 MeV injector cyclotrons.

1. Introduction

Customarily large proton synchrotrons have utilized a linear accelerator to preaccelerate particles up to an energy appropriate for injection into the synchrotron. The choice of a linac in lieu of other possible devices has been dictated principally by the high density of the transverse x, p_x, y, p_y, phase space projections of the linac beam. Secondary factors have been: (1) the output energy of reasonably sized linacs matched moderately well with the desired injection energy, (2) the duty cycle of the synchrotron resulted in a linac duty cycle compatible with reasonable power consumption, and (3) the linac, though expensive compared with possible other devices, was still a moderately small fraction of the total synchrotron cost.

Results of recent developmental work on sector focused cyclotrons[1–3]) has led to results indicating such a cyclotron to be a possible likely choice as an injection device with possible special relevance[4]) for FFAG type synchrotrons. Specific factors are as follows:

(1) Detailed studies of orbit phenomena in such cyclotrons indicate that designs can be evolved which will transmit the beam from source to exterior of the machine without appreciable dilution of the x, p_x, y, p_y phase space density; if the cyclotron is provided with a source equivalent in emittance to that of the linac, it should then match the linac in transverse density of the extracted beam. (2) In the design of high performance synchrotrons there is an increasing trend to higher injection energies such that in some contemplated situations the large physical size of the linac has posed an awkward problem. (3) For FFAG synchrotrons, the possibility of enormously increasing the duty cycle with respect to that of pulsed field synchrotrons could lead to situations where the power requirements for the linac were an important economic consideration. In view of the above and of the established advantage of the cyclotron with respect to compactness and economy it appears appropriate to undertake a recomparison of the relative injection capabilities of cyclotrons and linacs. A further motivating factor for such a comparison arises from the distinct difference in the time profile of the output current for the two devices; if the cyclotron is established as a feasible injector, an additional group of r-f acceleration schemes can be considered for the synchrotron with possible gains in efficiency in particular situations.

Objective evaluation of the injection capability of cyclotrons is unfortunately handicapped at present by a sparsity of written reports on a

† A portion of the work described herein was performed during a summer visit by one of the authors (HGB) to the laboratories of the Midwestern Universities Research Association. A preliminary account of this work has been privately circulated as a MURA report (No. 593).

* Research supported in part by U.S. Atomic Energy Commission.

[1]) T. A. Welton, Proceedings of CERN 1959 conference on High Energy Accelerators and Instrumentation, p. 366; Also private communications.

[2]) M. M. Gordon, Proc. of Sea Island Conf. NAS-NRC **656** (1959) 234.

[3]) Blosser, Gordon and Arnette, manuscript in preparation.

[4]) Lee C. Teng, Rev. Sci. Instr. **27** (1956) 106.

number of pertinent aspects of cyclotron information and secondly, by the absence of experimental testing of a number of design features indicated to be desirable. The present report is an effort to partially alleviate the first of these handicaps by collecting and reviewing available information, principally from unpublished notes and private communications, relative to the performance to be anticipated from injector cyclotrons.

The discussion in this report is in terms of injector cyclotrons—it should be noted however, that desirable attributes of an effective injector cyclotron are essentially identical to those of a precision research cyclotron and hence the discussion could equally well be directed to performance of a device intended for the latter purpose. (The studies at Michigan State on which this report is largely based are in fact principally concerned with design of such a research cyclotron—with such an instrument a very intriguing research program can be envisaged. For those interested in further information in this regard, an unpublished report, MSUCP-1, is available from the authors.)

It will be convenient to divide the discussion into three sections. Section 2 summarizes existing data on phase space characteristics of cyclotron sources. Sections 3 and 4 view the cyclotron as a device for mapping source phase space characteristics into phase space characteristics of the extracted beam, section 3 considering specifically the transverse characteristics of the mapping $(x, p_x, y, p_y,)$ and section 4 considering longitudinal characteristics of the mapping (E, t).

As is obvious, but perhaps nevertheless worthy of mention, the design of every cyclotron is in many respects a unique problem. Performance, even with optimized designs, may vary considerably depending on a number of boundary conditions, and detailed performance estimates can therefore only be made after considerable study of a particular situation. The conclusions of this report will be drawn principally from results of detailed studies at Michigan State[3]) of the characteristics of a 40 MeV 3 sector low spiral cyclotron. The conclusions are then directly applicable to injector cyclotrons of energies up to perhaps 100 MeV. At energies of 200 MeV and higher a number of the problems discussed would be considerably different and would require additional detailed study before reliable performance estimates could be made. Lacking such detailed work, it is reasonable to assume that results comparable to the 40 MeV case can be achieved in the 200 MeV range; such an assumption is however quite qualitative and should be supplemented at an early stage with quantitative studies if active interest in such a device develops. (Rather extensive studies of an 850 MeV cyclotron have been performed[1,2,5,6]); problems encountered therein apparently indicate a considerably lower final energy to be more appropriate for such cyclotrons at least insofar as accelerator technology is concerned.)

2. The Cyclotron Source

Let the rectangular coordinates x and y designate displacement at right angles to the principal direction of motion of a beam of particles and p_x and p_y the corresponding conjugate momenta. The phase space density of some small element of the beam is then the current (particles per unit time) in the element divided by the product of the spreads in energy, in x, in p_x, in y, and in p_y of the element. For injection purposes the spread in energy of the particles leaving the source is usually of small consequence[7]) and it is therefore adequate to consider the density in the x, p_x, y, p_y, t projection of the total phase space. Experimental determinations of this projection can be accomplished by allowing the

[5]) J. A. Martin, Proc. of CERN 1959 Conf. on High Energy Accelerators and Instrumentation, p. 205.

[6]) M. M. Gordon and H. G. Blosser, Progress report on Beam Extraction Studies for Oak Ridge Cyclotron Analogue II (available from authors on request).

[7]) If the spread in energy of the output beam from a cyclotron were measured as a function of time with extremely fast equipment, an area of the form shown in the sketch at right would be obtained (with similar figures following in sequence spaced in time at intervals of 1 r-f period.) The energy spread δ arises from the source, the spread Δ from detailed features of the accelerating process. Due to matching difficulties between injector and synchrotron a phase figure of the form shown must normally be considered from the point of view of the synchrotron as having a spread $\Delta + \delta$ uniform in time. Since Δ is normally much greater than δ, the precise value of δ is unimportant.

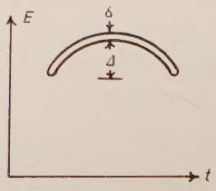

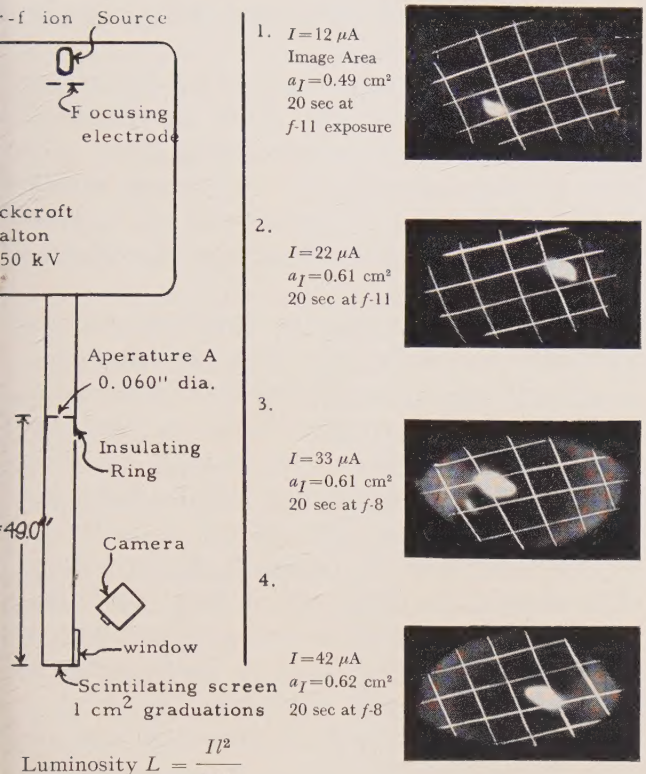

Fig. 1. Luminosity results for Oak Ridge National Laboratory Biology Division Cockcroft-Walton accelerator.

beam to illuminate an aperture and measuring the current and angular divergence of the beam passing through the aperture. The x, y spread of the beam is defined by the aperture, the p_x, p_y spread by the angular divergence (for small angles $\theta_x \simeq p_x/p$ etc.) Note that for given spread in p_x and p_y the angular divergence in each dimension will vary as p^{-1} as the particles are accelerated, and the solid angle as p^{-2}, where p is the total momentum.

Figure 1 gives the results of such a measurement on the beam of a Cockcroft-Walton accelerator of the Oak Ridge National Laboratory Biology Division[8]). The accelerator was equipped with a standard r-f ion source of the type normally used in synchrotron injector pre-accelerators. The results of the measurements give values from 21 to 58 (A/cm² sr), the range of values corresponding to increasing voltage on the source extractor electrode up to approximately the limiting value for reliable operation. Assuming the maximum can be achieved routinely, the value of 60 (A/cm² sr) for a DC instrument at 250 kV is set as a standard of comparison.

As a cross check we note that with the above value for the density, the full width full angle product for a 50 MeV linac with 120° acceptance time and 5 mA average output during the pulse is inferred to be 1.4 milli-rad cm which is in accord with normal operating expectation for such a device.

Comparable data on cyclotron ion sources are difficult to obtain. (A cyclotron source is closely tailored to the characteristics of the center of a cyclotron and will operate only in closely similar environments.) The detailed studies of the central region of the Canberra cyclotron by Smith[9]) afford perhaps the best source of data from which estimates of the phase space density can be drawn. Fig. 2 quotes pertinent material from Smith's results. The experimental situation is considerably different from that of fig. 1 in that the ions are continually under the influence of focusing fields. In such a situation it is easily shown that the spot size divergence product Q is given by

$$Q = \frac{\pi}{4}\frac{\nu}{R} A(0)A(\pi/2) \qquad (1)$$

where ν is focusing frequency, R the radius of the orbit, $A(0)$ and $A(\pi/2)$ the full width of the beam at the reference angle (0) and at a second angle $\frac{1}{4}$ cycle of the betatron wave length away, and where Q is then the product of full width and full divergence. It is unfortunately necessary in inferring Q's from Smith's results to refer to separate experiments to determine the radial and axial Q's respectively. Source and extractor geometries in the two situations were however identical so that the risk of error in inferring the two Q's from separate experiments appears slight. (To the author's knowledge no data are available from which the two Q's can be inferred simultaneously.) Since the cyclotron source is "on" for only a fraction of the time it is necessary

[8]) The measurements were made by one of the authors (HGB) and results were previously briefly reported in Proc. of Sea Island Conf. NAS-NRC pub. 656 p. 203.

[9]) W. I. B. Smith, Sector Focused Cyclotrons, NAS-NRC pub. 656 (1959) 183.

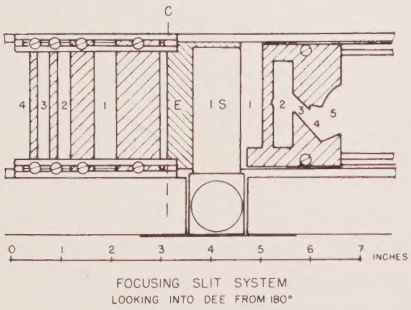

(figure from Smith, ref.[9])

RADIAL APERTURE

$\omega_r \simeq 1$, $R \simeq 1.7''$, $A(0) \simeq 0.29''$
$A(90) \simeq 0.29''$,

$$Q_r = \frac{\pi}{4}\frac{\omega_r}{R} A(0)\, A(90)$$

$\simeq$ 100 milli-rad cm.

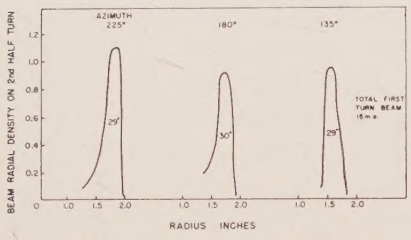

(figure from Smith, ref.[9])

AXIAL APERTURE:

Notches at digits 2, 3, 4 and 5 on right cut to fit beam. Notch pattern indicates $\omega_r \simeq 2$ and $A(90) \simeq 1$ cm.

$$A(0) = 1 \text{ cm}. \quad Q_z = \frac{\pi}{4}\frac{\omega_z}{R} A(0)\, A(90)$$

$\simeq$ 36 milli-rad cm.

Luminosity (150 keV):

$$L = \frac{I}{Q_r Q_z} = 4.2 \text{ A/cm}^2 \text{ sr}$$

Correct for 0.18 duty cycle (see text) and to 250 keV energy equivalent:

$$\text{L (DC, 250)} = 39 \text{ A/cm}^2 \text{ sr}$$

Fig. 2. Cyclotron source data from Smith, ref.[9]).

in order to compare with the Cockcroft Walton data to correct for the duty cycle in addition to the correction for difference in momentum mentioned previously. For the duty cycle correction, Livingston and Jones[10]) report the output of a source of the type used by Smith to be reduced by a factor 0.18 when r-f extraction voltage is substituted for D.C., other factors being held constant. Applying this correction and the p^{-2} correction gives an emittance (D.C., 250 kV equivalent) for the Smith source of 39 A/cm² sr.

The approximate equivalence of the result from the Smith data, and that from the Cockcroft Walton data is in accord with what would have been the most reasonable prior expectation, namely that the plasmas in the two sources are approximately equally effective as producers of collimated ions.

At the risk of belaboring the obvious it is perhaps worthwhile to note that equivalence of source luminosity in no way necessarily implies equivalence in luminosity in the extracted beams of Cockcroft Walton and cyclotron. As an example, measurements on the extracted beam of the Oak Ridge 86″ cyclotron gave luminosity values[8]) a factor of 5×10^3 lower than the Cockcroft Walton values, after correction for energy and r-f duty cycle (0.18), even though the cyclotron was equipped with a source of the same type used by Smith and with presumably comparable emittance. The result is indicative of the enormous dilution of filled phase space with unfilled which can occur in some circumstances. Fortunately, in the sector focused cyclotron, detailed orbit computations indicate that such dilution can be largely avoided as is discussed in sections 3 and 4 which follow.

3. Cyclotron Orbit Dynamics—Transverse Characteristics

As indicated in the introduction, this and the following section view the acceleration of particles in the cyclotron as a phase space transformation. A certain interior low energy phase space volume defined by the characteristics of the beam as it leaves the source extractor slit is transformed by the cyclotron into an exterior high energy volume —it is desired to estimate the characteristics of this mapping. The coupling between longitudinal and transverse motions is comparatively weak in the cyclotron and it is therefore convenient to initially neglect the spreads in energy and time of particle's leaving the source. The beam to be considered thus has normal spot size and divergence but all particles leave the source extractor slit at the same time and

[10]) R. S. Livingston and R. S. Jones, Rev. Sci. Inst. **25** (1954) 532.

with the same energy. At a later time some fraction of such a beam will have successfully traversed the cyclotron and extractor and arrived at the exterior. The objective of this section is to estimate the survival fraction for this "instantaneous" beam and the phase space characteristics thereof.

Three distinct problems are encountered. (1) Near the center of the cyclotron, the operating point is at best extremely close to a non-linear resonance at $\nu_r = 1$, the effects of which can easily distort the phase area in a highly undesirable way. (2) In the intermediate radius region, though non-linear effects are inherently small, significant distortions can occur due to cumulative effects over the relatively large number of revolutions ($\simeq 90\%$ of the total) which the particles make in the region. (3) To accomplish extraction, conventional electrostatic techniques are inadequate at energies of interest for injection, and it is therefore necessary to utilize resonant magnetic techniques which can again easily distort the phase area in an undesirable way. In the following subsections each of these problems is considered in turn.

3.1. CENTRAL REGION ORBITS

Maxwell's equations require that the flutter field must approach zero near the center of a sector focused cyclotron as $(r/g)^N$ where g is a quantity proportional to the magnet gap, r is the distance from the center, and N is the number of sectors. As a consequence a region results in which axial focusing is more or less marginal depending on the number of sectors. To alleviate this difficulty the azimuthal average of the field, $< B >$, is often designed to decrease with radius ("fall off") near

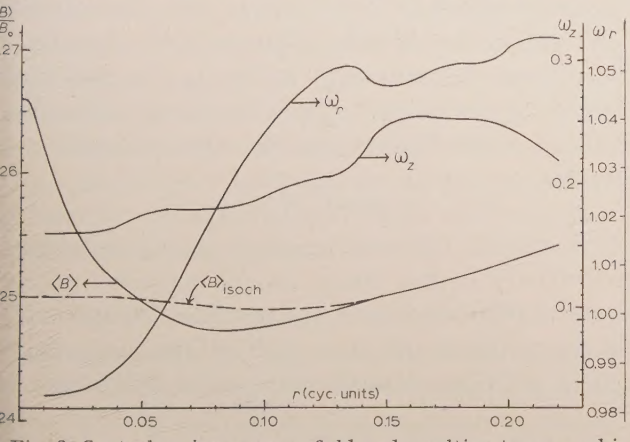

Fig. 3. Central region average field and resulting tunes used in studies of ref.[13]). For comparison isochronous average field is also shown. One cyc. unit equal velocity of light divided by angular velocity of r-f accelerating voltage.

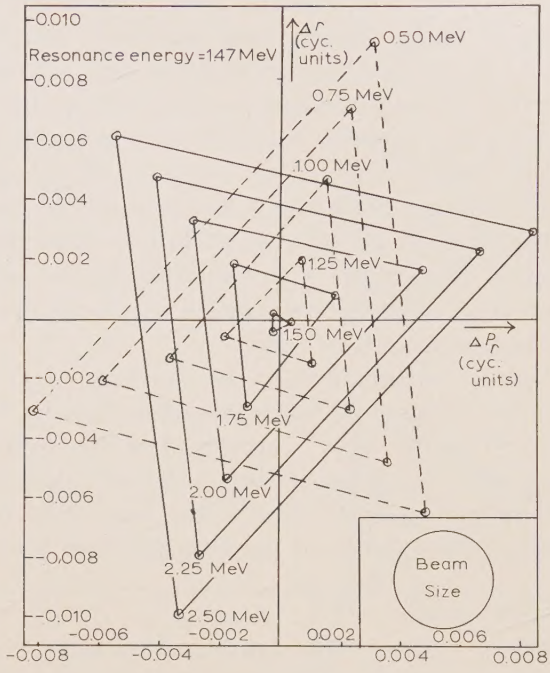

Fig. 4. Radial stability limits at a sequence of energies for field of fig. 3 (from ref.[13])). Stability limit position inferred from tracking of unstable fixed points.

the center to supplement the axial focusing; at the point where the sectors reach a strength sufficient to provide the desired focusing, $< B >$ reverts to an increasing function of radius as is required for isochronism, and in the transition the radial tune passes through the $\nu_r = 1$ resonance. If $N = 3$ the flutter rises sufficiently rapidly to also allow consideration of designs in which $< B >$ is set for isochronism all the way to the center, and so no resonance transition is encountered.

An average field decreasing with radius has been successfully employed in the central region of the four sector Delft[11]) and Illinois cyclotrons[12]). The operation of these cyclotrons, unfortunately, gives little detailed insight as to distortions of the radial phase area in the transition through $\nu_r = \frac{4}{4}$, but at

[11]) Heyn and Khoe Kong Tat, Proc. Sea Island Conf. NAS-NRC **656** (1959) 29.

[12]) Allen, Chatterjee, Ernest and Yavin, Rev. Sci. Inst. **31** (1960) 813.

least it is indicated that the transition is not disastrous.

For the three sector case, model magnet and computer studies of both field fall off[13]) and isochronous $< B >$[14]) designs have been made at Michigan State. Results obtained show that for either type of field, source locations can be found such that with adequate accelerating voltage, the x, p_x, y, p_y area from the source maps into the intermediate radius region of the cyclotron with negligible distortion. Field fall off designs would perhaps be preferred in an injector cyclotron since they result in acceptance of a somewhat larger axial phase area; we therefore consider results for fields of this type in further detail.

Typical performance to be expected are illustrated in figs. 3–6, which are taken from ref.[13]). Fig. 3 shows the $< B >$ employed in the studies, along with the corresponding radial and axial focusing frequencies ("tunes"), the tune data beginning at the radius of the first half turn for an assumed accelerating voltage of 280 kV per turn. The strong ν_z, in conjunction with a relative absence of axial non-linearities, implies at once that the axial motion will be free of appreciable distortion. The large ν_z in addition enhances both the axial phase space acceptance given by eq. (1), and the axial space charge limit, the latter given in the absence of neutralization by the approximate expression

$$I_{\text{lim}} = A\, \varepsilon_0 \omega_0 \nu_z^2\, (\Delta\phi/2\pi)\, (\Delta E/e) \qquad (2)$$

where A is the full axial height of the beam, ε_0 the permittivity of free space, ω_0 the particles' rotational angular velocity, e the particles' charge, ΔE the energy gain per turn and $\Delta\phi$ the azimuthal spread of the accelerated beam, all in MKS units.

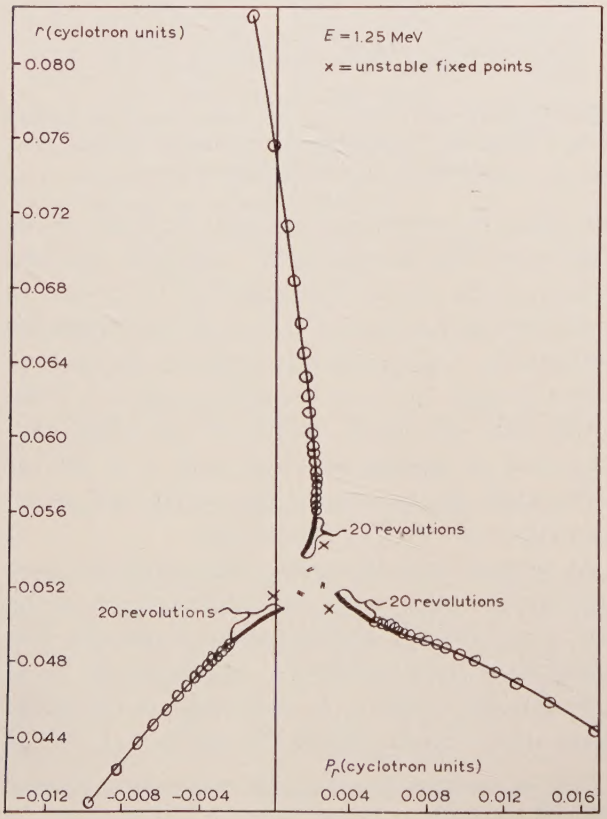

Fig. 5.
Static phase plot at 1.25 MeV for field of fig. 3 (from ref.[13]).

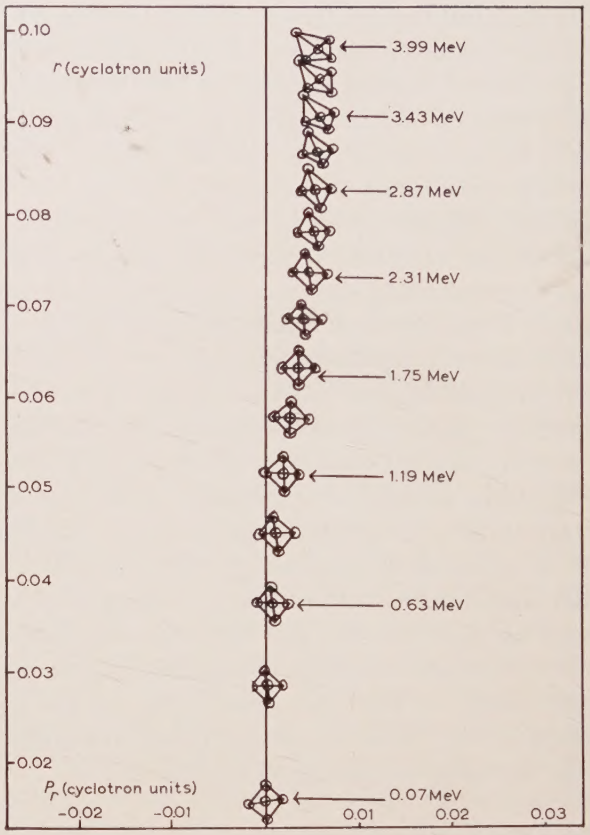

Fig. 6. Radial phase plot of beam sized group of particles accelerated from source in field of fig. 3 with energy gain of 280 keV per turn (from ref.[13]).

[13]) J. E. Stover, Michigan State University Cyclotron Project Report **3** (Aug. 1960).

[14]) M. M. Gordon and H. G. Blosser, manuscript in preparation.

The effect on the space charge limit is particularly important in view of the quadratic dependence of the limit on ν_z and the fact that the output of present cyclotrons appears from comparison with eq. (2) to be approximately directly determined by the space charge limit (increasing the limit should therefore allow a corresponding increase in the accelerated current as compared with presently operating cyclotrons).

Fig. 4 shows stability limits for the radial motion at successive energy values corresponding approximately to successive full revolutions of the accelerated particles. For comparison, the circle at the bottom right of the figure is the phase area of a beam with 0.3″ radial amplitude (the distribution observed by Smith[9])). For several turns in the vicinity of the resonance, a substantial fraction of the beam must be outside the stability limit. The limited number of turns accomplished in the unstable region in combination with the slow motion of the phase "fluid", shown in fig. 5, results, however, in a tolerable situation as can be seen in fig. 6 which shows successive snapshots of an array of particles also with 0.3″ radial amplitude, accelerated upward from the source through the resonance and well into the intermediate radius region of the cyclotron. The geometry of the array of particles is well preserved which implies transmission of the beam phase area without introduction of significant distortion.

The results shown in fig. 6 will clearly be quite sensitive to reduction of the accelerating voltage, as is currently being explored in further detail. The 280 kV/turn used in the studies is however easily achievable in a fixed energy injector type cyclotron; hence for this application the results establish that a field of the type shown will allow acceleration of particles out of the central region with negligible distortion of beam optics.

3.2. INTERMEDIATE RADIUS REGION ORBITS

Orbit problems in the intermediate radius region of the cyclotron are minor in comparison with either the central region or the extraction region. Stability limits are much larger than the beam size, the radial stability limit for example typically corresponding to a factor of 10 to 40 larger amplitude

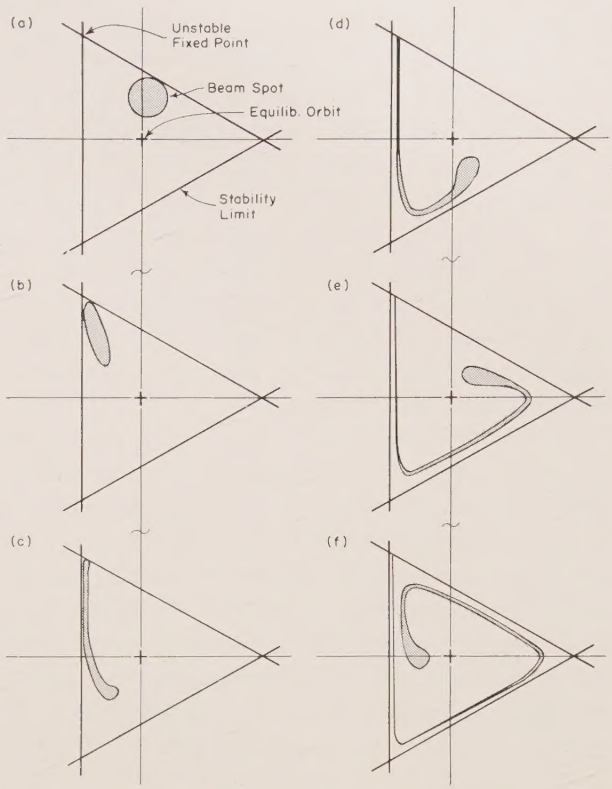

Fig. 7. Schematic radial phase plots illustrating distortion effect to be expected if beam spot circulates in vicinity of stability limit for sizable no. of revolutions.

(depending on the amount of spiral employed) than the amplitude expected from the source. One aspect of the motion in this region does however merit careful consideration. In the results shown in fig. 6 it was found that the beam area at the final energy was considerably displaced from the equilibrium orbit, or, in the usual terminology, a coherent betatron amplitude of approximately 20 mm was superimposed on the random distribution of amplitudes from the source. Such a coherent amplitude is apparently a typical result of the optimum central region solution. Moreover, the substantial radial separation of turns in this region of the cyclotron implies that, averaged over a group of turns, there will always be an amount of coherent amplitude at least equal to half the radial separation of equilibrium orbits for successive half turns[15]).

In the intermediate radius region such a coherent

[15]) One of the authors (H.G.B.) is indebted to K. M. Terwilliger for some very helpful discussions of this point.

amplitude could result in extensive distortion if the speed of the precessional motion of off center orbits, given by ν_r, varies appreciably with amplitude. The effect is sketched in fig. 7, where the precession rate is assumed to decrease with amplitude. Large amplitude particles rotate slower, hence lag behind those of somewhat smaller amplitude and stretch the phase figure into a long contorted spiral. If coherent amplitudes are present sufficient to place. the beam near the stability limit for a moderately large number of revolutions, distortions of the sort shown in fig. 7 will always result.

A limit on the amount of coherent amplitude tolerable without introduction of appreciable distortions may be estimated from the data of fig. 8, which are numerical results for the shift in ν_r with amplitude for particles of energy 28 MeV in the magnetic field of the proposed Michigan State University cyclotron. The shift in ν_r is seen to be extremely small out to a relatively large fraction of the total stable amplitude. As a consequence, relatively large coherent ampltudes can be tolerated. As an example, let us arbitrarily define "excessive distortion" to be a precessional difference of $\frac{1}{25}$ of 2π between inside and outside of the beam spot and compute the resulting limit on coherent amplitude in the intermediate radius region of Michigan State type magnets. For such a magnet, stability limits are typically $\simeq$100 mm, and making use of the data of fig. 8, it is found that a source spot of 7.5 mm diameter (the expected radial phase area inferred from ref.[9]) circulating for 200 turns can have a coherent amplitude of up to 40% of the limiting value (i.e. 40 mm) before distortion becomes "excessive". Such a value for the coherent amplitude is well beyond the range which arises or is desirable in customary design situations. The results therefore indicate that the beam phase area will also map through the intermediate radius region with negligible distortion.

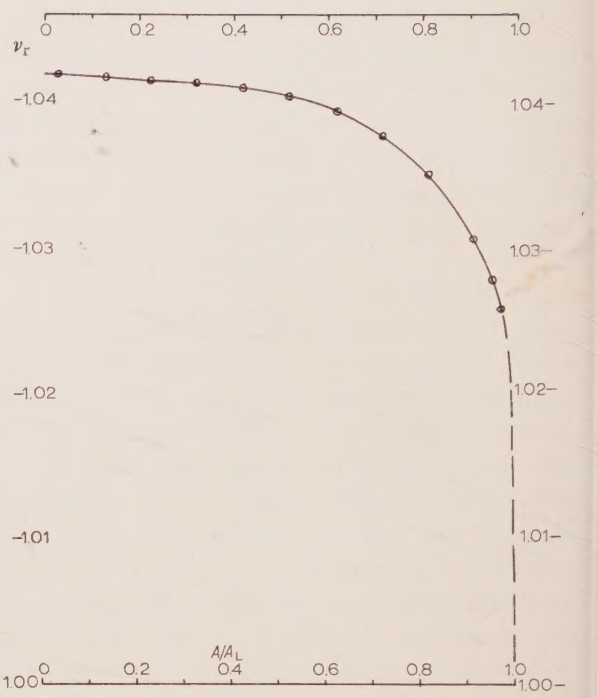

Fig. 8. ν_r as function of amplitude at 28 MeV in magnetic field of proposed MSU cyclotron, ν_r is determined from the number of revolutions required to complete a full precessional cycle on the phase diagram.

3.3. EXTRACTION REGION ORBITS

The cyclotron has earned a reputation as an efficient, straight forward device for producing intense internal beams; equally it has earned a reputation as a poor device for producing well-collimated external beams. Typically 80 to 95% of the internal beam is lost in the extraction process and in addition the surviving beam tends to emerge in a broad fan. Manifestly, major improvement in the effectiveness of the extraction process is required if a cyclotron is to function as an effective injector.

Low energy cyclotrons normally accomplish beam extraction by using an electrostatic channel, the region of strong electric field being separated from the region of normal orbits by a thin electrode called a septum. In principle the septum is placed between successive turns so that particles on one turn move just inside the septum and on the next just outside and the electric field is made sufficiently strong to bend the latter turn out of the cyclotron. As the energy of the cyclotron is raised several effects act to markedly reduce the effectiveness of such devices. (1) The radial separation of successive equilibrium orbits decreases, due to the r^2 dependence of the energy and quickly becomes comparable with the thickness of feasible septums; more particles then strike the septum, reducing the extraction efficiency and enhancing the

engineering problems of septum design. (2) The radial separation of successive equilibrium orbits becomes small with respect to the spread in radius of the particles from a particular turn; particles from a number of turns with a corresponding broad distribution in energy enter the channel. (3) As the velocity increases, successively stronger electric fields are required to obtain a given angular deflection (the electric force must balance a given fraction of the magnetic force and the magnetic force increases linearly with v); the required field strengths quickly approach technological limits.

The first of the above difficulties is set purely by the turn separation and may be alleviated by introduction of features to appropriately magnify the separation. The second is related but somewhat different in that magnification of the separation without corresponding magnification of the radial spread of a given turn is required. The third is basically also a function of turn separation in that the choice of E field is, to begin with, dictated by small turn separation (electrodes can be made thinner than magnetic shields); if the turn separation is adequate, magnetic shields can be employed at all energies, hence eliminating the velocity difficulty.

The Tuck, Teng, LeCouteur extraction system[16]) normally employed in high energy synchrocyclotrons amplifies orbit separation by introducing magnetic field perturbations of a type such as to resonantly excite the radial betatron oscillation. The usual perturbation strengthens the field over a narrow angular region near the maximum energy orbit and in some cases an accompanying weakened field region is introduced 60° to 90° away. Fourier analysis of the perturbation results in a variety of harmonics; in most cases the $\cos\theta$ and $\cos 2\theta$ components appear to be the dominant perturbing factors in the motion. Fig. 9 is a series of sketches depicting qualitatively the features of radial phase plots at a sequence of energies near the maximum energy[17]). The initial large stable region corresponding to centered orbits shrinks under the influence of the perturbation, finally disappearing completely. The shaded area in the figure depicts the behavior of a group of particles being slowly accelerated. As the particle energy increases the separatrix defining the stable region pulls gradually in through the beam

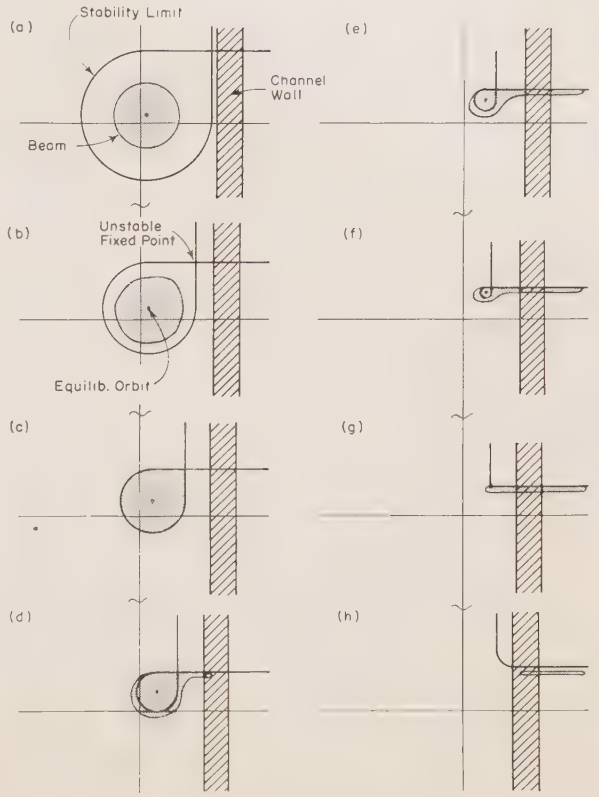

Fig. 9. Schematic radial phase plots illustrating operation of synchrocyclotron regenerative extractors.

spot, dumping particles into the unstable region; the particles in the unstable region move out along the asymptote until they reach the channel radius, at which point they either enter the channel or are lost depending on whether their position coincides with the channel aperture. Viewed as a mechanism for getting particles into a channel, the procedure is quite effective. If the inner wall of the channel has radial width a, and the channel aperture radial width b, channel entry efficiencies of up to $b/(a+b)$ can be achieved, the maximum efficiency occurring if the channel is placed at a radius where the growth in radial oscillation amplitude per turn is just $a+b$. Entry efficiencies of 50% or more are often achieved.

Unfortunately, other aspects of the process are

[16]) J. L. Tuck and L. C. Teng, Univ. of Chicago 170 in. Synchrocyclotron Progress Report III, Chap. VIII (1950);
J. L. Tuck and L. C. Teng, Phys. Rev. **81** (1951) 305;
K. J. LeCouteur, Proc. Roy. Soc. (London) B **64** (1951) 1039.

[17]) See for example, N. F. Verster, Proc. of Sea Island Conf. NAS-NRC **656** (1959) p. 199.

not similarly effective. First of all, particles entering the magnetic channel will have an energy spread corresponding approximately to the energy difference between sketches (c) and (g) of fig. 9, i.e. between the energy at which the stable region is just equal to the beam spot area and the energy at which the stable region has just vanished. In addition to the energy spread itself, the asymtote position shifts in position on the phase diagram as the stable region shrinks, thereby imparting an additional spread in angle (coherent with the energy spread) into the beam entering the channel.

The combination of energy spread, angular spread, and a distorted object shape combine to make design of the channel an extremely difficult problem. The customary channel design appears in fact to be a rather highly selective energy monochrometer; the result is that most beam is lost in the channel but the output beam is highly monochromatic. Typically 50% of the internal beam will enter the channel and of this, approximately $\frac{1}{10}$ or 5% of the original beam, will be transmitted. The beam entering the channel will have an energy spread of about 1% whereas the exit beam will have spread of only a few tenths of a percent.

For sector focused cyclotrons, a situation exactly analogous to conventional cyclotrons is found; at low energies an electrostatic peeler can be effectively employed, but as the energy is increased the same difficulties listed previously are encountered. In a sector focused cyclotron the operating point is, however, never far from some linear or non-linear resonance and hence the first and third of the aforementioned difficulties can be avoided with almost trivial ease by taking the operating point onto a resonance. Oscillations will be excited sufficient to swing the beam into a magnetic channel in a manner quite analogous to the Tuck, Teng, LeCouteur system.

There is, however, one crucially important difference between sector focused and synchrocyclotrons, to wit, the sector focused cyclotron is a fixed frequency device and can hence have an r-f system with enormously higher volts/turn than can be achieved in the synchrocyclotron. Rather than slowly shrinking the stable area thru the beam giving the diffusing effect shown in fig. 9, it is possible (as is shown in more detail in following paragraphs) with the large energy gain to effectively snap the stable region instantaneously out from under the beam whereupon the beam walks as a spot out to the channel radius. Since the beam is a spot rather than a streamer, 100% channel entrance efficiency is easily achievable[18]). In addition, the energy spread of the beam entering the channel should be extremely small and the angular divergence essentially no larger than the damped divergence from the source. With such a beam, the problem of channel design is almost trivially easy compared with the synchrocyclotron case and it is therefore quite probable that 100% channel transmission could also be achieved.

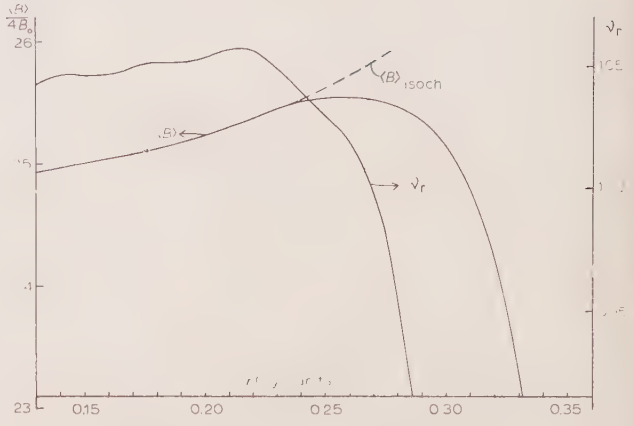

Fig. 10. Extraction region average field (and resulting radial tune) used in MSU extraction studies.

The principal features of such a system, as applied to the 3 sector 40 MeV cyclotron, are sketched qualitatively in figs. 10 and 11. In this case the most convenient resonance to employ is at $\nu_r = 1 (= \frac{3}{3})$ which is reached of necessity[19]), as

[18]) It is perhaps worthwile to recall to the reader's attention that throughout this section we are discussing a group of particles leaving the source at fixed time and with no energy spread. While 100% efficiency is achievable for such particles, a considerable reduction in efficiency will result when averaged over time as is discussed in section 4.

[19]) $\nu_r = 1$ will of course always occur near the edge of any isochronous cyclotron at the transition from increasing to decreasing $< B >$ vs. radius. Immediately preceding this resonance is a region of non-isochronous orbits and hence in order to reach the resonance the accelerating voltage must be high enough to limit the particle phase slip to an acceptable value. In view of this it may be convenient in many circumstances to use a different resonance, a likely choice being simply the resonance closest to the isochronous tune at the maximum energy.

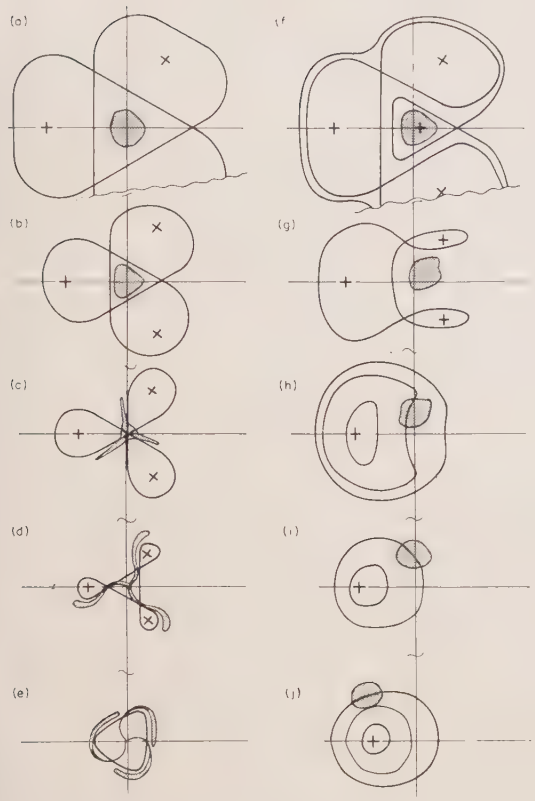

Fig. 11. Schematic radial phase plots illustrative behavior at $r = 0$ without (left) and with (right) $\cos\theta$ field perturbation. Sequence from top to bottom depicts transition from above to below resonance.

hown in fig. 10 when the isochronous field region erminates and changes into the usual edge region all off. The left hand side of fig. 11 depicts the behavior of the phase space[20]) as the resonance is raversed assuming a pure 3 sector field. If the beam spot were approximately on center prior to he resonance, the beam would diffuse out in 3 places as shown by the gray area in the figure, the non-linearity giving an undesirable stretching effect quite similar to the stretching caused by the slow acceleration in fig. 9.

If a field component with $\cos\theta$ angular dependence is included, a number of helpful changes occur as are indicated at the right of fig. 11. Pairs of "fixed" points[21]) move together and vanish corresponding to the disappearance of the original center stable region followed by two of the outer stable regions leaving, as shown in 7 (j), a phase plot corresponding to approximately linear motion about a displaced stable fixed point. If the accelerating voltage is high enough to shift the particle energy from (f) to (i) of fig. 7 in a few turns, the beam effectively jumps from linear motion about a nearby fixed point to approximately linear motion about a considerably distant fixed point, hence yielding turn separation of magnitude determined by the amplitude and effective ν_r of the oscillation about the final fixed point and with a minimum of distortion, since for almost the entire process the beam spot is in a reasonably linear region. The gray spot in the right hand sketches of

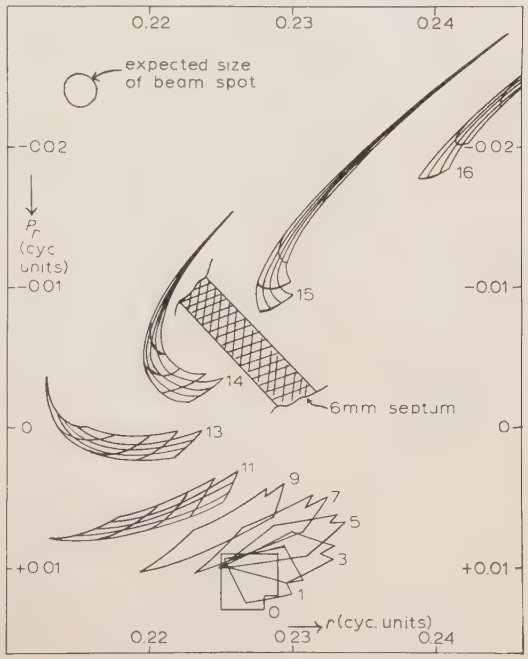

Fig. 12. Computational results for grid of particles accelerated with 280 keV/turn from initial energy of 30 MeV in field of proposed MSU cyclotron. Field has $\cos\theta$ component of amplitude 1 %. Circle at upper left corresponds to radial phase acceptance of 76 milli-radian cm at 70 keV.

[20]) Non-linearities in the magnetic field give rise to the set f distinct topological regions in the phase space, the boundaries f which are sketched in the figure. The characteristics of these egions have been discussed by many authors—see for example: P. A. Sturrock, Annals of Physics **3** (1958) 113; Hagedorn, Hine and Schoch, CERN Proceedings **1** (1956) 237; and L. J. Laslett, Mura Reports 452, 459, 461, 463, and 490 unpublished). A report by the authors, MSUCP-9, is also vailable which shows the relation of the phase regions to articular features of the magnetic field.

[21]) A "fixed" or self repeating point in the phase space indicates an orbit which closes smoothly on itself after one revolution. Such orbits are subdivided into stable or unstable lassifications according as near neighbor orbits remain close to r drift away from the fixed point orbit respectively.

fig. 11 indicates qualitatively the behavior of a beam spot in such circumstances.

The rapidity of the transition from 7 (f) to 7 (i) is approximately proportional to dv_r/dn (the change in v_r per turn) in the extraction region. To enhance dv_r/dn requires high volts (large change in E per turn) and/or a small magnet gap (small gap allows large dv_r/dE).

Actual beam behavior in such a process is illustrated[22]) in fig. 12. The figure shows results of orbit integrations in which a grid of particles (again in the magnetic field of the proposed 3 sector 40 MeV MSU cyclotron) are accelerated into the resonance with an energy gain of 280 keV/turn. The grid is initially positioned near the center of the stable region of the r, p_r phase space as can be seen in fig. 13 which shows the initial grid on its static phase plot as well as corresponding displays at the end of 1st and 2nd full turns. At the end of the third and following turns no stable region exists. The second turn is then the only one on which the grid overlaps the stability boundary and even on this turn the overlap is on a well behaved portion of the boundary, well removed from the proximity of the unstable fixed point. Referring again to fig. 12 it is seen that on the initial turns the grid positions fairly fully superimpose corresponding to motion about a nearby stable fixed point (for clarity results from the 2nd, 4th, 6th, 8th, 10th and 12th turns have not been plotted and, in addition, on the early turns only the outline of the grid is shown). After the normal stable region has vanished the grid moves off, corresponding to motion about a considerably displaced stable fixed point. The separation of the 14th and 15th turns is 15 mm, that of the 15th and 16th 35 mm. With careful design a magnetic septum could probably be inserted between the 14th and 15th turns. The cross hatched area on the figure (fig. 12) corresponds approximately for example to a 6 mm thick septum[23]). Between the 15th and 16th turns a 20 mm thick septum could easily be inserted. In either case, since the turn separation is considerably larger than the septum width, 100% channel entry efficiency would result for the particles here considered.

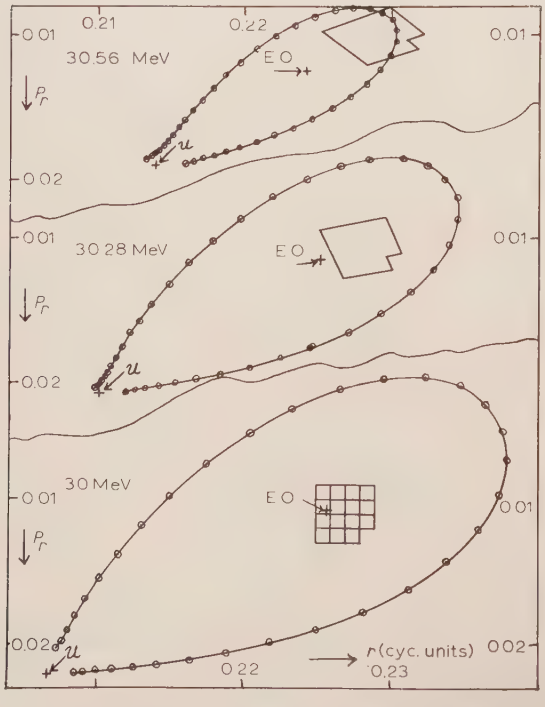

Fig. 13. Grids from zeroth first and second turns of fig. 12 superimposed on corresponding static phase plots.

The grid as a whole is seen to distort rather severely, particularly on the later turns where the separation is large. Sub-areas of the grid are, however, much better behaved. The circle at the upper left of fig. 12 corresponds to a beam with spot size divergence at the source (70 keV) of 76 milli-radian cm. (This area is somewhat smaller than the area from an unapertured source which from fig. 2 would be 190 milli-radian cm at this energy, but also somewhat larger than the area which would probably be used in most actual designs due to space charge effects, as will be discussed in section 5.) Sub-areas of the grid comparable in size to the beam spot are seen to have much less distortion than the grid as a whole. The area in the vicinity of the notched corner is particularly well behaved. If a septum were successfully fitted between the 14th and 15th turns, distortion of a beam of area corresponding to the circle in the figure would be negligible, when

[22]) These results are taken from a report, MSUCP-9, by and available from the authors. Considerably more detailed discussion of the phenomena is given therein.

[23]) The optimum azimuth for the septum is clearly not that at which the phase plot in fig. 12 is made. The slanting of the septum area in the phase space indicates a projection of the septum area from the optimum septum azimuth to the azimuth of the phase plot.

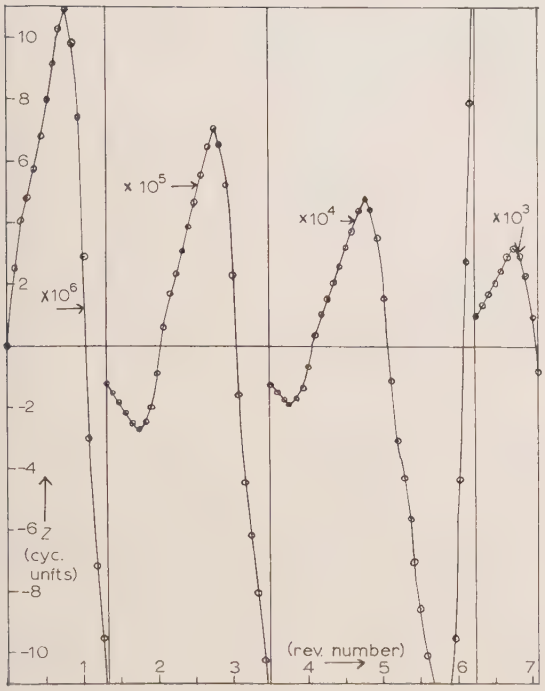

Fig. 14.
Vertical motion of beam in the vicinity of $\nu_r = 2\nu_z$ resonance.

considered from the practical viewpoint of design of subsequent optical elements.

As in the Tuck, Teng, LeCouteur extraction process, a considerable tendency toward axial instability is found in extraction processes of the type considered here. The origin of this instability is quite easy to understand as are the steps necessary to alleviate the difficulty. In the extraction process the beam is moving off center rather rapidly, particularly in the final two or three revolutions and hence on one side of the magnet successive orbits move further and further into the strong field fall off at the edge of the magnet. The fall off gives a strong axial focusing impulse to the particles—much stronger than any other axial force encountered on the revolution. In the extreme situation, axial motion of the type shown in fig. 14 often results; the particles are sharply focused once per revolution, crossing the median plane shortly thereafter and proceeding to drift off the opposite side of the median plane for the remainder of the revolution until they again return to the focusing region whereupon the cycle is repeated. The motion repeats once each 2 revolutions and, since $\nu_r = 1$, the amplitude buildup corresponds to the $\nu_r = 2\nu_z$ coupling resonance.

To alleviate the difficulty it is necessary to reduce the field fall off in the vicinity of the protruding orbits. Two rather different approaches can be employed in the design of magnet structures to accomplish this objective. Simplest from the magnet design viewpoint is to extend the field on one side of the magnet via a cam-like structure designed to give a gentle slope to the field for a distance of 15 or so cm beyond the main field, such that the focusing impulse in the region is weak enough not to cause trouble. A more complicated but possibly more economical technique is to attempt "terracing" of the edge of the field in the vicinity of the last two turns by bringing iron close to the median plane. The last two turns are sufficiently separated from previous turns and from each other to make such terracing feasible and in most circumstances these are the only turns on which the instability is a serious problem. The dees can terminate at an earlier radius since acceleration is not really important on the last several turns, thereby permitting iron to be brought close to the beam space, as is required to accomplish the terracing. While neither the cam-sided nor the terraced field have been developed in detail at the present time, both are sufficiently straightforward as to make it essentially certain that at least one can be developed, and probably both, without undue difficulty.

The problem of magnetic channel design for such a beam, while also not yet treated in detail, should clearly be vastly easier than the comparable synchrocyclotron problem. Since by assumption the beam has left the source at fixed time and with fixed energy the only energy spread comes from a phenomenon which is effectively a slight coupling between betatron and synchrotron oscillations, principally in the central region of the cyclotron. For the 40 MeV case this coupling gives an energy spread of roughly 1 in 2000 so that to all intents and purposes the instantaneous beam is monochromatic. In addition both radial and axial phase areas are compact approximately elliptical figures. In view of these factors it appears quite reasonable to assume that channel designs can be evolved which will transmit the instantaneous beam with negligible additional

distortion and with essentially 100% efficiency.

Before proceeding to consideration of the E, t phase space characteristics, it is perhaps worthwhile to summarize the results of this section. Combining the conclusions of subsections 3.1, 3.2 and 3.3, it is seen that the instantaneous beam can be expected to negotiate the entire acceleration-extraction process with small, essentially negligible x, p_x, y, p_y distortion and 100% efficiency, or at least for the 3 sector 40 MeV MSU design such performance is clearly indicated. Qualitative considerations lead to the conclusion that similar results can be achieved for other sector numbers and for final resonances other than $\nu_r = 1$.

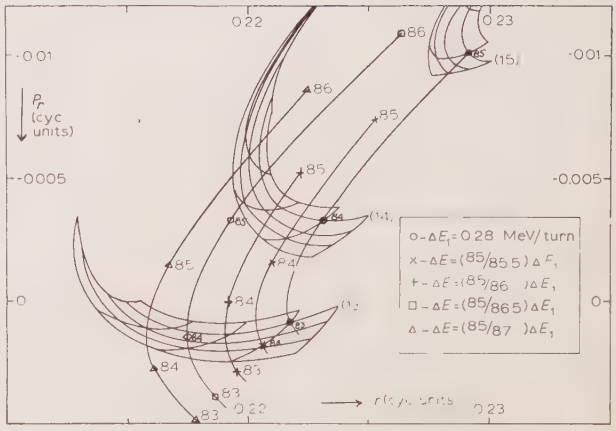

Fig. 15.
Accelerated orbits with varying voltages as shown.

4. Cyclotron Orbit Dynamics—Longitudinal Characteristics

We now remove the restriction of the previous section and consider the behavior of a beam of particles leaving the source over a finite time interval. For particles leaving the source at different times the principal different physical factor is the accelerating voltage (possible time variations in the magnetic field are readily reducible to a negligible level with presently available techniques). Differences in the accelerating voltage experienced by the particles are of two types, one due to time variations of the amplitude of the r-f voltage and the other arising from differences in the starting phase of the particles with respect to the r-f voltage. The first of these can in principle be reduced to a negligible level although techniques comparable to those available for control of the magnetic field are not as yet available. Considerable progress[24]) has been made, however, and in view of this it seems reasonable to assume in considering injector cyclotrons that developmental work will have been done sufficient to reduce amplitude time variations of the r-f to a negligible level (say to less than $\pm 1/(40n)$ of the total voltage where n is the number of turns). We are left then with the effect of variations in the initial phase. The phase at which particles depart from the source is of course not a controllable factor. Particles leaving at certain phases will be extracted, those at other phases will not. Our objective is to estimate the fractional time during which particles can be accepted from the source and still be extracted.

Note first of all that in an exactly isochronous cyclotron, the particle's initial phase is maintained throughout the acceleration process so that from the point of view of the particle an initial phase off from the peak voltage value is completely equivalent to acceleration on the peak but with reduced volts per turn. Looking again at fig. 12 it is seen that the r, p_r areas of the 0th and 1st turns largely overlap, yet 14 turns later for each, i.e. on the areas labeled 14 and 15 in the figure, the overlap has completely disappeared. The factor which determines whether a particular point in the overlapping region of 0 and 1 arrives, after 14 turns, in area 14 or in area 15 must then be the particle energy since this is the only distinguishing coordinate in the overlap region. Consider then a particle in the overlapping region but with energy half way between the energies of 0 and 1. After 14 turns this particle would qualitatively be expected to be spatially half way between 14 and 15 of the figure, or right where the septum is positioned, and hence would be lost.

Fig. 15 depicts the effect quantitatively. The particle at the notched corner of the fig. 12 grid has been traced backward with deacceleration for 85 revolutions from turn 15 of fig. 12, i.e. 70 turns back from the beginning of fig. 12. The final point of this backward deacceleration run has then been used as the initial condition for a set of 4 forward accelerations runs, each forward run starting at the

[24]) H. Fauska, J. W. Orth and F. H. Schmidt, Nucl. Instr. and Meth. 10 (1961) 73.

same position and with the same energy particle but with acclerating voltages in the ratio of 85/85.5, 85/86, 85/86.5, and 85/87 respectively to that of the deaccelerated run. Hence after 85 and 86 turns the first and third respectively of the accelerated particles have energies differing from that of the reference notch particle by $\frac{1}{2}$ the energy gain per turn. As is seen in the figure, these particles fall approximately half way between the 14th and 15th grid positions and will collide with the septum as expected. The second and fourth of the accelerated particles after 86 and 87 turns respectively have identical energies to that of the reference notch particle and on the basis of the qualitative argument would be expected to arrive at the same position. From fig. 15 it is seen however, that they fail to do so by a considerable amount such that even though they successfully entered the channel, their direction would be different and the probability of surviving the channel consequently small.

From the above results a safe criterion as to fractional "on time" of the cyclotron is to assert that only those particles survive which depart from the source in a phase interval such that the effective voltage gain per turn felt by all particles in the interval is on the average constant to $\pm 1/(10)n$ where n is the total number of turns in the cyclotron. Within such limits the composite r, p_r phase area would be enlarged due to the time wandering of the beam by no more than a factor 2, the turns would continue to be spatially separated, the energy spread would be essentially $\pm 1/(10n)$ (since spreads arising from other effects are negligibly smaller), and the beam would still have compact radial and axial phase areas; with such conditions, achievement of near perfect channel performance remains a reasonable expectation.

The range of initial phases for which the composite energy gain (for complete source to extractor trajectories) is constant to the specified tolerance can be readily estimated. Making the usual smooth energy gain approximation, one has

$$\frac{\mathrm{d}E}{\mathrm{d}n} = V\cos\phi\,(E), \qquad \frac{\mathrm{d}\phi}{\mathrm{d}n} = 2\pi\,[1 - \omega_{\mathrm{rf}}/\omega_{\mathrm{p}}(E)] \quad (3)$$

where E is the energy of the particle, V the voltage gain per turn, n the revolution number, $\phi(E)$ the difference between particle and r-f phase (positive ϕ corresponding to particle ahead of r-f maximum), ω_{rf} the angular velocity of the accelerating voltage, and $\omega_{\mathrm{p}}(E)$ the angular velocity of the particle of energy E. Combining equations (3) and integrating yields the well known result

$$\sin\phi(E) = \sin\phi_0 + V^{-1}\int_0^E 2\pi\,[1 - (\omega_{\mathrm{rf}}/\omega_{\mathrm{p}}(E)]\,\mathrm{d}E\,. \quad (4)$$

If the second term on the right of (4) is written as $\sin\phi_1(E)$, (i.e. $\phi_1(E)$ is the phase of the particle starting exactly at the peak of the r-f) then for given initial ϕ the number of turns required to reach a particular energy is from the first of equations (3)

$$n(E) = V^{-1}\int_0^E \frac{\mathrm{d}E}{\cos\phi(E)} = V^{-1}\int_0^E [1 - (\sin\phi_1(E) + \sin\phi_0)^2]^{-\frac{1}{2}}\,\mathrm{d}E\,. \quad (5)$$

Expanding the integrand of the integral in (5) yields

$$n(E) = V^{-1}\,[E\sec\phi_0 + f_1(\phi_0)\int_0^E \sin\phi_1(E)\,\mathrm{d}E + f_2(\phi_0)\int_0^E \sin^2\phi_1(E)\,\mathrm{d}E + \ldots] \quad (6)$$

where $f_1(\phi_0)$ is an odd or even function of ϕ_0 as 1 is odd or even.

If the cyclotron is strictly isochronus, $\phi_1(E) \equiv 0$ and hence all terms in (6) except the first vanish. In such case, if $E_{\max}/V$ is 200 for example, as would be a likely choice of parameters for an injector cyclotron, then one obtains a phase interval of $\pm 2.6°$ or 1.4% total for which the energy gain is constant to the required $\pm 1/(10n)$. For non-isochronous fields the higher terms in (6) operate to reduce the acceptable phase interval[25]). The first essential contribution in this regard arises from the third term of (6) since the second term can always be made to vanish by appropriate balancing of positive and negative phase excursions of the $\phi_0 = 0$ particles. Fortunately the third and higher terms appear to be typically small in normal design situations for injector cyclotron. As an example, for the non-isochronous field considered in § 3.1, and with energy gain per turn of 280 keV, the higher order terms in (6) reduce the acceptable phase interval by less than 10% which, for purposes herein, is quite negligible. For simplicity we therefore in the

[25]) One of the authors (HGB) is indebted to D. L. Judd for several helpful discussions of this phenomena.

following paragraphs consider only the first term of (6).

The range of acceptable phases can be broadened by partial flat-topping of the r-f as has been suggested by Rossi[26]) and independently suggested and experimentally tested by Goodman[27]). The figure of $\pm 2.6°$ obtained above (for $n = 200$) can for example be extended to $\pm 18.3°$ or $\frac{1}{10}$ of D.C. by adding a third harmonic of amplitude 11.9% to the r-f wave.

Before passing to summations it should be noted that a longitudinal space charge effect has been pointed out by Welton[28]) which leads to an increased rate of acceleration for particles of positive ϕ_0. This effect could, if ignored, considerably increase the energy spread in the beam and decrease the efficiency of the extraction process. Methods for alleviating this difficulty have also been pointed out by Welton. Basically the second term on the right of (6), or an equivalent term if the r-f is partially flat topped, must be programmed to a slightly non zero value with sign such as to cancel the imbalance in acceleration arising from the space charge effect. This solution appears straightforward —the effect will therefore not be considered further.

5. Conclusions

The results of the previous sections are now combined to obtain composite performance estimates for the complete system. Section 2 concluded that cyclotron type sources could furnish beams with D.C. luminosity, at 250 keV, of at least 40 A/cm² sr. Sections 3 and 4 together defined a procedure for estimating the fractional time during which the source beam would be transmitted thru cyclotron and extractor. For $n = 200$, this fractional on time was 1 in 70 for pure sinusoidal accelerating voltage and 1 in 10 if optimum third harmonic voltage was included. For normal choice of field strengths and r-f frequency, the cyclotron output would consist of a continous train of pulses, the time separation between pulses corresponding to a frequency of approximately 20 Mc/s. The transmitted beam would have an energy spread of $\simeq 1$ in 1000 for the 200 turn example, the major part of the energy spread arising from a coherent variation of energy[29]) with time of the sort sketched in footnote[7]). A coherent spatial oscillation also accompanies the energy spread, the oscillation as described in section 4, being such as to effectively double the radial phase area of the beam.

With respect to the axial motion, little mention has been made of the subject thus far in this report except to point out that possible instabilities arising in the extraction process appear amenable to solution. The apparent neglect of this topic is not accidental, but rather, is a reflection of the fact that throughout the remainder of the cyclotron the axial motion is well behaved, the principal responsible factor being the relatively large distance

Table 1

Estimated performance characteristics of 40 MeV injector cyclotron for two choices of axial aperture. In the table the radial aperture at the source is assumed to be restricted to yield a net accelerated current of $\frac{1}{2}$ the space charge limit. Source luminosity at 250 keV and D. C. Is assumed to be 40 A/cm² sterradian, Radial spot-size divergence of output beam is enlarged by × 2 to account for time wandering of beam.

Axial aperture	25 mm	50 mm
Volts/turn	2.8×10^5	2.8×10^5
Number of turns	140	140
Central magnetic field (kilogauss)	14	14
Duty cycle:		
sin ωt voltage	1.7%	1.7%
sin $\omega t + a \sin 3\omega t$ voltage	11.1%	11.1%
Repetition rate (pulse/sec)	21×10^6	21×10^6
Source extraction energy	70 keV	70 keV
Phase space acceptance from source (full width-full angle):		
Radial (milli-radian cm)	45	23
Axial (milli-radian cm)	470	1880
Output beam current (time average):		
sin ωt voltage	2.8 mA	5.6 mA
sin $\omega t + a \sin 3\omega t$ voltage	18.3 mA	36.6 mA
Output beam spot size-divergence (full width-full angle):		
Radial (milli-radian cm)	3.8	1.9
Axial (milli-radian cm)	20	80
Output beam energy spread	± 30 keV	± 30 keV

[26]) G. B. Rossi, Cyclotron Square Wave R-F System, U.S. Patent No. 2, 778, 937.

[27]) C. D. Goodman, Oak Ridge National Laboratory, Report ORNL-2403 (unpublished).

[28]) T. A. Welton, Proc. of Sea Island Conf. NAS-NRC 656 (1959) 192.

[29]) The coherent energy spread could of course be eliminated by a properly phased accelerating cavity acting on the extracted beam. The residual energy spread in such case would be difficult to estimate.

between the magnet poles and the beam space in cyclotron structures of normal type which drastically limits axial nonlinearities in the aperature. The actual choice of axial aperature arises principally from economic factors; apertures in the range from 25 to 50 mm would appear likely choices. With appropriate choice of major parameters along the lines of section 3.1, an initial ν_z of 0.2 appears easily achievable.

With an initial ν_z of 0.2 and assuming an energy of 70 keV as a typical value for beam leaving the source extractor slit (the point at which the data of Smith[9]) are applicable), an axial phase space acceptance of 470 and 1900 milli-rad cm results for 25 and 50 mm aperture respectively. By appropriate use of apertures near the center, the radial phase area can be set for any value from near zero up to $\simeq$ 200 milli-rad cm (the 70 keV equivalent of Smith's results[9])). In many situations depending on the energy gain, the combination of radial and axial acceptances listed will yield currents in excess of the space charge limit. In such case, for optimum design, either radial or axial acceptance should be restricted to reduce the initial current to conform with the limit.

Combining the above statements, detailed estimates of the performance of a given cyclotron can be obtained. As an example, table 1 is a summary of properties to be expected from the 40 MeV cyclotron for the two choices of axial aperture mentioned above. In each case the radial phase space acceptance is assumed limited by aperatures such that the total accepted current is $\frac{1}{2}$ the space charge limited current. In this computation the effective axial phase space acceptance is reduced in a self consistent way to allow for the reduction in ν_z due to the space charge repulsion. Table 2 is a considerably less certain summary of properties of a possible 200 MeV cyclotron, the table being derived by simply assuming that all the conclusions herein relative to 40 MeV performance are also valid at 200 MeV.

Finally, it is appropriate to hazard a few remarks as to relative merits of such a beam for synchrotron injection. It is at once clear, as mentioned in the introduction, that the optimum radiofrequency system in the synchrotron is considerably different when a cyclotron is used as the injector. The cyclotron beam is rather tightly bunched in time and one is at once led to consideration of synchronous synchrotron r-f systems in which each cyclotron pulse at injection comes into the approximate center of an already turned on "bucket"[30]). Very interesting possibilities for achieving extremely high intensities ensue, although apparently at the expense of considerably enhanced fabricational problems in the synchrotron r-f system. The cyclotron beam is also novel with respect to large transverse phase space area of the beam (in conjunction with high density this means very large currents indeed during the cyclotron pulse) principally in the axial direction. The large area means that the phase area of a synchrotron can be filled in fewer turns and, since on every turn, some empty phase space (corresponding to the inflector) is always injected, filling in fewer turns results in more efficient filling. Cyclotrons can be constructed with approximately equal ease in either horizontal or vertical orientations so that the large axial phase area in the cyclotron can be either axial or radial in the synchrotron.

TABLE 2

Estimated performance characteristics of 200 MeV injector cyclotron for two choices of axial aperture. Radial aperture of source assumed to be restricted as described in table 1 caption

Axial aperture	25 mm	50 mm
Volts/turn	5×10^5	5×10^5
Number of turns	400	400
Central magnetic field (kilogauss)	14	14
Duty cycle:		
sin ωt voltage	1.0 %	1.0 %
sin $\omega t + a \sin 3\omega t$ voltage	8.5 %	8.5 %
Repetition rate (pulse/sec)	21×10^6	21×10^6
Source extraction energy	125 keV	125 keV
Phase space acceptance from source (full width-full angle):		
Radial (milli-radian cm)	60	30
Axial (milli-radian cm)	350	1400
Output beam current (time average):		
sin ωt voltage	3 mA	6 mA
sin $\omega t + a \sin 3\omega t$ voltage	25 mA	50 mA
Output beam spot size-divergence (full width-full angle):		
Radial (milli-radian cm)	3	1.5
Axial (milli-radian cm)	9	35
Output beam energy spread	$\pm$ 50 keV	$\pm$ 50 keV

[30]) Symon and Sessler, CERN Proceedings 1 (1956) 44.

NUCLEAR INSTRUMENTS AND METHODS 13 (1961) 118–123; NORTH-HOLLAND PUBLISHING CO.

MEASURING MACHINE FOR BUBBLE CHAMBER PHOTOGRAPHS

B. B. CULWICK† and S. J. GOLDSACK††

Department of Physics, University of Birmingham

Received 12 May 1961

A semi-automatic measuring machine is described which is primarily designed for analysing the tracks of particles in a bubble chamber. The accuracy of a measurement on the film is about 2.5 microns in each coordinate, and measurements can be made at a rate of one every few seconds.

1. Introduction

The recent success of hydrogen-filled bubble chambers as instruments of high energy nuclear physics has prompted the development in many laboratories of devices intended to speed up the measurements on photographs taken with the chambers.

The purpose of the present article is to describe the machine which the authors have constructed at the University of Birmingham to fulfil the needs of the 9″ hydrogen bubble chamber built in this laboratory (Colley *et al.*, 1959)[1]) and to obtain experience for future work with the British National Bubble Chamber.

The apparatus has now been in use for about six months, and measurements have been made on about 1000 proton scattering events at 970 MeV in the Birmingham bubble chamber, and on about 200 events from the CERN 30 cm bubble chamber exposed to a beam of 16 GeV pions. It has proved itself generally reliable and capable of maintaining its specified accuracy for long periods with little trouble.

The first group to appreciate that the rate of accumulation of data from bubble chambers could outstrip the possibilities of measurement was that of Alvarez at Berkeley, and the machines developed there by Franck and his collaborators have formed a basis for many other designs. It is a pleasure to acknowledge that many of the ideas incorporated in our machine were originally those of the Berkeley group.

The aim of a measuring machine is two fold. One hopes to improve the speed of measurement directly, but it is also possible to improve accuracy both in the sense of freedom from human error (incorrect recording of numbers, etc.) and perhaps the actual accuracy of setting. Further, the speed of measurement may be increased indirectly by making the work less fatiguing and therefore making longer working periods possible. It is hoped that all these results are achieved in the machine we have constructed.

The way in which these objectives are achieved in different machines varies, but probably the most important step is the removal of the time-consuming and fatiguing process of reading scales, often to four or five figure accuracy, and writing down the results. It is in this process, moreover, that errors most readily occur, due to mis-reading of the scales. In most machines which have been devised, as in ours, this process is made automatic. In order that the measurement may be printed out or punched in coded form on perforated cards or tape, it must first be converted from a continuous variable to a number, rounded to the nearest integer in a suitable scale. This conversion from analogue to digital form is known as digitizing.

It is further useful if the output can be made in a form suitable for immediate input to a digital computor, since invariably there are large amounts of calculation to be performed on the data.

The remaining steps are then the provision of

† Now at Brookhaven National Laboratory, U.S.A.
†† Now at Imperial College, London.

[1]) Colley, Kinson and Riddiford, Nucl. Instr. and Meth. 4 (1959) 26.

controls for setting the apparatus for a given measurement, and the provision of an arrangement to facilitate the selection of the required setting. In the most advanced machines this last process is achieved automatically by the use of a servo-mechanism, so that the machine makes its own readings entirely. The present machine has recently been modified to incorporate this facility, and the circuits used for this are described in the next paper.

2. Principle of Operation

The instrument described here is designed to facilitate the measurements of X and Y co-ordinates of points on the film selected by the operator. To this extent its use is not limited to the measurements of bubble-chamber tracks.

A schematic diagram of the apparatus is given in fig. 1, and a general view of it in plate 1. The film is fixed in the plane F, and its image is formed on a screen S, with a magnification $\times$ 10, by a 3″ "Dalmac" lens at L.

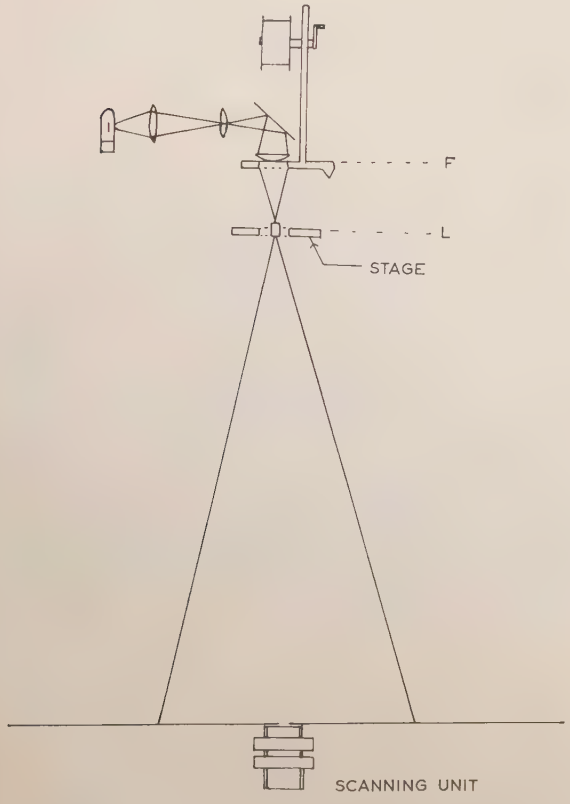

Fig. 1. Schematic diagram of the apparatus (not to scale).

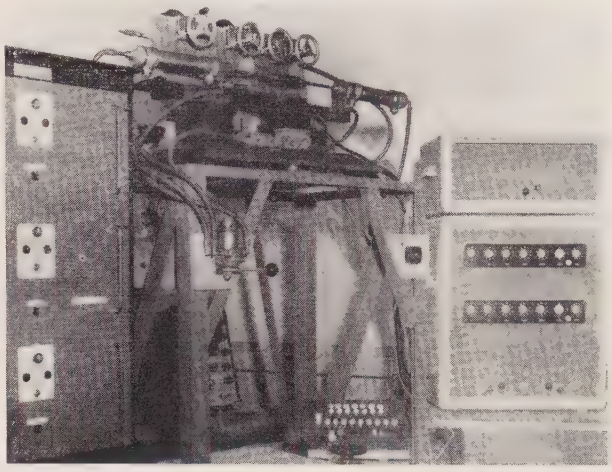

Plate 1. General view of the apparatus.

Provision is made to introduce any one of the three stereo views of the chamber into the position of measurement directly above the projection objective. The measurements are made by moving the projection objective to bring the image of the required point on the film to a fixed spot on the projection screen. The measurements of the position $(X'Y')$ of the lens are related to the co-ordinates of the points on the film XY by the simple factor $X = X'(1 + 1/m)$ where m is the magnification of the optical projection.

Illumination is obtained from a 300 watt incandescent projection bulb, and, since the projection lens is to move, this must be adjusted with the condenser system to give a parallel beam of light onto the film†, so that the illumination is equivalent whatever the position of the projection lens.

A measurement consists of adjusting the lens position to bring the chosen point of the image onto the central point of the screen, and recording the XY coordinate pair. Digitizers have been provided to record the coordinate pairs automatically, while the stage has been equipped with servo-motors for convenient control of the stage while making the settings. These motors are arranged as velocity control servos, so that their speed is proportional to the applied voltage. They are then fed with voltages proportional to the sine and cosine of a direction chosen by the operator, so that the stage can be

† More exactly the beam should converge to an image of the filament at the position of the projection screen.

caused to move in the chosen direction. (This may be, for example, the direction of the track which is being measured.)

Lastly, a scanning device has been constructed to facilitate the setting of the track image on the fixed reference point. In what follows these parts will be described in greater detail.

3. The Stage and Digitizers

The measuring stage is the commercially-available U-10 2-coordinate measuring table made by the Société Genèvoise des Instruments de Physique. The travel is $2'' \times 3''$, though some modifications were required of the standard pattern to make this useful range available with the optical arrangements used. We are grateful to the company for their help in this respect. The stage moves in the X and Y directions on a system of needle rollers, giving very low friction. However the motion, and, in the normal use, the measurement is obtained from lead screws, backlash in the screw and its bearings being removed by spring loading.

On this stage we have mounted the Ferranti "Moiré Fringe" digitizers. This is a system in which a diffraction grating fixed on the upper stage, moves over a similar grating on the lower stage, there being a small angle between the lines.

The system of moiré fringes produced is "viewed" by four photo-transistors. The signals from these are fed into a two-way decade scaler using "Dekatron" counting tubes. Each "count" in the scaler corresponds to the passage of $\frac{1}{4}$ of a line of the moving grating over the fixed, and the accuracy of measurement in no way depends on the lead screw, but only on the grating spacing, for which an N.P.L. certificate can be obtained.

We have used gratings with 2500 lines/inch which give a "digit size" of 1/10000" or approximately 2.5 microns. If finer precision is required, gratings with 2500 lines/cm are available, though the maximum speed of travel, limited by the scaler response, is reduced in proportion. In our machine this is not a limitation.

The Ferranti laboratories have further perfected a circuit by which these Dekatrons may be "read" automatically and their contents punched on paper tape in binary-coded decimal form (Mercury Code) using a Creed Model-25 reperforator. The Dekatron cathodes are "scanned" in turn with a Siemens "digit switch", a type of fast Uniselector switch, and when a glow is detected the corresponding character is punched. The print-out of an X and Y coordinate pair of five digits each takes about 2 seconds on the average. The movements of the stage must of course cease during the punching sequence†.

The design for mounting the digitizers on the Société Genèvoise stage was taken over from a similar design at CERN, and we are most grateful to Dr. Y. Goldschmidt-Clermont for sending us not only full drawings but also the necessary castings to simplify our work. Much of the work of adapting the stage in this way was performed by Sogenique Service Ltd., Newport Pagnell, a British subsidiary company of the Société Genèvoise.

4. The Film Carrier

The three views of the chamber are presented side by side on an auxiliary slide, as can be seen in plate 2. The selected view may be brought into line with the optic axis of the system by a pair of pneumatic pistons and a three position valve. This slide is not intended to have the accuracy of the measuring stage, so all measurements must be performed on one view before moving to the next.

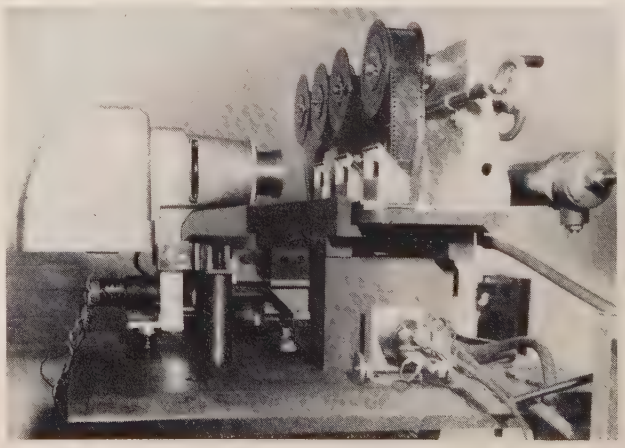

Plate 2. The stage and film assembly, showing the servo-motors and illumination arrangements.

† Since this was written, the Dekatron unit has been replaced by a fast transistorised scaler incorporating a buffer store, enabling a correct punch out to be obtained without stopping the stage. This is specially useful when automatic track following is incorporated.

The film is held firmly in position by vacuum suction on the back of the film.

5. The Servo-Motors

These are Muirhead 400 c/s 2 phase size 18 servo motors, with built-in tachometer generators. They drive the lead screws of the stage through 10:1 reduction gearboxes. Since the screws move with the stage, the motors are mounted, on wheels in the X direction and on ball castors in the Y direction, to allow the motors to follow the movements of the stage. The output shaft of the motor is coupled through a flexible link to the screw shaft of the stage, and in the Y-motor the additional unwanted degree of freedom, that of swinging about the flexible link, is inhibited by coupling the motor to the upper stage platform by strips of spring steel. This arrangement, orginally intended to be temporary, has proved entirely successful in use.

6. The Control System

A block diagram of the control system is given in fig. 2. The servo motors are arranged as velocity servos by the use of feed back from the tacho-generators. The control voltages to which they respond are obtained from a sine cosine resolver, a type of variable transformer whose circuit is illustrated in fig. 3. When coil A of the rotor is energised (input 1) voltages are induced in the coils X and Y of the stator proportional to the cosine and sine of the angle θ respectively. Thus if those voltages are used to energise the motors, the stage moves with a constant resultant velocity, but in a direction θ to the X axis.

If the same input voltage is applied to input 2,

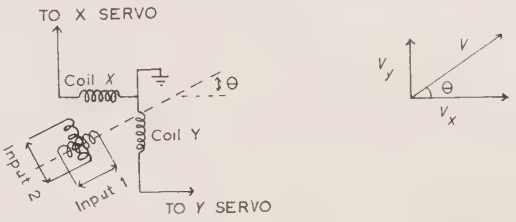

Fig. 3. The resolver.

the coil B of the rotor, voltages proportional to the sine and cosine of θ are induced in X and Y respectively, and the stage moves at the same velocity, but perpendicular to the chosen direction θ. Finally, if the phase of the input to either of these coils is reversed, the stages move along the same line but in the opposite sense.

To control the position of the stage, bringing the chosen image point to the centre of measurement, the operator uses, mainly, a key switch which admits a certain voltage into input 1, causing the stage to move forward, and a steering wheel, which rotates the resolver axis thus giving control of direction of travel. Thus while working along a track the direction selected is that of the tracks, so that successive measurements follow naturally one after the other. To provide higher speed of travel the same switch may be pushed in the opposite direction.

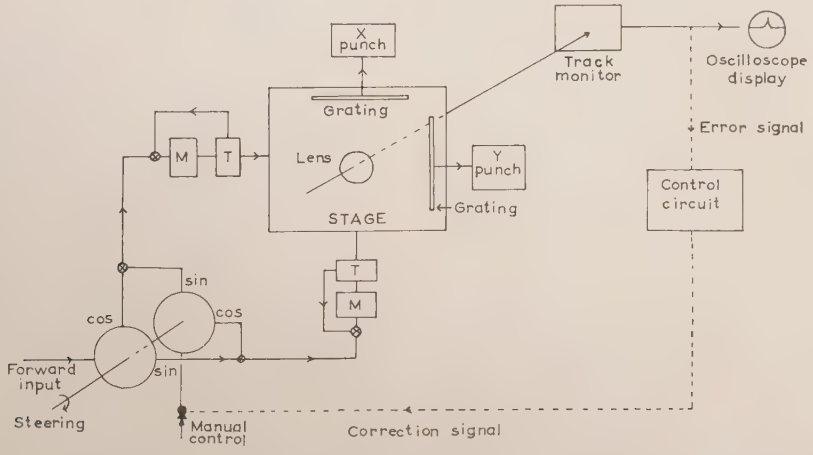

Fig. 2. Block diagram of the servo-control systems. The connection shown dotted is the subject of the next paper.

When the spot on the track to be measured is reached, it will be necessary to make fine adjustments to bring the track accurately onto the centre. This is done by energising the second input, so causing motion at right angles to the track. However, though buttons are provided to introduce voltages of either phase into this coil, giving left or right motion relative to the track direction, this control is too fierce for fine setting, as the response time of the motors is a few milliseconds. A set of inching buttons is therefore provided. A push on one of these discharges a condenser through a relay and so closes a switch for a few milliseconds. One push therefore gives a sideways step which depends on the size of the condenser. In our case four buttons have been provided corresponding to steps of about 8 and 2 microns in each direction: these enable the operator to make a precise setting with great ease.

Lastly, a push button is provided to cause the stage to move backwards along the chosen direction.

6. The Scanning Device

In the above section the method by which sufficiently fine control of the stage position is achieved has been described. There remains the question of how the operator decides when a chosen point to be measured is set on the centre of the screen, which corresponds to the cross hairs on a microscope. For this purpose a scanning device has been provided.

The principle of operation of this device is illustrated in fig. 4. When a ray of light passes through an oblique glass plate it undergoes a parallel displacement. Thus if an image is formed on a slit by projection through such a plate, the image will be scanned across the slit as the plate is rotated. In practice we have used a four-sided glass block, so that after each scan the next pair of faces causes the scan to start again in the same direction. The glass block is $\frac{1}{4}''$ square section and $1''$ long and rotates about its long axis, which is parallel to the slit S; the light penetrating this slit falls on the photo-cathode of the photomultiplier. When the image of a track parallel to the slit is cast on the system, a pulse appears on the photomultiplier, which can be displayed on a cathode ray oscillograph. The position of the pulse in time changes as the track is moved transversely across the slit, and the adjustment consists of setting the track so that it obscures the light on the slit at the instant when

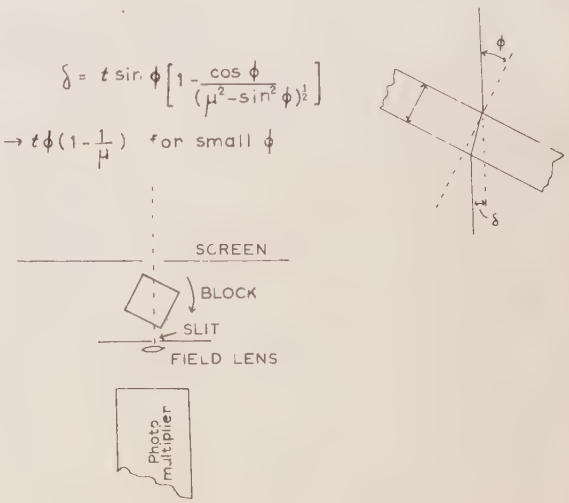

Fig. 4. The rotating glass block scanner.

the face of the block is normal to the incident light direction.

To indicate this, marker pulses are produced by an auxiliary optical system, consisting of a light source and photo transistor, which produces a

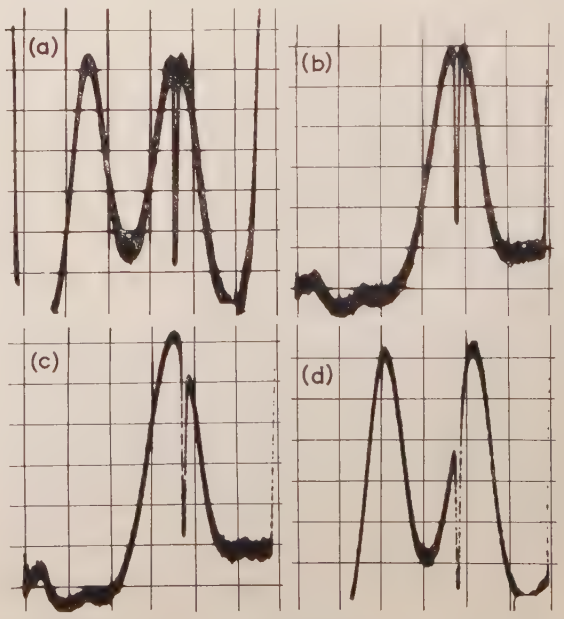

Plate 3. Track signals on the oscilloscope. In a) and d) the two tracks were 100 microns apart on the film. The fiduciary mark is shown centred in a) and b), 10 microns off in c) and 25 microns off in d).

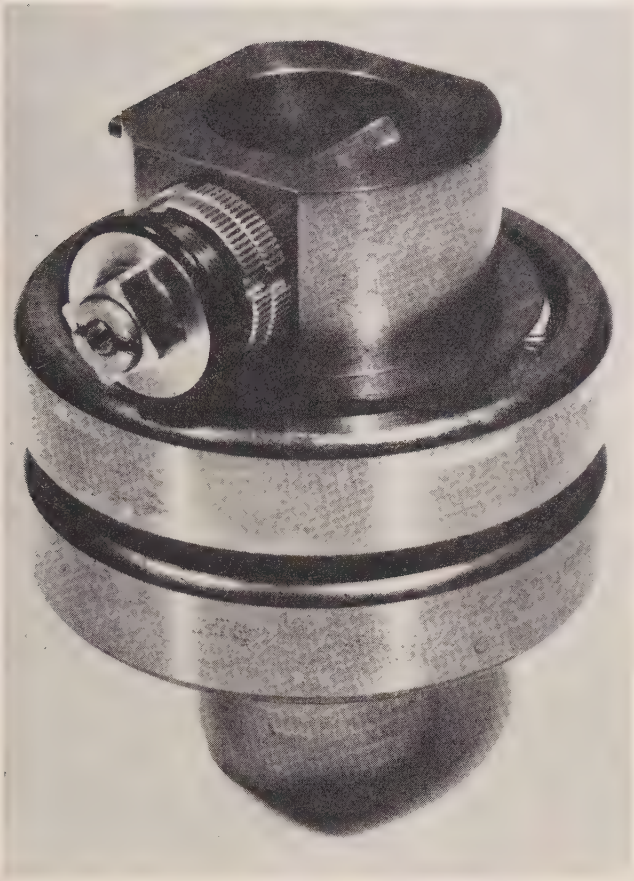

Plate 4. The rotating glass block scanning unit.

pulse by reflection off a four faced metal block mounted on the same axis of rotation as the glass prism. The appearance of the cathode ray tube screen when a track image falls on the glass block is shown in plate 3. The broad upward pulse represents the track; the short downward one is the fiduciary mark obtained by the reflection.

This provides an excellent and accurate method of centreing the track to make a reading. However, the slit must be set parallel to the track, and the way this can be done and yet continue to obtain the necessary drive to the block is shown in plate 4, which is a photograph of the actual unit. The upper ball race is a kind of friction "crown wheel' on which runs the rubber tyred pulley wheel, which acts as the "pinion". The crown wheel is caused to rotate at constant speed by a standard gramophone motor, and the motion is transmitted to the glass block through the pulley no matter what orientation the system may have. To permit rotation about its axis, the whole unit is mounted in a second bearing, a tight roller bearing to avoid side play. The polished metal block referred to above is also visible in this photo, attached to the pinion wheel.

Lastly, since one usually wishes to work along the direction of the track being measured, the rotation of the slit to the direction of the track is coupled to the resolver with a 1 : 1 gear, so that the setting of the slit parallel to the track simultaneously sets the resolver at the angle required to cause motion along the track, the inching buttons producing motion at right angles to it.

The signals on the photo-multiplier and phototransistor carry, of course, the measure of the error in the existing setting from the track. It is possible to derive from them the necessary electrical signals to cause the stage to "home" on the track and follow it automatically. The next paper describes how this has been done.

Acknowledgements

We would like to thank Professor P. B. Moon for his enthusiastic support of this project, and for many helpful suggestions.

We would also like to thank the several members of the workshop staff of the Physics Department who helped in its construction, but especially Mr. G. Young who contributed largely to the success of this machine.

The project was supported in part by a grant from the D.S.I.R.

NUCLEAR INSTRUMENTS AND METHODS 13 (1961) 124–126; NORTH-HOLLAND PUBLISHING CO.

AN AUTOMATIC TRACK FOLLOWING DEVICE

G. A. DORAN and M. JOBES

Department of Physics, University of Birmingham

Received 12 May 1961

This paper describes a method of automatic track following which is used on the measuring machine for bubble chamber photographs described in the previous paper. An error signal is derived from the relative positions of the peak of the track pulse and a marker pulse. Correction signals are then applied to servo-motors to reverse the sign of the error signal. A non-linear system is used; the magnitude of the correction signal is constant but its sign is changed when the sign of the error signal changes. An electrical signal to print out co-ordinates is produced when the error signal is zero.

1. Introduction

The preceding paper describes a measuring machine for bubble chamber photographs. In its original form Ferranti reversible "Dekatron" scalers were used to record the measuring stage position, and since the uniselectors used took about two seconds to transfer the co-ordinates to computer tape it was necessary for the stage to be stationary during this process.

Recently the Dekatron scalers have been replaced by a Ferranti transistorized scaler, which is intended eventually to be part of the National Bubble Chamber measuring machine. This scaler has the advantage of a store into which the co-ordinates may be transferred without stopping the main scaler; the co-ordinates are then printed out from the store on computer tape.

With this modification it seemed desirable to replace the manual setting on tracks with an automatic device. This would enable the operator to make measurements more rapidly and would eliminate errors due to faulty setting by the operator. This is the subject of the present paper.

2. Design Considerations

The system consists of an error signal generator, a computer and a correction signal generator. The error signal is obtained by comparing the relative positions of the marker pulse and the track pulse. Zero error signal corresponds to the marker pulse occurring at the peak of the track pulse. The correction signal is applied to input 2 (see previous paper) of the resolver; the phase and magnitude of this 400 c.p.s. signal then determine the direction and speed of motion perpendicular to the track.

The track pulse approximates to half a sine wave of frequency in the order of 250 c.p.s., depending on the operating conditions of the bubble chamber. The pulse is obtained from a photomultiplier, the peak of the pulse corresponding to a reduction of current in the photomultiplier. There is therefore a considerable amount of noise in signal.

To determine the sign of an error signal two possible methods have been considered. In the first method the track pulse is integrated over a fixed time interval up to the marker pulse and then integrated again for the same time interval after the marker pulse. The difference of these two integrals would give the magnitude and direction of the error signal. This method has the advantage of not being unduly affected by noise. The second method is to differentiate the track pulse. The point where the differentiated signal is zero then defines the peak of the track pulse and the position of the marker pulse relative to this gives the error signal. The advantage of this method is that the peak is being defined, whereas the integral method defines the peak only if the track pulse is symmetrical about it. The differential method causes a serious reduction in the signal-to-noise ratio. Preliminary tests, however, showed that with care the differentiated track pulse could be made substantially free from noise and this method was used.

With any servo system it would be impossible to

keep the marker pulse continuously on the peak of the track pulse. A signal to print out co-ordinates, a track crossing signal, is required when the marker pulse is on the peak of the track pulse. With this signal a linear servo system is no longer necessary. All that is required is that the track be moved from side to side across the marker pulse and a track crossing signal be produced at the appropriate time. If a linear system is not to be used then the magnitude of the error signal is not needed; only its sign need be known. This simplifies the design considerably.

After taking all the usual precautions with the photomultiplier, noise was still a problem. This could only be reduced by bandwidth limitation which inevitably introduced some phase shift of the wanted signal, and therefore a time displacement of the peak of the track pulse. This in itself is not important unless it varies with the width of the track pulse, but if the displacement is fixed the marker pulse may be displaced by the same amount and therefore gives the same setting. With a triple RC circuit as bandwidth limiter this condition is satisfied up to a phase shift of about 15 degrees. Similar considerations apply to the choice of differentiating time constant. If this is too short then noise is troublesome; if it is too long time displacement depends on track width.

It has been found possible to design a system on this basis which will work on all but the poorest tracks, that is, tracks which could not be measured manually with any accuracy.

3. The Circuit

A block diagram of the circuit used is shown in fig. 1. The track pulse is fed through a bandwidth limiter, a triple RC circuit, the time constant of each section being 28 μsec. It is amplified and then differentiated. The differentiation time constant is 120 μsec. After further amplification the positive and negative halves of the differentiated track pulse are separated and squared. These squared pulses are then put into coincidence with the marker pulse. Coincidences between the negative squared pulse and the marker pulse indicate an error in one direction and the coincidence pulses are used to switch a bistable circuit. Coincidences between the positive squared pulse and the marker pulse indicate an error in the opposite direction and switch the bistable to its other stable position. One of the two 400 c.p.s. gates is always kept open by the bistable and the appropriate phase for correction is fed to the resolver.

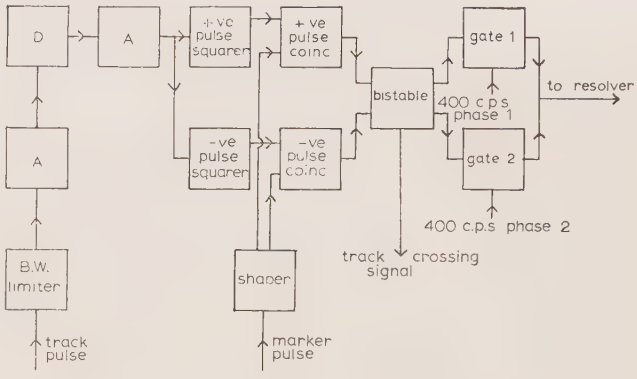

Fig. 1.

Track pulses are produced by the rotating glass block system at the rate of 80 per second. This is therefore the rate of sampling the error signal. The bistable remains in one of its stable states allowing the correct phase of A.C. to be fed to the resolver until the sign of the error signal changes. When this happens the bistable changes to the other stable state and opens the second gate. The correction signal is reversed and the stage moves across the track in the opposite direction until the sign of error signal changes again. A track crossing signal is produced by the bistable when its stable state is changed.

4. Operation of the Circuit

The speed of response is proportional to the amplitude of the signal fed to the servo-motors. If this is too small the device cannot follow a track at fast forward speeds along the track. If the amplitude is too large then large scale oscillations across the track take place. The setting, however, is not critical.

Tests were performed first of all with no movement along a track. The marker pulse was set manually on the peak of the track pulse and the co-ordinates of the point observed. Then the co-ordinates were observed with the circuit switched on and without a track crossing signal. The

coordinates printed out were never more than one digit different from the hand-set co-ordinates.

The track crossing signal is open to criticism since it occurs not when the marker pulse is on the peak of the track pulse but at the first error sampling after this. In order that the error introduced is never more than one digit the speed of movement of the measuring stage is limited. This speed, however, is within the stable range mentioned in the first paragraph of this section.

To test the device operationally events have been measured by manual setting and then using the automatic device. The results obtained from computation of the measurements were the same in each case.

The speed of measuring co-ordinates is approximately three times that with manual setting. The speed of measuring complete events is perhaps $1\frac{1}{2}$ times that with manual setting since operations other than measurements of track co-ordinates are involved.

No provision has yet been made for automatically maintaining the axis of rotation of the glass block in the scanning device parallel to the track, but a circuit is being designed for this purpose.

Acknowledgement

When this work was being carried out, one of us, M. Jobes, was in receipt of a maintenance grant from D.S.I.R.

NUCLEAR INSTRUMENTS AND METHODS 13 (1961) 127–130; NORTH-HOLLAND PUBLISHING CO

OPERATION OF A 9-INCH BUBBLE CHAMBER WITH DEUTERIUM

W. P. DODD, G. A. DORAN, J. B. KINSON, L. RIDDIFORD and B. TALLINI

Department of Physics, University of Birmingham

Received 12 May 1961

A 9-inch bubble chamber in a pulsed magnetic field has been successfully operated with deuterium. The closed circuit system for the use and storage of the deuterium is described. The operating conditions of the chamber are discussed, and compared with those of the same chamber when used with hydrogen.

1. Introduction

The purpose of this note is to report the operation with deuterium of the 9-inch bubble chamber in use with the Birmingham synchrotron. A description of the chamber has already been given[1,2]). The usefulness of deuterium is due to the fact that at high energies the neutron appears free to the bombarding particles[3]). The chamber has been exposed to a high energy neutron beam, and plate 1 is a photograph showing at the right a typical neutron-neutron interaction of type

$$n + n(+ p) \rightarrow n + p + \pi^-(+ p) .$$

The neutron enters from the left of the photograph, and the charged tracks are curved in the 15 kilogauss field. The track of noticeable curvature is the negative meson. The short track is due to the "spectator" proton, which takes little part in the reaction and has an energy of only eeveral MeV. At the left is a reaction of type

$$n + p(+ n) \rightarrow p + p + \pi^-(+ n).$$

The backward going track is the meson, and one of the proton tracks has a high bubble density.

2. Apparatus

Deuterium is expensive and difficult to obtain in large quantities, so the apparatus used forms an enclosed system enabling storage, use, and recovery of the gas with a minimum of loss. Fig. 1 is a line drawing of the system, and plate 2 a photograph of the storage vessel and other apparatus. This vessel, R1, has a volume of 100 cu.ft. and contains at low pressure the 170 standard cu.ft. of gas required to fill the chamber, plus sufficient ballast to ensure that the pressure in no part of the system is less than atmospheric under operating conditions. It also serves as a "dump" tank to which gas from the chamber can be rapidly transferred via the needle valve N or the gate valve V2 whilst warming the chamber to operating temperature, or should an emergency arise during operation. In the event of a chamber overpressure the spring-loaded safety valve S2 releases deuterium to the tank.

To transfer gas from the storage vessel to the smaller high pressure supply vessel R3 (volume 1 cu.ft.) necessary to fill and maintain the correct operating pressure on the chamber, a small totally enclosed piston type refrigerator compressor C1 (pressure 0–200 PSIG, motor 1.5 HP) is used. This is employed quite intermittently since the loss from the chamber is normally very small. Total enclosure avoids the need for seals on the driving shaft. Experiment has shown that any exchange of the deuterium with hydrogen in the lubricating oil is small; mass spectrometric analysis of gas samples exposed to hot oil for long periods of time, and taken from the tank before and after experimental runs, show the hydrogen content to be 0.5–1.0%. The compressor body will not stand high pressure,

[1]) D. C. Colley, J. B. Kinson and L. Riddiford, Nucl. Instr. and Meth. 4 (1959) 26.

[2]) G. A. Doran, J. G. Hill, J. B. Kinson and L. Riddiford, Intern. Conf. High-Energy Accel. and Instrum. CERN 1959.

[3]) A. P. Batson, B. B. Culwick, H. B. Klepp and L. Riddiford Proc. Roy. Soc. A 251 (1959) 233.

Plate 1. Typical n-n and n-p interactions.

so the regulating valve P1 maintains the input pressure at a value slightly in excess of atmospheric; further protection is provided by the overpressure switch S and the valve V1 which is manually operated as the pressure in R3 approaches the required value. The regulating valve P2 is set at the chamber operating pressure. Any oil is removed from the gas by the filter F and final cleaning is achieved by the De–Oxo unit D, the silica gel trap T1 and the charcoal trap T2, which is immersed in liquid nitrogen. The filter incorporates a mechanism for returning oil to the sump.

The seals between the chamber body and the armourplate glass windows are provided by double tin gaskets the space between which is evacuated. This is done by a further smaller totally enclosed compressor C2 (pressure 0–50 PSIG, motor $\frac{1}{8}$ HP), this time of the rotary vane type and capable of maintaining a pressure of about 1 mm of mercury in the pump-out space whilst returning the gas pumped to R1 through the exhaust line. The filling and exhaust lines are usually disconnected from the chamber between runs, so all are flushed with deuterium and evacuated twice before use. At the end of a run, the gas left in the chamber and lines is collected by sorption in the Vibrac steel cylinder C (volume 2 l) filled with activated charcoal, which is then also used to reduce the pressure in apparatus other than R1 to slightly above atmospheric. At present, in the event of a chamber window failure, the deuterium in it would be released to the atmosphere through B, rather than to R1. This is because the liquid hydrogen (H) and nitrogen reservoirs are not designed to withstand high pressure

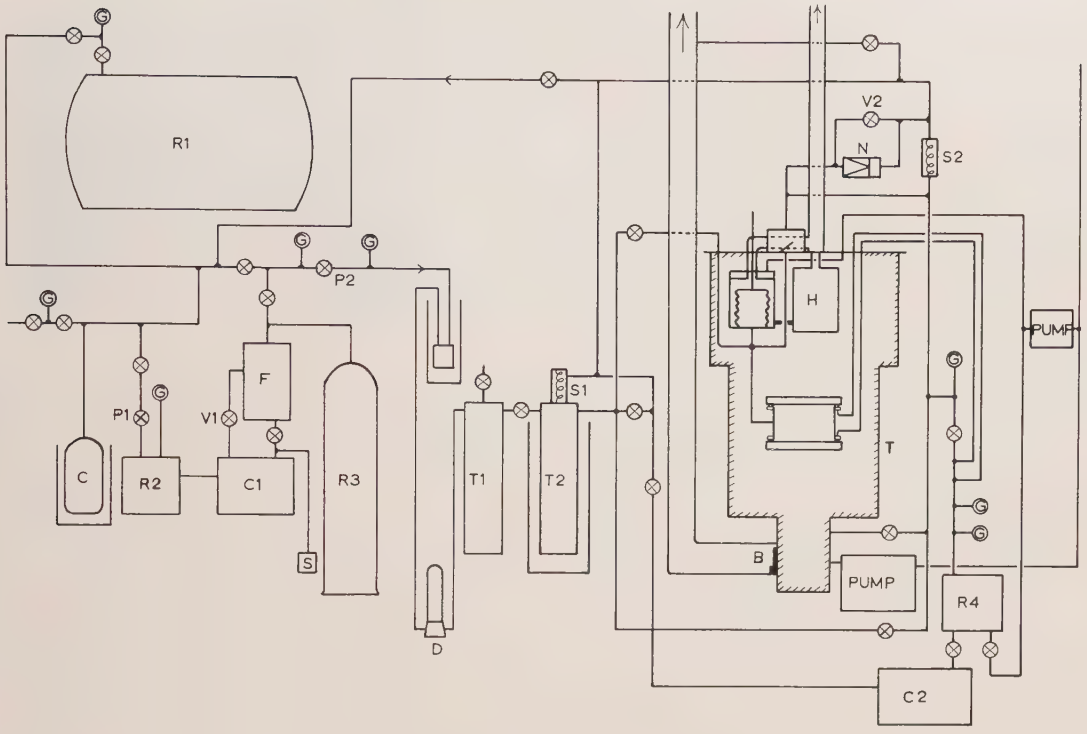

Fig. 1. Line drawing of the apparatus.

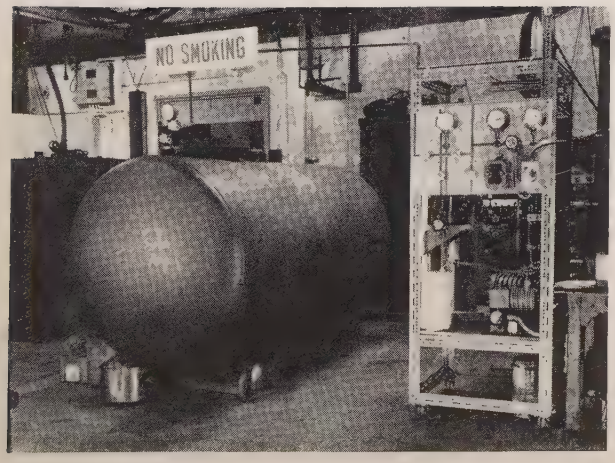

Plate 2. The deuterium system.

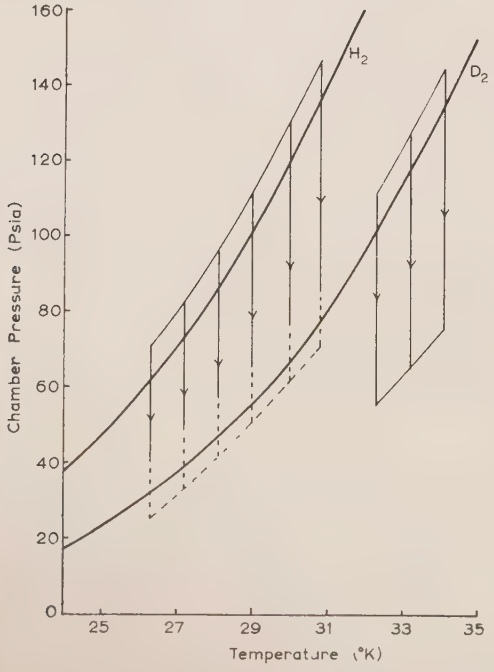

Fig. 2. Operating ranges for the 9-inch chamber.

and would probably collapse, thereby mixing their contents with the deuterium and also probably breaking the vacuum vessel T.

3. Operation

The boiling point of deuterium is 23.6° K whilst that of hydrogen is 20.4° K. To obtain a sufficient degree of superheat for track formation in deuterium it has therefore been necessary to operate at higher temperatures and pressures than for hydrogen. The higher pressure makes maintaining a good vacuum ($\approx 10^{-5}$ mm) more difficult; further, boiling at the walls and track distortions increase with temperature. We have found the minimal useful temperatures to be about 32.5° K (vapour pressure 103 PSIA) for deuterium and 27.3° K (73 PSIA) for hydrogen; a wide range of operating conditions is however possible, as indicated in fig. 2. The upper limit to pressure was set by the apparatus. The parameters used by other workers have been collected and plotted by Barford[4]). The 15-inch diameter Berkeley chamber is the largest one so far operated with deuterium[5]).

To ensure reliability with deuterium the operating temperature of the 9-inch chamber is chosen to be 33.9°(130 PSIA). The expansion ratio is 1.5%, the same as for hydrogen. At this temperature performance is excellent, as it is with hydrogen at lower temperatures (usually 27.4° K, 75 PSIA), and a run of 20000 pictures has been made. There is no noticeable background due to tritium contamination, often a source of trouble in diffusion cloud chambers. A typical pressure-time trace from the transducer (1), with the flash trigger superimposed, is shown in fig. 3. As with hydrogen, although the base pressure is apparently reached after about 10 ms, the chamber remains insensitive for a further ten; the subsequent rate of bubble growth is however quite rapid. The synchrotron provides bursts of particles of duration about 1 ms, the instants of occurrence of which may vary by $\pm$ 1 ms from pulse to pulse. The shortest flash delay interval used is therefore about 2 ms; this is adequate for hydrogen but for deuterium a delay of 3–4 ms is normally required to obtain good tracks of minimum bubble density. The total usage of liquid hydrogen is almost twice that for hydrogen[1]), since about 50 watts are required to maintain the chamber at the operating temperature (33.9° K). It is not possible to decrease this in a convenient way since the heat is transported by convection in the expansion tube between the chamber and the bellows[1]).

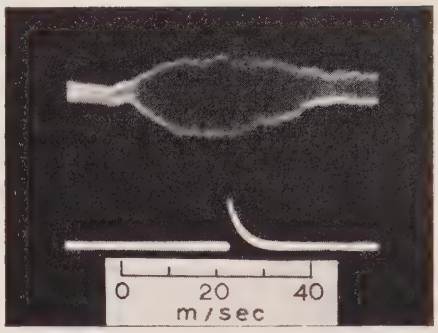

Fig. 3. Pressure trace and flash trigger.

Acknowledgements

Early work on the apparatus was done by Drs. D. C. Colley and J. G. Hill. Mr. M. Jobes, and Mr. C. W. Barrow, by whom the apparatus was largely assembled, have helped with the runs. We are grateful to Mr. G. H. Guest for reliable operation of the liquifier, and Mr. J. V. Houghton of A.E.R.E. Harwell for arranging to supply the deuterium.

[4]) N. C. Barford, Progress in Cryogenics (1960) p. 89.

[5]) R. D. Tripp, Intern. Conf. High Energy Physics, CERN 1958, p. 184.

NUCLEAR INSTRUMENTS AND METHODS 13 (1961) 131–140; NORTH-HOLLAND PUBLISHING CO.

ELECTRO-SPRAYING: A METHOD OF MAKING SAMPLES FOR β COUNTING ALLOWING ACCURATE CORRECTION FOR SELF-SCATTERING AND SELF-ABSORPTION

E. BRUNINX and G. RUDSTAM

CERN, Geneva

Received 18 May 1961

The different aspects of preparing thin, uniform samples by electro-spraying are described. The technique is used in the determination of a set of self-scattering and self-absorption factors for three different β emitters with low, medium and high energy. A general method is outlined for the determination of these factors under different conditions.

1. Introduction

The determination of the formation cross-section of a nuclide produced in a nuclear reaction involves in most cases the determination of the disintegration rate, via the β counting rate, of a suitable sample. This sample contains the radioactive isotope together with inactive carrier of the element of interest. The preparation of samples for β counting requires procedures such as: electrodeposition, precipitation, evaporation and distillation.

The conversion of β counting rates to disintegration rates involves the application of several correction factors[1–4]). Most of these factors depend only on the counter set-up and on the β energy. They can conveniently be put together into one factor; which is determined once and for all with a set of standardized samples of nuclides with different β energies. There is one correction factor, however, which varies from experiment to experiment, and this is the correction for self-scattering and self-absorption which depends strongly on the thickness and chemical composition of the sample and on the energy of the β particles[5]). A successful correction for this effect implies the preparation of thin and uniformly spread sources.

Electrodeposition gives smooth, uniform samples in a fairly easy and reproducible way. At low carrier concentrations some special precautions have to be taken in order to ensure quantitative deposition[6,7]). However, the method is limited to certain elements.

Distillation of some organic compounds has been proposed by Pate and Yaffe[8]). The equipment is somewhat complicated in that a vacuum system is necessary. It also has its limitations in the possibility of obtaining suitable organic compounds.

The precipitation technique is very versatile for carrier quantities above 1 mg. The self-scattering and self-absorption factor is, however, large and in many cases difficult to estimate because filtered and dried samples tend to become quite uneven.

In cases where the amount of carrier is small (< 1 mg) evaporation is a common method for source preparation. Samples prepared by this method often become very unevenly spread, however, with most of the material forming a ring. Addition of insulin[9]), colloidal silica[10]), or cupric ferrocyanide[11]) to the drop before evaporation improves the samples, but as is shown later neither of these methods is satisfactory. Besides the addition of some solid compound is required, which will of

[1]) B. P. Burtt, Nucleonics **5**, No. 2 (1949) 28.

[2]) L. R. Zumwalt, U.S. Atomic Energy Commission Unclassified Report AECU-567 (1950).

[3]) A. C. Pappas, American Report LNS-MIT-63, AECU-2806 (1953) Part IV; Inaugeral Dissertation, University of Oslo.

[4]) E. P. Steinberg, American Report ANL-5622 (1956).

[5]) W. E. Nervik and P. C. Stevenson, Nucleonics **10**, No. 3 (1952) 18.

[6]) R. W. Dodson, Miscellaneous Physical and Chemical Techniques of the Los Alamos Project Vol. 3, Edited by A. C. Graves and D. Froman (McGraw-Hill, New York, 1952).

[7]) L. J. Maletskos and J. W. Irvine, Nucleonics **14** (1956) 84.

[8]) B. D. Pate and L. Yaffe, Can. J. Chem. **34** (1956) 265.

[9]) L. M. Langer, Rev. Sci. Instr. **20** (1949) 216.

[10]) J. S. Merrit, J. Taylor and P. Campion, Can. J. Chem. **37** (1959) 1109.

[11]) G. Rudstam, Inaugural Dissertation, University of Uppsala (Uppsala, 1956).

course increase the self-scattering and self-absorption factor.

The need for finding a suitable way of preparing samples for β counting has led us to explore in detail the electro-spraying method originally proposed by Carswell and Milsted[12]). After different modifications and improvements the method was found very successful in making uniform samples of almost any element. A number of self-scattering and self-absorption measurements has shown that the correction for these effects can easily be carried out with an accuracy of better than 1%. As the method is also very rapid and simple to carry out, it can be recommended for the preparation of samples for β counting, β spectroscopy, etc.

2. Principle

The original apparatus, as proposed by Carswell and Milsted, consisted of a small glass tube drawn

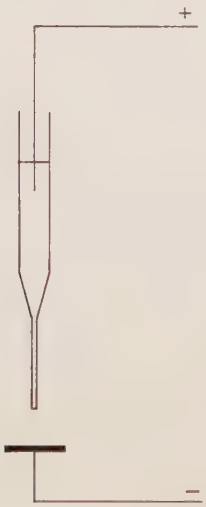

Fig. 1. Principle of electro-spraying.

at one end to a capillary. The material to be sprayed is dissolved in a small amount of organic liquid, and introduced into the tube (fig. 1). An electrode connected to the positive pole of the high-voltage supply is immersed into the liquid. A foil on to which the liquid is to be sprayed is connected to the negative pole. The distance between the tip of the capillary and the foil is about 10 mm. Upon applying a tension of about 5 000–10 000 V, DC, the liquid is forced out of the capillary and dispersed as extremely small droplets. Due to the fast evaporation of the organic phase, only the solid particles reach the collector foil. This is essential since otherwise a non-uniform deposit will be formed.

3. Experimental Set-Up

Since the capillary is the vital part of the whole set-up it was necessary to find some way of making reproducible capillaries. Drawing glass tubes to a capillary[12]) required a large amount of trial and selection until a good one was found.

In these experiments, capillary tubing of diameter varying from 0.1 to 0.5 mm, calibrated to within 0.01 mm, was used. Three different lengths

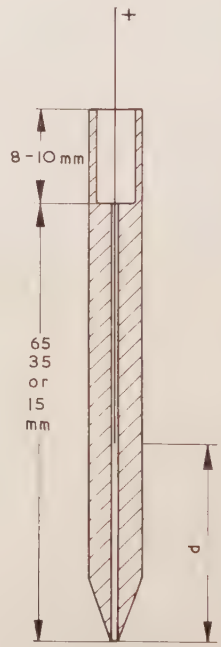

Fig. 2. Capillary used in the experiments.

were tested, namely 65 mm, 35 mm and 15 mm. The form and dimensions of the capillaries are shown in fig. 2. As collector foils, thin aluminium foils of 0.01 mm thickness were used. The foils were put on a small rotating metallic table ($\approx$ 10 cm diameter; 2–3 r.p.m.) and covered with a thin plexiglass disc into which a hole of about 10 mm diameter was drilled so as to obtain a spot of well-defined area. The rotating table ensured uniform distribution of the spray over the uncovered part

[12]) D. Carswell and J. Milsted, J. Nucl. En. 4 (1957) 51.

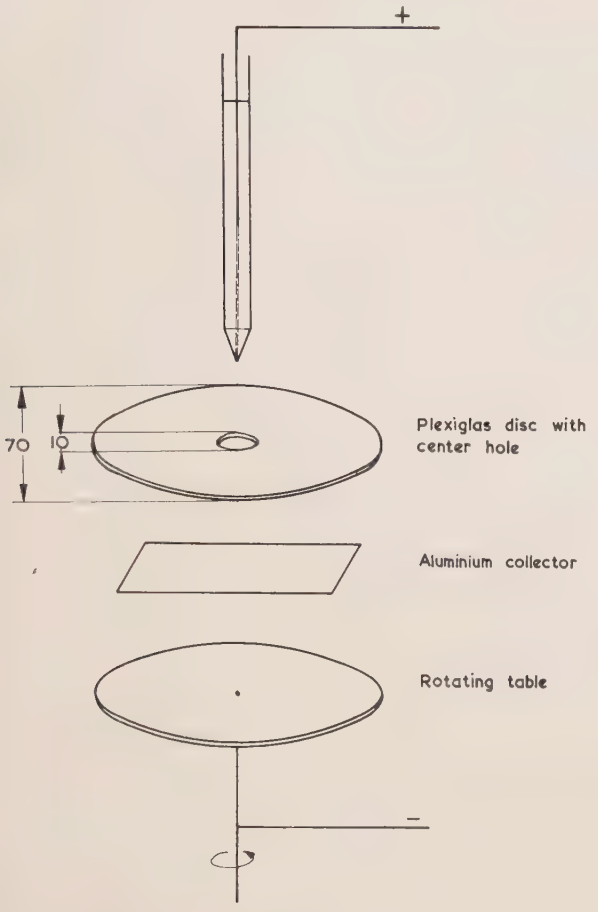

Fig. 3. Exploded view of the experimental arrangement.

of the aluminium foil. A wire of stainless steel or platinum was used as an electrode.

The high-voltage supply is continuously variable between 1 000–10 000 V, and a micro-amperemeter gives a rough indication of the current flowing through the cell. Usually a current of the order 0.1–0.5 μA was used.

The experimental arrangement is shown schematically in fig. 3, and the HV supply in fig. 4.

Three precautions should be taken:

i) wire and capillary should be completely degreased;

ii) no air bubbles should be left in the capillary, since they might cause small drops to fall on the collector plate;

iii) no undissolved material, such as dust or small particles, should be present.

4. Spraying Conditions

4.1. CHOICE OF CAPILLARY AND ELECTRODE

In order to see whether a certain combination of capillary and wire will work, a quick test is as follows. The capillary is filled with liquid and the wire inserted down to the tip of the capillary. If the liquid drops out, no satisfactory operation can be

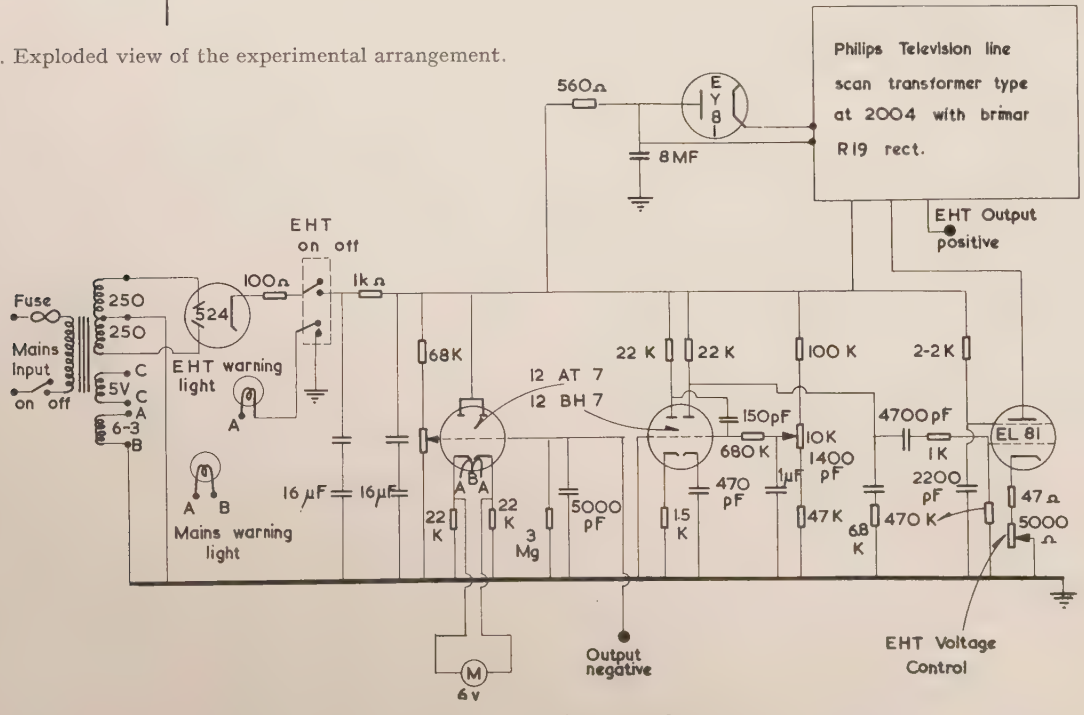

Fig. 4. High-voltage supply.

TABLE I

Capillary		Wire diameter (mm)	d*	t†	I**	Remarks
Diameter (mm)	Length (mm)					
			32	4.5	2.3	
0.5	65	0.43	17	6.8	1.7	
			8	9	1.5	
			8	4	3	
0.4	65	0.30	5	4	2.2	Difficult to spray
			43	3.5	2.5	Uniform sample
0.4	65	0.32	32	7	2	Uniform sample
			8	10.5	1.7	Uniform sample
			25	3	3	Difficult to spray
0.4	35	0.32	18	5	3	Uniform sample
			8	8	2.3	
			48	3.7	3	
0.3	65	0.22	43	5	2.5	
			32	7.5	1.8	
			7	16	1.8	
			32	4.5	2.8	Difficult to spray
0.3	65	0.20	24	5.5	2.5	
			7	8	2.4	
0.1	35	— ††	—	27	1	Uniform sample

* d = distance from tip of capillary to end of wire in mm (see fig. 2).

† t = time to empty capillary, expressed in minutes.

** I = intensity of current microampere.

†† = no wire is inserted into the capillary itself. Electrical contact is made by dipping the wire into the liquid in the small reservoir on the top of the capillary.

expected, and a larger wire or smaller capillary should be chosen. With this in mind, a few capillary-wire combinations giving good results were tested out more extensively.

As a test solution, potassium iodide (500 μg K/ml) in ethanol was chosen. The distance from the tip of the capillary to the collector plate was kept at 7 mm. In each case 50 μl of the alcoholic solution was sprayed. The results are given in table 1, and the following conclusions can be drawn.

a) Good and uniform spraying can be obtained with different types of capillaries, provided the wire has the right dimensions.

b) Increasing the length of the capillary increases the time necessary to spray a given volume of liquid.

c) For a given capillary, one can increase the distance d and decrease the total spraying time. An upper limit is set by the liquid dropping out of the capillary. The variation of spraying time is more or less a linear function of d.

4.2. INFLUENCE OF THE ORGANIC SOLVENT

In their experiment, Carswell and Milsted used acetone as solvent. We have found that several other liquids can be used equally well.

Important factors for good spraying are:

i) low surface tension (γ) to facilitate the formation of very small drops;

ii) low viscosity (η) in order to keep the flow rate reasonably fast;

iii) vapour pressure low enough to allow the solvent to be evaporated in flight.

These conditions are not sufficient for the choice of solvent, however. For example, hexane with $\gamma = 18.43$ and $\eta = 0.324$ does not spray, while

acetone with $\gamma = 23.70$ and $\eta = 0.316$ does. Probably the dielectric constant plays a role. In table 2 several solvents are listed together with their surface tension, viscosity, dielectric constant and boiling point. A + or — sign indicates that it was, or was not, possible to spray the liquid.

at the tip of the capillary, and the spraying starts (region I). At higher voltages the single drop disappears gradually and the rate of spraying increases with the voltage applied (region II). At still higher voltage the spraying becomes very irregular and frequent discharges occur (region III).

TABLE 2

Solvent		$\gamma(20°)$ (dynes/cm)	$\eta(20°)$ (centipoises)	$\varepsilon(20°)$	Boiling point
Acetone	(+)	23.70	0.32	21.4	57°
Ethyl ether	(+)	17.01	0.23	4.33	35°
Carbon disulphide	(—)	32.33	0.35	2.64	46°
Methanol	(+)	22.61	0.60	33.1	65°
Ethyl acetate	(+)	23.90	0.46	6.4	77°
n Butyl alcohol	(+)	24.6	2.95	7.8	118°
n Hexane	(—)	18.43	0.33	1.84	69°
Ethanol	(+)	22.75	1.20	25.7	79°
Ethanol: water					
= 100: 1	(+)	21.5	1.20	25.7	
= 75: 25	(+)	24.7	$\approx$ 2.15	$\approx$ 36	
= 50: 50	(—)	27.5	2.87	49.4	
Water	(—)	73.05	1.01	80.36	100°

In the case of carbon disulphide and hexane, the liquid did not leave the capillary at all.

The highest ratio of alcohol/water that could be sprayed was alcohol (70), water (30).

4.3. INFLUENCE OF HIGH VOLTAGE

The current flowing through the cell as a function of the high voltage is plotted in fig. 5. At low voltages no current flows and no liquid is expelled. As the tension is increased a conical drop is formed

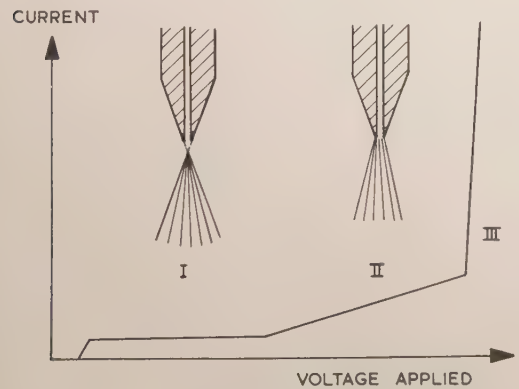

Fig. 5. Current and shape of the spray as a function of the applied voltage.

Region II is most suitable for spraying, but region I can also be used, especially with capillaries of small diameter.

Stainless steel, copper and platinum have been used as wire materials. Stainless steel usually works well, but if there is danger of deposition of the active material on the wire (i.e., spraying of the noble metals), platinum should be used.

4.4. EFFECTIVE YIELD

A few trials were made in order to get an idea of how much of the material sprayed is collected on the plate. The results are compared with the same quantity directly evaporated on an aluminium foil (table 3).

TABLE 3

Element and concentration	Directly evaporated	% Yield 1st spray	1st and 2nd spray †
Cs (carrier free)	100 %	30	38
Cs with carrier	100 %	58	67
Nb with carrier	100 %	58	68

† 50 μl of alcohol were put into the small top reservoir and sprayed onto the collector plate.

The major losses occur at the tip of the capillary, in the small top vessel, and by adsorption on the wire. A carrier-free solution shows a somewhat lower spraying yield than a solution containing carrier, probably due to adsorption. Part of the liquid is also lost on the plexiglass disc.

4.5. SPRAYING CONDITIONS FOR DIFFERENT ELEMENTS

Table 4 summarizes spraying conditions for different elements. Undoubtedly many other organic solutions are feasible. In most cases inorganic solutes have been tried but organic compounds of

TABLE 4

Element	Compound sprayed	Solvent	Remarks
Ag	$AgNO_3$	Ethanol, acetone, ethyl ether	
As	As_2S_3	Ethanol	As_2S_3 dissolved in NaOH (equiv. quant.). Evap. to dryness. Take up in ethanol.
Au	$AuBr_3$	Ethyl, ether, acetone	
Ba	$BaBr_2$	Methanol	Capill. 0.4 mm Wire 0.34 mm
Br	KBr	Ethanol	
	NH_4Br	Ethanol	
Ca	$CaCl_2$	Ethanol	
Cd	$Cd(NO_3)_2$	Ethanol	
Ce	$Ce(NO_3)_3$	Ethanol	
Co	$CoCl_2$	Ethanol	
Cs	CsI	Ethanol	
Cu	$CuCl_2$	Ethanol	
Fe	$FeCl_3$	Ethyl ether	
	oxinate	Ethanol	
Ga	$GaCl_3$	Ethanol	
	$Ga(OH)_3$	Ethanol	$Ga(OH)_3$ + equiv. NaOH Dry. Take up in ethanol.
Hg	$HgCl_2$	Ethanol	
I	KI	Ethanol	
In	$In(NO_3)_3$	Ethanol	
K	KI	Ethanol	
La	$LaBr_3$	Ethanol	
	$La(NO_3)_3$	Ethanol	
Mg	$MgCl_2$	Ethanol	
Mn	$MnCl_2$	Ethanol	
Mo	Chloride	Ethyl ether	
Na	NaOH	Ethanol	
Nb	$NbCl_5$	Ethanol	
Ni	$NiCl_2$	Ethanol	
Pb	$Pb(NO_3)_2$	Ethanol	
Pd	$PdCl_2$	Acetone	
Ru	$RuCl_3$	Ethanol	
Sb	$SbCl_5$	Ethyl ether	
Sc	$Sc(NO_3)_3$	Ethanol	
Se	H_2SeO_4	Ethanol	
Sn	$SnCl_2$	Ethanol	Black ppt.
Sr	$SrCl_2$	Ethanol + H_2O ($< 5\%$)	
Ti	oxinate	Ethanol	
U	$UO_2(C_2H_3O_2)_2$	Ethanol	
V	VCl_5	Ethanol	
Y	$Y(NO_3)_3$	Ethanol	Difficult to obtain good results
Zn	$Zn(C_2H_3O_2)_2$	Ethanol	

metals can also be used as is shown in the case of iron and titanium. Sometimes the compound sprayed decomposes (reduction of selenium). This is no drawback as long as the composition of the compound is known. This decomposition occurs on the foil after the spraying. The aluminium foils can be heated up to 600°C without any harm; this results in a firmly adhering precipitate. The quantity of metal sprayed ranges up to 500 μg which is a useful region for radiochemical and spectrophotometric analyses. The capillary and wire used had a diameter of 0.40 and 0.32 mm.

If hygroscopic compounds are sprayed, the samples should be kept in a dessicator in order to avoid increase of thickness by the uptake of water.

4.6. MICRO-STRUCTURE OF THE SPRAYED SAMPLES

In order to compare the structure of the sprayed samples with the evaporated ones, a few microphotographs have been taken. The results are shown in Plates 1 to 4. In all cases cesium iodide was used, the average thickness being 450 μg/cm^2.

Plate 1 shows the central part of a sprayed sample. Plate 2 gives the central part of an evaporated sample with cupric ferrocyanide. Plate 3 shows the border region of a sprayed sample, while Plate 4 shows the same region of a sample evaporated under an infrared lamp.

These plates show the quality and fine grain size of the sprayed samples. From the scale one can estimate the grain size to be of the order of 1 micron.

5. Self-Scattering and Self-Absorption Measurements

The self-scattering and self-absorption effect for small sample thicknesses has been investigated using samples prepared by the spraying method. This experiment was carried out in the following way. A carrier-free alcoholic solution of a suitable tracer nuclide was prepared. From this solution a series of samples were made by spraying on aluminium discs. The samples were counted both with β and γ counters, and the ratio β/γ was determined. This ratio was plotted versus the γ activity, and a curve was drawn through the experimental points. Its intercept for zero activity (or $(\beta/\gamma)_0$) represents the β/γ ratio for a weightless sample without self-scattering and self-absorption effects.

Another series of samples were sprayed from a solution containing the same tracer as above, but in addition, also a compound of a suitable chemical composition. One of the thicker samples was sprayed onto a thin weighed aluminium foil, and its weight was determined by means of a micro balance. The weight of the other samples was then deduced from the relative γ counting rates. The β/γ ratios of the samples were then measured. When divided by $(\beta/\gamma)_0$, determined as described above, they represent the self-scattering and self-absorption effect F_S for aluminium. Different backings might yield slightly different results.

As tracers the following nuclides were chosen:

Nb^{95} with β energy, 0.158 MeV;
Cs^{137} with average β energy 0.56 MeV; and
Ru^{106} in equilibrium with Rh^{106} with average β energy 3.3 MeV. (The 0.039 MeV β particles from Ru^{106} are absorbed by air and counter window.)

Compounds added were:

Methylene blue with $Z_{\text{eff}} = 8$ [Z_{eff} defined according to Pappas (ref.[3])]†;
zinc bromide with $Z_{\text{eff}} = 33.5$;
cesium iodide with $Z_{\text{eff}} = 54$.

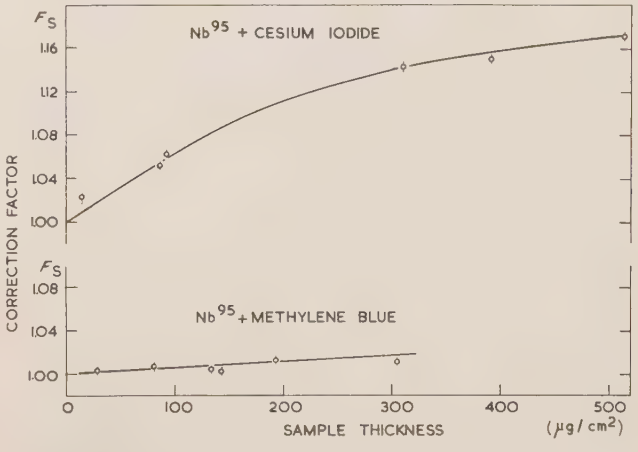

Fig. 6.
Self-scattering and self-absorption factor for 0.158 MeV β energy.

† For a compound $(Z_1A_1)n_1\ (Z_2A_2)n_2 \ldots (Z_mA_m)n_m$ the value Z_{eff} is given by

$$Z_{\text{eff}} = \frac{\sum_1^m A_i n_i Z_i}{\sum_1^m A_i n_i}.$$

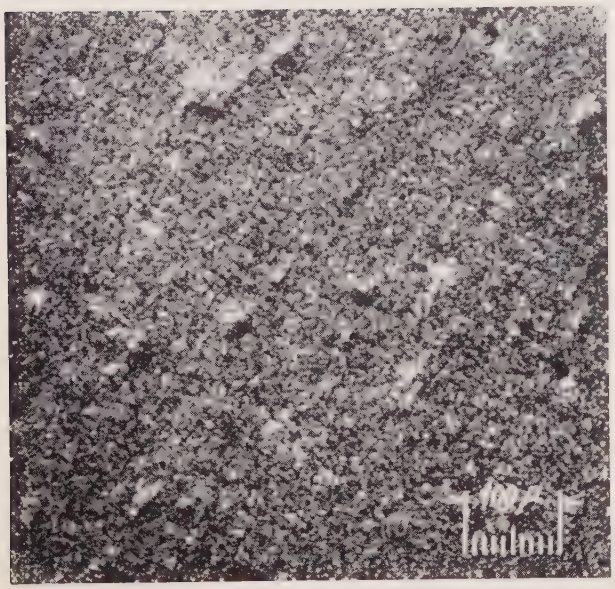

Plate 1.

Plate 2.

Plate 3.

Plate 4.

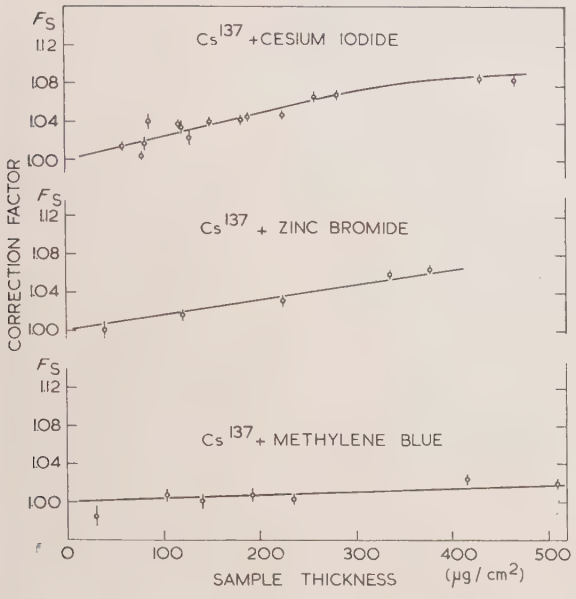

Fig. 8.
Self-scattering and self-absorption factor for 3.3 MeV β energy.

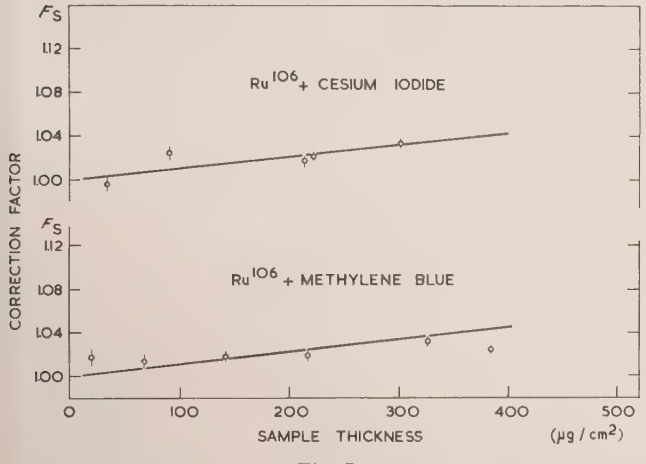

Fig. 7.
Self-scattering and self-absorption factor for 0.56 MeV β energy.

The resulting self-scattering and self-absorption curves are presented in figs. 6–8. These curves confirm that the effect is large even for thin samples (cf. ref.[4]).

In order to study different evaporation methods, samples were prepared by evaporating a Cs^{137} solution containing CsI and different additives (insulin, colloidal silica: "ludox", cupric ferrocyanide) to give thickness of about 400 $\mu g/cm^2$. The results are given in table 5.

Only the sample containing cupric ferrocyanide was uniformly spread; the other formed a ring. Thus the insulin and the ludox methods do not seem useful for sample thicknesses of a few hundred $\mu g/cm^2$. The cupric ferrocyanide method is quite good, but it is limited by the fact that the solution of this compound has to be ammoniacal. Consequently, the solution to be evaporated must not contain acids which could form ammonium salts.

6. Applications of the Electro-Spraying Method

The results of the self-scattering and self-absorption experiments show that the effect is serious even for thin samples. The correction may amount to 10–20%. As the effect depends on several parameters (β energy, sample thickness and composition), it is not advisable to determine a series of curves like those in figs. 6–8 and to interpolate between these curves. If an accuracy of $\pm$ 1% is aimed at, one should make instead a special determination of the self-scattering and self-absorption effect for each sample. This is easily done if the nuclide to be measured emits γ radiation as well as β particles in its decay. In such a case two or three samples are sprayed, with at least one sample very

Table 5
F_S measurements for evaporated Cs^{137} samples

Substance added		Average thickness of sample	F_S measured	F_S estimated from fig. 7	Difference
compound	amount				
—	—	460 $\mu g/cm^2$	1.156	1.094	+ 6.2 %
insulin	25 $\mu g/cm^2$	350 $\mu g/cm^2$	1.167	1.077	+ 9.0 %
ludox	5 $\mu g/cm^2$	350 $\mu g/cm^2$	1.155	1.077	+ 7.8 %
$Cu_2Fe(CN)_6$	40 $\mu g/cm^2$	450 $\mu g/cm^2$	1.112	1.093	+ 1.9 %

thin. The β/γ ratio of the samples is plotted versus the γ activity, and a line is drawn through the point. Its intercept for zero activity is taken to be the β/γ ratio for a weightless sample ($= (\beta/\gamma)_0$), and the F_S value for any of the samples is obtained by dividing the corresponding β/γ ratio by $(\beta/\gamma)_0$. The correctness of this approach, at least for samples below 500 $\mu g/cm^2$, is evident from figs. 6–8. By this method the self-scattering and self-absorption effect can easily be corrected for with an accuracy of $\pm$ 1%.

Only in cases with no γ radiation the self-scattering and self-absorption effect should be estimated from general curves, using tracers with similar β energy and chemical composition. Even then it might be better to perform a direct determination by adding to the solution some isotopic tracer which emits γ rays but no β particles, for instance, a nuclide decaying to 100% by electron capture.

A drawback with the electro-spraying method is that the amount of solution caught on the catcher foil is not well known (cf. 4.4). For the determination of chemical yields it is often necessary to know the exact amount of carrier in a sample. This drawback is not serious, however. One can either evaporate a measured amount of the solution (sometimes it is better to do this after converting it into an aqueous solution) and compare the γ activities of this sample and the sprayed ones. Another way is to spray the sample on backing of pure aluminium. The sample is then dissolved after the activity measurements, and the element of interest is analysed quantitatively, e.g., by spectro-photometric methods.

Acknowledgements

We wish to thank Mr. P. Laubereau† for help and assistance during the earlier phases of this work. His experiments were very useful in eliminating and avoiding many errors and pitfalls.

We thank Professor A. C. Pappas for kindly reading and discussing the paper. We also thank Dr. G. Vanderhaeghe for advice and help in preparing the microphotographs.

The assistance of Mr. L. King and Mr. C. Nichols in constructing respectively the high-voltage supply and capillaries is gratefully acknowledged.

† CERN Summer student 1960.

NUCLEAR INSTRUMENTS AND METHODS 13 (1961) 141–146; NORTH-HOLLAND PUBLISHING CO.

COINCIDENCE SUMMING AND NON-LINEARITY STUDIES WITH A TWO-CRYSTAL SCINTILLATION GAMMA SPECTROMETER†

J. KANTELE†† and R. W. FINK

Department of Chemistry, University of Arkansas, Fayetteville

Received 20 June 1961

A two-crystal 4π NaI(Tl) scintillation gamma spectrometer has been used for studying coincidence summing effects with special reference to the energy calibration in the region 0.5 to 4 MeV of coincidence sum peaks of cascade gammas. From observed deviations of the sum peak positions from those expected according to calibrations with single photopeaks, the nonlinear response of NaI(Tl) has been investigated. The pulse height per unit energy as a function of energy appears to approach a constant value with increasing energy up to 4 MeV. A slight shift in single photopeak position when collimation is introduced was observed at most gamma energies with a single crystal spectrometer. Possible reasons for the apparent non-linearity are discussed.

1. Introduction

In gamma spectroscopy it is frequently necessary to use detectors of high efficiency such as well-crystals[1]) which suffer the disadvantages of poor resolution and high cost. One of the advantages of high efficiency detectors is the summing of coincident events which often gives important information on cascade relationships of gammas. It is known that sum peaks lie at a somewhat higher energy than a single photopeak of the same energy[2]), probably due to a non-linear response[3]) of the NaI(Tl) crystal as discussed by Peelle and Love[2]), who suggested the use of the summing phenomenon for studying the non-linearity itself.

In order to work in the energy region up to several MeV, we have constructed a spectrometer similar to the two-crystal 4π arrangement used by Ketelle, Thomas, and Brosi[4]) to study the very low energy region (< 200 keV). From a study of the pulse height/unit energy vs. energy curve[3]) and other experiments reported below, some information could be gathered on the complex photon interactions in NaI(Tl), many details of which are still quite poorly understood.

2. The Two Crystal 4π Scintillation Spectrometer

The scintillation heads used were two "integral-line" Harshaw 3 × 3-inch NaI(Tl) crystals both coupled with DuMont 6363 photomultiplier tubes. The heads were placed face-to-face as close as possible with the thin radioactive source between them. Output gains of the photomultipliers were equalized by adjustment of the high voltage to find the largest peak-to-valley ratio for the Co^{60} gamma spectrum. The output pulses were fed to one preamplifier followed by a linear, non-overloading DD2 amplifier and a RIDL 200-channel transistorized analyzer. By connecting both photomultiplier outputs directly to one preamplifier, considerable attenuation in the primary output pulses from the photomultipliers occurs, but this does not change the shape of the pulses or of the spectrum.

Owing to the finite thickness of the gamma-ray sources, aluminum crystal windows and MgO reflectors, the actual distance between the crystal

[1]) See for example, D. C. Lu and M. L. Wiedenbeck, Phys. Rev. **94** (1954) 501;
P. R. Bell, in Beta- and Gamma-ray Spectroscopy, K. Siegbahn, Ed. (North-Holland Publishing Co., Amsterdam, 1955).

[2]) R. W. Peelle and T. A. Love, Rev. Sci. Instr. **31** (1960) 205.

[3]) D. Engelkemeir, Rev. Sci. Instr. **27** (1956) 589.

[4]) B. H. Ketelle, H. Thomas and A. R. Brosi, Phys. Rev. **103** (1956) 190.

† Supported in part by the U.S. Atomic Energy Commission.

†† Postdoctoral visitor, 1960/62, on leave from Institute of Physics, University of Helsinki, Finland.

surfaces was about 8 mm, and hence the total solid angle subtended by the crystals to the source about 90% of 4π steradians.

According to efficiency curves given by Heath[5]), the total absolute efficiency of the 4π detector exceeds 30% for gammas of all energies at least up to 10 MeV. Peak-to-total ratio is noticeably larger for the 4π detector than for a single crystal, particularly at energies of a few MeV, where the probability of escape of annihilation quanta is appreciably smaller. Owing to the high efficiency, the probability of detecting two or more simultaneous events also is large, and hence coincident gamma rays give rise to rather intense sum peaks. For example, the intensity of the sum peak at 4.1 MeV from the Na^{24} cascade gammas at 1.37 and 2.75 MeV is about 30% of that of the latter gamma peak. In comparison with a single 3×3-inch NaI(Tl) crystal, the sum peak efficiency of the two-crystal system for Na^{24} is about six times as large. The summing performance of the two-crystal spectrometer is demonstrated by fig. 1 in the case of Na^{22} decay. As can be seen from the figure, each $(\beta^+)(\gamma)$ coincidence gives rise to two sum peaks which are often useful in placing positron transitions in the decay scheme.

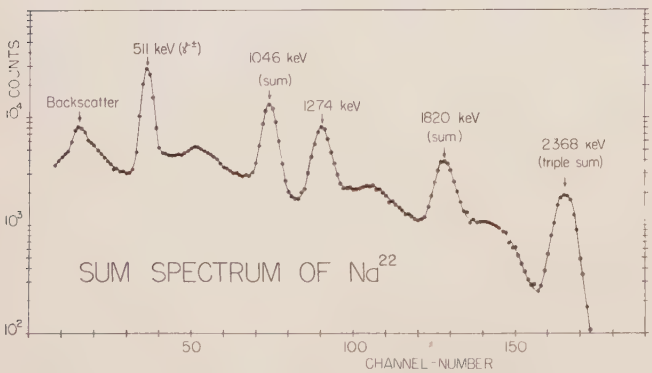

Fig. 1. Sum spectrum of Na^{22} taken with 4π spectrometer consisting of two 3×3-inch NaI(Tl) crystals situated face-to-face, the distance between windows being 1 mm. The peaks due to annihilation radiation and to the 1274 keV gamma are accompanied by three sum peaks at 1046, 1820, and 2368 keV (based on single photopeak calibration) which are 24, 35, and 72 keV larger, respectively, than the values obtained by computing the energy sums corresponding to summing of two annihilation quanta, one annihilation plus the nuclear gamma, and the gamma plus two annihilation quanta. Note that the $(\beta^+)(\gamma)$ coincidence in Na^{22} decay gives rise to two sum peaks which are often useful in placing positron transitions in the decay scheme.

In the present equipment the resolution for the Cs^{137} photopeak of one of the scintillation heads is 8.0% and that of the other, 8.4%, the resolution of the 4π combination being 8.25%. For the 4.1 MeV sum peak of Na^{24} the resolution of the 4π system is 3.8% which is only a little more than half that of a typical large well-crystal of same efficiency. The linearity of the present spectrometer appears to be excellent from about 0.2 MeV up to the highest energy studied, 6.14 MeV. The behavior in low-energy regions was not studied in detail, because of the uncertain response of the lowest channels of the pulse height analyzer. The stability in all of these experiments was excellent, the typical fluctuation in photopeak positions being less than 0.2% during several hours.

3. Measurements and Results

In all energy determinations, the total crystal counting rate was kept well below 10^5 cpm, where the well-known counting rate shift due to the photomultipliers appears. The actual position of both single and sum peaks was defined as that of the vertical line dividing the peak area into two equal parts. This line can be considered to represent best the average pulse height under the total absorption peak. In all cases, when intercomparisons between accurately determined gamma-ray energy standards were performed, the results agreed with those reported from precision beta spectrometry[6]) to within a few keV.

To justify the use of sum peaks for non-linearity studies, the positions of sum peaks from Y^{88}, Co^{60}, and Na^{24} were determined with both the 4π detector and with a single crystal, the other one being removed without any changes in connections, applied voltage, or amplification. Since the results in both cases agreed precisely, one concludes that the sum peak position is independent of whether the two events are detected one in each crystal and added electronically or both summed in one crystal which is interpreted to mean that two simultaneous light producing and collecting events in one crystal,

[5]) R. L. Heath, Scintillation Spectrometry Gamma-ray Spectrum Catalogue, U.S. Atomic Energy Commission Report IDO-16408, (1957) (unpublished).

[6]) Nuclear Data Sheets, National Research Council, Washington 25, D.C.

TABLE 1
Data on sum peaks of some well-known coincident gamma-rays[6]).

Source	Coincident gammas (keV)	Apparent sum peak energy E_a(keV)	Calculated sum peak energy E_c(keV)	$\Delta = E_a - E_c$(keV)	$\Delta\, \frac{1}{4}E_c^2$ (10^{-5} keV^{-1})	Calibration standards
Na^{22}	511, 511	1046 ± 5	1022	24 ± 5	9.2	Y^{88}, Zn^{65}
In^{114}	556, 722	1308 ± 5	1278	30 ± 5	7.3	Na^{22}
Na^{22}	511, 1274	1820 ± 6	1785	35 ± 6	4.4	Y^{88}
Sc^{48}	986, 1040	2054 ± 8	2026	28 ± 8	2.7	Y^{88}, Na^{24}
Na^{22}	511, 511, 1274	2368 ± 10	2296	72 ± 10		Y^{88}, Na^{24}
Co^{60}	1172.8, 1332.5	2549 ± 8	2505	44 ± 8	2.8	Na^{24}
Y^{88}	899, 1840	2767 ± 8	2739	28 ± 8	1.5	Na^{24}
Na^{24}	1368.7, 2754.7	4170 ± 20	4123	47 ± 20	1.1	Na^{24}, N^{16}

† A 4π gamma scintillation detector consisting of two 3 × 3-inch NaI(Tl) crystals was used for the energy determinations. Calibrations were performed by using single photopeak energies only. The quantity $\Delta/\frac{1}{4}E_c^2$ in the table is related to the slope of the pulse height per unit energy vs. energy curve.

occur and are added together fully independently, without interference. Therefore, comparisons of the sum peak and single peak positions provide a method to obtain *differences* between pulse height per unit energy at two gamma ray energies.

A number of coincidence sums of gamma-rays of well-known[6]) energies were studied, using precisely determined single photopeak energies as standard. Results of these measurements are summarized in table 1. In all cases the measurements have been repeated many times, and the limits of error given are conservative, being at least twice the standard deviations. The result on the Y^{88} sum peak agrees well with that of Peelle and Love[2]). One triple coincidence sum, namely that of Na^{22}, is included in the table to show how surprisingly large the deviations from such sum peaks can become.

If the difference between the apparent and calculated energies of sum peaks of two coincident gammas is denoted by $\Delta = E_a - E_c$, the quantity $\Delta/\frac{1}{2}E_c$ gives approximately the difference in pulse height per unit energy between energies $\frac{1}{2}E_c$ and E_c. If the gamma energies are equal, the difference given will be exact. When the difference is divided by the energy interval $\frac{1}{2}E_c$, the quantity $\Delta/\frac{1}{4}E_c^2$ is obtained which is a qualitative measure of the slope of the pulse height per unit energy vs. energy curve between the energy values $\frac{1}{2}E_c$ and E_c. As one can see from column 6 of table 1, this decreases towards higher energies.

It must be emphasized that these results are true only for 3 × 3-inch NaI(Tl) crystals. According to Engelkemeir[3]), however, non-linear behavior does not seem to depend much on crystal dimensions.

In the present work, an experiment supporting this was performed, where the Co^{60} sum peak position was determined with a $1\frac{1}{2}$ × 1-inch cylindrical crystal and with a $2\frac{1}{4}$ × $2\frac{1}{2}$-inch NaI(Tl) well-crystal. In each case the deviation from the single photopeak calibration line was the same within experimental limits as in the case of the 3 × 3-inch crystal.

To study the effects of light collection and escape of secondary radiations (e.g., bremsstrahlung and multiply-scattered Compton quanta) from the crystal, positions of photopeaks from 0.5-inch dia. collimated gamma beams from RaD, Hg^{203}, Cs^{137}, and Na^{24} sources were compared with those from uncollimated sources at the closest distance. In each case the sources were placed on the crystal axis, with weaker sources being used for the latter case to give equal counting rates at both geometries, always well below the point where counting rate shifts occur. After a careful series of measurements, it was established that at energies 47 and 72 keV, no measurable changes (statistically less than 0.3 keV) were observed, but both at 279 and 661 keV, the peak from the collimated source was definitely about 2 keV higher than that from the uncollimated one. At 1369 and 2755 keV from Na^{24}, results averaged from a long series of comparisons show that the above difference also is about 2 keV

in the same direction, but owing to the smaller percentage difference at higher energies, this result is somewhat inconclusive. To summarize, these experiments seem to suggest that below, say, 100 keV, the effect of axial collimation on the photopeak position is negligible, but at energies from approximately 300 keV up to 3 MeV, the difference, which is *essentially constant*, can be observed with extremely stable equipment. This difference may well depend on crystal size or other factors, but it is believed that the present value of about 2 keV is the correct order of magnitude.

In order to study the effect on photopeak position of the light collection process only, a radial collimation experiment was performed which minimized all the other effects. Each 3 × 3-inch NaI(Tl) crystal was exposed to 0.5-inch dia. collimated gamma beams at two positions perpendicular to the crystal axis; namely, position A, 1 cm from the photomultiplier end of the crystal, and position B, 1 cm from the front face of the crystal. In this arrangement any variation between A and B in photopeak position must be due only to a difference in the light collection.

For energies from 279 to 1840 keV, shifts in photopeak position between A and B were in opposite directions for the two crystals, but the magnitude of the shifts never exceeded 1.5%. This is attributed to a slight difference in quality between the two scintillation detectors. For energies of 47 and 70 keV, however, the photopeaks were about 5% higher in both crystals in position B (close to the front surface) than in position A. This is interpreted to be due to the fact that an appreciable fraction of the light produced at position A experiences total reflections at the exit window which causes the light collection efficiency to be slightly lower for position A than for position B.

4. Discussion

This 4π arrangement provides an additional method of obtaining coincidence information by means of sum peaks which avoids the problems associated with gating channels, matching of delay times, and which in the case of low intensity sources often is the only way to get coincidence results. In many laboratories crystals of large dimensions are used in studies of light nuclei with an electrostatic accelerator. In thin-target studies of small cross-section reactions, the large crystals could be connected in the above manner to give otherwise unobtainable coincidence information. A further development of this technique is in progress[7]) involving the use of the two crystals in a special coincidence setup which sums scintillation events occurring in both crystals simultaneously and rejects all other events.

One of the most important advantages of the two-crystal spectrometer over well-crystals at corresponding efficiency is the good resolution which is essentially the same as that of a single crystal, if the gain adjustment has been performed carefully. This type of spectrometer has also a reasonable efficiency for summing three coincident gamma-rays, as has been demonstrated in fig. 1.

The existence of some other summing effects should also be pointed out, particularly summing of K X-rays and gammas. This can cause additional peaks to appear in the spectrum in the usual sum peak manner, or it can shift the position of a single gamma photopeak, especially at higher energies, when the resolution is not sufficient to allow formation of a separate sum peak. In the present work the K X-ray summing shifted the 2614 keV gamma-ray peak of ThC″ to a higher energy by about 10 keV. (It is known[6]) that more than 10 per cent of these gamma-rays are emitted simultaneously with X-rays produced by internal conversion of cascade gamma-rays of lower energy.) X-ray and gamma summing also may occur to some extent at very close source-to-crystal distances in ordinary spectroscopy, owing to the large efficiency and high peak to-total ratio for K X-rays. This effect can often be observed in electron-capture decay of high Z nuclides.

Summing of gammas and bremsstrahlung quanta produced by beta particles may sometimes be observed. For example, in this work a sample of Co^{60} was wrapped with a 1 mm thick lead plate and the sum peak position compared to that without lead wrapping. A slight shift of a few keV towards higher energy was observed, but owing to the limited resolution this result must be considered inconclusive.

[7]) J. Kantele and R. W. Fink, to be published.

The results summarized in table 1 do not show any definite trend in the "non-linearity excess", Δ. Although the number of cases in table 1 is too small to give detailed conclusions on parameters affecting the function Δ, one can say that at least up to about 2 MeV the non-linearity excess seems to be essentially constant, being of the order of 30 keV. It is interesting to note that the "non-proportionality excess" reported by Peelle and Love[2]) also is 30 keV.

Since the general way of treating the relative intensities of sum spectra has been studied by other authors[8]), it will not be discussed here.

The observed behavior of the slope of the pulse height per unit energy vs. energy curve is in good qualitative agreement with Engelkemeir's work[3]). It is also in accordance with the overall linearity of pulse height vs. energy function above 100–200 keV reported by him and other authors[9]).

The negative intercept $(-e)$ of the extrapolated linear portion of the pulse height vs. energy curve with the energy axis suggests that the pulse height (V) depends on photon energy (E) at higher energies according to the equation $V = k(E + e)$, where k is a constant. From this, one expects that the pulse height per unit energy, $V/E = k(1 + e/E)$ should approach a constant value with increasing E. The present measurements are in good qualitative agreement with this in the energy range studied, suggesting an approximate value of 30 keV for e.

The axial collimation experiments give some information on light collection and secondary energy escape processes in the crystals. As no axial collimation effects on the peak position were observed below 100 keV, where most of the absorption occurs very close to the crystal surface, the light collection process from all parts of the front surface of the crystal seems to be approximately the same. Escape of secondary energy from the crystal apparently has only a small influence on the average pulse height under the total absorption peak. This can be immediately deduced from the magnitude of the collimation effect ($\approx$ 2 keV) at all energies, and from the fact that the observed non-linearity is essentially independent of crystal dimensions. Probably low energy Compton quanta from multiple scattering processes leave the crystal to a greater extent when there is no axial collimation, and this gives rise to escape which broadens the low energy side of the photopeak causing it to appear to lie at a slightly lower energy.

Since the escape of secondary energy has very little effect on the photopeak position, it is apparent that the main reason for the observed non-linearity lies in the process by which electron energy is converted into light and/or possibly in statistical processes in the photomultiplier. One might expect the influence of two phenomena: (1) Energy dependence of the energy-to-light conversion efficiency, (2) Energy dependence of the spectral distribution of the fluorescent light, so that some shift occurs with respect to the spectral response of the photomultiplier.

There is one further effect occurring in photon interaction with NaI(Tl) that also has some influence on the response, namely Čerenkov radiation of secondary electrons. It is known[10]) that above a certain energy [about 110 keV in NaI(Tl)] electrons produce Čerenkov light when moving in transparent media. The spectrum of this light overlaps in part the spectral response of the photocathode. Hence, certainly some fraction of the total amount of light produced in a scintillation of sufficient energy is due to the Čerenkov effect. In the current literature there does not seem to be available data to make a conclusive estimate of the correct order of magnitude of the intensity of this radiation. However, general knowledge[10]) of the Čerenkov effect suggests that in a medium of rather high refractive index [that of NaI(Tl) is 1.77 for the Na D-line] a few tenths percent of the total energy of electrons up to several MeV is dissipated by means of Čerenkov radiation. As the total conversion efficiency of NaI(Tl) is[11]) about 0.084, the Čerenkov light output may amount to several percent of the total amount of light produced. In other words, the conversion efficiency is very high for the small fraction of the initial energy dissipated in the form

[8]) See, e.g., R. K. Gupta and S. Jha, Nucl. Phys. **1** (1956) 2; P. Shapiro and R. W. Higgs, Rev. Sci. Instr. **28** (1957) 939.

[9]) See, e.g., W. Bernstein, Nucleonics **14**, No. 4 (1956) 46.

[10]) J. V. Jelley, Čerenkov Radiation and its Applications (Pergamon Press, New York, 1958).

[11]) J. B. Birks, Scintillation Counters (McGraw-Hill Book Co., New York, 1953) p. 52.

of Čerenkov radiation. If this is really so, then this effect actually *increases* noticeably the observed pulse height at secondary electron energies above the Čerenkov threshold, and so counteracts the otherwise more non-linear trend of NaI(Tl) response. Perhaps the Čerenkov effect is in part responsible for the behavior of the pulse height per unit energy vs. energy function, which approaches a constant value at higher energies, where the Čerenkov light output increases.

Acknowledgement

We are indebted to Mr. R. Rogers for technical assistance in constructing the spectrometer. We wish to thank Dr. D. G. Gardner for help in obtaining the facilities necessary for this work.

NUCLEAR INSTRUMENTS AND METHODS 13 (1961) 147–152; NORTH-HOLLAND PUBLISHING CO.

HYDROGEN AND CARBON TARGET PREPARATION FOR A POSITIVE ION ACCELERATOR†

R. D. McCORMICK and J. D. McCORMACK

Hanford Laboratories Operation, General Electric Company, Richland, Washington, U.S.A.

Received 24 May 1961

A detailed description is given of the techniques used to make hydrogen and carbon targets for the Hanford 2 MeV positive ion accelerator. The hydrogen targets were made by adsorbing deuterium or tritium onto either titanium or zirconium. These metals were mounted on their platinum and tantalum backing disks by evaporation or by sintering. Targets ranged in thickness from 200 to 15000 μg per square centimeter with atomic ratios of 1 to 1. Carbon targets were made by mounting carbon on platinum backing disks by evaporation, painting, or cracking. Targets ranged in thickness from 100 to 5000 μg per square centimeter.

1. Introduction

At Hanford, a program of nuclear research using a 2 MeV Van de Graaff accelerator required the preparation of a variety of targets. In order to supply this specific need, detailed target preparation techniques had to be developed. It is the object of this paper to present these techniques in sufficient detail that they may be easily used by others.

2. Apparatus Used

The apparatus used consisted of three main components: a glass vacuum system, a vacuum evaporator, and an induction heater. The glass vacuum System McLeod used a liquid nitrogen trapped mercury diffusion pump, two gauges which gave a pressure range of 1×10^{-5} to 5 mm of Hg, a quartz furnace tube, and a Toepler pump.

The vacuum evaporator consisted of an eighteen-inch bell jar and a liquid nitrogen trapped mercury diffusion pump. It was equipped with an AC glow discharge electrode, a cold cathode discharge vacuum gauge, and a variable voltage high current power supply.

The induction heater, rated at 1 kW output, had a water cooled work coil made from $\frac{1}{8}$-inch copper tubing which was shaped into a two turn flat spiral.

The target holder, which is shown in fig. 1, was made from a sheet of 0.032-inch thick copper bent into a hexagon with a $\frac{3}{4}$-inch diameter hole in each of five faces to receive the backing disks. A small piece of copper sheet with a $\frac{3}{8}$-inch diameter hole in it was bolted to the inside surface over each $\frac{3}{4}$-inch hole so that the holes were concentric. This served to mask the disk from the filament and restrict the deposition to the desired size. The backing disks were held into the recesses with steel paper clips.

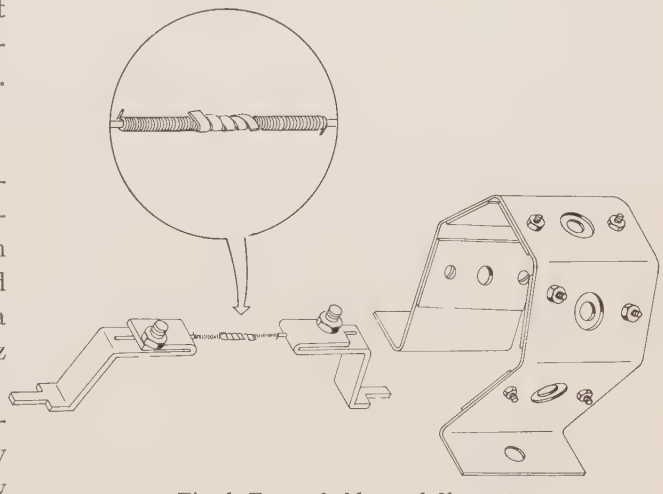

Fig. 1. Target holder and filament.

All the targets were on $\frac{3}{4}$-inch diameter disks with a target diameter of $\frac{3}{8}$-inch or $\frac{1}{2}$-inch. The thickness of the backing disks was 0.005 inch for tungsten, 0.010 inch for platinum, and 0.015 inch for tantalum.

† General Electric Company, Richland, Washington. Work performed under Contract No. AT(45-1)-1350 for the U.S. Atomic Energy Commission.

3. Gas Filled Targets[1–5])

3.1. PREPARATION OF BACKING DISKS AND FILAMENT

Platinum disks were prepared for targets with a great deal of care. The smoother side of the disk was finished by number "0" emery polishing paper to remove all blemishes, while the other side was marked for identification. Next the disks were cleaned in trichlorethylene and then in ethyl alcohol. The disks were now outgassed in vacuo at about 1000°C in the quartz furnace tube for ten minutes. After being cooled and removed from the furnace they were weighed and again cleaned in alcohol.

Initially, in the development of the procedures, temperatures were measured with a Leeds and Northrup optical pyrometer. Later it was found that adequate temperature control could be maintained by observing the color of the heated disk.

Tantalum disks were marked for identification, finished with the number "0" emery polishing paper, and cleaned in alcohol. Trichlorethylene was not used because it appeared to react with the tantalum. The disks were outgassed at 1000°C for a few seconds and then for five minutes at a dull red heat. If more than dull red heat was used for very long the tantalum evaporated on the inside of the vacuum furnace. After outgassing there was sometimes a discoloration on the disks which was removed by light polishing with fine emery paper. This discoloration was probably caused by exposing the disks to air while they were still hot. The disks were weighed and recleaned in alcohol. Just before evaporation, the disks were ion bombarded in an high voltage AC glow discharge by placing the target holder over the ungrounded electrode. The bombardment was conducted for ten minutes.

The filament consisted of a four-inch piece of 0.060-inch tungsten wire cleaned with emery paper and wrapped helically over a length of two inches with about 12 inches of 0.007-inch tungsten wire[6]). This serves to promote spreading of the melted zirconium or titanium on the filament. The filament was held between two copper electrodes, which were flexible enough to allow for some expansion. Sheet titanium 0.010-inch thick was cleaned with emery paper until the metal was bright, cut into thin strips weighing between 75 and 150 mg, and wrapped tightly around the filament in a helix. After the filament had been used once, care had to be taken in wrapping the titanium on the filament because the tungsten had become very brittle.

3.2. EVAPORATION OF ADSORBING METAL

The loaded filament was mounted on the evaporator, and the target holder containing the platinum disks (fig. 1) was placed over the filament after the ion bombardment of the targets. The bell jar was evacuated to 3×10^{-5} mm of Hg as measured by the cold cathode discharge tube. The titanium on the filament was raised to 1000°C by passing a current of 100 A through the filament. The outgassing was continued until the pressure dropped to 1×10^{-5} mm of Hg. The filament current was then increased slowly until the titanium melted, (about 140 A). As the titanium melted, the pressure rose sharply, then dropped to about 1×10^{-6} mm of Hg. The filament current was left at 140 A while the evaporation proceeded for three to four minutes or until the bell jar pressure raised to 1×10^{-5} mm of Hg. After evaporation was complete, the disks were allowed to cool 15 min. before the bell jar was opened. Occasionally it would be found that some or all of the disks had peeled, which may have been caused by contaminated disks or improperly outgassed evaporating metal. It has been found that highly polished disks tend to peel more readily.

In order to get semi-thick targets, the evaporation process was repeated up to four times. After the first evaporation, the filament was held at 140 A for only 30 sec at a time and allowed to "cool" a minute in between the 30-sec periods. This was repeated until a total evaporation time of three to four minutes was achieved for each loading of the filament. This was done because it seemed to reduce

[1]) W. J. Arrol, E. J. Wilson and C. Evans, AERE (Harwell) Report IR-1135 (1953).

[2]) E. R. Graves *et al.*, Rev. Sci. Instr. **20** (1949) 579.

[3]) A. B. Lillie and J. P. Conner, Rev. Sci. Instr. **22** (1951) 210.

[4]) B. J. Massey, Fifth National Symposium on Vacuum Technology Transactions, 1958 (Pergamon Press, New York, 1959) p. 72.

[5]) R. S. Rochlin, Rev. Sci. Instr. **23** (1952) 100.

[6]) J. G. S. Biram AERE (Harwell) Report EL-952 (1952).

the number of disks that peeled. Targets up to 2000 $\mu g/cm^2$ were made in a series of four evaporations. The amount of metal deposited depends, of course, on the amount of titanium on the filament, the length of time the filament is held at the proper temperature, and the filament to target distance. These parameters could be varied depending on the desired target thickness. In practice, however, the filament to target distance was fixed at 4.8 cm by the holder, and the time was usually ample to evaporate all of the load on the filament. Loading the filament too heavily with titanium caused the filaments to burn out because the titanium alloyed with the tungsten and lowered the melting point of the filament. After the targets were removed from the bell jar they were weighed and the thickness of the deposited metal was calculated.

The evaporation of zirconium was exactly the same as for titanium. No multiple evaporation of zirconium have been made. Titanium and zirconium evaporated equally well on platinum and tantalum.

3.3. SINTERING OF ADSORBING METAL

For the preparation of thicker deuterium or tritium targets a method other than evaporation was employed. An outgassed, weighed platinum backing disk was coated with the desired thickness (1000 to 15 000 $\mu g/cm^2$ for this work) of titanium hydride powder, 99 per cent less than 325 mesh†. Uniform coatings were achieved by allowing the titanium hydride to settle from a suspension in ethyl acetate. The settling chamber supported the backing disk on a pedestal, thereby keeping the disk free of any contact around the edge which improved the uniformity of coating. After the titanium hydride had settled, the ethyl acetate was slowly drained off and the disk left undisturbed to dry.

After the coating was dry it was dressed to the desired size using a fine sable brush. The excess titanium hydride was gently blown away, the coating was then measured and weighed to check the thickness. Care was required in handling the disk to avoid cracking or loosening the coating.

The disk was then heated in the quartz furnace to a temperature of 1200° C in a vacuum of less than 5×10^{-5} mm of Hg for five minutes to decompose the hydride and sinter the resultant titanium powder to an adherent hard coating.

Similar targets have also been made using tungsten backing and presumably other metals that do not form low melting point alloys with titanium could be used. The sintering time must be long enough to obtain coherence of the deposit and to permit some alloying with the backing, but excessive sintering time will give a deposit too brittle to absorb the stress produced upon gas adsorption and may lead to cracking and flaking.

† Metal Hydrides Inc., Beverly, Massachusetts.

3.4. LOADING THE ADSORBING METAL

Both titanium and zirconium evaporated targets were loaded with deuterium gas, and the techniques were the same for either metal. The target was placed in the furnace tube and the glass system was evacuated to a pressure of approximately 5×10^{-5} mm of Hg. Deuterium was let into the system to a pressure of 1 to 1.5 mm of Hg as measured on the McLeod gauge. The target was slowly brought up to the temperature at which adsorption started (300–400° C) by moving the furnace tube into the induction heater RF field. As the target began to adsorb gas, the system pressure decreased which caused the target temperature to increase. It was sometimes necessary, therefore, as the adsorption proceeded, to move the furnace slightly away from the RF field.

The length of time that a target adsorbed gas depended upon the thickness of the titanium film. For a 200 $\mu g/cm^2$ target, the adsorption was completed in a matter of a few seconds. In fact care had to be taken on these thin targets because slight overheating would ruin the gas adsorbing properties of the evaporated film, probably because of the alloying of titanium and the platinum or tantalum. On the other hand a target 2000 $\mu g/cm^2$ was held at the adsorbing temperature as long as 20 min.

Another method used to load targets was to heat them to a very dull red and cool them slowly in a gas atmosphere. This method worked best on evaporated targets in the 500 to 1000 $\mu g/cm^2$ range. Below 500 $\mu g/cm^2$ there was a chance the target would take no gas, and above 1000 $\mu g/cm^2$ it was sometimes necessary to repeat several times to get

enough gas adsorbed. This method allowed more alloying between the backing material and the evaporated film.

Sintered targets were loaded by heating to a dull red temperature and cooling slowly in a gas atmosphere. These targets were quite thick but they were also quite rough. That is, compared to an evaporated target the macroscopic surface of the sintered target is very rough and the sintered targets adsorb gas quickly for their thickness. It has been noted that evaporated targets with a flaw or slight break in the film will load rapidly compared to an equally thick film that is in good condition.

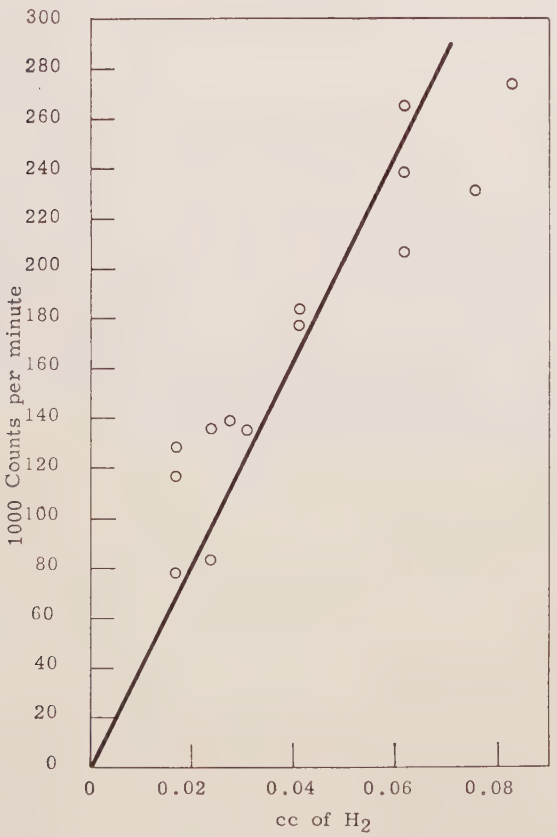

Fig. 2.
Tritium-titanium target counting rates versus tritium content.

In the loading of titanium targets with tritium, a tritiated uranium bed was used as the gas source. The technique of loading targets with tritium was identical with that for loading them with deuterium. More time was needed, however, because the uranium bed had to be heated to release gas and cooled to adsorb the gas left in the system after the target was loaded. Usually the uranium bed would be allowed to adsorb gas until the pressure dropped to 0.025 mm of Hg. In case the bed failed to adsorb the excess gas, a Toepler pump and a storage flask were available. The amount of gas adsorbed by the target was calculated from knowing the change in the gas pressure and the system volume. The ratio of gas atoms adsorbed to titanium or zirconium metal atoms was calculated for each target. For deuterium the ratio ran as high as 1.3 to 1, while for tritium the highest was about 1 to 1. In the sintered targets a special effort was made to keep the ratio below 1 to 1 so that the adsorber metal would not become brittle and flaky.

The bremsstrahlung from the tritium targets were counted using a NaI(Tl) crystal and a multiplier phototube. This was done as a check on the gas loading measurements made knowing the system volume and pressure change, and as a possible means to determine target condition after use. See fig. 2 for a comparison of the counting rate and the gas loading.

4. Carbon Targets

Carbon targets were made in three different ways: evaporation, cracking, and painting. In each case backing disks were prepared the same as for the hydrogen targets.

For the evaporation of carbon[7]), the filament assembly in the bell jar was replaced by a device which held two spectroscopic grade carbon electrodes†, one of which was moveable from the outside through a seal in the base plate. After the bell jar pressure had dropped to about 3×10^{-5} mm of Hg, the $\frac{1}{4}$-inch diameter carbon electrodes were outgassed by passing 50–60 A AC through them while they were touching. When the pressure dropped to 1×10^{-5} mm of Hg, an arc was drawn between the electrodes which lasted for 2 to 4 sec. After a cooling period of about a minute another arc was drawn. This was repeated until the desired amount of carbon had been deposited. For every 2 to 4 sec of arcing, 50 to 75 $\mu g/cm^2$ were deposited on the disks. Targets from 140 to 1300 $\mu g/cm^2$ were made this way.

† National Carbon Company, New York, N.Y. grade AGKSP.

[7]) D. E. Bradley, Brit. J. Appl. Phys. 5 (1954) 65.

Another method of making carbon targets was by cracking methyl iodide on the platinum backing[8]). A small quantity of methyl iodide was frozen in the vacuum system (using liquid nitrogen) and a platinum disk was put in the furnace tube. The system was then evacuated using only the mechanical pump. The methyl iodide was melted, and disk was heated to a dull red (500°C) whence carbon deposited on the disk. A methyl iodide pressure of 30 cm of Hg was used. It took several hours of cracking to get a target with a thickness of 107 $\mu g/cm^2$. The carbon coating seemed uniform and was hard and smooth, but the disks were coated on both sides. The residual iodine from cracking badly contaminated the glass system and the pumps.

A few targets were also prepared by painting a backing disk with colloidal carbon in alcohol†. The film was dried in air and baked at 1200°C in the vacuum furnace for ten minutes to evaporate any volatile impurities. This method produced useable targets but was not pursued because of uncertainties in carbon purity and thickness.

5. Target Durability

Targets of evaporated titanium or zirconium are unaffected by ordinary handling. In several cases the gas was released from part of from all of the target because of failure of the target cooling mechanism which allowed extreme temperatures to exist during bombardment by the beam.

Targets made by TiH settling techniques have proven very durable with ordinary handling.

Evaporated carbon targets have been ruined by careless handling and from excessive heat. Although the carbon surface is hard and scratch resistant, it is brittle. Accidental bending of the soft platinum backing material has caused the breaking of some of the carbon films. Excessive heat from ion bombardment has caused failures giving the targets a "blistered" appearance.

The painted carbon targets had low abrasion resistance and became somewhat pitted in time, but otherwise were reasonably durable.

6. Conclusions

The successful manufacture of targets is to some extent an art, and rigorous adherence to a procedure, once developed, is necessary to insure useable targets. Two primary modes of failure are peeling of the target material from the backing, and in the case of hydrogen targets, failure of the evaporated metal to adsorb the gas. Some observations pertinent to these modes are offered.

It was difficult to pinpoint the causes of peeling of the evaporated metal. The peeling took place in the evaporation process as well as in the gas loading process. Four suspected causes of peeling in the evaporator were excessively polished backing disks, unclean or greasy disks, insufficient outgassing of the metal to be evaporated, and excessive heating of the disks during evaporation. When the backing disks were finished slightly rough and cleaned very well, peeling definitely decreased. Inadequate outgassing of the evaporating metal was suspected as another cause of peeling. Keeping the temperature of the disks down while evaporating was accomplished by evaporating in 30-sec intervals, and this reduced the peeling in the evaporator. It was noticed, however, that the peeling in the loading process was subsequently increased if this method were used for the initial evaporation, so short interval evaporation was discontinued except when depositing additional layers for semithick targets.

Peeling in the gas loading process is believed to be initiated by surface flaws in the evaporated metal films or in some cases by a high gas loading ratio. It has been noted that evaporated films with surface flaws adsorb gas much more rapidly than those with perfect surfaces, and in many cases the result is peeling around the flaw or over the whole surface. This may really be a combination of poor adherence and over loading with gas. High gas loading ratios (gas to metal) say of over 1 to 1 make the evaporated metal brittle and flaky.

Failure of the evaporated film to adsorb the target gas can be attributed to two causes: (1) excessive alloying of the film and the backing disk, (2) contamination of the film during evaporation or filling. The alloying (or diffusion) difficulty can be reduced when filling the thinner films by heating the targets only enough (300–400°C) to promote

[8]) H. G. Holmgren *et al.*, Rev. Sci. Instr. **25** (1954) 1026.
† Acheson Colloids Co., Port Huron, Michigan.

the adsorption. The loading method, in which the target is heated to a dull red and cooled, may lead to lower loading ratios in the thin targets and in some cases complete lack of adsorption. As the target thickness increases the alloying becomes less important.

Contamination of the film during evaporation can be reduced by outgassing the evaporating metal, the backing disks, target holder, or any other parts in the vacuum system that are heated. Failure to maintain good vacuum during evaporation will lead to the reaction of the adsorbing metal with the residual air in the system. The subsequent oxides and nitrides formed and deposited on the disk are quite stable and not easily reduced, consequently the adsorbing properties of the film will be decreased.

In the filling, a similar process occurs except it is restricted to the surface. Upon the heating of the target the residual oxygen and nitrogen can react with the surface of the adsorbing metal creating a layer which may hinder the adsorption of the hydrogen.

With the carbon targets there were failures of the evaporated carbon films by bending the backing disks and by heat. The intense ion beam caused some targets to have a "blistered" appearance. The adherence of the evaporated films was not completely satisfactory, however, additional work on the technique seems justified because the method is quick, easy and controllable over a wide range of thickness. A harder backing material would stop breakage from bending.

Using a degreasing agent such as trichlorethylene seems somewhat risky since we found some which was contaminated with oil. Only reagent grade chemicals should be used and great care to avoid contamination should be taken.

NUCLEAR INSTRUMENTS AND METHODS **13** (1961) 153–160; NORTH-HOLLAND PUBLISHING CO.

A FAST PULSE-SHAPE DISCRIMINATOR WITH APPLICATIONS AS A SPECTROMETER AND SENSITIVE MONITOR FOR 1–30 MeV NEUTRONS

L. J. DE VRIES and F. UDO

Institute for Nuclear Physics Research, Amsterdam, Netherlands

Received 20 May 1961

The construction and operation is described of a neutron-gamma discrimination circuit. The discrimination is based on the differences in the shapes of light pulses initiated by protons and electrons in an organic crystal. The circuit separates these pulses above a proton energy of 0.5 MeV. The response to a gamma-source can be calculated as a pile-up effect with a time constant of about 0.1 μsec. The circuit is independent of normal temperature fluctuations and the multiplier voltage can be varied by 20 per cent. The circuit has been applied as a fast neutron spectrometer. The efficiency is 1.3×10^{-4} counts /neutron and the resolution 10 per cent at 14 MeV neutron energy.

A neutron monitor is designed, based on this circuit. This instrument can measure neutron fluxes down to 10 per cent of the maximum permissable dose and it can present information about the neutron spectra.

1. Introduction

The measurement of neutron spectra with organic scintillation crystals in the presence of a gamma-ray background is not possible on account of the high efficiency of the scintillator for gamma-quanta and of the nonlinear light yield of these materials for protons. In order to discriminate between the recoil protons and the gamma-induced electrons one can make use either of the difference between the specific ionisation densities, or of the difference between the ranges, or of the different pulse-shapes of these particles. The first two methods can only be applied in special cases and never give discrimination over a wide range of energies.

Pulse-shape discrimination is possible because in some scintillation materials the ratio of the intensities of the slow and the fast components of the scintillation light initiated by a proton is different from the intensity ratio of the same components of the light pulse initiated by an electron. In fact, Brooks[1]) proposed this discrimination principle.

We describe the scintillation decay as the sum of two exponentials. This is a simplification, not true in general for an organic scintillator, but in our case, where the circuit selects two components to some extent, this approximation will prove to give a good description. We assume the front edge of the scintillation pulse to be a step rise at $t = 0$. The current in the multiplier is then given by:

$$I(t) = I_0 \left[\exp\left(-t/T_1\right) + a \exp\left(-t/T_2\right)\right] . \qquad (1)$$

This equation and consequently the following calculation is different from the starting equation and the treatment of Brooks[2]).

According to Owen[3]) is for both particles in stilbene $T_1 \simeq 6$ nsec and $T_2 \simeq 370$ nsec. The constant a makes the differences between protons and electrons: $a_p \simeq 0.09$ and $a_e \simeq 0.05$.

Brooks obtains two voltage pulses from the photomultiplier: the first from a dynode connected to a low resistance R_1, the second from a dynode connected to a high resistance R_2. A stray capacitance C is present across each resistor. To simplify the results of the calculation the time constants of these RC circuits are chosen to be $R_1C \simeq T_1$ and $R_2C \simeq 2T_2$.

The fast pulse can be expressed by the equation:

$$V_{\text{fast}} \simeq \frac{I_0}{C} \left[t \exp\left(-t/T_1\right) + aT_1 \left\{ \exp\left(-t/T_2\right) - \exp\left(-t/T_1\right) \right\} \right] . \qquad (2)$$

This voltage reaches its maximum at a time $(t_{\text{fast}})_{\max} \simeq T_1$ and hence the maximum amplitude

[1]) F. D. Brooks, Brit. Patent Spec. 823263 (1957).
[2]) F. D. Brooks, Nucl. Instr. and Meth. 4 (1959) 151.
[3]) R. B. Owen, I.R.E. Trans. on Nucl. Sc. NS5 (1958) 198.

of the voltage pulse developed across R_1 is:

$$(V_{\text{fast}})_{\max} \simeq I_0 T_1 (Ce)^{-1} . \tag{3}$$

This maximum height is proportional to I_0 and therefore almost proportional to the intensity of the fast light component.

The slow pulse is given by:

$$V_{\text{slow}} \simeq \frac{I_0}{C} [T_1 \{ \exp(-t/2T_2) - \exp(-t/T_1) \} + 2aT_2 \{ \exp(-t/2T_2) - \exp(-t/T_2) \}] . \tag{4}$$

This pulse reaches its maximum at:

$$(t_{\text{slow}})_{\max} \simeq 2T_2 \ln 2 \simeq 0.5\ \mu\text{sec} .$$

The maximum amplitude is:

$$(V_{\text{slow}})_{\max} \simeq \frac{I_0}{2C} (T_1 + aT_2) . \tag{5}$$

This pulse V_{sm} mainly contains information on the slow component, because $T_2/T_1 \cong 60$, $a_{\text{p}} \simeq 0.09$ and $a_{\text{e}} \simeq 0.05$.

When equation (3) is multiplied by a factor $K = (T_1 + a_{\text{e}}T_2)e/(2T_1)$, and subtracted from (5), the difference is:

$$\Delta_{\text{e}} = V_{\text{sm}} - KV_{\text{fm}} = 0 .$$

for electrons and

$$\Delta_{\text{p}} = V_{\text{sm}} - KV_{\text{fm}} = \frac{I_0}{2C} (a_{\text{p}} - a_{\text{e}}) T_2$$

for protons.

For $K_1 > K$, Δ_{e} can also be made negative. In that case Δ_{p} decreases by the same amount.

The shapes and the times of the maxima of the pulses (3) and (5) are different. To subtract these pulses by an electronic circuit they must possess similar shapes. This can be done by reshaping the fast pulse with the help of a crystal diode stretcher. However, since a diode is a nonlinear device we have to stretch both pulses to about 10 μsec in order to compensate for any nonlinear behaviour. We may then subtract the stretched and equalized pulses to give the indication pulse Δ.

Our objections against this circuit, of which some are already enumerated by Brooks, are:

1) The information from the slow pulse is used only up to its peak. The contribution of the slow component relative to the fast component in this pulse increases with time (eq. (4)). This contribution is nearly zero at $t = T_1$, it is $(aT_2)/T_1$ at the time of the peak of the slow pulse and it is almost twice this value at $t = 1$ μsec.
2) The requirements given above are such that the pulses have to be longer then desired for minimizing the interference of electron pulses which may cause a false indication. This effect is proportional to the stretching time.
3) The nonlinear effects of the diodes may be made to cancel one another to some extent by selecting a pair with similar characteristics. Furthermore Brooks compensates remaining diode nonlinearity by admitting space charge saturation in the multiplier. The latter effect strongly depends on dynode voltage.

2. Operation of the Circuit

In our circuit most objections can be eliminated. Fig. 1 shows a disc of stilbene crystal (1 cm thick by 3.75 cm in diameter), which is attached to a Dumont 6292 photomultiplier. The slow and the fast pulse for the discrimination circuit are taken off the last two dynodes A and B. The anode is connected to a fast coïncidence circuit for application of the instrument as a spectrometer.

The RC times given in the introduction determine the dynode resistances. The fast pulse will now be stretched in a linear way by the network composed of the inductor L and capacitor C_1. The voltage across C_1 is a damped oscillation with a frequency of about 10 Mc/s. The ringing circuit can be adjusted in order to get an envelope of the signal, for protons and for electrons, which is equal to the pulse shape given by equation (4) with $a = a_{\text{p}}$.

After the adding of the slow pulse A to the damped oscillation in the adding circuit (UP in fig. 1), we obtain an oscillation which will be positive for a proton pulse and an oscillation of which the minima will be negative for an electron pulse (fig. 2 and fig. 3 where $a = 0.8a_{\text{p}}$). Fig. 4 shows a cathode ray oscilloscope (CRO) picture of proton and electron pulses selected by a single channel pulse height analyser (PHA) to give equal peak height amplitudes. In agreement with theory the minima of both pulses show an extremum at about 0.5 μsec. From the two oscillations we deduce $a_{\text{p}}/a_{\text{e}}$

by measuring the ratio of the amplitudes and their amplitude shift. This is done for $t = 0.8 - 1.4$ μsec. The results are $a_p = (1.9 \pm 0.1)\, a_e + 0.01$, assuming values for T_1 and T_2 which are given in the introduction. Owen derived the intensity ratio

The sum pulse is fed into a simple diode detector (diode 0A73 or 0A85 in series with capacitor C_2). At the negative peaks of the exciting voltage in the case of an electron pulse, the capacitor charges up to almost the peak of the applied voltage. It is not

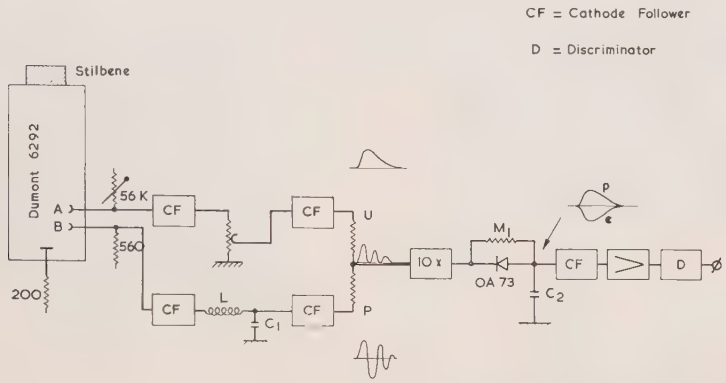

Fig. 1. Block layout of the discrimination circuit, showing wave forms at various points in the circuit.

a_p/a_e from the analysis of the slow pulse shapes obtained by photographing these pulses on a fast oscilloscope[3]). He found in good agreement an intensity ratio $a_p/a_e = 1.8$ for stilbene.

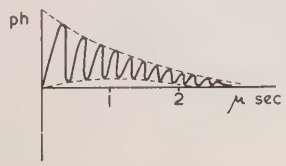

Fig. 2. Idealized proton pulse after the adding circuit.

Fig. 3. Idealized electron pulse after the adding circuit.

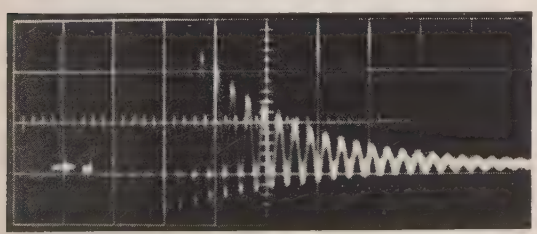

Fig. 4. Oscillograph pictures of proton and electron pulses immediately before the diode stretcher. The CRO is triggered by a single channel pulse height analyzer which passes pulses from about 6 MeV protons and 2 MeV electrons. Sweep speed 0.4 μsec/cm. Vertical sensivity 0.25 V/cm. The horizontal axis is indicated by an arrow.

essential that the forward resistance is constant. Since the back resistance of a real diode is not infinite, the positive proton pulse will give a small positive output signal. Fig. 5 shows the pulse on C_2

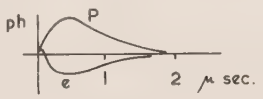

Fig. 5. Idealized proton and electron pulse on C_2, smoothed by a low-pass filter.

smoothed by a low-pass circuit ($RC = 0.1$ μsec), which is not indicated in fig. 1. This filter prevents the 10 Mc/s ripple voltage developed across C_2 from reaching the discriminator D and it also suppresses the small positive beginning of an electron pulse sufficiently. This small positive peak is caused by the first uncompensated oscillation. Two difficulties remain:

Firstly, the temperature dependence of the back resistance of the crystal diode is too high to get a good stability against temperature fluctuations. By means of a 100 kΩ resistor across the diode the influence of a temperature variation between 14 and 22°C turns out to be negligible. Secondly, for very small electron pulses the forward current of the diode is too small to cancel the current through this 100 kΩ resistor. A small positive pulse remains which reaches its largest amplitude for about

0.5 MeV gammas. These pulses can be eliminated by the discriminator D in fig. 1, which accepts positive pulses above a certain level only.

Fig. 6 shows the output pulse of the detector, exposing the stilbene crystal to the radiation of a

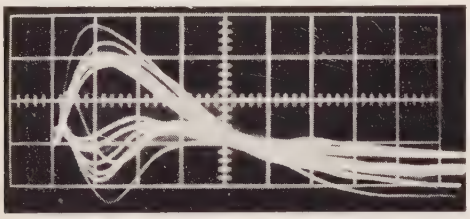

Fig. 6. Oscillograph picture of proton and electron pulses after diode and amplifier, in the case described in fig. 4. Sweep speed 1 μsec/cm. One of the pulses shows pile-up of a proton and electron pulse.

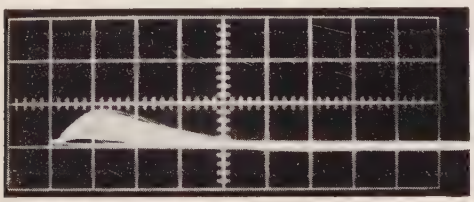

Fig. 7. Oscillograph picture of all gamma-pulses from a ^{88}Y source after diode and amplifier; sweep speed 1 μsec/cm.

PoBe neutron source. The CRO (a Tectronix 545) is triggered by the pulses from about 6 MeV protons and 2 MeV electrons. Fig. 7 illustrates the indicated maximum in the electron indication pulses.

Fig. 8, 9 and 10 demonstrate the merits of the circuit and make the discriminating qualities comparable with those of Brooks and Owen. These pictures are obtained with a "twinckle box" described by Brooks[2]) and Owen[3,4]). In this arrangement spots appear on the CRO screen. The horizontal position of a spot is proportional to the peak amplitude of the scintillation pulse A. The vertical position is proportional to the peak amplitude of the indication pulse on capacitor C_2. These spots lie along two distinct loci. Due to the fact that the pulse stretcher built in the display unit accepts positive pulses only, all pictures had to be composed of two parts. The upper half for positive pulses and the lower half for inverted negative pulses. The pictures show that it is possible to distinguish between a pulse height, which corresponds to 0.5 MeV proton recoil energy and electron pulses. This low-energy cut-off can be lowered at the cost of a partial loss of high energy neutrons. Protons up to 14 MeV or more can be discriminated with the chosen adjustment.

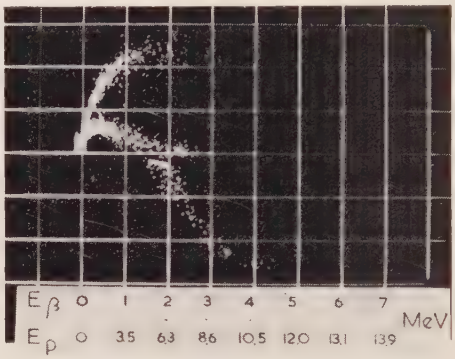

Po Be source

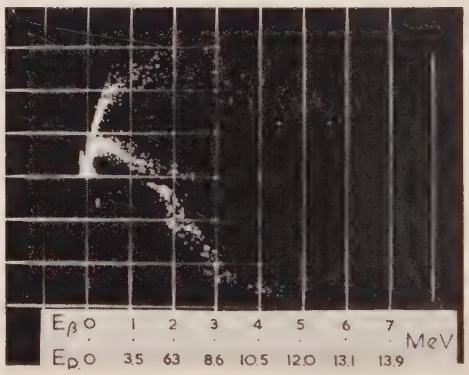

14 MeV n-generator

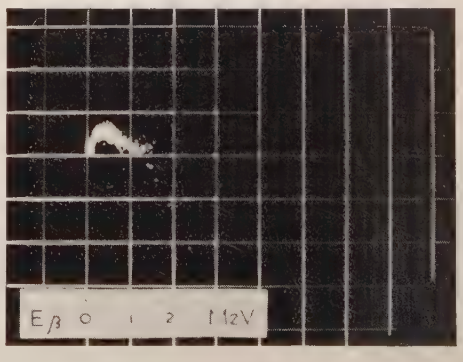

^{88}Y source

Fig. 8, 9 and 10. Peak height of the discrimination pulse as a function of recoil-proton or Compton-electron energy. The upper points represent the proton pulses. Sources were placed on the side of the crystal in order to get the maximum electron range of 3.75 cm in the crystal.

[4]) R. B. Owen, Nucleonics, **17** no. 9 (1959) 92.

The discriminator setting proved to be independent of the angle of incidence of the primary particle, although the peak amplitude, e.g. of 14 MeV neutrons, shows a small variation[12]). The discriminator setting is also independent of the variation of the multiplier voltage between 1200 and 1500 V.

3. Pile-up Effects

The gamma radiation, which always accompanies neutrons, can produce serious errors in neutron

In channel A the second pulse always adds on the tail of the previous one. In channel B an interference takes place between the damped harmonic motions of the successive pulses. This can be a constructive interference, that will not destroy the balancing, however, it may also lead to a false indication pulse, but only during the first two or three oscillations. If the second electron pulse arrives still later the diode circuit has become insensitive. If τ is the mean time during which a destructive interference can take place, N_t the

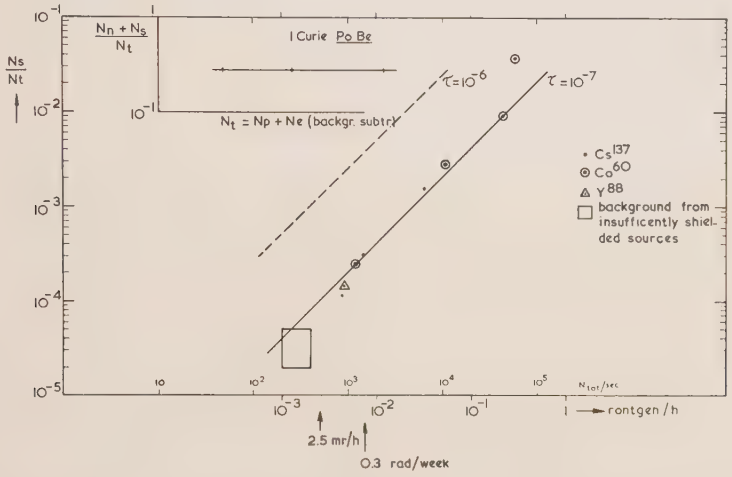

Fig. 11. Gamma-discrimination ratio as a function of gamma-intensity, by making use of different sources at various distances. N_s is the total number of spurious pulses above the threshold $\tau_t = 0$. N_t is the total number of pulses above the same threshold. The inset shows the number of indication pulses for a Po Be source at various distances between source and counter.

counting. As mentioned before, the Brooks circuit is sensitive to gamma pile-up, resulting in false indication pulses. These are caused by the fact that the pulses A and B are not of the same length. A second pulse, arriving at A, when a previous pulse is still present, will add on its "tail", since the photomultiplier acts like a current source.

In channel B addition of the pulses takes place as long as the fast pulse lasts; when the second pulse arrives later the higher one is selected by the diode stretcher. Therefore, a second pulse will always give a false indication pulse during the time that the amplitude of the first pulse is still above a certain level. This level depends on the pulse heights of both pulses.

In the presented circuit pile-up can only occur during a fraction of the pulse length:

total number of gamma-pulses and N_s the number of spurious counts, then

$$N_s = 2\tau N_t^2 . \tag{6}$$

Fig. 11 shows the ratio N_s/N_t as a function of gamma-ray intensity, of the gamma-ray sources ^{60}Co, ^{88}Y, ^{137}Cs. A straight line is obtained for a double log plot. This is in good agreement with formula (6). From the slope of the line we deduce $\tau = 0.1$ μsec. No other qualitative data are available for other circuits; however, from a preliminary result of Owen[4]) we estimate the resolving time for his circuit to be $\tau \simeq 9$ μsec.

The inset of fig. 11 shows the result of a similar measurement for a n-source†. The ratio N_s/N_t is

† 1 Curie PoBe from Amersham delivered Jan. 1960, measurement Sep. 1960.

independent of the neutron flux as is to be expected. The relative number of proton pulses is about 30 per cent of the total number of counts in the crystal.

To get the behaviour of τ at various electron pulse heights the gamma-spectra are measured on a 256 channel PHA in two cases: 1) the PHA gated with the pulses from the discriminator D in fig. 1 and 2) ungated (fig. 12). The gated spectrum shows a threshold, below which $\tau = 0$.

Due to the fact that a pile-up event always takes place before the first pulse reaches its maximum, the peak height of a pile-up pulse is almost equal to the sum of the pulse amplitudes of the composing pulses. Therefore, the pile-up spectrum can be written as:

$$n_k = \sum_{i+j=k} n_i n_j (\tau_i + \tau_j) \; ; \qquad (7)$$

n_k = number of pile-up pulses in channel k.
n_i = number of ungated pulses in channel i.
n_j = number of ungated pulses in channel j.
τ_j = resolving time of the pulses in channel i.
τ_j = resolving time of the pulses in channel j.

A curve of τ plotted as function of the pulse height, that can be constructed from eq. (7), is shown in fig. 12. It is calculated for the ^{60}Co source. In this figure the experimental pile-up spectrum is compared with the calculated curve. Assuming these τ-values the spectrum of the spurious pulses from a ^{88}Y source is calculated too. The calculated spectrum is again in agreement with the gated spectrum.

4. Applications

4.1. NEUTRON SPECTROMETER

Mozley and Shoemaker[6]) presented a new design of a two crystal proton recoil spectrometer in 1952, viz. a hydrogeneous crystal serves as a radiator of the recoil protons and measures the first part of the ionisation path, and a second crystal, viewing the first, measures the residual of the proton energy. The total proton recoil energy, that is the primary energy, is given by the sum of the two pulses.

Usually, a proportional counter is used as an electron-proton discriminator. We constructed a similar detector with pulse form discrimination instead of discrimination by means of a proportional counter. The pulse height spectrum of the added pulses is obtained from a PHA gated with the output of a 1 μsec triple coincidence between the two indication pulses and the output of a fast (10 nsec) coincidence between the two signal pulses.

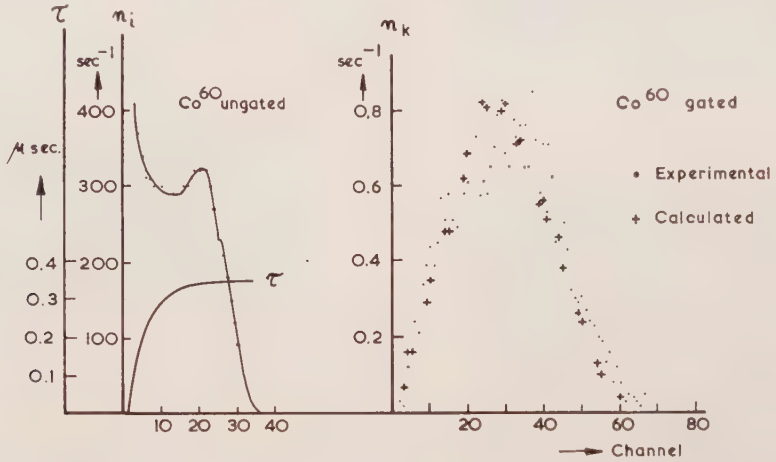

Fig. 12. Gated and ungated gamma-spectra of Co^{60}. Resolving time is presented as a function of pulse height as calculated by eq. (7).

The spectrum of the 14 MeV neutrons of the d-t reaction is presented in fig. 13. The distance between the crystals was 12 cm, the diameter of the crystals 3.75 cm.

The resolution of each crystal (from the differentiated one-crystal n-spectrum at 14 MeV) is about 5 per cent, the geometric resolution 5 per cent, while the channelwidth is 1.5 per cent in this case. The n-energy spread is not exactly known.

[5]) H. W. Broek and C. E. Anderson, Rev. Sci. Instr. **31** (1960) 1063.

[6]) R. F. Mozley and F. C. Shoemaker, Rev. Sci. Instr. **23** (L) (1952) 569.

The source is a Philips t(d,n) tube that is surrounded by a layer of transformer oil of about 1 cm in the neighbourhood of the target and a layer of a thickness of 10 cm on the top of the tube. Reifenschweiler[11]) describes the construction and operation of this tube. The measured full width at half

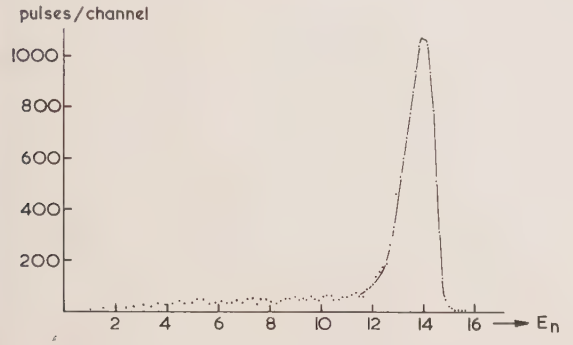

Fig. 13. Neutron energy spectrum from a t(d,n) source observed with the double crystal spectrometer. The full width at $\frac{1}{2}$ max is 10 per cent. Efficiency of the detector amounts to 1.3×10^{-4} counts per neutron. Integrated tail is 26 per cent of the peak value (calculated value for traversing neutrons 21 per cent).

max is 10 per cent in some cases with collimated neutrons 9 per cent (at the cost of an increased tail). This resolution could not be lowered appreciably by making use of a longer collimator between the crystals.

The calculated efficiency defined as the ratio of the counted neutrons to those, traversing the spectrometer parallel to the axis, is 1.3×10^{-4} counts/neutron. The efficiency of this telescope is about 10 times better than the efficiency of radiator-counter-crystal telescopes[7]), while its resolution is twice as large.

4.2. NEUTRON MONITOR

The described circuit is also very useful as n-monitor, for n-energies above 1 MeV.

Homogeneous organic scintillators can be of real value for fast neutron dosimetry, since they have a high efficiency and a good tissue equivalence if the integrated light output is measured; e.g. stilbene is tissue equivalent within 10 per cent from 2 till 20 MeV. Electrons, however, produce in these materials a relative greater light flash than protons. Therefore, we cannot eliminate gamma-radiation by higher bias settings of the counter. As a ZnS-Ag activated phosphor discriminates against electrons rather satisfactory neutron detectors are made by combining hydrogeneous materials with activated ZnS powder. The response at low energies and the energy resolution are poor, because of the granular structure of the ZnS. The proposed discriminator can resolve these difficulties.

In dosimetry the efficiency at energy E is usually defined as the number of counts (per sec) from the whole crystal, divided by the number of neutrons, incident per cm² (per sec) and coming from any direction, with energy E. Figure 14, curve A, shows this efficiency calculated for our stilbene crystal[5,7]). This curve can be compared with fig. 14 curve B, that shows the efficiency in the same units for the polyethylene-ZnS monitor of Moyer, according to Thompson[8]). Curve A surpasses curve B until 10 MeV. It is probable that curve B will turn down at higher energies. A four times larger stilbene crystal, instead of our 10 cm³ crystal, will give a much higher efficiency than Moyers monitor up to

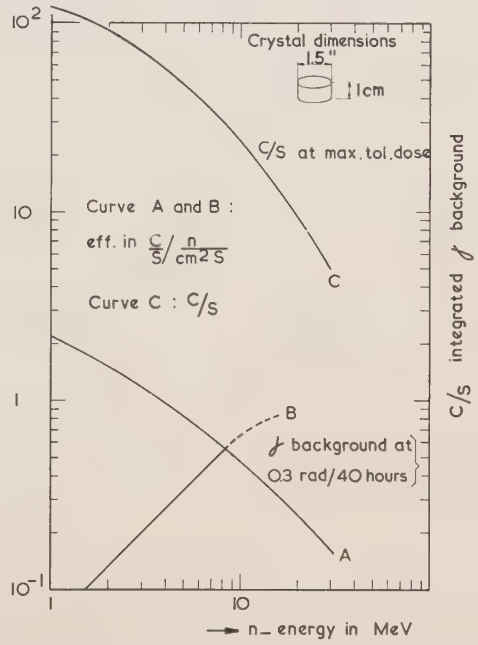

Fig. 14. A. Stilbene-monitor efficiency; B. Efficiency of polyethylene ZnS sphere; C. Monitor counting rate at a n-flux of 0.03 rad/40 hours.

[7]) S. J. Bame, E. Haddad, J. E. Perry and R. K. Smith, Rev. Sci. Instr. 28 (1957) 997.

[8]) B. W. Thompson, Nucleonics 12 no. 5 (1954) 43.

20 MeV and almost the same above this energy.

Our instrument gives a counting rate of 66 cps with a PoBe source, for a flux density of 75 n/cm² sec (as computed from a long-counter calibration). Hence the mean efficiency of the apparatus is 0.9 counts per neutron/cm².

Mean efficiency can be calculated by means of curve A if the shape of the neutron spectrum is known. This spectrum can be derived from the one-crystal pulse height spectrum with an accuracy that is sufficient for dosimetric purposes. Broek and Anderson[5]) gave a recent treatment of this method with a summary of corrections and the calculation of optimum crystal size for stilbene.

The efficiency calculated along these lines proved to be in agreement with the experimental result within statistical error. This result can also be compared with the measurements with a Hornyak counter. Handloser and Higinbotham[9]) found a mean efficiency of 0.01 for a ZnS-lucite button with equal volume.

We will show that the circuit can measure 10 per cent of the maximum permissible n-dose, 0.03 rad/week, when the gamma-radiation level is equal to the recommended permissible occupational exposure rate: 0.3 rad/40 hour week $\simeq$ 7.5 mr/h. We multiplied curve B by the neutron flux densities, which "singly" will deliver 0.03 rad/week $\simeq$ 0.3 rem/week[10]). This gives curve C. In the same figure is the total number of spurious gamma-indication pulses at a gamma-dose of 0.3 rad/week indicated by an arrow on the right scale. It is apparent that e.g. 10 per cent of the max. permissible dose for 14 MeV neutrons can be measured under these circumstances in 100 sec with a random error of $\pm$ 7 per cent and a systematic error of 22 per cent. A correction for this systematic error can easily be made if the total gamma-activity is known. This should be done by the same photomultiplier. If I_n is the uncorrected neutron counting rate and I_t the total counting rate, both in c/s, the following equation is obtained for $I_n \ll I_t$ and for $I_\gamma \simeq I_t$:

$$(I_n)_{corr} \simeq I_n - CI_\gamma^2 \ , \qquad (8)$$

where $C = 2 \times 10^{-7}$ (c/s)$^{-1}$.

This subtraction can be carried out electronically. In this case the monitor can be used at a relative higher gamma-level without any calculation. Statistics can be improved by using a larger crystal. As mentioned above we intend to use a four times larger crystal. This crystal will give as much pile-up pulses as the 10 cm³ crystal, in the presence of a gamma-background of 0.15 rad/week. A somewhat increased discrimination level may increase the tolerable background level.

At the moment a portable transistorised circuit is constructed. We inted to check the influence of higher discriminator settings, which may considerably improve the discrimination ratio at 14 MeV.

Acknowledgements

The authors are indebted to Prof. P. C. Gugelot for valuable discussions on the subject of this paper.

This work constitutes part of the research program of the Institute for Nuclear Physics Research, made possible by financial support from the Foundation for Fundamental Research of Matter (F.O.M.) and the Dutch Organisation for Pure Scientific Research (Z.W.O.).

[9]) J. S. Handloser and W. A. Higinbotham, Rev. Sci. Instr. **25** (1954) 98.

[10]) N.B.S. (U.S.), Handbook **63** (1957).

[11]) O. Reifenschweiler, Nucleonics **18** (1960) 69.

[12]) J. B. Marion and J. L. Fowler, Fast Neutron Physics I.

NUCLEAR INSTRUMENTS AND METHODS 13 (1961) 161–168; NORTH-HOLLAND PUBLISHING CO.

EXPERIENCES IN THE USE OF SCINTILLATION DETECTOR IN A β-SPECTROMETER OF TOROID-SECTOR TYPE

D. BERÉNYI and GY. MÁTHÉ

Institute of Nuclear Research (ATOMKI) of the Hung. Acad. of Sci., Debrecen

Received 28 April 1961

Experiences are reported regarding the adjustment of the electronic parameters and other operating conditions of a scintillation spectrometer used as a detector in a β-spectrometer of the toroid-sector type. Anthracene crystals and plastic phosphors were applied as scintillators, while the multipliers were types RCA 6342-A and 5819 respectively. The adjustment of the optimal parameters and the investigation of the operating conditions of the detector were carried out by taking the signal-to-noise characteristics and pulse-height distributions as well as by determining the efficiency curve of detection.

1. Introduction

In the last decade, the use of scintillation techniques instead of GM-counting has become more and more common in magnetic β-spectrometers†. This is mainly accounted for by the short decay time of scintillators in addition to the easier handling of the scintillation crystals and even more so of the plastic phosphors. The short decay time is particularly important in the case of coincidence spectrometers. On the other hand, the high sensitivity of the photo multiplier to magnetic fields, and the necessity of cooling at low electron energies are unfavourable.

A scintillation detector has been used in our β-spectrometer which is of the toroid-sector type[2]). This instrument was completed for coincidence work by a scintillation γ-spectrometer[3]). A spectrometer of the toroid type does not reveal any disturbing effects from the magnetic field since the field is closed inside the toroid-coil and there is no measurable magnetic field at the detector position. Thus there was no need for using any compensating field or light conductor. The detecting phosphor was placed directly upon the photo cathode of the multiplier and DC-silicone oil of high viscosity was used for the optical connection. The disc-shaped scintillator was held in the centre of the photocathode by a suitable plexi ring. The iron cylinder enveloping the multiplier was mounted in the vacuum chamber as reported in reference[3]). No cooling whatever was applied, and the multiplier was practically at room temperature. Under such experimental conditions and with its parameters properly adjusted the scintillation detector was equivalent to a GM-counter with a window-thickness of about 0.1 mg/cm^2 from the viewpoint of detecting electrons of low energy.

The following is a summary of our experiences in adjusting the parameters of the electronics and applying various scintillators and light-reflector foils.

2. Signal-to-Noise Ratio

It is well-known that adjusting the operating point for a GM-counter is a rather simple matter. It should be set at the centre of the plateau of the characteristics.

In the case of a given magnetic field in the β-spectrometer and a constant discrimination voltage, characteristics similar to those of GM-counters may be ascribed to scintillation detectors. At low voltages, the curve starts with a low counting rate arising from the radioactive contamination of the chamber and from the cosmic background. The abrupt rise and the plateau-like portion is due to

† Ramler and Freedman were some of the first to use it[1]).

[1]) W. J. Ramler and M. S. Freedman, Rev. Sci. Instr. **21** (1950) 784.

[2]) A. Szalay and D. Berényi, Acta Phys. Hung. **10** (1959) 57.

[3]) D. Berényi, Acta Universitatis Debreceniensis de L. Kossuth nom. **5** (1958) 187.

electrons focused on the detector. The further rise at higher voltages is due to the dark current of the multiplier. Obviously, the length of the scintillation detector plateau will depend on the energy of the incoming electrons.

Instead of taking the usual characteristics of GM-counters it was found more suitable to take the signal/noise ratio as a function of the high voltage fed to the multiplier. This was obtained by measuring the counting rate from the sample (Cs^{137}, Co^{60}) at a given magnetic field in the β-spectrometer (signal) and dividing by the counting rate of the background (noise)—with the magnetic field switched off and with the same value of the high voltage. A typical series of such curves is shown in fig. 1. The individual curves correspond to different values of the magnetic field, i.e. to different electron energies. It can be seen that the curves have got maxima which are shifted to higher voltages as the electron energies decrease.

The position of the signal-to-noise maxima as a function of the electron energy is shown in fig. 2. If measurements are to be carried out only in a particular energy region or above a particular energy value, the detector will be most favourably adjusted by setting the operating point at the maximum of the signal/noise curve pertaining to the energy in question. From the series of curves of the signal/noise ratio: it can then be predicted which energies will not be detected at all and which will be registered to a lower degree as compared to an optimal signal/noise ratio.

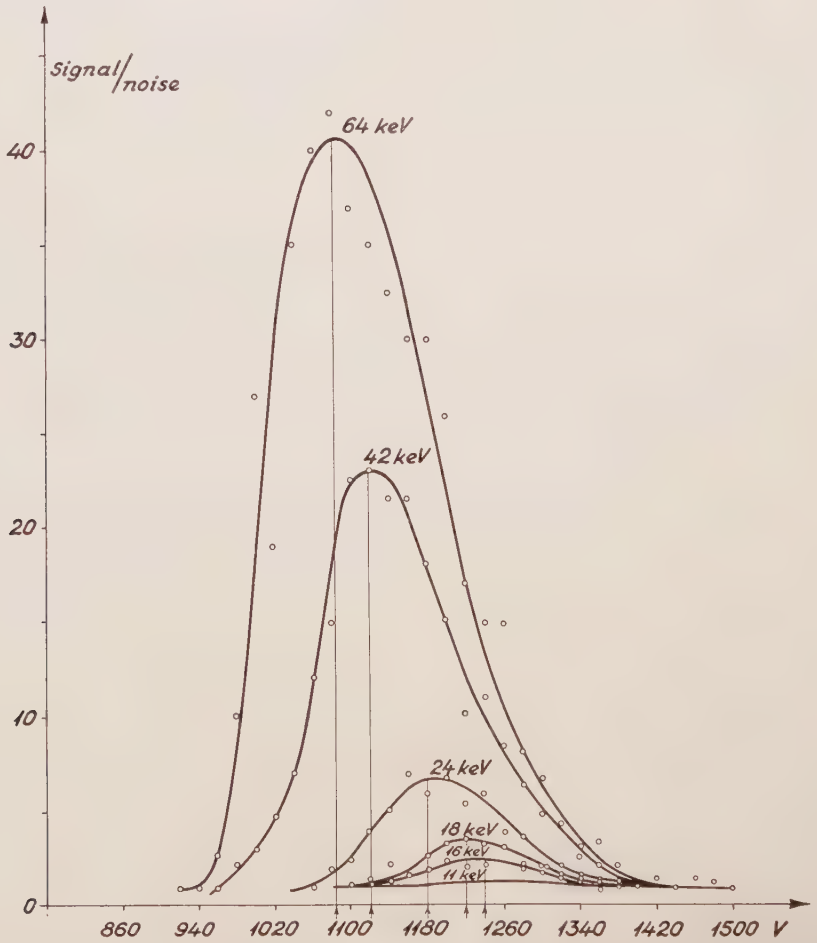

Fig. 1. Curves of the signal/noise ratio as a function of the high voltage of the multiplier. The individual curves refer to different magnetic fields of the β-spectrometer, i.e. different energies of the electrons entering the scintillation phosphor.

If, however, the aim is to count electrons of the lowest energy detectable under the given conditions, the high voltage due to the maximum of the lowest energy must be set at the energy where a maximum can develop at all. The same lowest energy value—that is the limit of detectability—is also given by the hyperbola to be seen in fig. 2, which, asymptotically approaches the curve $x = 9.5$ keV.

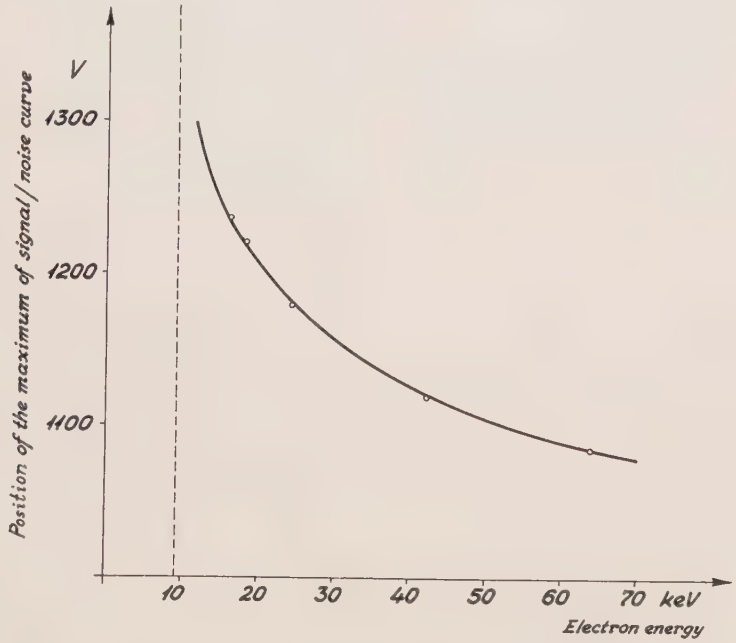

Fig. 2. Correlation between the energy of detected electrons and the position of the maximum of the corresponding signal/noise curve.

When the discriminating voltage or the amplification factor of the amplifier is altered, the curves remain essentially the same except for a shift towards lower or higher voltages†. Therefore the limit of detectability to electrons of low energy cannot be reduced by applying a higher amplification or a lower discriminator voltage. At too high an amplification, the signal/noise ratio even diminishes because of the considerably increasing noise of the amplifier.

3. Pulse-Height Distribution

The pulse-height distribution for a given magnetic field and a properly chosen high voltage, generally consists of a maximum, a shorter or longer tail attached to this maximum and the upturn due to the dark current near 0 V. Taking the peak positions for different values of the magnetic field the linearity of the energy-pulse height function of the scintillator can be checked. A series of pulse-height distributions curves also discloses at what energies the peak dissolves in the dark current background. This is the lowest electron energy still detectable (c.f. limit of detectability) under the given experimental conditions.

These curves reveal what bias should be used at a given high voltage for the elimination of the dark current and for the decrease of the chamber background, whenever the measurements are made only in a particular energy region or above a certain energy value. From an analysis of the ratio of the area, in the pulse height-counting rate diagram it can also be estimated by about what proportion the detecting efficiency for electrons of a given energy has been diminished at such a bias.

By investigating the pulse-height distributions we also found, at a particular electron energy, the double peak effect reported by Porter *et al.*[4]). In the pulse-height distribution shown in fig. 3. The

† In a lower high voltage region, the curves get narrower. This can be explained by the nonlinearity of the high voltage-amplification factor characteristics of the multiplier.

thickness of the detector is 0.1 mm and the double peaks arise over 60 keV. In the case of the 91 keV electrons the two peaks cannot be resolved and for 225 keV electrons, however, the higher energy peak appears at a higher pulse-height as the 100 V bias. This, as it has been stated[4]), is in connection with the thickness of the phosphor.

4. Determination of the Optimal Electronic Parameters of the Detector

On the basis of what has been discussed above the detector should be adjusted as follows: First, the curve series of signal/noise ratio for different values of the magnetic field are to be taken and the signal/noise maxima can then be plotted as a function of the energy (fig. 2). It is advisable to take the curves at a comparatively high integral discriminator level, say 5–10 V, in order to cut out network disturbances. If electrons of the lowest energy detectable under the given conditions are wanted to be detected the high voltage should be set, at which the curve of signal/noise maxima practically reaches the asymptote. The same result is obtained by setting the high voltage at the value corresponding to the maximum of the curve of the signal/noise series, that is the curve of the lowest energy still having a maximum. In this case, the background counting rate is rather high.

In many cases, however, it is not essential to register electrons of even the detectable lowest energy. Then the pulse-height distributions should be taken at the same high voltage and at some energies (particularly those in whose region the measurements are to be made). Being aware of this we are able to set the discriminator at a value that cuts off the large background, yet definitely admits the pulses to be measured. For a given energy, the decrease of the detecting efficiency resulting from the adjustment of the parameters of the detector can also be estimated from the pulse-height distribution[4]).

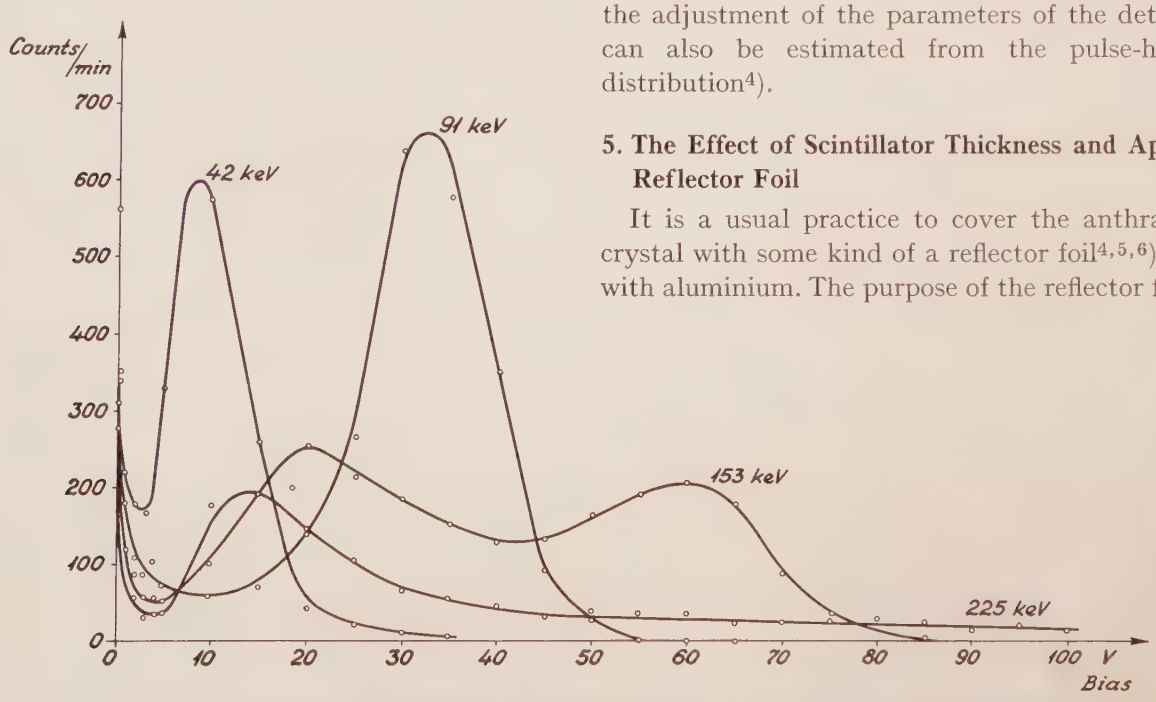

Fig. 3. Pulse-height distribution for electrons of different energies. The scintillator was a plastic phosphor disc. of 0.1 mm thickness (⌀ 14 mm).

5. The Effect of Scintillator Thickness and Applied Reflector Foil

It is a usual practice to cover the anthracene crystal with some kind of a reflector foil[4,5,6]), e.g. with aluminium. The purpose of the reflector foil is to increase light efficiency as well as to prevent evaporation from the anthracene crystal in vacuum. The latter point is particularly important in so far as thin anthracene crystals are concerned, considering that it takes a 0.1 mm thick anthracene

[4]) F. T. Porter, M. S. Freedman, T. B. Novey and F. Wagner, Jr. Phys. Rev. **103** (1956) 921.

[5]) J. Brünner, J. Halter and P. Scherrer, Helv. Acta Phys. **31** (1958) 338.

[6]) N. N. Delyagin, A. A. Sorokin, N. V. Forafontov and V. S. Spinel', Izv. An SSSP. Ser. Fiz. **20** (1956) 920 (in Russian).

foil about a week to ten days to completely evaporate in vacuum.

Electrons of low energy might benefit most from the increase of light efficiency, as in this way even low pulses would rise above background level and become registrable. This, however, is not supported by our measurements since in the case of electrons with low energy, the absorption in the reflector foil is far greater than its effect of light reflection and by that, its effect of increasing the pulses. This is well illustrated in figs. 4a and 4b. In case *a*, a 0.1 mm thick anthracene disc was used for detection and it was covered with the thinnest available aluminium foil (≈ 0.2 mg/cm^2). In case *b*, the thickness of the anthracene disc was 1 mm and the crystal was not covered with any reflector foil. The difference is clearly observable as case *a*, at 18 keV, already reveals a very strong distortion. On the other hand, when the anthracene is not covered (case *b*), the limit of detectability is 5–6 keV according to the analysis of the signal/noise curves. All this is in agreement with the latest investigations on electron absorption[7]) which have shown that the range of 8–10 keV electrons in aluminium is ≈ 0.2 mg/cm^2.

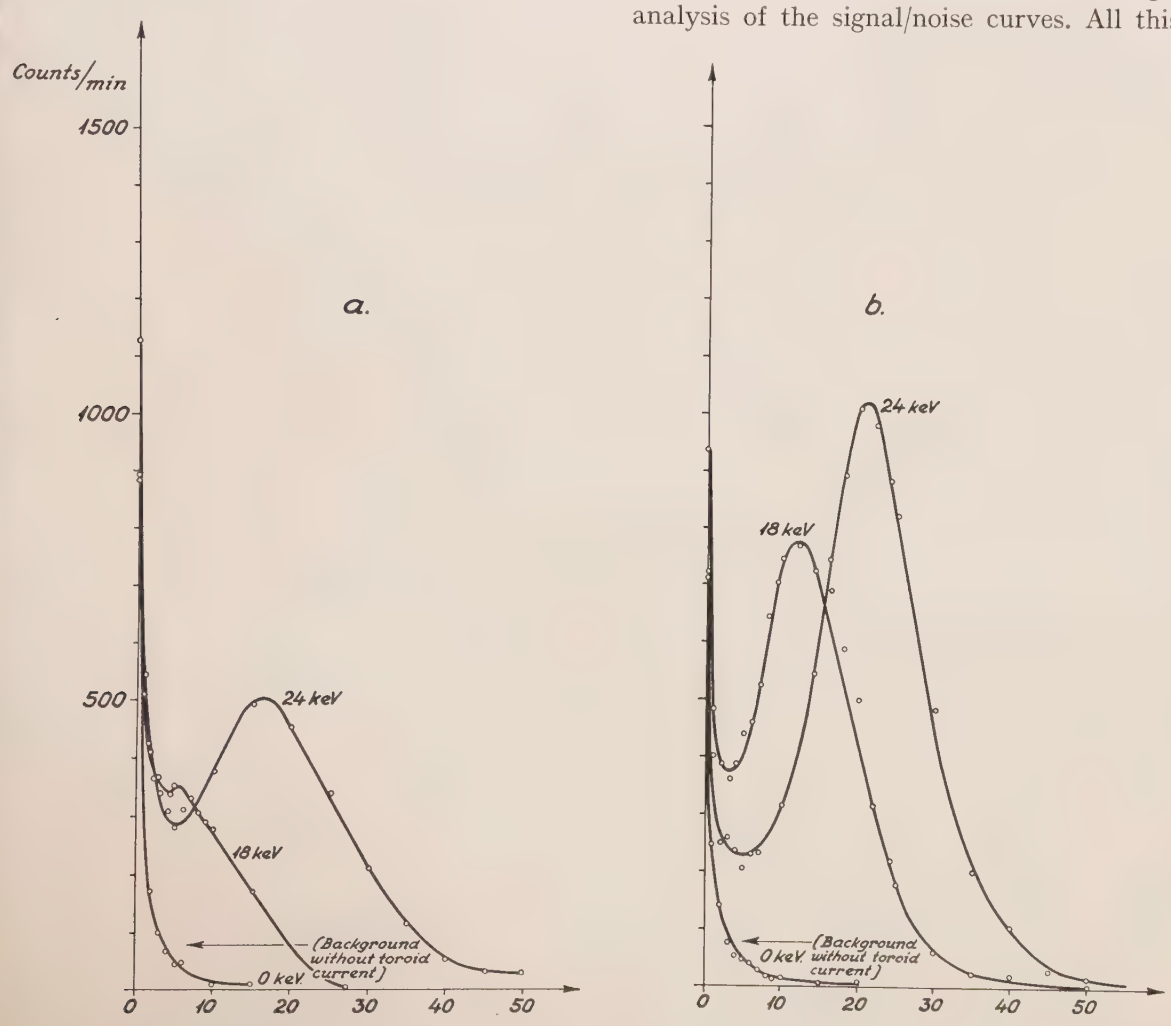

Fig. 4. Pulse-height distribution when the detector crystal was: a) a 0.1 mm thick anthracene with an Al-foil of ≈ 0.2 mg/cm^2 in front, and b) a 1 mm thick anthracene without any cover. Conditions were otherwise the same in both cases (e.g. the source in both cases was Cs^{137}, thus the fact that there is a difference of the heights of the maximums, also in case *b*, is first of all, due to the shape of the β-spectrum).

In the light of what has been stated, we find

[7]) O. Klemperer, A. Thetford and F. Lenz, Proc. Phys. Soc. **76** (1960) 718.

questionable the 80% efficiency of detection reported in ref.[5]) for electrons of 20 keV using a 5 μ Al foil (1.35 mg/cm^2) in front of the scintillator, fact that the smaller background—favourable to thinner crystals—is negligible when the adjustment is made to register low energies†.

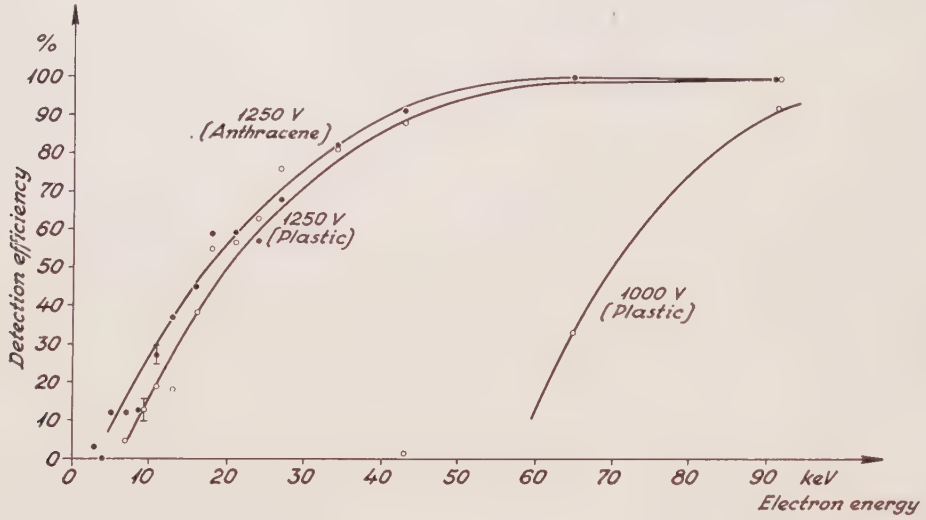

Fig. 5. Detecting efficiency determined from the Fermi-Kurie diagrams. At these measurements, the discriminator level was constant.

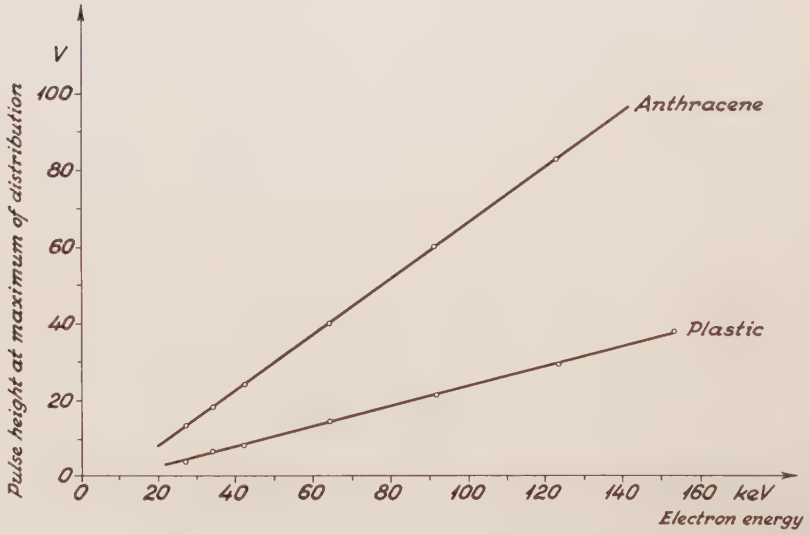

Fig. 6. Position of the maximum of the pulse-height distribution versus electron energy for anthracene and plastic phosphors.

although such foils correspond to the range of 20 keV electrons.

In view of the quick evaporation of thin anthracene foils in a vacuum and the necessity of having such foils covered for prolonged measurements, the use of thicker anthracene crystals without covering seems more appropriate. This is also stressed by the

[8]) H. De Waard, Thesis, Groningen, 1954, p. 71.

† According to de Waard[8]), another practicable way is to cover the surface of the anthracene crystal with a wet Zapon-foil and to evaporate it in vacuum with a thin Al layer. In previous experience, we also found that such a process actually prevented the crystal from evaporating in the vacuum. Nevertheless, at our present measurements, we have not investigated its effect on the detection of electrons of low energy. Considering, however, that the added thickness of the Zapon and Al layers is a few times 10 μg/cm^2 which corresponds to the range of $\approx$ 1–2 keV-electrons, it is likely that such a cover has a negligible effect above 5–6 keV.

6. Various Scintillators and Multipliers

Plastic scintillators have scarcely been used as detectors in magnetic β-spectrometers, because of their low light-energy efficiency.

We have tested the application of scintillators of various types and thicknesses. At room temperature and with a RCA 6342-A multiplier there was a anthracene detector† and 10–12 keV for a plastic†† scintillator. Fig. 5 shows the detecting efficiency as a function of energy obtained from the analysis of the Fermi-Kurie diagram. It clearly reveals the role of high voltage setting at a constant discrimination level.

Fig. 6 shows the correlation between the energy

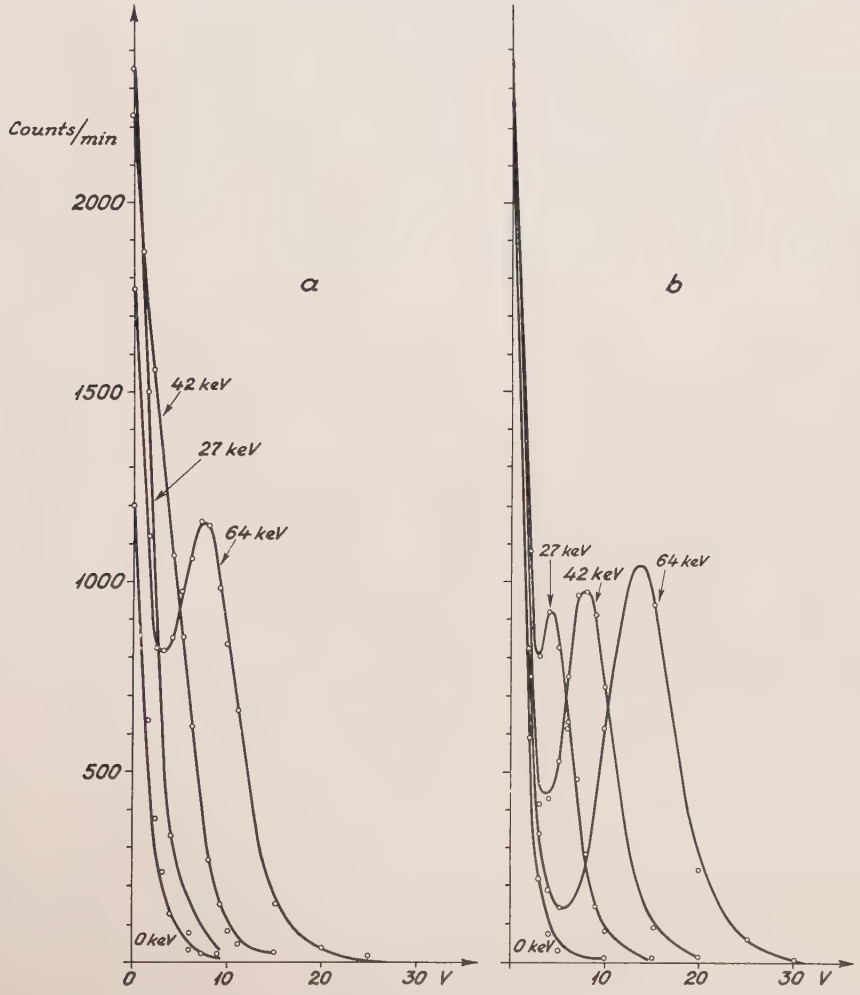

Fig. 7. Pulse-height distribution for different electron energies under identical conditions when (i) an RCA 5819 and (ii) an RCA 6342-A multiplier was applied.

pronounced difference between plastic and anthracene phosphors in so far as signal height and signal/noise characteristics are concerned. The limit of detectability, as we have mentioned is 5–6 keV for an and the positions of maxima in the pulse-height distribution for anthracene and plastic scintillators[9,10]). Both curves are linear in the measured region.

[9]) L. W. Johnston, R. D. Birkhoff, J. S. Cheka, H. H. Hubbell, Jr. and B. G. Saunders, Rev. Sci. Instr. **28** (1957) 765.

[10]) I. Rezanka and J. Frána, Czech. Journ. Phys. **10** (1960) 686.

† The anthracene crystals were produced by the Institute of Medical Physics, Budapest.

†† The plastic phosphors were made in Czechoslovakia (shipped by VUPEF) and in England (Nuclear Enterprises Ltd.).

No essential difference was found between scintillators of various types and thicknesses (from 0.1 to 1.5 mm).

Our conclusion is that under the given conditions it is satisfactory in most cases to use a plastic phosphor instead of an anthracene crystal which is more difficult to handle.

Finally the properties of the detector were studied when an RCA 5819 type multiplier was used instead of an RCA 6342-A-type. Owing to the lower operating voltage of the multiplier, the signal/noise curves shift towards lower voltages and become narrower. This should not generally cause any disadvantage. The RCA 5819-type multiplier, however, proved to be less favourable for detecting electrons of low energy. This is clearly shown in fig. 7. An analysis of the signal-to-noise curves for this multiplier yielded a low energy limit of detectability as high as 20 keV. This phenomenon may be due to the lower cathode sensitivity of tube 5819. From the point of view of detecting electrons of low energy, the multipliers having a low dark current and high cathode sensitivity to light are generally expected to be favourable.

Thanks are due to Prof. A. Szalay, director of this Institute for the special interest he has taken in this work. Acknowledgement is also due to Mrs. T. Halász for her conscientious technical help as well as to Dr. Cs. Ujhelyi, radiochemist, and Mr. Gy. Meszéna, mathematician, for the prompt and thorough source-preparations and mathematical calculations required.

NUCLEAR INSTRUMENTS AND METHODS 13 (1961) 169–176; NORTH-HOLLAND PUBLISHING CO.

THE DOUBLE-GRID IONIZATION CHAMBER

IWAO OGAWA, TADAYOSHI DOKE and MASAHIRO TSUKUDA

Department of Physics, Rikkyo (St. Paul's) University, Toshimaku, Tokyo

Received 28 June 1961

A new type of gridded ionization chamber is described. The chamber is provided with two sheets of grid between the cathode and the collector. Signals are taken out not only from the collector, but also from the grid closer to the cathode simultaneously. While the collector pulses afford the information on the energy of particles, the grid pulses give the information on the direction of emission. The other grid facing the collector is grounded and serves as a screen grid.

Owing to the efficient shielding action of this screen grid, it is possible to make full use of the grid pulses while keeping the energy resolution better than $1 \approx 2\%$. Several applications of the chamber are shown, including the improved "electronic collimation", low-background counting and the measurement of angular distribution of proton recoils.

1. Introduction

Gridded ionization chambers have been widely used as an excellent energy spectrometer for alpha-particles with a high resolution in energy as well as an outstanding luminosity. In some cases, however, it is desirable to obtain information not only on the energy, but on the direction of emission of the particles as well. Among the various methods[1–4]) that have been attempted for this purpose, the grid-pulse method proposed by Bochagov, Vorob'ev and Komar seems to be most promising.

Bochagov *et al.*[1]) pointed out that the negative amplitude of a pulse extracted from the grid of an ionization chamber is expressed as a linear function of $\cos\theta$, where θ is the angle between the particle track and the normal to the cathode. Making use of the fact, they succeeded in the so-called "electronic collimation", namely the method of selecting only those pulses which are produced by the particles with $\theta \cong 90°$ electronically with the help of grid pulses. In addition, they have suggested the application of grid pulses to the measurement of angular distribution of particles emitted from a source on the cathode of a chamber.

However, extraction of grid pulses affects strongly the shielding action of the grid. Therefore, it is difficult to obtain a high resolution in energy under simultaneous extraction of pulses from both the collector and the grid in a conventional *single*-grid chamber.

In order to overcome this difficulty, we have constructed a *double*-grid chamber[5])†. In addition to the grid for extracting the signal, the chamber is provided with another grid in front of the collector. The latter grid is grounded and serves as a screen grid. With the chamber, we have succeeded in extracting the grid pulses without any appreciable loss in energy resolution.

In the present article, we shall first give an account of the nature of grid pulses. Next we consider the shielding efficiency of a double-grid system. Then we describe the construction, operation and performance of our chamber. Finally we give several applications of the chamber, including the electronic collimation with an improved luminosity, low-background counting by the method of coincidence between the collector and the grid, together with the measurement of angular distribution of proton recoils with the help of grid pulses.

† Professor Komar has kindly informed the authors by a private communication that he, together with his colleagues, independently constructed such a double-grid chamber previously cf. Izv. Akad. Nauk. SSSR, Ser. Fiz. **22** (1958) 824.

[1]) B. A. Bochagov, A. A. Vorob'ev and A. P. Komar, Izv. Akad. Nauk SSSR, Ser. Fiz. **20** (1956) 1455; Zh. Tekhn. Fiz. **27** (1957) 1575.

[2]) Y. I. Filimonov and G. A. Petrov, Izv. Akad. Nauk SSSR, Ser. Fiz. **20** (1956) 1434.

[3]) R. Sherr and R. Peterson Rev., Sci. Instr. **18** (1947) 567.

[4]) U. Facchini, E. Gatti and F. Pellegrini, Nucl. Instr. and Meth. **4** (1959) 221.

[5]) I. Ogawa and T. Doke, J. Phys. Soc., Japan **16** (1961) 1025.

2. Nature of the Grid Pulses

In a double-grid chamber as shown schematically in fig. 1, the electrons liberated along the track of an alpha particle emitted from the cathode K at first drift towards the first ("signal-") grid G_1 keeping the original columnar distribution. After

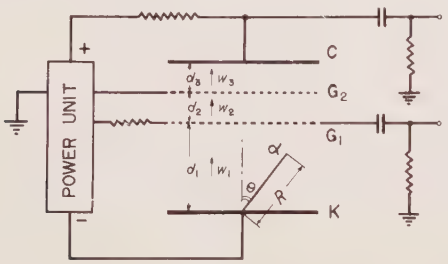

Fig. 1. Schematic view of a double-grid ionization chamber.

passing the two grids G_1 and G_2, they are eventually collected on the collector C. The positive ions may be regarded as at rest during the period of electron collection.

Such a drift of electrons gives rise to a saw-tooth-like negative pulse on G_1 as given in fig. 2.

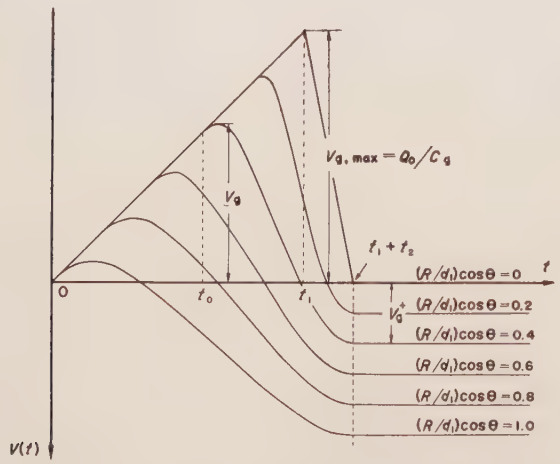

Fig. 2. Typical wave-forms of grid pulses. t_0 is the time when the head of an electron column passes through the G_1-plane. Other quantities are defined in the text.

The negative pulse-height V_g of the pulse is approximately given by a formula[1]):

$$V_g = \frac{Q_0}{C_g}\left(1 - \frac{R^*}{d_1}\cos\theta\right), \qquad (1)$$

where Q_0 denotes the total charge of the ions, C_g the capacity of the G_1-system, d_1 the distance between K and G_1, and θ the angle between the particle track and the normal to the cathode; R^* is a quantity which represents a length close to the particle range R independent of $\cos\theta$.

The fractional defect $\delta \equiv (R - R^*)/R$ has been worked out[6]) as a function of $\vartheta \equiv t_2/t_1$, where t_1, t_2,

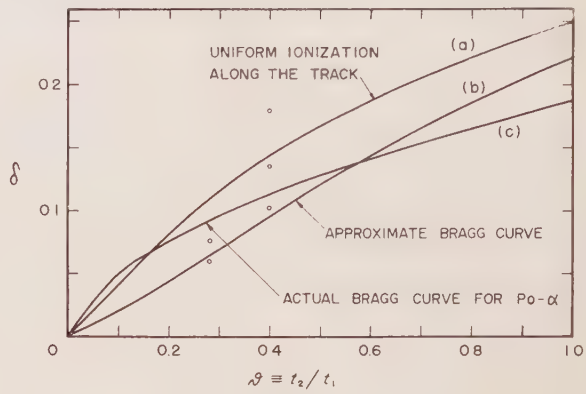

Fig. 3. δ *vs.* ϑ relation.

is the drift time of electrons in the $K - G_1$ and $G_1 - G_2$ space, respectively. The result is plotted in fig. 3 for different distributions of specific ionization along the track. Experimentally δ has been estimated for various ϑ from the pulse-height distribution for isotropic particles to be described below. The data are in fair agreement with the theoretical curves.

On the other hand, the positive pulse-height V_g^+ of the pulse is given by

$$V_g^+ = -\frac{Q_0}{C_g}\frac{\bar{X}}{d_1}\cos\theta$$

irrespective of ϑ, where $\bar{X}$ is the distance from the origin of the track to the centre of ion distribution.

It is seen from (1) that the pulse-height distribution of grid pulses due to monoenergetic alpha particles emitted isotropically from the cathode will be rectangular, ranging from $V_{g,\min} = (Q_0/C_g)\{1 - (R^*/d_1)\}$ up to $V_{g,\max} = Q_0/C_g$. If the particles are anistropic, then the pulse-height distribution will represent the angular distribution in terms of $\cos\theta$, where $V_{g,\min}$ and $V_{g,\max}$ correspond to $\cos\theta = 1$ and $\cos\theta = 0$ respectively.

In the case where the particles are neither monoenergetic nor isotropic, we may study the angular

[6]) I. Ogawa, Nuovo Cimento, Supplemento, in press.

distribution for a particular energy by measuring the pulse-height distribution of those grid pulses which are in coincidence with a collector pulse of a particular size.

It should be mentioned that the pulses extracted from the cathode may also give information on the track angle. Those pulses assume the shape of a rounded off step-function, and their *positive* pulse-heights V_k are given by the expression:

$$V_k = \frac{Q_0}{C_g}\left(1 - \frac{\bar{X}}{d_1}\cos\theta\right) \qquad (2)$$

where C_k is the capacity of the cathode system.

Cathode pulses are sometimes more convenient than grid pulses, since their shape suits better to low-noise amplification and since they may be extracted from a *single*-grid chamber without any loss in the energy resolution. However, the range of the pulse-height distribution corresponding to $\cos\theta = 1 \approx 0$ is $\bar{X}/R(\cong \frac{1}{2} \approx \frac{3}{5})$ times narrower than that of grid pulses.

3. Effect of the Screen Grid

Simultaneous extraction of pulses from both the collector and the grid of a single-grid chamber gives rise necessarily to an electrostatic induction between the collector and the grid. This affects the shielding efficiency σ of the grid seriously.

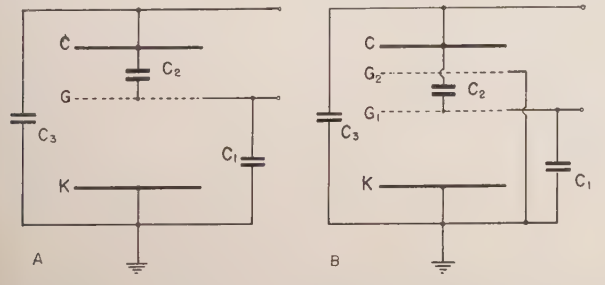

Fig. 4. Equivalent circuits of gridded chambers for calculating the shielding inefficiencies. A: single-grid chamber; B: double-grid chamber.

According to an elementary consideration, σ is given by the following expression:

$$\sigma \cong \frac{1}{1 + (c_1/c_2) + (c_1/c_3)}, \qquad (3)$$

where c_1, c_2 and c_3 designates the capacities between K — G, G — C, and C — K, respectively, in fig. 4A.

For an illustrative case of $c_1 \cong c_3 \cong 44$ pF and $c_2 \cong 40$ pF, which was actually met with in our chamber under the single-grid operation, (3) gives σ as large as 32%.

The corresponding spread ΔV_c in the collector pulse-height V_c for monoenergetic alpha particles can be calculated from the well-known formula[7]):

$$\frac{\Delta V_c}{V_c} = \sigma\frac{\bar{X}}{d_1}. \qquad (4)$$

For $\sigma = 32\%$ and $\bar{X}/d_1 = 0.46$, (4) gives the energy resolution $\Delta V_c/V_c$ as poor as 15%.

Let us now consider a *double*-grid chamber. In this case, σ is again expressed by (3) if only we alter the definition of c_1, c_2 and c_3 as given in fig. 4B. But in general $c_2 \ll c_1$, $c_2 \ll c_3$ owing to the screening effect of G_2, so that

$$\sigma \cong c_2/c_1 . \qquad (5)$$

c_1 may be regarded as composed of two capacities: $c_1 = c_{12} + c_{10}$, where c_{12} is the capacity between G_1 and G_2, and c_{10} the remaining capacity of G_1 against the ground including the cable capacity. On the other hand, $c_2 = c^{(1)} + c^{(2)}$, where $c^{(1)}$ denotes the capacity between G_1 and C due to the lines of force passing through the mesh of G_2, while $c^{(2)}$ the capacity between G_1 and C due to the détour lines of force round the periphery of G_2. Thus

$$\sigma \cong \frac{c^{(1)} + c^{(2)}}{c_{12} + c_{10}}.$$

In view of the relation

$$\sigma_2 = c^{(1)}/c_{12}$$

where σ_2 is the "intrinsic" shielding inefficiency for G_2 as introduced by Bunemann, Cranshaw and Harvey[7]), it is concluded that σ may be greater or smalle than σ_2 depending on whether $c^{(2)}/c^{(1)} \gtrless c_{10}/c_{12}$. To minimize σ, it is required to reduce not only σ_2, but the ratio $c^{(2)}/c^{(1)}$ as well by an appropriate design of electrodes.

4. Design and Construction of a Double-Grid Chamber

The double-grid chamber we have constructed is provided with an electrode arrangement as shown

[7]) O. Bunemann, T. E. Cranshaw and J. A. Harvey, Canad. J. Res. 27 (1949) 191.

in fig. 5. The vessel, made of iron, is plated with nickel. The grids, G_1 and G_2, consist of tungsten wires, 0.1 mm in diameter. The wire-spacing is 2 mm for G_1 and 1 mm for G_2. The potentials of the electrodes, given in fig. 6, are so chosen to avoid

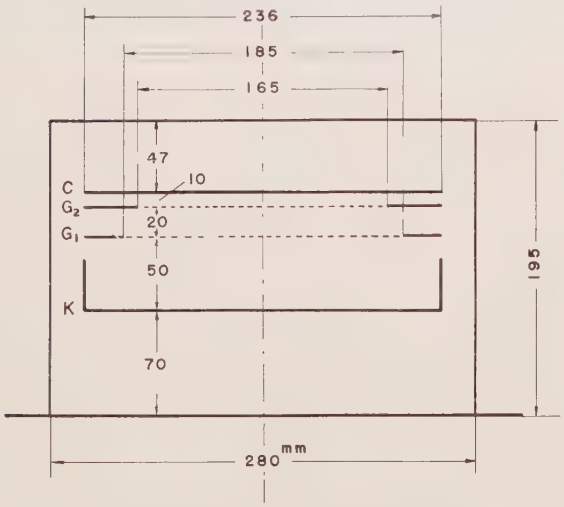

Fig. 5. Electrode arrangement of the chamber.

the collection of electrons by G_1 and G_2.

The "intrinsic" shielding inefficiency σ_2 for G_2 is calculated to be 1.82% from the formula by Bunemann *et al.*[7]). On the other hand, the measured shielding inefficiency σ for the double-grid system is about 2%. This may perhaps imply that $c^{(2)}/c^{(1)} \approx c_{10}/c_{12}$ incidentally in our chamber.

The chamber was filled with pure argon or with a mixture of argon plus methane, ethylene, carbon-dioxide or nitrogen for different purposes. The

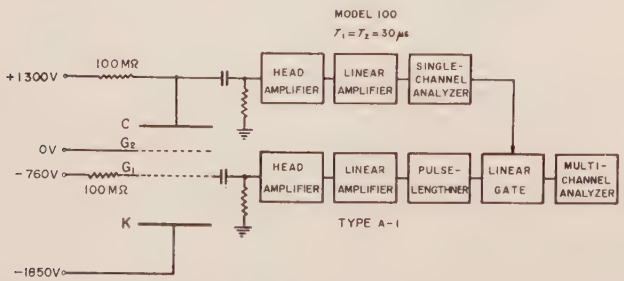

Fig. 6. Block diagram of the electronic circuit for measuring the distribution of grid pulse-heights.

alpha-sources, 16.5 cm² in area, were placed at the centre of the cathode.

Fig. 6 gives the block diagram of a typical circuit used with the chamber for measuring the pulse-height distribution of the grid pulses.

Pulses from G_1 are amplified, lengthened and passed through a linear gate circuit to a multi-channel analyzer[8]). The amplified pulses from the collector C are selected by a single-channel analyzer and then control the gate.

The maximum rise time T was as large as 14 μsec for both the grid pulses and the collector pulses, when the chamber was filled with pure argon. Thus the differentiating and integrating time constants T_1 and T_2 of the amplifier were always chosen as $T_1 = T_2 = 30$ μsec for the collector pulses. The r.m.s. noise level was then about 800 when expressed in equivalent ion pairs across the input capacity of about 84 pF. For the grid-pulse amplifier, various combinations of T_1 and T_2 were used for different gas fillings so as to fulfill the condition for linearity: $T_1 \gg T \gtrsim T_2$ with a band-width as narrow as possible to lower the noise level. For pure argon we adopted $T_1 = 46$ μsec and $T_2 = 5$ μsec.

5. Performances

Fig. 7A shows the energy spectrum of the alpha particles from a sufficiently thin Po^{210} source obtained with the chamber. The half-value width of

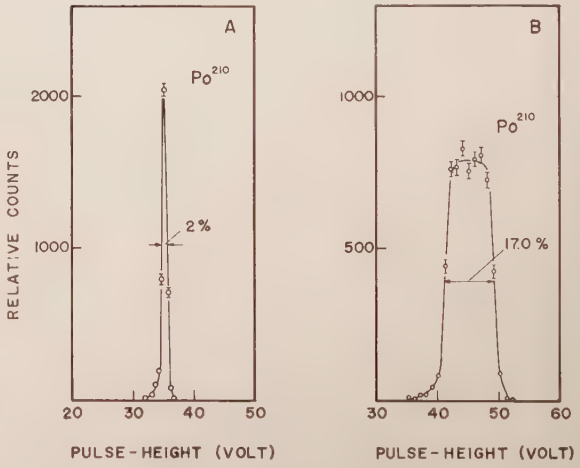

Fig. 7. Improvement of energy resolution by the screen grid.. A: energy spectrum of Po^{210}-α obtained with a double-grid chamber; B: spectrum obtained with a single-grid chamber under the extraction of grid pulses.

the peak is about 100 keV. The effect of the screen grid is evident since the above result was obtained

[8]) M. Tsukuda, to be published.

with G_1 connected to a high resistor for signal-extraction.

It should be pointed out that the energy resolution will be much more improved by widening the spacing d_3 between the collector and the screen grid, or by mounting a guard ring around the collector or the signal grid. The former procedure will be more effective than the latter, since it will not only reduce σ, but also lower the noise level by diminishing the collector capacity.

particles with close energies is first possible with a double-grid arrangement.

6. Applications

6.1. ELECTRONIC COLLIMATION

Electronic collimation is one of the most important applications of the grid pulses. Bochagov *et al.*[1]) demonstrated that the alpha particles emitted nearly perpendicularly to the cathode may be selected electronically† by counting only those

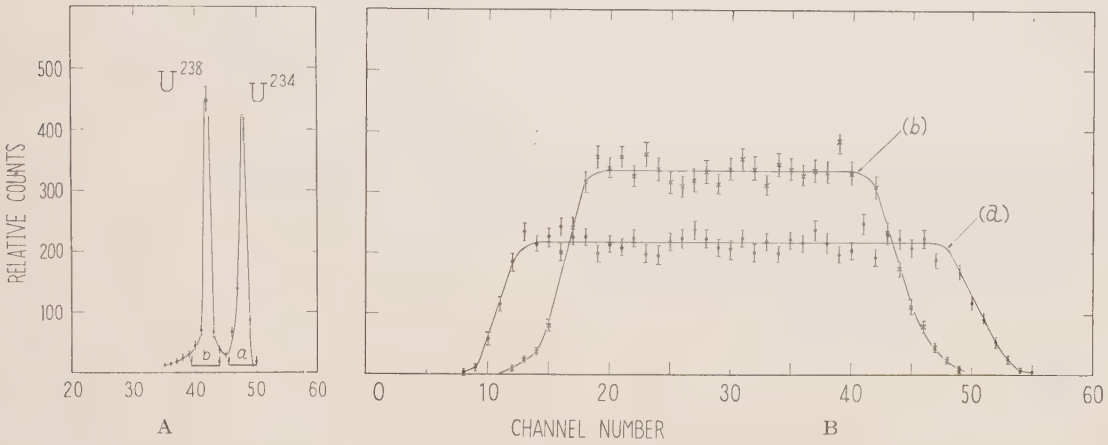

Fig. 8. Pulse-height distribution of collector pulses (A) and grid pulses (B) due to alpha particles from natural uranium.

For comparison, we measured the energy spectrum of the same alpha particles *without* the screen grid. In the actual measurement, G_1 was removed and G_2 connected to a high resistor. The result is given in fig. 7B, showing an energy resolution as poor as 17%. For the electrode arrangement and the input circuit used, the capacities c_1, c_2, c_3 (see fig. 4A), together with the ratio $\overline{X}/d_1$, were just as quoted in sec. 3, giving $(\Delta V_c/V_c)_{calc} = 15\%$. This is in good accordance with the observed value.

Fig. 8A shows the energy spectrum for natural uranium, about 50 μg/cm^2 thick, obtained under the double-grid arrangement. Fig. 8B gives the pulse-height distributions of those *grid*-pulses which were counted in coincidence with a collector pulse in the range (a) or (b) indicated in fig. 8A. The two rectangular distributions, (a) and (b) in fig. 8B, are interpreted as showing the isotropy of the alpha particles from U^{234} and U^{238} separately. It is clear that such a separate measurement of angular distribution among the groups of alpha collector pulses which are in coincidence with a grid pulse of an amplitude close to $V_{g,\,min} = (Q_0/C_g)\{1 - (R^*/d_1)\}$. Since the whole area of the source is effective, the method enables a very luminous counting compared to the collimation with multi-hole collimators. In addition, the method of itself accomplishes a marked elimination of backgrounds (see sec. 6.3).

In a single-grid chamber, however, simultaneous extraction of pulses from both the grid and the collector is necessarily accompanied by an increase of shielding inefficiency factor σ for the grid. It is thus required to limit the pulse-height of the grid pulses to a very narrow range in order to reduce the spread due to σ (see eq. (4)) of a line in the energy spectrum down to the order of noise level. This limitation for the grid pulse-height is generally much

† Hanna has independently suggested that the cathode-grid space may be used in order to get information on track orientation. Cf. G. C. Hanna, Article in Experimental Nuclear Physics, Vol. III, E. Segrè, Ed. (John Wiley & Sons, Inc., New York, 1959).

more severe than required merely to reduce the effect of source thickness. This implies that the collimation angle must be unnecessarily small at a sacrifice in the counting rate.

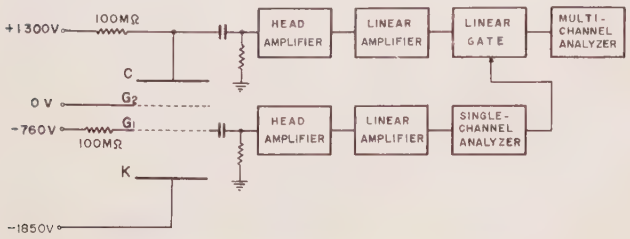

Fig. 9. Circuit for the electronic collimation.

Fig. 9 gives the block diagram of a circuit for the collimation. Fig. 10 illustrates the effect of such a collimation on the energy spectrum of alpha particles from natural uranium with a moderate thickness ($\approx 80\ \mu g/cm^2$). The minor peak due to U^{235} is clearly observed under the electronic collimation as shown in A, whereas it is rather vague without collimation (shown in B). The pulse-height range determining the collimation angle is shown with a hatched area in the total distribution of grid pulse-heights given in C.

It is also possible to select only those alpha particles which are emitted into any direction θ with the help of the same circuit. This method may

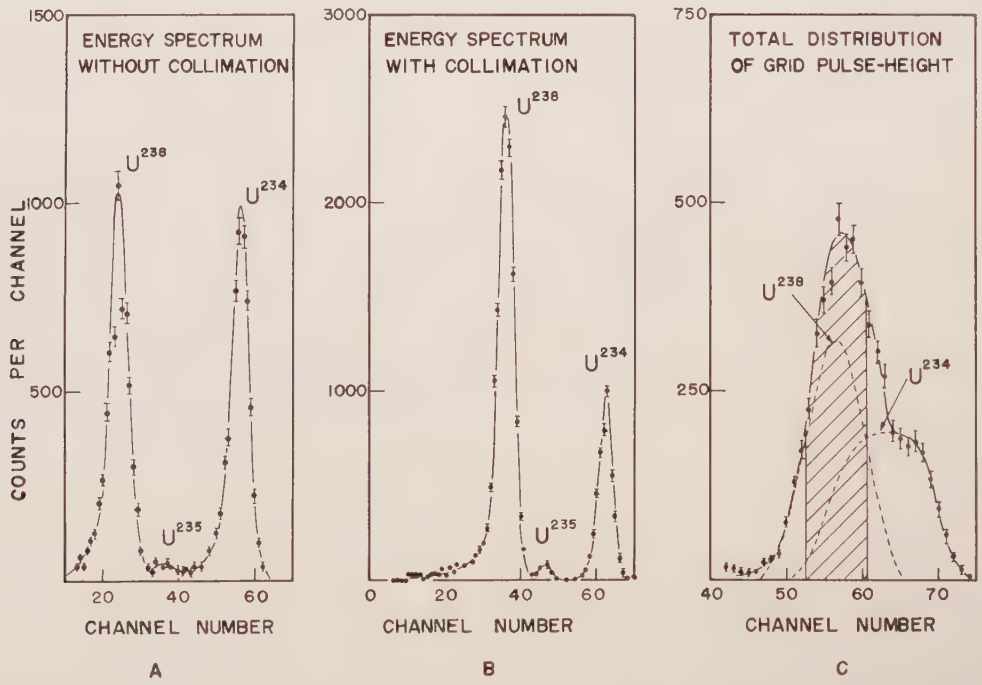

Fig. 10. Effect of electronic collimation on the energy spectrum of alpha particles from natural uranium, about 90 $\mu g/cm^2$ thick. A: under the collimation; B: without collimation.

Now in a double-grid chamber σ can be readily made practically negligible. Hence the solid angle for collimation may be taken several times as large compared to the case of single-grid to suppress the low-energy tail of a spectral line due to thickness down to the noise level. Thus it is possible to obtain a counting rate several times higher than the single-grid collimation.

be applied to measure σ for the chamber under use, or to study the angular dependence of columnar recombination, electron attachment or the electron collection at the grid in the filling gas used. Indeed, it was by this method that the authors measured σ for our chamber to be about 2%. Also, it has been confirmed by the same method that the electron collection to the screen grid G_2, artificially made to

take place in the chamber filled with A + 4% CH_4, shows a small, nevertheless definite angular dependence.

6.2. MEASUREMENT OF THE ANGULAR DISTRIBUTION OF NUCLEAR REACTIONS

The double-grid chamber can be conveniently used for a rapid measurement of the angular distribution of alpha particles or protons from a nuclear reaction. A thin target is placed on the cathode and irradiated by neutrons or gamma rays incident at a right angle. The pulse-height distribution of the grid pulses to be obtained with the circuit given in fig. 6 will then just represent the angular distribution (in the laboratory frame) in $\cos\theta$ of the particles with a selected energy for $0 < \theta < \frac{1}{2}\pi$.

The primary advantage of the method consists in the high efficiency of detection for product particles. Almost all the particles with the particular energy entering the solid angle of 2π are counted to give angular information. Besides, the back-d grounds due to recoils and reaction products from other electrodes than the cathode are automatically rejected in this method for the reason to be described in sec. 6.3. Moreover, angular distribution directly obtained in terms of $\cos\theta$ is sometimes very convenient for physical interpretation.

As a preliminary test of the method, measurements were performed on the angular and energy distributions of proton recoils from a paraffin radiator[9]). The radiator, about 0.6 mg/cm² thick, was placed on the cathode of the chamber and irradiated perpendicularly by d–d neutrons (E_n = 2.48 MeV) from a Cockcroft-Walton accelerator., The gas filling used was 2.17 atm of pure argon without any polyatomic admixture to minimize gas recoils.

Fig. 11 shows the energy spectrum of recoils thus obtained. The well-known rectangular distribution is reproduced fairly well. Backgrounds mainly due to recoil protons from the collector and the insulators were reduced considerably by the coincidence counting between the collector and the grid. The remaining backgrounds were subtracted from the counts with the radiator.

[9]) I. Ogawa, St. Paul's Review of Arts and Sciences, No. 11 (1961).

Fig. 12 gives the observed pulse-height distributions of the grid pulses for recoil energies indicated by hatched areas in fig. 11. For both energies E_{pA} and E_{pB}, the distribution shows a narrow peak at

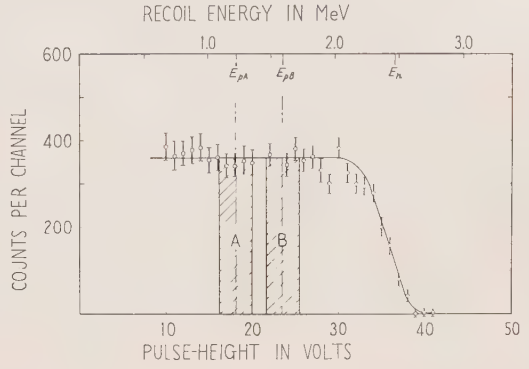

Fig. 11. Energy spectrum of proton recoils from a thin radiator, about 0.6 mg/cm² thick.

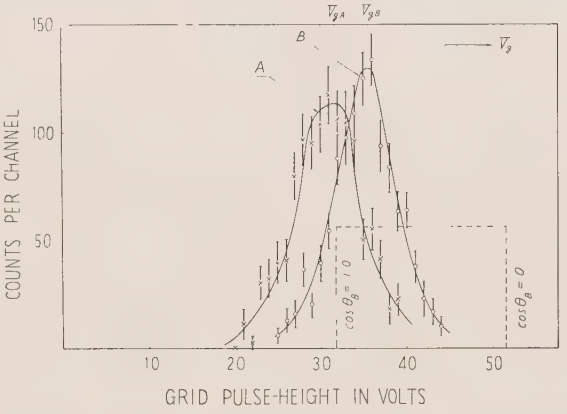

Fig. 12. Pulse-height distributions of grid pulses showing the angular distributions (in the laboratory frame) of recoil protons with energies indicated in fig. 11 by hatched areas.

different positions. This is just as is expected from the familiar relation $E_p = E_n \cos^2\theta$, where E_p denotes the recoil energy and θ the recoil angle. If the recoils with the energy E_p were isotropic in the laboratory frame, then the distribution would be a rectangular one as shown in fig. 12 by a broken line. The resolution in $\cos\theta$ is mainly determined by the amplifier noise.

6.3. LOW-BACKGROUND COUNTING

One of the main sources of background in an ionization chamber is the alpha particles from the radioactive contamination on the collector and the

grid. When the chamber is irradiated by fast neutrons, recoil protons from the hydrogeneous contamination on these electrodes often constitute a dominant origin of background.

Now it can be shown from a simple consideration[10]) that the grid pulses due to those background particles are essentially of the opposite (positive) polarity compared to those due to particles originated from the cathode. Making use of the fact, we may reduce the background considerably by counting only those collector pulses which are accompanied by a *negative* grid pulse.

In fact, we have succeeded in reducing the background by a factor of about three in a tentative test of the method attempted without paying any particular attention to the cathode material. Better performances may be obtained if we use low-background material for the cathode.

Precisely speaking, grid pulses due to particles from G_1 (the grid facing the cathode) are preceded, in general, by a *negative* pulse of small magnitude[6]). Taking the fact into account, background grid-pulses should be discriminated by a slightly negative bias voltage. The bias will also help to eliminate the random coincidence of background collector pulses with the grid noise.

The method will enable the low-background spectrometry of weak alpha rays over a broad range of energy without any loss in the counting efficiency.

Mayneord and Hill[11]) have stated that the two-electrode cylindrical chamber, though limited in the energy resolution, is definitely superior to the gridded chamber with respect to the low-background character, since the larger electrode area in the latter will result in an increased background. By the method described here, however, a low-background performance at least comparable with the cylindrical chamber may be accomplished in a gridded chamber with a higher resolution in energy.

In some cases, cathode pulses may be used instead of grid pulses. Although this alternative method does not require a *double*-grid, it involves a rather critical adjustment of the gas pressure and of the discriminator bias, and may be probably less universal.

[10]) T. Doke, J. Phys. Soc. Japan, to be published.

[11]) W. V. Mayneord and C. R. Hill, Nature **184** (1959) 667.

6.4. MEASUREMENT OF α–γ ANGULAR CORRELATION

Another important application of the chamber will be the measurement of angular correlation between the alpha particles and the gamma rays emitted in cascade. The basic advantage of the grid-pulse method as applied to such a measurement has been already discussed by Bochagov *et al.*[1]). By the use of a double-grid chamber, separate correlation measurements on two alpha groups having nearly equal energies would be made possible.

7. Conclusion

The double-grid chamber we have constructed proved to be useful in several applications. With the chamber, the grid-pulse method originated by Bochagov *et al.* were greatly improved, with little complication in construction and operation. In addition, a new method of background discrimination with the grid pulses was found to be promising. The chamber may be superior to the recent solid-state detectors with respect to the luminosity and the availability of angular information.

It should finally be mentioned that the luminosity and the low-background performances would be improved significantly if we construct a double-grid chamber of a *cylindrical* type, under a tolerable sacrifice in the linearity between V_g and $\cos\theta$.

The authors sincerely express their gratitude to Professor E. Tajima for reading the manuscript and for many valuable comments. Also, one of the authors (I.O.) would like to thank Professor P. Huber and Professor E. Baumgartner for their hospitality and encouragements during his temporary stay at the University of Basel. Finally, the authors are greatly indebted to Mr. A. Sasaki for continuous aid in electronics.

NUCLEAR INSTRUMENTS AND METHODS 13 (1961) 177–182; NORTH-HOLLAND PUBLISHING CO.

FAST TUNNEL DIODE CIRCUITS FOR NaI(Tl) DETECTORS†

GEORGES C. BRET†† and ERWIN F. SHRADER

Case Institute of Technology, Cleveland, Ohio. U.S.A.

Received 22 June 1961

A detector system using a NaI(Tl) crystal, an RCA 6810A photomultiplier and a tunnel diode discriminator is described. The output from the anode of the high gain photomultiplier corresponding to the emission of three photoelectrons from the photocathode even though it is not big enough to drive an electron tube from cut off to saturation can, however, easily trigger a tunnel diode fast discriminator. The system introduces a 4 mμsec spread in time when detecting gamma rays over a wide range of energies and only 1 mμsec when a 10% energy selection is performed using a parallel slow channel. A tunnel diode time-to-pulse height converter having a resolving time better than 2 mμsec which can be used in conjunction with the system is also described.

1. Introduction

The circuits to be discussed here were developed for the study of (n,γ) angular correlation in (p,nγ) and (n,n'γ) reactions. In this type of experiment the gamma ray channel must have an extremely good resolution both in time and in amplitude to discriminate against the background. NaI(Tl) has been chosen because of its good energy resolution and efficiency, but since the light signal from the crystal has a long decay time we have been primarily concerned with the possibility of obtaining fast standard pulses related to the first photons emitted in the crystal. This has been achieved using a tunnel diode fast discriminator. The resolving time of this detector is about 4 mμsec over a wide range of gamma energies and only 1 mμsec when a 10% energy selection is performed using a parallel slow channel.

The experiments to be described were carried out with the pulsed Van de Graaff generator at Case Institute of Technology. In this type of generator the capture gamma photon source can be pulsed by means of sweeping the proton beam across an aperture giving bursts a few mμsec long, the repetition time being 110 mμsec. The pulsing system enables one to observe groups of emitted neutrons by the usual time-of-flight technique using a time-to-pulse height converter. A time-to-pulse height converter of a very simple kind involving a tunnel diode circuit has been designed for this purpose. The gamma ray detection system which includes the Na(Tl) crystal, photomultiplier, fast discriminator and the converter has a 4 mμsec resolution over a wide range of pulse heights.

2. Time Resolution Considerations

As we have stated the use of a Na(Tl) detector has been necessary to achieve the required gamma energy resolution. For timing purposes it has been shown[1]) that the variance in the timing signal is in general smaller for the non-linear method than for the linear method. However, the non-linear method introduces systematic variations of the timing signal with pulse amplitude. If one desires to operate the detector over wide ranges of signal amplitude some method must be used to eliminate this dependence. One method is to operate the non-linear element on as few photoelectrons as possible. In this way the systematic dependence of the timing signal can be made comparable to the variance in timing due to the statistical nature of the detection process.

† Work supported in part by the United States Atomic Energy Commission.

†† Fulbright grantee from Ecole Superieure d'Electricite of Paris. Present address 12 Cours d'Herbouville, Lyon 4, France.

[1]) S. Colombo, E. Pignanelli and E. Gatti, Nuovo Cim. 5 (1957) 1739.

[2]) M. Vergne's and R. David-Boyer, J. Phys. Radium 21 (1960) 65.

A Na(Tl) crystal coupled to a photomultiplier gives rise to a mean distribution of photoelectrons from the photocathode[2]).

$$I(t)\,\mathrm{d}t = R\,\lambda\,\mathrm{e}^{-\lambda t}\,\mathrm{d}t$$

where $I(t)\,\mathrm{d}t$ is the number of photoelectrons emitted in an interval between t and $t + \mathrm{d}t$, R is the total number of photoelectrons, and $\lambda^{-1} = \tau$ is the Na(Tl) decay time which is of the order of 0.25 μsec. It has been shown that for reasonable light collection efficiency and photoelectron conversion efficiency $R \approx E$, the energy of the photon expressed in keV.

The mean time required for the emission of the first N photoelectrons is

$$t = \frac{\tau N}{R} \quad \text{if} \quad \frac{N}{R} \ll 1\,.$$

The variance in the time of emission can be shown under these same conditions to be[3])

$$\overline{\Delta t^2} = \frac{\tau^2 N}{R^2}\,.$$

The mean voltage obtained by collecting the charge from the first few photoelectrons is of course

$$V = \frac{Ne\bar{G}}{C}$$

where e is the electronic charge, $\bar{G}$ the mean current gain of the photomultiplier and C the capacitance of the anode of the photomultiplier and associated wiring capacitance. If this voltage pulse is used to work on a non-linear element such as a discriminator there are at least two other effects which contribute to the variance of the time at which the signal is detected and these are associated with the statistics of the photomultiplier. One is the variance of the gain of the photomultiplier and the other is the variance of the transit time from photocathode to anode.

The variance of the centroid of the pulse whose duration is that required to collect a certain charge Q is approximately[1])

$$\overline{\Delta t^2} = \frac{\tau^2}{2R^2}\,(1 + \varepsilon_{\mathrm{A}}^2)\,N + \frac{\varepsilon_{\mathrm{ph}}^2}{N}\,; \qquad N \geqslant 1\,, \qquad (2)$$

where $\bar{N} = Q/e\bar{G}$ i.e. mean number of photoelectrons required for charge Q, $\varepsilon_{\mathrm{A}} (= \frac{1}{3})$ is the fractional variance of the gain G, and $\varepsilon_{\mathrm{ph}}^2$ is the variance ascribed to the transit time jitter of single photoelectron pulses here assumed to be of the order of 1 or 2 mμsec.

To keep the variation in $\bar{t}$ with R over a considerable range of pulse amplitudes comparable to the sqaure root of the variance due to the statistical processes requires N to be of the order of only a few photoelectrons.

If say this number is of the order of three, then for a photomultiplier with a maximum gain of 2×10^7 and an output capacity of 30 pF three photoelectrons will produce on the average an output voltage of approximately 0.10 V. Therefore, further signal amplification is usually needed when using conventional discriminators[4]). We shall see however, that if we use a simple tunnel diode circuit the voltage required to trigger the diode is about 0.1 V.

3. Tunnel Diode Circuit

There is no simple way to analyze the transient behavior of a circuit involving non linear devices such as a tunnel diode but the investigation of some limiting cases can give us some useful insight into the general behavior of the circuit.

Let us suppose first that no stray capacity exists between the anode of the phototube and the ground and that the tunnel diode is the only load as shown on fig. 1(a). The photomultiplier behaves like a current generator and at any moment the load line on the diode characteristics is parallel to the voltage axis.

If initially the stable point is ξ an increase of current will bring it to δ and then the voltage across the diode will jump from δ to η taking a value V_1, since the current source is supposed to have an infinite internal resistance.

If on the other hand we suppose that the stray capacity is big, and that the main part of the photomultiplier current goes into it, the diode is effectively fed by a voltage generator and the load line of the circuit is parallel to the current axis (fig. 1(b)) and only a variation of current occurs through the diode. This current could be recorded by means of a

[3]) R. Post and L. Schiff, Phys. Rev. **80** (1950) 1113.

[4]) R. E. Holland, F. J. Lynch and E. N. Shipley, Bull. American Phys. Soc., Series II, **5** (1961) 424.

small resistance in series with the diode but the current signal reproduces merely the shape of the diode characteristic.

Since in the real case we have a stray capacity C of about 30 pF, we must introduce a resistance R to isolate the diode from C as shown on fig. 1(c).

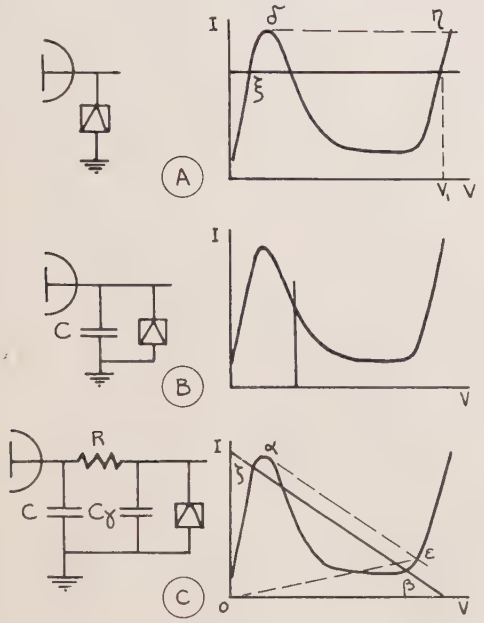

Fig. 1. (a) Tunnel diode operation for photomultiplier idealized as a current generator; (b) Tunnel diode operation for photomultiplier acting as a voltage generator i.e. large output capacity; (c) Actual circuit for using tunnel diode as a photomultiplier output discriminator.

The value of this resistance must fulfill three conditions:

1. If C_γ is the parallel capacity across the diode the time needed to charge C_γ through R must be smaller than the revolving time Δt

$$RC_\gamma < \Delta t .$$

2. Let us call ρ the maximum resistance of the diode during a transient period, such a maximum would be given for instance by the slope the line $O\varepsilon$ on fig. 1(c). C must have a small influence on the behavior of the diode; therefore:

$$RC >> \rho C_\gamma .$$

If we suppose the following values:

$$\rho = 800\Omega$$
$$C_\gamma = 5 \text{ pF}$$
$$\Delta t = 2 \text{ m}\mu\text{sec}$$
$$C = 30 \text{ pF} .$$

The first condition yields:

$$R < 400\Omega . \tag{3}$$

The second condition yields:

$$R >> 133\Omega . \tag{4}$$

3. If we want an output pulse which does not depend on the input current after the triggering period the second stable point ε on the diode characteristic must be on the second vertical part of the characteristic when the diode switches as shown on fig. 1(c).

This implies a maximum slope of the load line $\overline{\alpha\varepsilon}$ and therefore a minimum value of the resistance R which is for the diodes used:

$$R > 500\Omega . \tag{5}$$

We chose:

$$R = 500\Omega$$

which fulfills roughly conditions (3), (4) and (5). The diodes we use switch for a current $I_s = 1$ mA. If the zero signal current I_0 through the diode is 0.8 of the switching current a signal of amplitude 0.1 V will trigger the circuit. This value of I_0 should be limited to $0.8I_s$ or less in order to avoid instabilities.

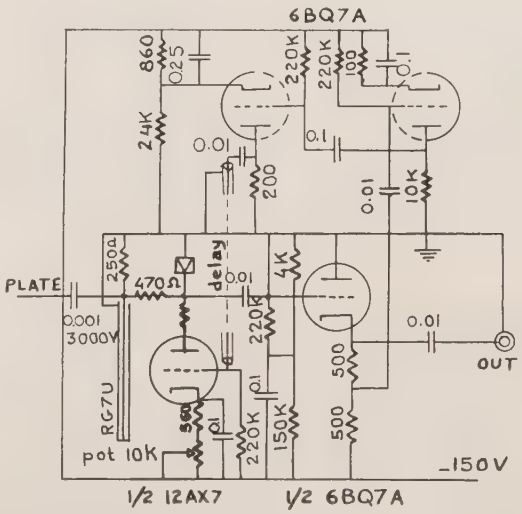

Fig. 2. Schematic circuit diagram of the fast tunnel diode discriminator.

4. Fast Discriminator

The circuit is built around a 1N2929 or a 1N2940 General Electric tunnel diode having a peak current of 1 mA. Fig. 2 shows the schematic circuit dia-

gram. The zero signal current through the diode is provided by a 12AX7 tube. A reset circuit involving a 6BQ7A tube applies negative pulses delayed by an RG7U cable to the grid of the 12AX7 after each gamma pulse in order to bring the diode back to its original stable condition. The load of the phototube is a 250 resistances in parallel with a short piece of RG7U cable (7 mμsec) which eliminates the possibility of damage to the diode by large signal pulses from cosmic rays.

The wave forms shown on fig. 3 were obtained using the 0.66 MeV gamma ray of Cs^{137}. Fig. 3(a) gives the shape of the slow pulses observed at the eleventh dynode. Fig. 3(b) gives the shape of the fast output pulses after the clipping cable. Fig. 3(c) gives the shape of the pulses coming from the diode. One can see that the rise of this output signal is always the same and is determined more by the diode circuit than by the size of the input pulses. In this experiment the gamma rays whose energy was bigger than 0.4 MeV were recorded.

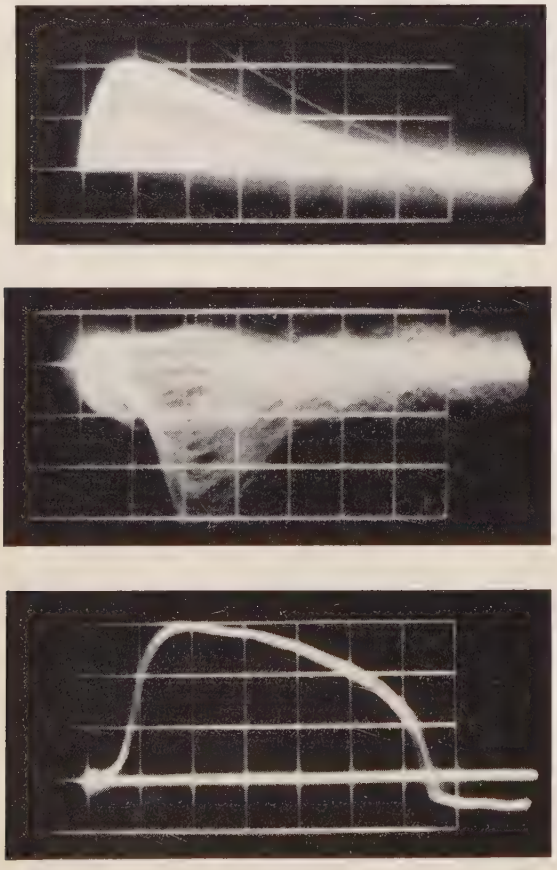

Fig. 3. Pulse wave forms from the detector-discriminator system for Cs^{137} gamma rays; (a) Slow pulses at eleventh dynode: Sweep speed 0.25 μsec/cm, sensitivity 0.1 V/cm; (b) Fast pulses at clipping cable: Sweep speed 10 ns/cm, sensitivity 0.1 V/cm; (c) Shaped pulses from tunnel diode: Sweep speed 20 ns/cm, sensitivity 0.15 V/cm. Wave forms displayed on a Tektronix Model 517 A CRO.

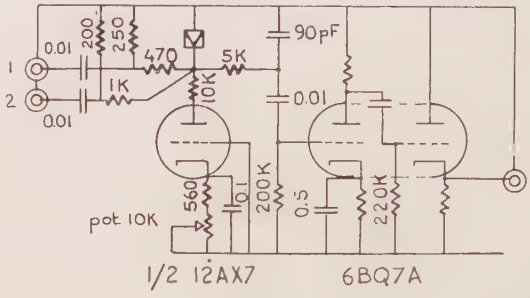

Fig. 4.
Schematic circuit diagram of the time-to-pulse height converter.

5. Time to Pulse Height Converter

Let us go back to fig. 1C and suppose that the normal setting of the diode is the point ζ. If we apply a short positive pulse the diode will switch to the point β giving rise to a constant voltage until a negative signal is applied. If we integrate the resulting rectangular signal we have a time to pulse height converter of a very simple kind. Since we are not really integrating the output voltage of the diode alone but the sum of this output voltage and of the two pulses we had used to switch the diode this converter must work with very short pulses of a relatively well defined size. Such pulses are available from the fast discriminator after proper clipping "start" and from the beam deflection oscillator "stop".

The converter involves a 1N2960 or a 1N2939 General Electric tunnel diode fed by a 12AX7. The complete circuit is shown on fig. 4. Two imputs are available: Imput 1 receives "start" pulses coming from a discriminator of the sort described earlier after amplification and clipping. Input 2 receives "stop" pulses coming from the oscillator pulsing the beam of the Van de Graaff generator. An amplification and a cathode follower enable us to feed directly a 256 channel pulse height analyser.

It is possible to use the discriminator described earlier as a time-to-pulse height converter since both circuits work in the same way. Nevertheless

pulses coming from the photopulse have different sizes and since the converter integrates the total charge going through the diode the resolving time is good only for a drastic energy selection in a parallel slow channel. Even so it was never possible during the experiments to obtain a resolving time better than 9 mμsec.

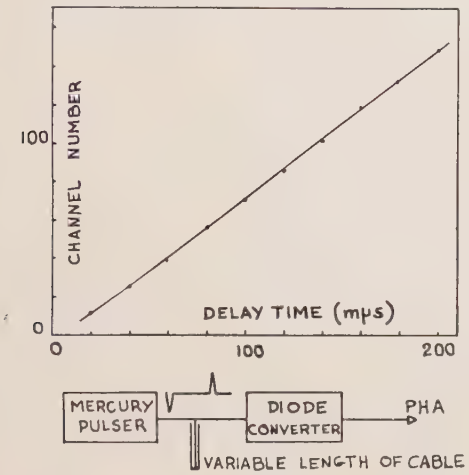

Fig. 5. Linearity and precision of the time-to-pulse height converter. The mercury pulses gives negative pulses 2 mμs long which start the converter, a variable length of cable reflects a positive pulse stopping the converter after a known variable time.

6. Tests and Results

A check of the stability and of the linearity of the converter has been done using a mercury pulser giving negative 2 mμsec long pulses of various amplitudes. The pulser was connected to one of the inputs of the converter and to a shorted cable reflecting a positive pulse after a time depending on the length of the cable (see fig. 5). The other input of the converter was grounded through a 200 Ω resistance. The output signal of the converter was displayed on a 256 channel pulse height analyser. The uncertainty in time was less than 2 mμsec for all time intervals. The converter is fairly linear between 20 and 200 mμsec but is sensible to the size of the input pulses. With pulses 2 mμsec long and of 0.3 V amplitude we obtained pulses corresponding to a given time T. If the amplitude was now increased to 1 V it results in a change in time ΔT of 3 mμsec for any time T.

A test of the effect of overlapping start and stop pulses was made using "start" pulses from the 0.66 MeV gamma ray of Cs^{137} on one input and "stop" pulses coming from a 4.6 Mc/s oscillator on the other input. The random time spectrum to be expected is displayed on fig. 6 which shows unusable regions totalling only 10 mμsec.

Since this apparatus was designed to be used in a time of flight measurement we established the minimum revolving time of the detector associated with the fast discriminator by the following method. The beam of the Van de Graaff generator was pulsed and the protons striking an aluminum target produced gamma rays up to 12.5 MeV from the reaction A^{27} (p,γ) Si^{28}. The gain of the 6810A photomultiplier was set in such a way that any gamma ray greater than 5 MeV would trigger the discriminator and could give a fast pulse. These pulses started a time to pulse height converter of the type described by Weber *et al.*[5]). The stop signal was derived from the deflection voltage used for pulsing the beam. A time spectrum was displayed

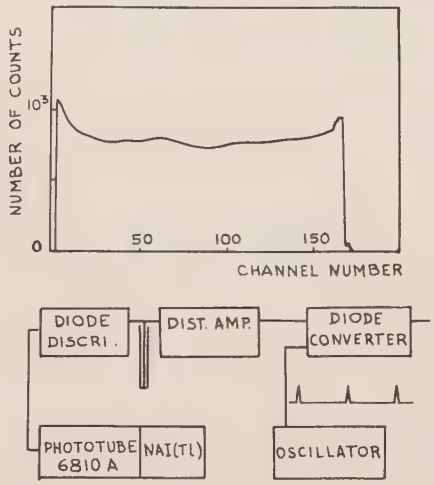

Fig. 6. A random spectrum was obtained using two independent sources. The converter was started by the gamma rays coming from a Cs^{137} source and stopped by the pulses coming from a 4.5 Mc/s oscillator. The output was displayed on a 256 channel pulse height analyser. The total length of the spectrum, 165 channels, represented 100 mμsec.

on a 256 channel pulse height analyser for a proton energy $E_p = 2.3$ MeV. This spectrum is shown on fig. 7.

[5]) W. Weber, C. W. Johnson and L. Cranberg, Rev. Sci. Instr. **27** (1956) 166.

The width of the line is 6 mμsec and the background is extremely small (less than 5 counts per channel).

Since the length of the protons bursts was known to be of the order of 4 mμsec several such spectra were recorded for different protons energies. Since in this method of pulsing the beam the length of the proton bursts is proportional to the square of the energy of the proton one can plot the square of the width of each time display against the square of the proton energy and obtain a linear plot. On extrapolation to zero energy we obtain the square of the resolving time of the electronics alone. This resolving time is 4 mμsec as seen from curve (a) of fig. 8.

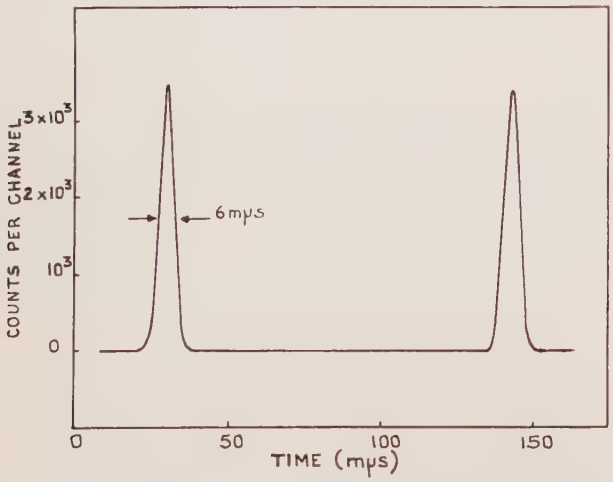

Fig. 7. The resolving time of the discriminator alone as determined by using the high energy gamma rays produced in the reaction Al^{27} (p,γ) Si^{28}. Using a pulsed proton beam of the Van de Graaff generator a time to pulse height converter was used to display this time spectrum on a 256 channel pulse height analyser.

When using the 0.9 MeV gamma ray occurring in the reaction Mn^{55} (p,n) Fe^{55} which is discussed later, the tunnel diode time to pulse height converter gives similar results. The width of gamma ray time distribution as a function of proton energy is shown on the curve (b) of fig. 8.

Both of these experiments showed that for a proton energy $E_p = 2.4$ MeV the length of the protons bursts was 3 mμsec. Under these same conditions another spectrum was recorded using the fast tunnel diode discriminator and the vacuum tube time to pulse height converter and employing a 10% energy selection on a parallel slow channel. The gamma rays were provided by the reaction Al^{27} (p,γ) Si^{28}, and the purpose of the experiment was to determine the resolving of the electronics alone when using high energy gamma rays (negligible time uncertainty introduced by the statistics

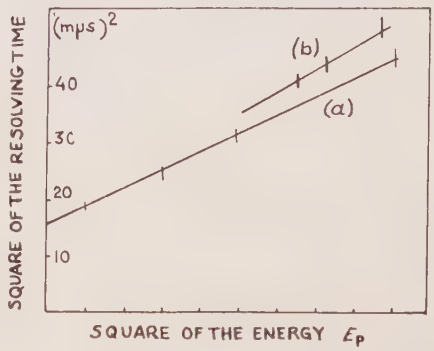

Fig. 8. The time width Δt of the spectrum shown on fig. 7 is composed of two parts; the uncertainty introduced by the electronics the mean value of which is Δt_1 and the length of the bursts of protons the mean value of which is Δt_2. Δt_2 is proportional to the proton energy E because of the pulsing device used. Plotting $(\Delta t_1^2 + \Delta t_2^2)$ as a function of E_p^2. One can obtain the resolving time of the electronics alone by extrapolating to $E_p = 0$. The curve (a) was obtained with the Al^{27} (p,γ) Si^{28} reaction and a conventional time to pulse height converter.

of photoelectron emission) and constant size pulses. The resulting time spectrum is shown on fig. 9. One can see the flat top showing that the resolution time from other causes is much smaller than the length of the proton bursts, it seems to be of the order of 1 mμsec and is probably mainly due to the electron transit time spread in the photomultiplier.

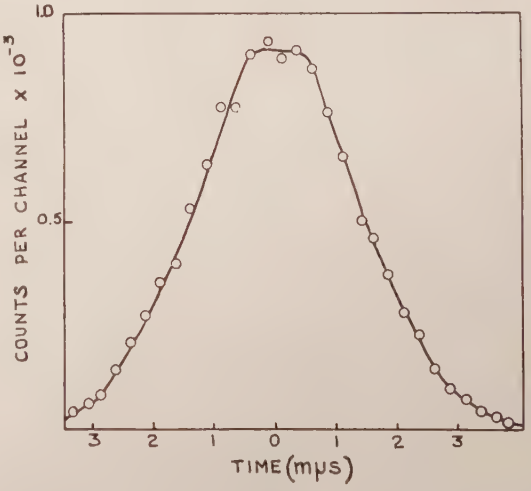

Fig. 9. This spectrum is similar to the spectrum displayed on fig. 7 but 10% energy selection of the gamma rays was done in a slow channel. The length of the bursts of protons was about 2.5 mμsec. The uncertainty in time introduced by the whole detector is of the order of 1 mμsec.

NUCLEAR INSTRUMENTS AND METHODS 13 (1961) 183–189; NORTH-HOLLAND PUBLISHING CO.

IMPROVED FISSION COUNTING METHOD FOR URANIUM ISOTOPE ANALYSIS

GÖSTA NILSSON

AB Atomenergi, Nuclear Chemistry Section, Stockholm, Sweden

Received 19 May 1961

The fission rates of an unknown sample and a standard sample are compared by a simultaneous fission counting of the samples when placed back-to-back in a pile neutron flux, the radio of the uranium contents of the samples is determined spectrophotometrically and ε = atom % U^{235} (unknown)/atom % U^{235} (standard) thereby calculated. The useful range of this method was extended by increasing the resolving power of the fission counter, the systematic error in ε was re-determined and found to be within 0.04 % and the precision was increased. It was thus found using 100–140 μg samples of uranium that, in the range 0.72–100 % U^{235}, ε in a single determination can be determained with a precision of $\pm$ 0.7 % with 95 % confidence limits. Almost the same relative precision in atom % U^{235} of the unknown sample can be ontained by using as standard samples uranium isotope standards from the National Bureau of Standards.

1. Introduction

If an unknown sample (u) and a standard sample (s) are placed in the same thermal neutron flux for equal times, and if fissions in U^{234} and U^{238} are neglected, then

$$\varepsilon = \frac{p_{235,u}}{p_{235,s}} \sim \frac{F_u/F_s}{A_u/A_s} = \frac{X_F}{X_A} \qquad (1)$$

where p is the abundance of the isotope in atom %, F the number of fissions and A the number of uranium atoms.

In a Geneva paper (1958)[1]), a preliminary report was given of a method where X_F was determined with an air-filled fission counter inside the R1 pile and X_A was determined spectrophotometrically.

The counter consists of two ion chambers, with a common high tension electrode, fitted to one end of an aluminium tube, the other end being connected to an iron block for radiation shielding (fig. 1). The two uranium samples (standard and unknown) are placed back to back on the common sample holder shown in fig. 2. The sample holder is charged outside the reactor and then introduced through the cavity shown in fig. 1 and loosely fitted to a movable steel rod by a fish-tail shaped connection. The rod is used to transport the sample holder to and from the position shown in fig. 2 (counting position). This arrangement permits sample changing at full reactor power (1 MW).

When in the counting position, the sample holder is at the same time the high tension electrode due to its contact with the spring loaded pin, P_1. It is also accurately guided by means of its cylindrical section and a steel pin, P_2, in such a way that its front part and the two collector plates, which function at ground potential, form two almost identical ion chambers.

To eliminate the small difference in the counting efficiencies of the two detector systems, each sample in a pair is counted in both chambers. They are interchanged by pulling out the sample holder a little, rotating it through 180° and pushing it back into position. This is done by means of the steel rod. To make the counting times equal for the two samples, the scalers are started and stopped with the same switch. No time measurement is needed.

The fission ratio is calculated from the relation

$$X_F = \sqrt{\left(\frac{N_{u,1}}{N_{s,2}}\right)_{t_1}\left(\frac{N_{u,2}}{N_{s,1}}\right)_{t_2}}, \qquad (2)$$

where $(N_{u,1})_{t_1}$ is the number of fissions recorded in time t_1 when the unknown sample is placed in ion chamber 1, and so on.

The uranium samples are prepared by electroplating 100–150 μg of uranium on to Pt discs[1]). The diameter of the deposit is about 18 mm and the sample thickness is so small that self-absorption can be neglecred. When the determination of X_F has been made, the uranium deposit is quantitatively removed from the discs for spectrophotometric analysis[1]).

Due to the long resolving time of the air-filled counter (50 μsec), ε had to be extremely small or the counting rate impractically low to avoid large systematic errors due to counting losses. This considerably limited the usefulness of the method since, with a small ε, $p_{235,u}$ had to be very close to $p_{235,s}$ and it was impossible to cover the intervals between the uranium isotope standards made available by the National Bureau of Standards at the end of 1958.

This paper will deal with some changes made in the fission counter to decrease the resolving time to

[1]) G. Nilsson, Progress in Nuclear Energy, Series IX, Vol. 1, Analytical Chemistry (Pergamon Press, 1959) p 104.

0.7 μsec, which makes possible the analysis of unknown samples at every value of $p_{235,u}$ in the range 0.72–100%. The error due to fissions in U^{238} has been re-determined, thus leading to a more reliable estimation of the systematic error of the method which was checked with the measurements on one of the NBS standards. The precision of the method was at the same time increased.

This method needs less uranium and gives a higher precision than the fission counting methods used at U.S. gaseous diffusing plants where the counters consist of a radium beryllium source and four ionization chambers housed in a lead shielding assembly[2,3,4]).

velocity is estimated to be about 3.6 cm/μsec for $E/p > 1$ volt cm^{-1} mm Hg^{-1} as comapred with 0.4 cm/μsec for pure argon. The counter potential was chosen to be −500 V and the electrode spacing 0.6 cm—this will give a collection time of about 0.16 μsec.

The effect on the discriminator bias curve of the gas pressure, p, and the electrode spacing, d, has been studied by Abson *et al.*[7]). They found that the product pd, where d is shorter than the range of both the fission fragments and the α-particles, should lie in the range 0.4–1.0 atm cm. There is, however, no optimum value for this product. With increasing pd, the response to α-particles increases

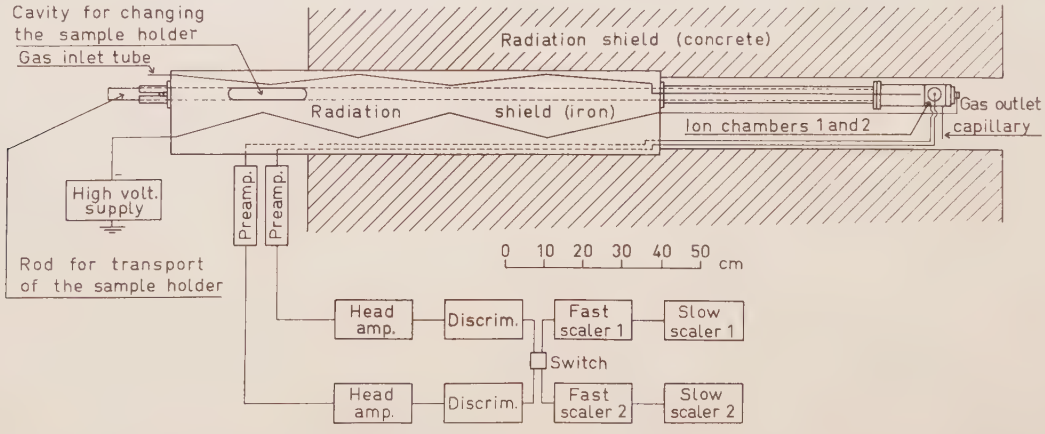

Fig. 1. The fission counter in one of the channels of R1 and a block diagram of the associated electronics.

2. Increase of Resolving Power

In order to decrease the resolving time, the counter was modified to work with a mixture of 98% A and 2% N_2, both of which permit electron collection. As shown by figs. 1 and 2 the counter was provided with a gas inlet tube and a gas outlet capillary. The ion chambers were made gastight by means of O-rings and the electronics was completely changed.

The gas flows through the chambers at a rate of 20 ml/min. After each sample changing a 3 min pre-flushing at the same flow rate makes the counter ready for operation.

The A-2% N_2 mixture was chosen because of its low sensitivity to oxygen[5]). The mixture also gives higher electron drift velocities than argon alone and therefore shorter collection times[6]). The drift relatively more than the response to fission fragments due to their different modes of ionization. In this case, pd equals 0.6 since the pressure is only slightly above atmospheric.

To obtain a high signal to noise ratio, the capacity collector to ground is only 60 pF and the high tension electrode, where the fissile material is located, is at a negative potential. The pulses from each chamber, about 3 mV in amplitude, are fed successively to a pre-amplifier with a gain of about 60, a head amplifier with gain control and variable differentiation time constant (TMC Model AL-4A),

[2]) A. E. Cameron, TID-5213 (1950) 131.
[3]) F. S. Voss, TID-7531 (1957) 130.
[4]) C. L. Truman, Nuclear Scie. and Eng. **6** (1959) 252.
[5]) U. Faccini and A. Malvicini, Nucleonics **13**, No. 4 (1955) 36.
[6]) L. Colli and U. Facchini, Rev. Sci. Instr. **23** (1952) 39.

a Schmitt discriminator with a resolving time of 0.3 μsec, a fast scaler (Hewlett Packard Model 520A), and a slow scaler.

The resolving time of the fast scaler is so short that the resolving time of the entire system only depends on the pulse shape at the discriminator input and on the setting of the discriminator level. As a guide for such a situation, Gillespie[8]) has shown that, when a short resolving time is required, the amplifier integration time constant should be set to a value comparable with the counter collection time and the amplifier differentiation time constant should be set to give the best compromise between resolving time and pulse amplitude. The integration time constant, about 0.15 μsec, is here given by the fixed rise time of the amplifiers. A sufficiently short differentiation time constant could not be selected at the head amplifier. A differentiation time constant of 0.12 μsec is therefore used at the preamplifier input and 5 μsec in the head amplifier.

The bias curves, fig. 3, show that α-pulses are easily discriminated, and there is no risk for α-

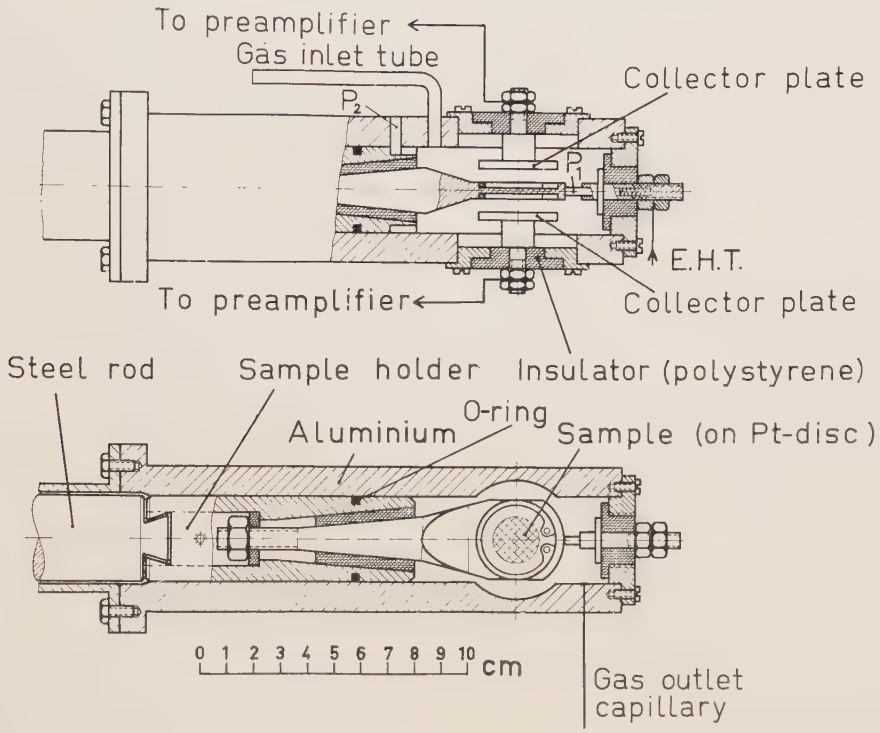

Fig. 2. Detailed view of the ion chambers.

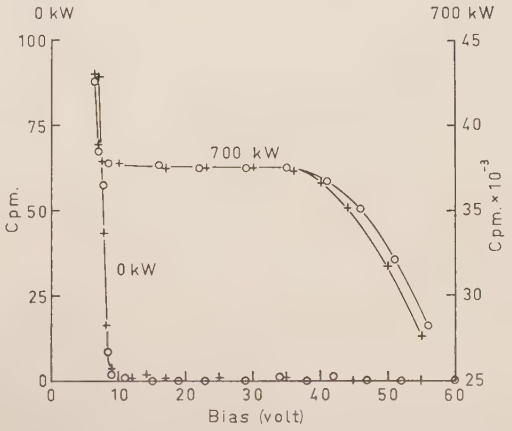

Fig. 3. Bias curves for the ion chambers at 0 kW (noise and alpha pulses) and at 700 kW (noise, alpha and fission pulses). Sample: 0.14 mg nat. U ($\approx$ 200 dpm α) and counter potential = — 500 V.

[7]) W. Abson, P. G. Salmon and S. Pyrah, Proc. of the Inst. of Electrical Eng. **105**, Part B, No. 22 (1958) 349.

[8]) A. B. Gillespie, Signal, Noise and Resolution in Nuclear Amplifiers (Pergamon Press, 1953).

build-up since the maximum α-emission rate (99% U^{235}) is about 5000 per min. The bias setting chosen was 30 volt. The background counting rates at 700 kW are then about 4 cpm for both chambers and the chambers were found not to interact.

The plateau curves are shown in fig. 4. The slightly bent counting rate-reactor power curves, fig. 5, fit the relation $r' = re^{-r\tau}$ where r' is the observed counting rate, r the input pulse rate and τ the resolving time. The resolving time was thus found to be about 0.7 μsec.

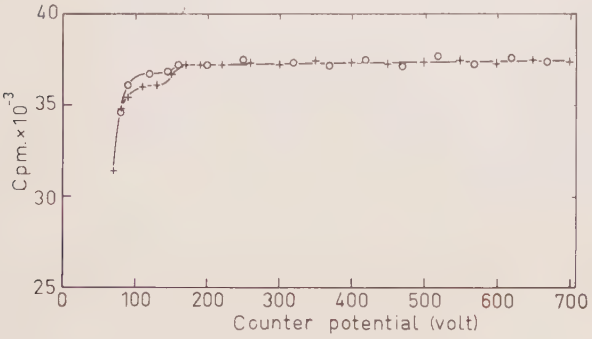

Fig. 4. Plateau curves for the ion chambers at 700 kW. Sample: 0.14 mg nat. U and bias setting = 30 V.

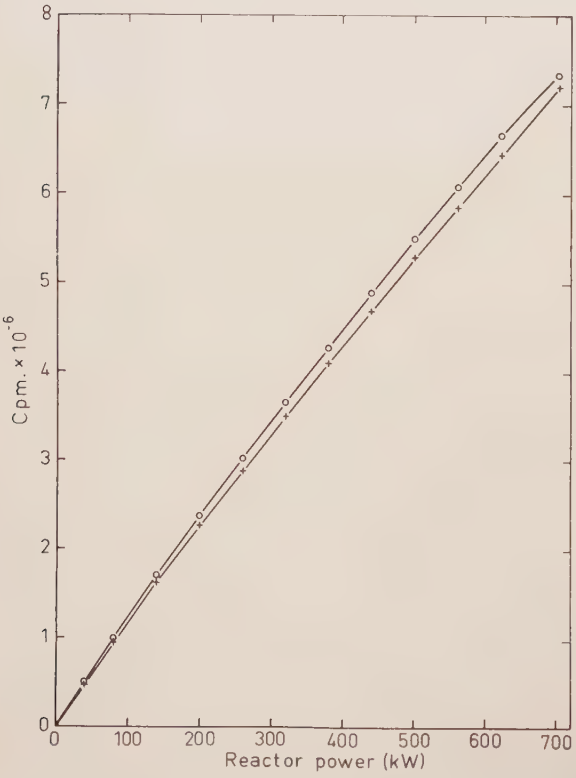

Fig. 5. Counting rate vs. reactor power for the ion chambers. Enriched uranium sample, counter potential = — 500 V and bias setting = 30 V.

3. Estimation of Systematic Errors

In the determination of ε we have to consider systematic errors since ε is calculated from the approximate eq. (1). Another source of such errors is counting losses due to the limited resolving power.

The number of fissions during time t in a uranium sample placed in a neutron flux $\phi(E,t)$ is:

$$F_t = \frac{A}{100}\sum_i p_i \int_0^\infty \int_0^t \sigma_i(E)\phi(E,t)\,\mathrm{d}E\,\mathrm{d}t = \frac{A}{100}\sum_i p_i I_{i,t} \quad (3)$$

where A is the number of uranium atoms, p_i the abundance in atom % and σ_i the cross-section of the isotope i. The summation is performed over the isotopes U^{234}, U^{235} and U^{238}.

If eq. (3) is applied to the unknown and standard samples, we obtain the following exact expression for ε.

$$\varepsilon = \frac{p_{235,u}}{p_{235,s}} = \frac{X_F I_{235,s}\,(1+\alpha_s+\beta_s)}{X_A I_{235,u}\,(1+\alpha_u+\beta_u)} = \frac{X_F I_{235,s}}{X_A I_{235,u}} Z\,, \quad (4)$$

where

$\alpha_s = p_{238,s}I_{238,s}/p_{235,s}I_{235,s}$,

$\beta_s = p_{234,s}I_{234,s}/p_{235,s}I_{235,s}$

and α_u and β_u are the corresponding values for the unknown sample. The time index has been omitted since the samples are counted for equal times (about 30 min) in each position.

The first approximation made in eq. (1) was to put $I_{235,s} = I_{235,u}$ which means that the two samples are in the same neutron flux. This is very nearly true since the samples are separated by a distance of only 2 mm. A calculation has shown that also their mutual flux depression is extremely small.

The second approximation made in eq. (1) was to put Z equal to unity which introduces the systematic error

$$\frac{\Delta Z}{Z} = Z - 1 = \frac{\alpha_s - \alpha_u + \beta_s - \beta_u}{1+\alpha_u+\beta_u}, \quad (5)$$

where β is about 10^{-5} also for high enrichments. A new measurement of α was performed because the old value was unexpectedly high ($\alpha_{max} = 1.7 \times 10^{-3}$) (ref. [1])). An uranium impurity in a thorium sample used for this determination was suspected to cause the high value.

The counter was loaded with a sample of spectroscopically pure ThO_2 and a sample of natural uranium, and the ratio F_U/F_{Th} was then recorded. The same measurement was performed when the counter was in the thermal column of the reactor. The Th-sample activity recorded in the latter case was assumed to be due to a uranium impurity which could thus be corrected for and α was calculated from the relation $\alpha \approx 4.12 p_{238} I_{Th}/p_{235} I_{235}$. In this way we found $\alpha = 5 \times 10^{-6}\, p_{238}/p_{235}$, $\alpha_{max} = 0.7 \times 10^{-3}$ (if $p_{235} \geqslant 0.7204$) and

$$\frac{\Delta Z}{Z} \approx \alpha_s - \alpha_u \approx \frac{5 \times 10^{-4}}{p_{235,s}} \left(1 - \frac{1}{\varepsilon}\right);$$

$$(\alpha_s > \alpha_u\,; \quad 0 < \alpha < 0.7 \times 10^{-3}) \qquad (6)$$

with a maximum value of 0.07%.

The relative systematic error in ε due to counting losses E_τ can be shown to be (Appendix)

$$E_\tau \sim \frac{\tau}{T\sigma^2}\left(\varepsilon - \frac{1}{\varepsilon}\right), \qquad (7)$$

where T is the total counting time and σ the relative standard deviation in X_F due to the counting statistics. For $\tau = 0.7\ \mu$sec, $T = 3600$ sec, $\sigma = 10^{-3}$ and $\varepsilon = 2.13$ which are all approximately valid for the data given in the table of the next section, E_τ is found to be about 0.03%. Since τ is known, this small error can readily be corrected for. (It had been impossible to correct for E_τ when $\tau = 50\ \mu$sec, especially as τ was not completely constant but varied slightly with the counting rate[1]).)

The only systematic error in ε to be considered is then $\Delta Z/Z$ for which it is, however, hard to make an exact correction. Nevertheless, for $\varepsilon = 2.13$ as in the following experiment this error is only about 0.04%.

4. Experimental Determination of Systematic Error and Precision

To determine the systematic error and the precision of the method, ten independent determinations of ε were made. The samples, containing 100–140 μg of uranium, were prepared from the National Bureau of Standards' standard samples, 950 (nat. U) and U-015 (1.5% U^{235}). All measurements were made in a thermal neutron flux of about 3×10^8 neutrons/cm^2 sec and the counting time was chosen to give a standard deviation in X_F of about 0.1%. The value of X_F could then be reproduced within 0.2%.

The main difficulty in uranium isotope analysis by fission counting is the uranium determination, i.e. the determination of X_A. This problem has been solved in different ways[2,3]). However, there did not seem to be any reason to abandon the spectrophotometric method described in the previous paper[1]). For small amounts of uranium it is probably the most precise one and the best precision is obtained if the unknown and standard samples contain about equal amounts of uranium. In this investigation X_A was therefore determined as originally described[1]). The time required for each of the steps, viz, sample preparation, counting and spectrophotometrie analysis, is about one hour.

The results are shown in the following table where the recorded counts are corrected for background and the absorbances (A_1 and A_2) for the differences in transmittance of the spectrophotometer cells.

The mean value for ε is 2.1256 $\pm$ 0.0019 (stand. dev.). The abundance of U^{235} in natural uranium is 0.7204 $\pm$ 0.0007% (stand. dev.)[9]). The sample U-105 was thus found to contain, with 95% confidence limits, 1.531 $\pm$ 0.004% U^{235}. With the same confidence limits, the value given by Wichers, National Bureau of Standards, is 1.531 $\pm$ 0.001% U^{235} (ref.[10])). If we assume, as is certainly true, that the value given by Wichers is corrected for systematic errors we thus find that the precision in our value and in Wicher's are not sufficient to show the small systematic error in our measurement. However, this error was estimated in the previous section and found to be about 0.04%.

The precision, with 95% confidence limits, in a single determination of ε is $\pm$ 0.014 or $\pm$ 0.7%, the largest contribution to the error coming from the X_A-determination. With the same confidence limits, the previously reported precision was $\pm$ 0.84%[1]). The increase in precision is due to a more careful determination of X_A (frequent

[9]) M. Lounsbury, Can. J. Chem. **34** (1956) 259.

[10]) Private communication from E. Wichers, National Bureau of Standards, Washington 25, D.C.

TABLE

Sample	Ion chamber	Counts	X_F	A_1	A_2	X_A	ε
U-015-1	1	1 808 195					
950-1	2	834 726					
950-1	1	742 918	2.1765	1.298	0.031	1.0238	2.1259
U-015-1	2	1 624 650					
U-015-2	1	1 994 683					
950-2	2	946 403					
950-2	1	1 033 491	2.0941	1.004	0.013	0.9872	2.1212
U-015-2	2	2 150 354					
U-015-3	1	1 925 139					
950-3	2	875 512					
950-3	1	973 863	2.2066	1.186	0.039	1.0328	2.1365
U-015-3	2	2 156 443					
U-015-4	1	1 988 998					
950-4	2	912 841					
950-4	1	749 106	2.1864	1.154	0.036	1.0311	2.1204
U-015-4	2	1 643 422					
U-015-5	1	1 738 096					
950-5	2	713 324					
950-5	1	805 229	2.4507	1.272	0.187	1.1470	2.1366
U-015-5	2	1 984 802					
U-015-6	1	2 359 336					
950-6	2	1 099 709					
950-6	1	965 440	2.1495	1.237	0.013	1.0105	2.1271
U-015-6	2	2 079 125					
U-015-7	1	2 267 731					
950-7	2	1 067 286					
950-7	1	1 621 651	2.1248	1.394	0.001	1.0007	2.1233
U-015-7	2	3 445 654					
U-015-8	1	3 335 282					
950-8	2	1 562 479					
950-8	1	1 165 082	2.1381	1.321	0.011	1.0083	2.1204
U-015-8	2	2 495 153					
U-015-9	1	2 099 079					
950-9	2	923 720					
950-9	1	860 213	2.2703	1.227	0.084	1.0684	2.1249
U-015-9	2	1 951 128					
U-015-10	1	2 229 331					
950-10	2	942 421					
950-10	1	781 842	2.3691	1.218	0.143	1.1174	2.1201
U-015-10	2	1 855 035					

matching of the spectrophotometer cells). This precision can of course be obtained in the whole range 0.72–100% U^{235}.

5. Conclusion

Eq. (6) shows that the systematic error in ε decreases with decreasing ε. Small values of ε, however, necessitate a large number of standard samples to cover the whole internal 0.72–100% U^{235}. A suitable compromise with regard to the NBS isotope standards available is $\varepsilon \leqslant 2$. The systematic error is then within 0.04% and eight isotope standards are needed (nat. U, U-015, U-030, U-050, U-100, U-200, U-350 and U-750).

The precision with 95% confidence limits in a single determination of ε was $\pm$ 0.7% and very nearly the same precision is now obtained in $p_{235,u}$ in the range 0.72–3% U^{235} by use of natural uranium and U-015 as standard samples. This precision will be extended to 100% U^{235} as soon as the U^{235} content of the remaining isotope standards is given with the same precision as that of U-015.

Appendix

If eq. (2) is differentiated and the approximations $t_1 \sim t_2 = t_1$, $N_{u,1} \sim N_{u,2} = N_u$ and $N_{s,1} \sim N_{s,2} = N_s$ are introduced then the relative systematic error in ε due to counting losses is

$$E_\tau = \frac{\Delta N_u}{N_u} - \frac{\Delta N_s}{N_s} = \frac{\Delta r_u}{r_u} - \frac{\Delta r_s}{r_s} = \tau\,(r_u - r_s) \qquad (8)$$

where r is the counting rate.

The relative standard deviation in X_F due to counting statistics is

$$\sigma = \pm\sqrt{\frac{1}{2}\left(\frac{1}{N_u} + \frac{1}{N_s}\right)} = \pm\sqrt{\frac{1}{2t}\left(\frac{1}{r_u} + \frac{1}{r_s}\right)} \qquad (9)$$

if the same approximations are introduced.

From eqs. (8) and (9) we obtain eq. (7) if we put $2t = T$ and note that $r_u \sim C p_{235,u}$, $r_s \sim C p_{235,s}$ (C = constant) and

$$\varepsilon = \frac{p_{235,u}}{p_{235,s}}.$$

NUCLEAR INSTRUMENTS AND METHODS 13 (1961) 190–196; NORTH-HOLLAND PUBLISHING CO.

A MINIATURE FAST FISSION COUNTER

G. D. HICKMAN

Knolls Atomic Power Laboratory†, Schenectady, New York

Received 19 May 1961

A small, $\frac{1}{4}$ inch diameter by $\frac{1}{2}$ inch in length, fast neutron fission counter probe employing highly depleted uranium as the fission material has been developed. The isotopic analysis of the uranium, obtained by the 3-stage mass spectrometer at this Laboratory, is as follows: U^{238} (essentially 100%), U^{236} (0.03 ± 0.02 ppm), U^{235} (0.90 ± 0.20 ppm), and U^{234} (0.04 ± 0.02 ppm). The uranium was plated out of solution to a yield of approximately 1.72 mg/cm². Detailed measurements of the fast neutron flux in the Flexible Plastic Reactor (10^5–10^6 ncm^{-2} sec^{-1}) at KAPL, obtained with the U^{238} fission counter, have shown it to be insensitive to both thermal neutrons and high energy (> 5.3 MeV) gamma rays. The photofission of the U_3O_8 was checked in the critical assembly by making a fast neutron scan with red phosphorus ($\frac{1}{2}'' \times \frac{1}{10}''$) pellets). Since the (n,p) threshold reaction in phosphorus (≈ 1 MeV) is approximately the same as the (n,f) reaction in U^{238}, the two scans should yield, as is found to be the case, identical results provided there is no appreciable influence of photofission in the U_3O_8.

There have been many excellent methods developed for the study of fast neutrons and a fairly complete survey of these methods is to be found in Lamphere[1]). The relatively sharp fast fission thresholds which exist for some of the fissile isotopes make the fission chamber one of the most useful tools of the reactor physicist. The ability to make small fission counters which yield results having high spatial resolution is an important advantage of the fission counter. A small fast fission chamber might be used to investigate 1) the streaming of fast neutrons through small reactor voids, or 2) fast neutrons in the near vicinity of or even through moderating or control regions. However, the fast fission counters which have been developed in the past all suffer from one defect. If the counter is to be used in the presence of a large thermal flux, it must be covered with a thermal (cadmium) shield. This procedure is due to the presence of small amounts of thermal fissile material in the counter, which exhibit large thermal fission cross sections. Since the cadmium shield surrounding the counter produces perturbations of the neutron fluxes, it would be advantageous to be able to eliminate the shield.

Of all the possible fissile isotopes which exhibit fairly sharp fast fission thresholds, it was decided to use U^{238} as the fissile material for a fast fission chamber. The two main reasons for using U^{238} as the fissile material of the counter are 1) the effective threshold†† for U^{238} of 1.4 MeV is one of the highest threshold energies of all the fissile isotopes, and makes possible the comparison of the experimental fast flux with a calculated high energy neutron group†††, and 2) U^{238} can be obtained relatively free of U^{234}, U^{235}, and U^{236}. Both U^{234} and U^{236} have relatively high energy threshold fission cross sections, i.e., 0.26 MeV and 0.70 MeV respectively, which being fairly close to the U^{238} fission threshold would probably not yield results appreciably different from those obtained with a "pure" U^{238} fission counter. However, U^{235} has a large thermal cross section (≈ 600 barns), and must be eliminated to a very high degree to enable one to use the high energy threshold characteristics of U^{238}.

A small, $\frac{1}{4}$ inch diameter × $\frac{1}{2}$ inch in length, fast neutron fission probe counter, employing depleted uranium as the fission source was constructed by

† Operated by the General Electric Company for the U.S. Atomic Energy Commission.

†† Effective threshold energy as defined by Hughes[2]).

††† In performing diffusion calculations for neutrons in reactors, the neutrons are broken up into 3 or 4 energy groups. The highest energy group is usually in the range of approximately 1 MeV–10 MeV.

[1]) R. W. Lamphere, Fission Detectors, Fast Neutron Physics, edited by J. B. Marion and J. L. Fowler (Interscience Publishers, Inc., New York, 1960).

[2]) D. J. Hughes, Pile Neutron Research (Addison-Wesley Co., Cambridge, Mass., 1953).

the Westinghouse Electronic Tube Department at Elmira, New York. A schematic diagram of this counter, type WX-4336, is shown in fig. 1. The

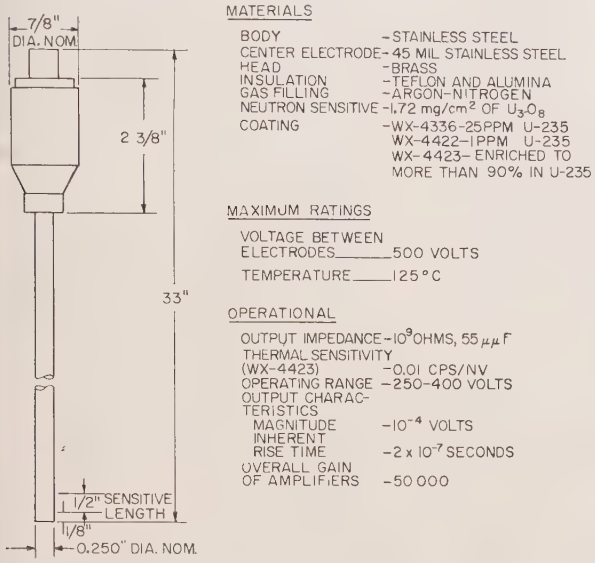

Fig. 1. Schematic diagram of fission counters WX-4336, WX-4422, and WX-4423.

U_3O_8 which was employed in the counter was obtained by the author from the Oak Ridge National Laboratory. The U_3O_8 was put into solution and plated out to yield a foil approximately 1.72 mg/cm². This foil in the form of a cylinder, formed the sensitive area of the fission counter. An isotopic analysis of the U_3O_8 was performed by the Mass Spectrometer Group at this Laboratory using a three-stage high resolution mass spectrometer.

Table 1

Isotopic analysis of U_3O_8 used in fission probe counter WX-4422

Isotope	Abundance
U^{238}	essentially 100 %
U^{236}	0.03 ± 0.02 ppm
U^{235}	0.90 ± 0.20 ppm
U^{234}	0.04 ± 0.02 ppm

The results of this analysis showed a U^{235} content of approximately 25 ppm. Due to this relatively large U^{235} content, it was decided to attempt construction of a second counter, type WX-4422, this one containing the highest purity U^{238} available. This counter, identical in geometry to WX-4336, was

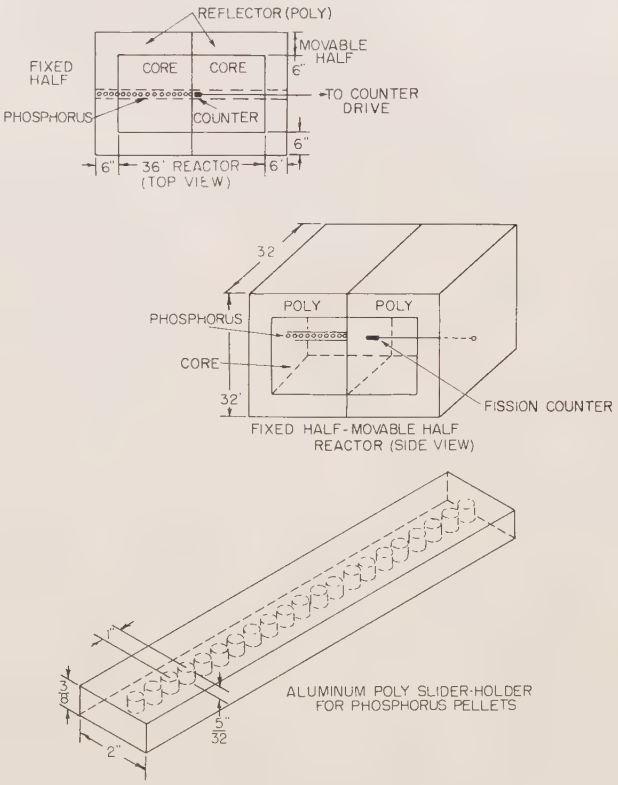

Fig. 2. Location of fission counters and phosphorus pellets in reactor core.

also fabricated by the Westinghouse group. The U_3O_8 was again obtained from Oak Ridge. The isotopic analysis of this highly depleted uranium is given in table 1.

While the U^{235} content in the WX-4336 counter was of the order of 25 ppm, it was approximately 1 ppm in the WX-4422 counter. This is the first time a U^{238} fission counter employing such highly depleted uranium has been reported†. The merits of such a high purity U^{238} fission counter will become evident from the following discussion.

Both of the fast neutron fission counters, WX-4336 and WX-4422, were used in the Flexible Plastic Reactor (10^5–10^6 n cm^{-2} sec^{-1}) at the Knolls Laboratory in the investigation of fast neutrons.

† Glover[3]) reports a fission counter employing U^{238} depleted to 7 ppm U^{235}, while Lamphere[4]) reports using a U^{238} counter depleted to 6.1 ppm U^{235}.

[3]) R. N. Glover, Nucl. Instr. **3** (1958) 320.

[4]) R. W. Lamphere, Phys. Rev. **104** (1956) 1654.

TABLE 2
Fast neutron scans taken with counter WX-4336

Position of center of counter from center of core (in.)	Total counts bare counter	Total counts Cd covered counter	Bare counter counts/6443	Cd covered counts/6443	% diff. bare-Cd covered
0.6	6443 ± 80	6337 ± 80	1.000 ± 0.012	0.983 ± 0.012	1.7
1.6		6258 ± 79		0.971 ± 0.012	
2.6	6523 ± 81	6325 ± 80	1.012 ± 0.012	0.982 ± 0.012	3.0
3.6		6179 ± 78		0.959 ± 0.012	
4.6	6150 ± 79		0.954 ± 0.012		
5.6	6190 ± 79	5834 ± 76	0.961 ± 0.012	0.905 ± 0.012	5.8
7.6	5715 ± 75	5485 ± 74	0.887 ± 0.012	0.851 ± 0.011	4.1
9.6	5225 ± 72	4924 ± 70	0.811 ± 0.011	0.764 ± 0.011	5.8
11.6	4669 ± 68	4329 ± 66	0.725 ± 0.011	0.672 ± 0.010	7.3
13.6	3904 ± 62	3753 ± 61	0.606 ± 0.010	0.582 ± 0.009	4.0
15.6	3030 ± 55	2837 ± 53	0.470 ± 0.009	0.440 ± 0.008	6.5
17.6	2064 ± 45	1947 ± 44	0.320 ± 0.007	0.302 ± 0.007	5.6
18.6	1364 ± 37	1220 ± 35	0.219 ± 0.006	0.194 ± 0.005	11.4
19.6	893 ± 30	701 ± 26	0.144 ± 0.005	0.112 ± 0.004	22.2
20.6	595 ± 24	446 ± 21	0.095 ± 0.004	0.071 ± 0.003	25.3
21.6		276 ± 17		0.044 ± 0.003	

Profiles of the fast flux were obtained with and without a thermal (cadmium) shield surrounding the counters. The counters were attached to a calibrated control rod mechanism enabling the movement of the counters in the reactor core and polyethylene reflector by remote control (fig. 2). The data which was obtained with counter WX-4336 is given in table 2. The difference between the bare and cadmium covered counter is approximately 5% in the core, but as great as 25% in the reflector. This is the type of variation which would be expected if thermal fissile material were present in the counter. In the center of the reactor core, both the fast and thermal neutron flux are large. However, in the reflector, the fast flux continues to rapidly decrease while the thermal flux is peaking at a distance of about 2 inches from the core reflector interface, after which it also rapidly decreases. The thermal neutron flux for this reactor, observed with a thermal fission counter, is given in fig. 3. There-

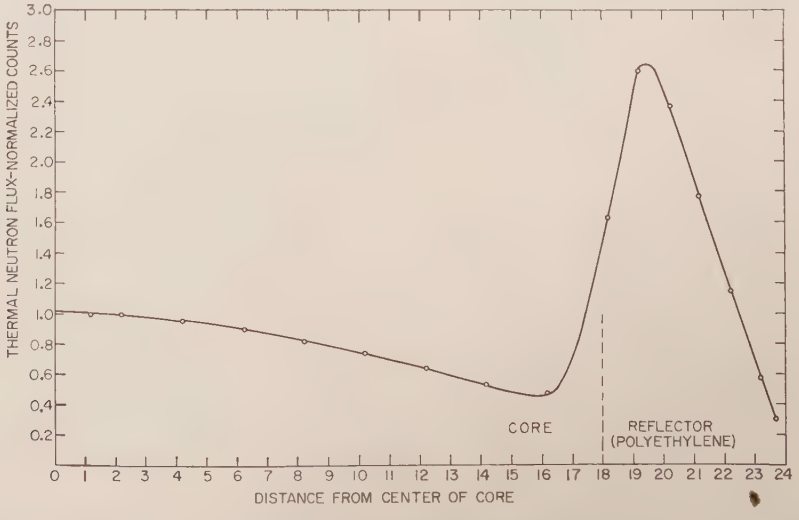

Fig. 3. Thermal neutron flux scan as observed with thermal fission counter WX-4423.

Table 3
Fast neutron scans taken with counter WX-4422

Position of center of counter from center of core(in.)	Average counts in 12 min. bare counter	Average counts in 12 min. Cd covered ctr.	Bare counter counts/1041	Cd covered counts/1041	% diff. bare Cd-covered
1.0	1041 ± 14	1000 ± 13	1.000 ± 0.014	0.961 ± 0.012	3.9
2.0	1018 ± 15		0.978 ± 0.013		
4.0	993 ± 14		0.954 ± 0.013		
6.0	943 ± 12		0.905 ± 0.012		
8.0	852 ± 12		0.818 ± 0.011		
10.0	780 ± 10		0.749 ± 0.009		
12.0	677 ± 9		0.650 ± 0.008		
14.0	557 ± 8		0.535 ± 0.008		
16.0	436 ± 7		0.419 ± 0.006		
18.0	280 ± 5	274 ± 5	0.269 ± 0.004	0.263 ± 0.005	2.2
19.0	159 ± 3		0.153 ± 0.003		
20.0	93 ± 2	91 ± 2	0.089 ± 0.002	0.087 ± 0.002	2.3
21.0	55 ± 1		0.053 ± 0.001		
23.0	22 ± 1		0.021 ± 0.001		

fore, if thermal fissile material were present in the fast fission counter, the contribution to the count rate from thermal neutrons would be greatest in the reflector, in agreement with the observed results.

The results of the fast neutron scans taken with the counter containing the highly depleted uranium, WX-4422, are given in table 3 and fig. 4. It is interesting to note that with the counter at the center of the reactor core, a 4% difference in the results obtained with the bare and cadmium covered counter still exists. However, this difference vanishes when the counter is moved into the reflector, which is good evidence for believing the difference is due to something other than to thermal fission of the U^{235}. The majority of the 4–5% difference in count rate obtained by both WX-4336 and WX-4422 counters (Cd covered-uncovered), when the counters were in the reactor core, is thought to be the result of the depression of the thermal flux. The thermal depression which is caused by the cadmium shield of the counter in turns reduces the fast neutron flux in the vicinity of the counter. This effect is, of course, not observed in the reflector where no fissile material is present. Since the uranium in counter WX-4422 was depleted in U^{235} to approximately 1 ppm in contrast to the 25 ppm U^{235} in counter WX-4336, WX-4422 should experience only $\frac{1}{25}$ as large a thermal influence as was observed with WX-4336. At the maximum observed interference of 25% for WX-4336, this would amount to 1% for WX-4422, well within the 2% statistics which were obtained.

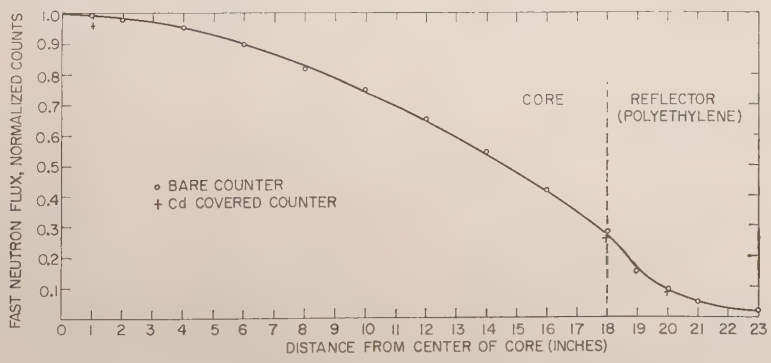

Fig. 4. Fast neutron flux scan as observed with counter WX-4422, with and without a Cd shield.

Any fission counter which employs uranium or thorium can be influenced by high energy gamma rays through the photofission process. Koch *et al.*[5]), in 1950, found that the threshold for the (γ,f) reaction in Pu^{239}, U^{238}, U^{235}, U^{233}, and Th^{232} were all approximately 5.3 MeV. The excitation function for U^{238} has a value of 125 mb for the cross section at maximum amplitude. The peak of the curve is at 14 MeV and has a width of 8.8 MeV at half-maximum[6,7]).

Glover[3,8]) pointed out that photofission was probably the major cause for the disagreement which was found to exist between fast flux measurements obtained by (n,p) threshold activation techniques, and those obtained using a U^{238} fission counter (7 ppm-U^{235}). The experiments were performed in a water tank which surrounds the LIDO reactor. The photofission was thought to be primarily caused by the 7.7 MeV capture gamma rays from neutron capture in the reactor core aluminum. The photofission interference did not appear until the fission counter was, in the water, a distance of 30 to 40 cm from the core-water interface. At this distance, in the water, the fast neutrons which are affected to a much greater extent in the water than are the high energy gamma rays, were decreased to such an extent that it was possible to see the influence of the (γ,f) reaction in the uranium.

In the present experiments, the neutron flux scans were performed in the reactor core and a few inches out into the polyethylene reflector. Therefore, even though the reactor contained a considerable amount of aluminum, it was felt that the photofission contribution would be found to be very small compared with the (n,f) reaction in U^{238}. The photofission interference in the counter was determined by a comparison of a fast neutron flux scan obtained by the U^{238} fission counter with a fast neutron scan obtained by the (n,p) reaction in red phosphorus. The fission counter is subject to both (n,f) and (γ,f) reactions, while the red phosphorus activates only by the (n,p) reaction. Therefore, the photofission of the U^{238} in the fission counter can be assumed negligible if the two scans are shown to have identical shapes. Some of the more important properties of phosphorus are (1) only one naturally occurring isotope, P^{31}; (2) reasonable half-life of 170 min; (3) relatively large (n,p) cross section for fission neutrons (31.2 mb); (4) effective threshold energy of 3.5 MeV, which approximates the threshold fission cross section for U^{238}; and (5) is very easy to handle in the form of red phosphorus powder. The excitation function for phosphorus was measured between 1.9 and 3.6 MeV by Ricamo[9]) and later between 1.6 and 10.0 MeV by Grundl *et al.*[10]). These results show a value of 1.31 mb at 1.6 MeV for the (n,p) cross section. It then increases fairly sharply to 0.14 barns at 5.5 MeV, and remains constant at this value until 9.5 MeV. Forbes[11]) obtained a cross section which was considerably less at 14 MeV. The red phosphorus in the form of a fine powder was cold pressed into pellets $\frac{1}{16}''$ in diameter by $\frac{5}{32}''$ thickness and weighing approximately 1.65 g by the Ceramic Group at the Knolls Atomic Power Laboratory. A wax compound, Ceremul C, made by Socony Vacuum, was used in the pressing operation to add strength to the pellets. The pellets were still very brittle and were placed in thin-walled aluminum cups. The phosphorus pellets were activated in the same equivalent locations in the reactor as the U^{238} counters sampled. Both the WX-4422 U^{238} counter and the phosphorus pellets were activated at the same time. The U^{238} data was remotely recorded during the activation, while the phosphorus pellets, after a period of approximately six hours of activation, were removed from the reactor and beta counted. Schematic diagrams of the reactor showing location of the fission counters and phosphorus pellets, along with a diagram of the loading of the phosphorus pellets are given in fig. 2. The activity produced in one of the phosphorus pellets from the scan was followed for approximately three weeks to determine its half-life. One day after activation,

[5]) H. W. Koch, J. McElhinney and E. L. Gasteiger, Phys. Rev. **77** (1950) 320.

[6]) R. B. Duffield and J. R. Huizenga, Phys. Rev. **89** (1953) 1042.

[7]) Katz, Kavanaugh, Cameron, Bailey and Spinks, Phys. Rev. **99** (1955) 98.

[8]) R. N. Glover, Nucl. Instr. **3** (1958) 316.

[9]) R. Ricamo, Nuovo Cimento **8**, No. 6 (1951) 383.

[10]) J. A. Grundl, R. L. Henkel and B. L. Perkins, WADC TN57-298, Pt. I (1958) 214.

[11]) S. G. Forbes, Phys. Rev. **88** (1952) 1309.

TABLE 4
Fast neutron scan obtained by P^{31} (n,p) Si^{31} reaction

Distance of center of phosphorus pellets from center of core (in.)	Counts (total)	Counts (bkg. corr.)	Counts due to 14 d activity corrected back to T_0	Counts corrected for bkg. and 14d activity	Counts (corr.) normalized to postion 1
1	83 065	82 859	3304	79 555 ± 294	1.000 ± 0.004
2	84 777	84 571	3168	81 403 ± 298	1.023 ± 0.004
4	78 706	78 500	2988	75 512 ± 287	0.949 ± 0.004
6	72 970	72 764	2664	70 100 ± 276	0.881 ± 0.004
10	60 173	59 967	2260	57 707 ± 250	0.725 ± 0.003
12	51 599	51 393	1952	49 441 ± 232	0.621 ± 0.003
14	42 038	41 832	1612	40 220 ± 209	0.506 ± 0.003
16	32 344	32 138	1324	30 814 ± 184	0.387 ± 0.002
18	24 701	24 495	3024	21 471 ± 168	0.270 ± 0.002
19	18 177	17 971	6236	11 735 ± 162	0.147 ± 0.002
20	13 625	13 419	6528	6 891 ± 149	0.087 ± 0.002
21	9 677	9 471	5196	4 275 ± 128	0.054 ± 0.002
22	6 124	5 918	3368	2 550 ± 101	0.032 ± 0.001
23	3 892	3 686	2016	1 670 ± 78	0.021 ± 0.001

TABLE 5
Comparison of fast neutron scans obtained by WX-4422 U^{238} fission counter and P^{31} (n,p) Si^{31} reaction

Center of phoshorus or U^{238} fission counter from center of core (in.)	Fast neutron flux as obtained by WX-4422 counter (normalized)	Fast neutron flux as obtained by P^{31} (n,p) Si^{31} reaction (normalized)	Per cent differences of columns 2 and 3
1	1.000 ± 0.014	1.000 ± 0.004	—
2	0.978 ± 0.013	1.023 ± 0.004	4.6
4	0.954 ± 0.013	0.949 ± 0.004	0.5
6	0.905 ± 0.012	0.881 ± 0.004	2.7
8	0.818 ± 0.011	—	—
10	0.744 ± 0.009	0.725 ± 0.003	3.2
12	0.650 ± 0.008	0.621 ± 0.003	4.5
14	0.535 ± 0.008	0.506 ± 0.003	5.4
16	0.419 ± 0.006	0.387 ± 0.002	7.6
18	0.269 ± 0.004	0.270 ± 0.002	0.5
19	0.153 ± 0.003	0.147 ± 0.002	3.9
20	0.089 ± 0.002	0.087 ± 0.002	2.3
	†0.085 ± 0.002		
21	0.053 ± 0.001	0.054 ± 0.002	1.8
22	†0.032 ± 0.001	0.032 ± 0.001	0
23	0.021 ± 0.001	0.021 ± 0.001	0

† Results obtained with WX-4422 counter with counter scan hole in core (18″ in length) filled with polyethylene to prevent streaming.

the only detectable activity was that produced by the reaction P^{31} (n,γ) $P^{32} \xrightarrow{(\beta^-)\ 14d} S^{32}$. After subtracting background and the 14 day contribution from the total observed activity (table 4), a single half-life of approximately 170 min was obtained. This is the expected activity for the threshold reaction P^{31} (n,p) $Si^{31} \xrightarrow{(\beta^-)\ 170\ min} P^{31}$. A small deviation from the 170 min half-life was found to exist for the first couple of hours after end of activation and is primarily due to the (n,γ) and (n,p) reactions in the aluminum cups which contained the phosphorus pellets, i.e.,

$$Al^{27}\ (n,\gamma)\ Al^{28} \xrightarrow{2.3\ min} Si^{28}$$
$$Al^{27}\ (n,p)\ Mg^{27} \xrightarrow{9.5\ min} Al^{27}\ .$$

The correction factor for the 14 day activity which must be applied to all the phosphorus pellets is not the same for all samples of the scan; but since the long lived activity is due to the thermal (n,γ) reaction, must be weighted by the thermal neutron flux as seen by the phosphorus. The 14 day activity (at end of activation T_0) in the phosphorus samples was obtained by recounting the samples a week after the first counting, and correcting for background and time elapsed since T_0. The final results of the phosphorus scan (170 min activity) normalized to the first position of the scan in the core, and listed in Column 6 of table 4, are listed again along with the final fast fission counter results (table 3) in table 5. Table 5 shows the phosphorus fast neutron activation results in good agreement with those obtained with the fast fission counter. This is essentially true in the reflector where the interference to the count rate of the fission counter by photofission of the uranium would be expected to be greatest. The approximate 4% difference between the phosphorus and the U^{238} results which exist for some of the points is about the spread in the weights of the phosphorus pellets.

The fast fission counter WX-4422 which employs highly depleted U^{238} (1 ppm U-235) has therefore been shown within the experimental accuracy to be insensitive to both thermal neutrons and high energy (> 5.3 MeV) gamma rays when used in the core or reflector of the FPR critical assembly. The result is an excellent, small geometry fast neutron probe. More recently a fast fission counter (1 ppm U^{238}) having a smaller sensitive area than those previously described has been obtained. This counter (WX-4576) is identical to the other counters except the sensitive length has been reduced from $\frac{1}{2}''$ to $\frac{1}{4}''$.

Acknowledgment

The author would like to acknowledge Al Boshoff and Bob Dwyer, for the operation of the FPR Critical Assembly and for their help in performing the flux scan measurements. The Mass Spectrometer and Ceramic groups of this Laboratory are gratefully acknowledged for their isotopic analysis of the U_3O_8, and for the pressing of the red phosphorus pellets, respectively. Westinghouse Electronic Tube Department at Elmira, New York, is also gratefully acknowledged for their prompt fabrication of the fission counters.

NUCLEAR INSTRUMENTS AND METHODS 13 (1961) 197–200; NORTH-HOLLAND PUBLISHING CO.

100 Mc/s TUNNEL-DIODE DISCRIMINATOR AND PULSE-SHAPER

A. ADLER, M. PALMAI and V. PEREZ-MENDEZ†

Department of Physics, The Hebrew University, Jerusalem, Israel

Received 10 June 1961

A discriminator circuit for use with nanosecond pulses at high repetition rates is described. Fast tunnel diodes are used in both the discriminating and pulse shaping stages. The effect of circuit parameters on the operation of the tunnel diode stages is discussed, and the results of various measurements on the performance of the circuit are given.

1. Introduction

A discriminator device which produces a standard shaped output pulse for input pulses above a given amplitude, is an essential element in electronic devices for nuclear particle detection and other applications. The trend in such experiments, to work with very high counting rates, especially in the case of experiments involving pulsed particle accelerators, necessitates the use of discriminators with recovery times in the nanosecond region and capable of operating stably with very short input pulses.

The discriminator described here uses tunnel-diodes[1]) as the discriminator and pulse shaping elements. Due to the very short switching and recovery times of tunnel diodes which are now available[2]) it was possible to design a circuit which can separate random pulses occurring at intervals as short as 10^{-8} sec.

2. Description of Circuit

The circuit diagram of the discriminator is shown in fig. 1. Designed for negative input pulses, it consists of a transistor emitter follower driving

† On leave from Lawrence Radiation Laboratory, University of California, Berkeley.

[1]) L. Esaki, Phys. Rev. **109** (1958) 603.
H. S. Sommers, Proc. I.R.E. **47** (1959) 1201.

[2]) R.C.A. Bulletin on Tunnel Diodes IN3128, IN3129, IN3130, IN3138.

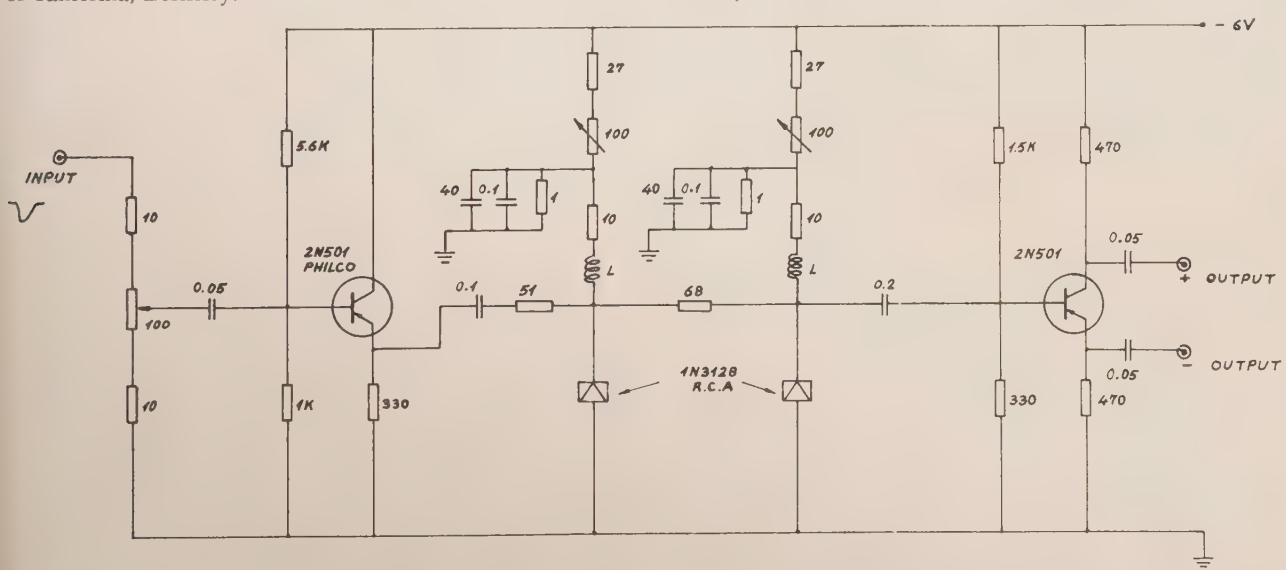

Fig. 1. Circuit diagram of 100 Mc/s discriminator.
1. All capacitances in μF. 2. Resistances in Ohms. 3. $L \approx 3$ Turns, 1 cm diam. coil.

the first tunnel diode which is the discriminating element. The second tunnel diode serves to produce a standard shaped pulse when triggered by the previous stage. The output is a transistor stage with unit gain from the emitter and collector.

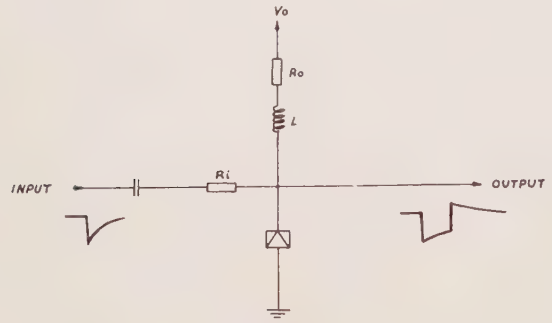

Fig. 2a.

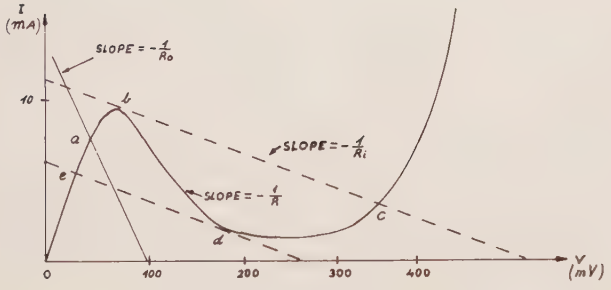

Fig. 2b.

Fig. 2. (a) Circuit connections of tunnel diode, (b) characteristic curve tunnel diodes showing load lines and biassing point.

The input pulses are fed into the circuit through a low inductance carbon potentiometer which selects the discriminating level. The minimum input pulse which can trigger the tunnel diode is then ≈ 0.1 V when it is biased to a potential of ≈ -30 mV as indicated in fig. 2b. This biassing level was chosen as a suitable compromise between the maximum sensitivity of the circuit and a satisfactory degree of stability for the tunnel diode.

The output pulse of the first diode is ≈ 0.4 V for input pulses just above the triggering level; it increases to ≈ 0.8 V for input pulses which are a factor of 10 larger than the triggering level. This variation in output pulse makes it desirable to use a second tunnel diode as a limiter and shaping element; with the circuit parameters shown in the figure the output pulse is uniform in amplitude and width to within 10% for all input pulses in this range. By increasing the inductance L, in series with the second diode it can be made to produce a satisfactory gate whose width is determined by the L/R time constant as discussed below.

The bias potential of the diodes is provided by a low impedence resistance divider fed from a -6 V stabilized power supply. Due to the rather low impedance of these diodes, it is especially necessary to keep the inductance of the leads from the power supply, and other connections, down to a minimum.

3. Circuit Design Considerations

The amplitude and shape of the output pulses produced by the tunnel diodes can be understood with reference to figs. 2a, 2b. V_0 is the negative d.c. supply which biases the diodes through the series connection of R_0 and L to a stable operating point located to the left of the current peak. To permit stable biassing close to the current peak, R_0 is chosen smaller than $-R$. The value of R_i was chosen as a compromise between having the corresponding load line approximately parallel to the voltage axis (thus obtaining a fairly constant output pulse) and keeping R_i low enough to avoid excessive integration of the input pulse.

The rise and decay times of the output pulse—which is the time to go from b to c and from d to e are given by $\alpha \mid -R \mid c$ where $\alpha \approx 6$, $-R =$ the negative resistance of the diode, and C the diode capacity[3]).

The width of the pulse—which is the time taken to traverse the characteristic from c to d is determined by the time constant $T_w = L/R_t$ where $L =$ series inductance including that of the diode.

$$R_t = R_0 + \frac{R_i R_{cd}}{R_i + R_{cd}}$$

where R_{cd} is the resistance corresponding to an appropriate average of the slope of the diode's characteristic between points c and d. Since the maximum value of R_0 is determined by the stability criterion given above, the width of the output pulse can be varied from a few nsec well into the μsec range by a suitable choice of L.

[3]) R. H. Bergman, I.R.E. Transactions on Electronic Computers. E.C. 9 (1960) 430.

The overshoot at the end of the output pulse, which corresponds to the output signal while the diode traverses its characteristic from e to a, recovers with a time constant

$$T_0 = \frac{L}{R_0 + \dfrac{R_1 R_{ea}}{R_1 + R_{ea}}}$$

where R_{ea} = resistance corresponding to the average slope of the characteristic between e and a. Thus, to obtain a short pulse, both in width and recovery time it is sufficient to choose L sufficiently small, as indicated in fig. 1.

4. Performance Tests

The circuit was tested for stability, sensitivity to input pulse width, and recovery time by the methods discussed below.

(a) Long term stability was tested using a standard delay line pulser. The drift in discriminator level over a period of 24 hours was less than 10 mV for a discriminator setting of 0.5 V.

(b) The pulse height as a function of pulse width is shown in fig. 3a; as can be seen it is essentially constant for pulses from 8 ns and larger. The pulse height was checked also as a function of the rise time of the input pulse (for pulses 50 ns long) and found to vary as shown in fig. 3(b).

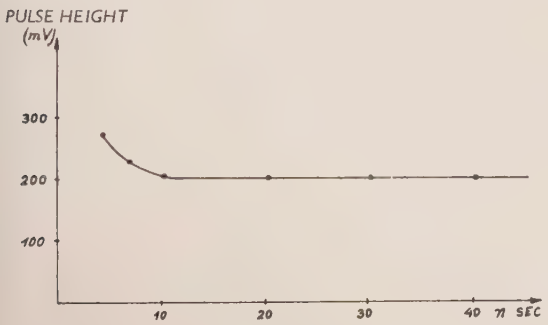

Fig. 3a.

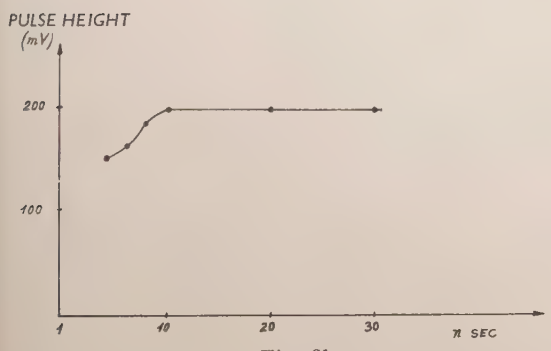

Fig. 3b.

Fig. 3.(a) Input pulse height as function of input pulse length for constant discrimination level, (b) height of 50 ns input pulse as function of its rise time for constant discrimination level.

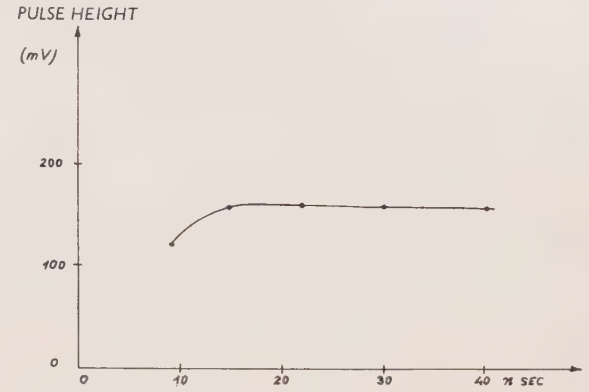

Fig. 4. Double pulse resolution as a function of separation of pulses, for 5 ns wide input pulses.

(c) The time resolution of the circuit was tested in 2 ways: (1) by feeding in from a mercury relay pulser two equal amplitude pulses with a separation between them determined by the relative lengths of the coaxial cables to the discriminator, the curve in fig. 4 is obtained. (2) The resolution for a group of equally spaced pulses was obtained as a function of frequency and number of pulses. These trains of pulses were obtained using the circuit shown in fig. 5(a). A negative input gate pulse from a standard pulse generator is fed to the tunnel diode of the pulse generator with an amplitude which brings the diode to an operating point in the negative resistance region. By suitable choice of the values of the series resistance and inductance, the tunnel diode can be made to perform relaxation oscillations. The amplitude of these oscillations is quite constant and therefore provides a sensitive check of the discriminator circuit. Fig. 5(b) shows the variation in disc level for trains of pulses at 50 and 85 Mc/s.

The general behaviour of the circuit indicated that the limiting performance at high frequencies was due mainly to the input transistor. Therefore, a better performance can be expected if this input stage is replaced by a good high frequency compensated switch attenuator, which would have the

additional merit of providing a linear scale for the instrument.

Acknowledgements

We would like to thank Dr. Henry Sommers of he R.C.A. Research Laboratory in Princeton for supplying us with the R.C.A. tunnel diodes used here. We are also indebted to him for many useful comments and suggestions concerning the use of these diodes in counting circuitry. We would also like to thank Prof. S. G. Cohen for his help and support of this work.

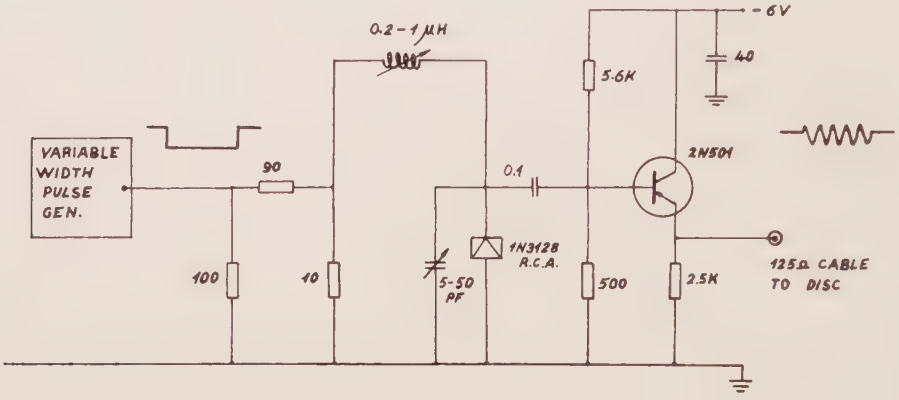

Fig. 5a.

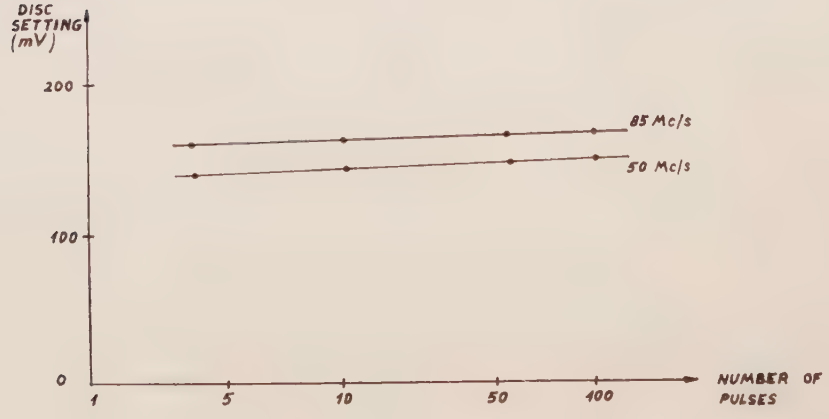

Fig. 5b.

Fig. 5. (a) Circuit diagram of gated pulse generator using tunnel diode, (b) variation in level setting of discriminator as function of n = number of consecutive output pulses per gating pulse of generator.

NUCLEAR INSTRUMENTS AND METHODS 13 (1961) 201–205; NORTH-HOLLAND PUBLISHING CO.

SOME CHARACTERISTICS OF A TOROIDAL PINCH WITH A REVERSED FIELD

S. BERGLUND and S. SVENNERSTEDT

Department of Physics, University of Uppsala

Received 22 June 1961

A description is given of an experimental set up for a large toroidal pinch. The primary system creates in the following order: 1) a weak quasi-stationary axial field, 2) the main gas current, and 3) a strong pulsed axial field in opposite direction to the weak one. The plasma fields and associated motions have been studied by magnetic probes, and the ionization stages of various elements in the discharge by optical spectroscopy. Results on the stability and the general behaviour of different discharge types are given.

1. Introduction

One method of confining and heating a plasma is by utilizing the pinch effect. However, a pinch discharge is extremely complex and the stability problem is very difficult to master, though great progress has been made in recent years on the theoretical side. Necessary and sufficient conditions for the hydromagnetic stability of the pinch have been derived for arbitrary field configurations with axial symmetry[1,2]). According to these conditions stable equilibria should exist, but they may be extremely hard to realize experimentally. A stringent criterion is given by Suydam[3]):

$$\left(\frac{\mu'}{\mu}\right)^2 + \frac{8\mu_0}{rB_z^2}\frac{\mathrm{d}p}{\mathrm{d}r} > 0\,. \quad \text{Here } \mu = B_\theta/rB_z\,, \quad \mu' = \mathrm{d}\mu/\mathrm{d}r\,,$$

and p, the pressure, is assumed scalar. The fulfillment of this inequality is necessary for stability. The first term is a measure of the magnetic field shear, which should be as large as possible. This is realized if the axial field inside the pinch has the opposite direction to the field outside. The necessity of this field reversal has also been shown in the limit of an infinitely thin current layer[4]).

The following report deals with some experiments with a toroidal pinch apparatus, in which a reversed field configuration is applied.

2. Apparatus

A schematic drawing of the apparatus is shown in fig. 1. The discharge tube is a porcelain torus, main diameter 102 cm, bore diameter 22 cm, and wall thickness 1.5 cm. The tube is made in two halves, carefully joined by glass fabric imbedded in epoxy resin. Three pipes serve as pump outlets and also as viewing ports for spectroscopic investigations. There are also several holes for insertion of probes. Although the vacuum system is not bakable, a base pressure down to 2×10^{-6} mm Hg is obtained by a large molecular pump and with a liquid air trap in the pump lead.

The discharge torus is closely surrounded by a 4 mm copper shell, which is cut along two directions, perpendicular to each other, as not only the axial gas current but also the axial magnetical fields are to be pulsed.

Outside the copper shell 24 B_z-coil units are equally spaced along the torus, each unit containing four 6-turn coils of the clock spring type. Outermost there are the coils for the induction of the main discharge, the B_φ-windings, and they consist of 80 turns of insulated copper wire, held in place by machined grooves in two wooden blocks, that surround the entire coil system.

In the present experiments the B_φ windings have been coupled to give a 2:1 turns ratio between the primary system and the gas. Part of the B_z coils has been used to give a comparatively weak quasi-

[1]) William A. Newcomb, Ann. Phys. **10** (1960) p. 232.

[2]) Bergen R. Suydam; Stability of a Linear Pinch, Part II LAMS 2381 (1960).

[3]) Bergen R. Suydam, Proc. 2nd Int. Conf. on the Peaceful Uses of Atomic Energy **31** (Geneva, 1958) p. 157.

[4]) M. N. Rosenbluth, Proc. 2nd Int. Conf. on the Peaceful Uses of Atomic Energy **31** (Geneva, 1958) p. 85.

steady field, whereas the other part has been used to create a stronger pulsed field.

The condenser bank has been charged to 10 kV. The stored energy for the B_φ windings is then 50 kJ and the ringing frequency is 3.3 kHz. The corresponding data for the weak field are 10 kJ and 0.25–1.3 kHz and for the strong field 60 kJ and 3.4 kHz.

The gas has been preionized by an RF oscillator working on a pair of electrodes on the porcelain torus, and the discharge has been started at the maximum of the weak field. The strong field is normally delayed with respect to the gas current,

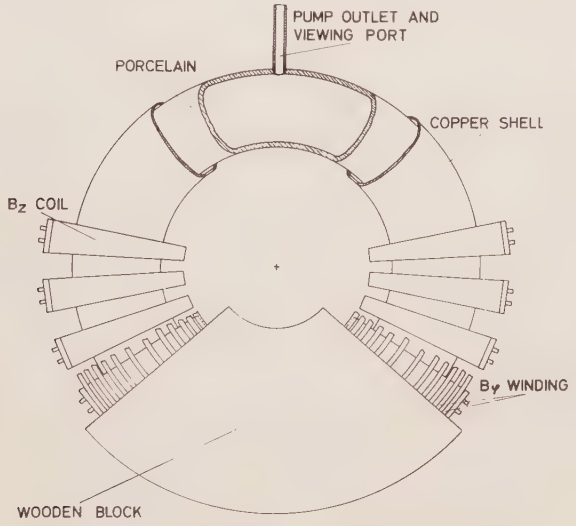

Fig. 1. Cutaway view of the apparatus.

the proper choice for this delay being a subject for investigations. Ignitrons of the type WX-3993 are used for switching. In order to limit the wear on these and on the condenser bank, a type of variable series resistors have been used in the primary circuits. They are made from steel wire and are carefully adjusted with respect to resistance and heat capacitance in such a way that they heat up considerably during the first half cycle and thus become very efficient in damping out the primary oscillation, although the effect on the first half period is small.

3. Diagnostic Equipment and Techniques

The electric measurements are aimed towards a direct measurement of the plasma current, the field and current distributions and plasma motions; the primary circuits have been continuously controlled with respect to the correct sequence of triggering etc.

The induced voltage on the gas has been measured by a voltage divider connected to the copper shell, and the total axial gas current by a Rogowsky coil placed around the porcelain body, inside this shell.

The magnetic field distributions inside the discharge have been studied by magnetic probes. A lot of experimental work has been devoted to these probes so as to give reliable results with a high signal to noise ratio and a wide frequency response. Several probe constructions have been tried including single as well as differential coils. In order to reduce the number of discharges required for such measurements, multiple probes are normally employed. The largest one consists of three pairs of mutually perpendicular coils, with a distance of 2 cm between the pairs. Thus two field components are simultaneously measured at three points. This probe is placed in a quartz tube, 7 mm in diameter. All measurements have been made along a main diameter crossing the torus bore center.

Integration of the signals has been done by simple RC circuits or by transistorized Miller integrators with a frequency range up to 2 MHz. The former integrators are placed at the receiving end of the transmission cable, the latter ones at the probe end, thus permitting the best loading conditions to be chosen for the coils.

Spectroscopic investigations have been made in the wavelength region 2000–4500 Å, employing a Hilger medium quartz spectrograph. A rotating disk is used for time gating and resolution of the spectra, and the discharge is synchronized with the disk rotation. A wide slit in the disk acts as a shutter for gating of the spectrum, while for time resolution, the light beam passes through a narrow slit and is swept along the slit of the spectrograph. As the two slits are perpendicular to each other and the light beam, the result is a streak spectrogram of a point source.

4. Results

Without preionization the gas breaks down within the pressure range 10–100 microns, but in an

irreproducible way. The time jitter is always too large, and the general behaviour of the discharge also becomes irregular. By means of the RF preionization in conjunction with the weak field used for stabilization, the time jitter has been decreased to 0.5 μs.

At first some investigations were made on the toroidal pinch, stabilized by the weak field, which is trapped inside the current layer. The amplitude of the gas current depends slightly on the initial gas pressure. Furthermore it increases with the weak field, which has been varied within the range $B_{z0} = 50$–300 gauss.

For a discharge with $B_{z0} = 280$ gauss and deuterium pressure $p = 25$ microns, the first half period of the gas current is 100 μs and the amplitude 70 kA. The B_z and B_θ field distributions have been measured by a multiple probe. Probe signals from several discharges are usually superposed on each oscillogram and a typical example of this is given in fig. 2, which shows the integrated signals from three discharges. The reproducibility is quite good for the first 20 μs, but then flutterings start, which indicate instabilities.

In fig. 3 the axial current density, i_z, is shown in a three dimensional model as a function of space and time. The discharge starts as a skin current

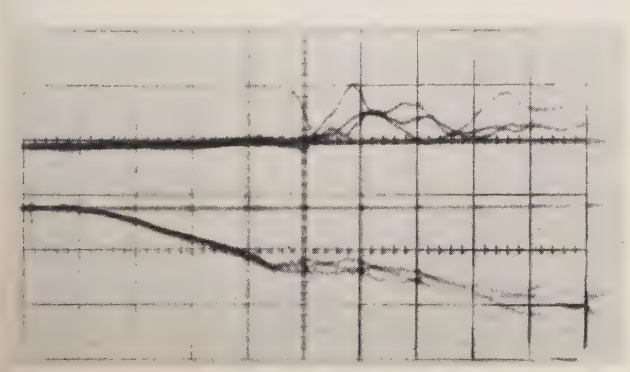

Fig. 2. Example of integrated probe signals to show reproducibility and onset of instabilities. Time scale 5 μs/div.

near the walls and during the subsequent compression the center of the current channel moves outwards. The confinement is not very good since the current density at the outer wall does not remain negligible. After about 25 μs the discharge becomes violently unstable and the confinement is lost. Application of the Suydam criterion indeed shows that the configuration is unstable, the criterion being violated at first in the outer parts of the current channel. The B_z probe data show that the

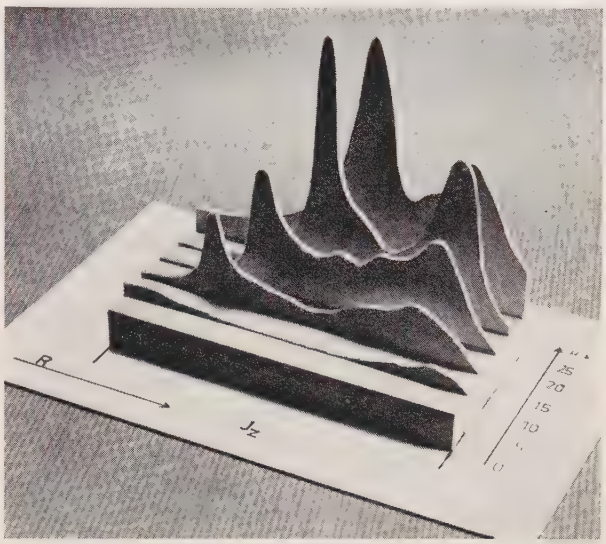

Fig. 3. A model of the i_z distribution for the case with only weak B_z field. Time 0–25 μs, the outer wall to the right.

initial flux is compressed inside the pinch, although not completely. The field rises from 280 gauss to a maximum of 1800 gauss, which is about 60% of a theoretical value if complete trapping is assumed.

The spectroscopic work has been concerned with the existence and time variation of different elements and their ionization stages in the discharge. Fig. 4 shows a time resolved spectrogram from the center viewing port for the discharge described above. For clarity a schematic representation of the spectrogram has also been made, see fig. 5. During the first half period, which is the most interesting, lines only from D, C, N, and O appear, while wall impurities such as Si and Al appear later on. Thus the plasma seems to be reasonably free from impurities. From the variation of the different ionization stages it is concluded that the electron energy is highest in the first half period. The current is not much lower during the second half period and therefore a cooling by impurities should be responsible for the lower electron energy. A gated spectrogram of the first half period has shown that the OV and CIV lines originate from the center of the discharge. Some lines between the second and third

half periods in fig. 5 are due to flashes in the viewing port. They are eliminated in later experiments.

Some spectrograms were taken with the probe inserted in such a way as to come within the

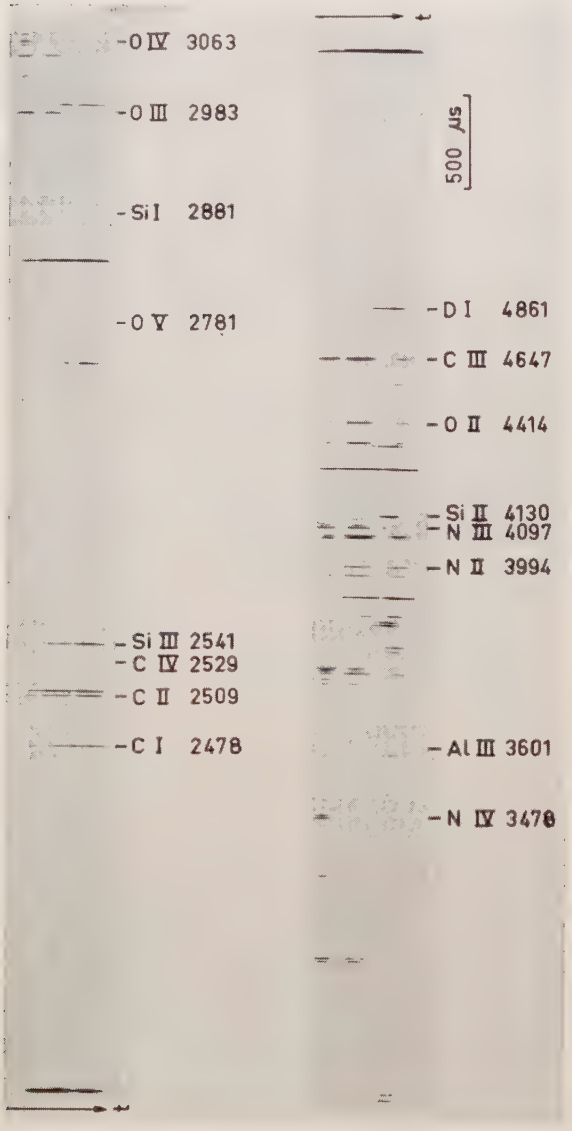

Fig. 4. Time resolved spectrogram for the discharge type shown in fig. 3. Exposure: 10 shots.

viewing angle of the spectrograph. Then the lines from OV and CIV disappeared, but no increase in the intensity of the Si lines was detected. Thus the plasma seems to be cooled in the vicinity of the probe even though the amount of evaporation is small.

The strong B_z field, peak value 5.5 kgauss, has been used in several ways. If it is started before or at the same time as the gas current, the latter can reach high values, up to 200 kA. However, a strong field inside the current channel prevents pinching. A spectrogram from such a discharge also showed an intense impurity spectrum with no lines from high ionization stages.

It is thus essential to delay the B_z field, and ac-

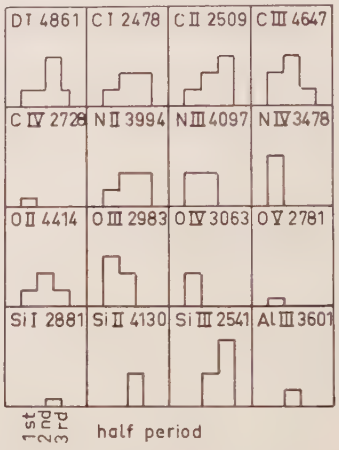

Fig. 5. Schematic representation of the spectrogram in fig. 4 by means of estimated intensities.

cording to the theories it should be given a direction opposite to that of the weak field. Both field directions were tried at first, but only the reversed field did give effects of interest.

Oscillograms of the gas current and the induced voltage on the copper shell are given in fig. 6, for a case where the reversed field is delayed by 15 μs from the onset of the gas current. The field has a very small influence on the total gas current but a pronounced influence on the discharge impedance. The small dip in the voltage curve at the very start of the reversed field is probably due to a current increase in the outermost regions, and the following sharp rise is a consequence of the plasma compression and the change in $i\theta$, resulting in a higher inductance.

The effects of the reversed field are superposed on the ordinary pinch dynamics and careful probe measurements are required to obtain a more detailed information. The B_z probe data confirm an additional compression of the current channel; the trapped weak field reaches a higher value. The

interdiffusion between the plasma and the reversed field is fairly slow in the beginning, but the final collaps of the hollow current channel is very rapid.

The i_z distribution for a case with $B_{z0} = 280$ gauss, reversed field delay 15 μs, is shown in fig. 7. An important difference in comparison with fig. 3 is the improved confinement, especially from the outer wall, where the current density is now negligible. The confinement also lasts for a longer time, about 30 μs.

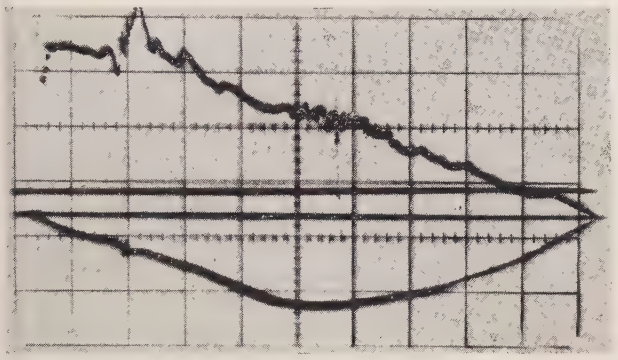

Fig. 6. Oscillograms of the axial gas current, lower beam, and the voltage per turn, measured on the copper shell, upper beam. Time scale 10 μs/div. Both weak and strong B_z fields. The latter starts at 17.5 μs.

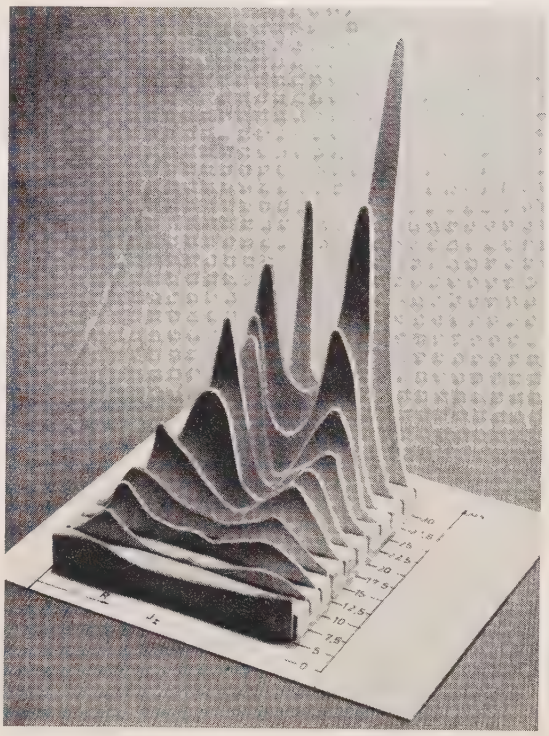

Fig. 7. The i_z distribution shown as in fig. 3 for the case with both weak and strong B_z field, $B_{z0} = 280$ gauss. Time 0–30 μs; the strong reversed field starts at 17.5 μs.

No wide conclusions on the possibilities of plasma confinement and heating by this method will be given here, however, as they require more detailed measurements and further variations of parameters. Such variations have indeed indicated that the stability is strongly dependent upon the initial gas pressure, the weak field and the gas current. For certain sets of these parameters with the peak gas current lower than 30 kA, it has even been possible to produce discharges, that are stable during the whole first half period, 100 μs.

Acknowledgements

We wish to express our sincere gratitude to Professors Per Ohlin and Kai Siegbahn for their interest and support during these investigations. Thanks are also due to Dr. Kjell Bockasten, who has guided the spectroscopic work. Technical and financial support has been given by ASEA and the work has been sponsored by The Swedish State Power Board and by the Air Research and Development Command, United States Air Force, through its European Office.

NUCLEAR INSTRUMENTS AND METHODS 13 (1961) 206–210; NORTH-HOLLAND PUBLISHING CO.

DIODE A BARRIERE DE SURFACE POUR LA DETECTION DE PARTICULES NUCLEAIRES

J. BOK et J. P. NOEL

Centre d'Etudes Nucléaires de Fontenay aux Roses, France

Reçu le 13 avril 1961

A method is described for the preparation of p-n junctions by surface-barrier for nuclear particles detection. The method used is the surface oxidation. Ozone is employed to stabilize the inversion layer. The main characteristics of this detector and the results obtained are given.

1. Principe du détecteur a barrière de surface

Considérons une jonction n,p dans un semiconducteur. Cette jonction étant polarisée en inverse, il existe une barrière d'épaisseur e donnée par la formule:

$$e^2 = \frac{V}{N} \times 1.33 \times 10^{15} \quad \textit{pour le silicium}$$

où e est en microns
V est la différence de potentiel appliquée en volts
N est le nombre de porteurs en cm^{-3} (fig. 1.)

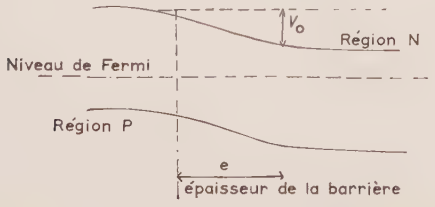

Fig. 1. Schéma de la barrière.

Le courant qui passe en inverse est extrêmement faible car la barrière est isolante (elle no contient pas de porteurs).

Une particule ionisante (α, proton, etc...) arrivant dans la barrière crée des paires électrons-trous qui sont collectées par les électrodes.

La quantité de paires électrons-trous crée est:

$$n = \frac{E}{\varepsilon_i}$$

Où E est l'énergie de la particule incidente et ε_i l'énergie necessaire pour faire 1 paire électron-trou.

Cette énergie est de 3.5 eV pour le *silicium*.

La charge Q libérée dans le barrière est donc:

$$Q = 2ne$$

$$Q = 2e\frac{E}{\varepsilon_i}$$

(e charge de l'électron).

et l'impulsion de tension recueillie est de hauteur:

$$V = \frac{Q}{C}$$

où C est la capacité de la jonction.

On a donc:

$$V = \frac{2e}{C}\frac{E}{\varepsilon_i}.$$

Nous avons donc une impulsion par particule absorbée, les système est donc détecteur.

D'autre part, la hauteur de l'impulsion est proportionnelle à E, le dispositif constitue donc un *spectromètre.*

2. Paramètres importants pour le détecteur

Les caractéristique physiques importantes du spectromètre sont:

2.1. L'ÉPAISSEUR DE LA BARRIÈRE e

En effet, la hauteur de l'impulsion est proportionnelle à l'énergie tant que toute l'énergie E de la particule est absorbée dans la barrière. L'épaisseur de la barrière nous donne donc l'énergi e maximum de la particule que l'on pourra mesurer.

Les deux moyens d'augmenter V sont donc:

1°) Diminuer N c'est à dire prendre un semiconducteur avec très peu de porteurs donc très pur.

On a utilisé du silicium pour lequel N était compris entre 3×10^{13} cm^{-3} et 2×10^{12} cm^{-3}.

2°) Augmenter V, on est limité dans cette voie par le courant continu qui passe dans la jonction.

2.2. LE COURANT INVERSE i_s

Ce courant doit être le plus faible possible car un fort courant diminue le rapport signal sur bruit c'est à dire la résolution du spectromètre.

L'expérience montre que ce courant est surtout un courant de surface. En effet le courant théorique de saturation calculé est très inférieur au courant observé même dans les cas les plus favorables.

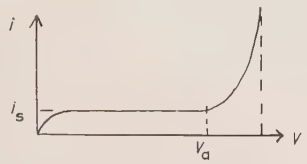

Fig. 2. Schéma de courant inverse.

Nous pouvons limiter le courant dû au courant de surface par l'utilisation d'un anneau de garde (voir fig. 7 et photographie). Celui-ci est relié directement à la haute tension. De cette manière, le courant de surface ne passe pas dans la résistance de charge et ne donne pas de bruit. Le courant inverse a la forme suivante (voir fig. 2).

On a un courant de saturation I_s, puis une montée rapide (avalanche). La tension inverse maximum applicable est précisément cette tension d'avalanche V_a.

Nous donnons (fig. 4) les caractéristiques inverses des jonctions que nous avons fabriquées.

2.3. LA SURFACE

Deux facteurs dépendent de la surface:

1) la sensibilité du détecteur

2) la résolution

1) La sensibilité augmente évidemment avec la surface.

2) On est cependant limité dans cette voie car la résolution diminue quand augmente la surface. En effet, la capacité de la jonction augmente, donc le signal diminue. D'autre part le courant augmente avec la surface, donc le rapport signal sur bruit diminue fortement.

En résumé une diode doit avoir:

- V maximum pour I donné.
- N le plus faible possible – silicium de départ très pur.
- Surface la plus grande possible pour une résolution donnée.

D'autres considérations entrent en ligne de compte:

- solidité mécanique
- et surtout stabilité des caractéristiques dans le temps.

2.4. CHOIX DU PROCÉDÉ DE FABRICATION

La méthode couramment employée pour faire des jonctions n,p dans du silicium est la diffusion d'impuretés.

Cette méthode présente les inconvénients suivants:

l'épaisseur diffusée est en général assez grande. Elle est de l'ordre du micron, ce qui fait une sorte de fenêtre pour les particules où elles perdent une partie de leur énergie.

pour du matériau de base de type p, la surface est sensible à l'oxydation et ces diodes ne se conservent pas à l'air. Par contre en partant de type n très pur, il est impossible de chauffer et de garder la pureté initiale.

Nous avons choisi le méthode qui consiste à faire une barrière de surface (jonction à la surface) par oxydation[1,2]).

Cette méthode élimine lesdeux inconvénients précédents (on part de type n, et on ne chauffe pas).

3. Mode de fabrication du détecteur (fig. 3)

3.1. RÉALISATION MÉCANIQUE DU COMPTEUR†

La technologie utilisée est très proche de celle employée dans la technique des transistors, toutefois les matériaux servant à la construction ont été choisis parmi coux présentant une faible section efficace d'activation. Ce compteur a été fait aussi discret que possible afin que dans les milieux de mesure sa perturbation soit faible.

[1]) J. L. Blankenship et J. C. Borkowski, Trans. I.R.E. on nuclear Science 5, 1 (1961) 17.

[2]) G. Dearnaley, Trans I.R.E. on nuclear Science 5, 1 (1961) 11.

† Les chiffres entre parenthèses se rapportant au schéma du détecteur de la figure 3.

Le matériau de base: le silicum est livré sous forme de billette d'un diamètre variant de 1 à 3 cm et d'une longueur de 10 cm de minces plaquettes de 0.5 mm à a mm d'épaisseur y sont découpées (1) au moyen d'une scie diamantée tournant à grande

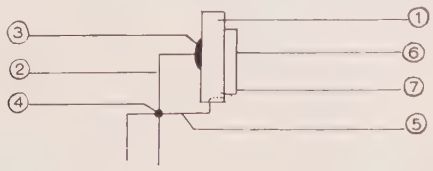

Fig. 3. Schéma de la diode.

vitesse. Une des faces de chaque plaquettes est soigneusement polie au moyen d'abrasif de différentes graduations afin de faire disparaitre toutes détériorations de la surface ayant pu être causées par le sciage, le polissage est terminé à la peau de chamois. Ces plaquettes sont lavées soigneusement dans une solution d'acide fluorhydrique diluée, puis ces dernières sont placées dans un bain de nickelage, après nickelage une piéce d'aluminium A G (2) est soudée au moyon d'indium (3) sur le revêtement de nickel assurant ainsi un bon contact électrique avec le silicum la pièce d'aluminium (2) possède un passage isolant fait au moyen de résine araldite afin d'assurer ultérieurement le contact électrique de la barrière.

3.2. FORMATION DE LA COUCHE D'INVERSION

Le traitement pour obtenir une couche d'inversion du type p sur du silicium N consiste à faire une attaque chimique de la surface parfaitement polie, en milieu oxydant la méthode expérimentale est la suivante.

a) La surface polie est attaquée pendant 5 minutes dans une solution conteneant 25 cc d'acide fluorhydrique et 50 cc d'acide nitrique.

b) Après attaque, la solution est diluée dans l'eau distillée, la plaquette de silicium est sortie de la solution lorsque la concentration en acide est très faible.

c) La surface de la plaquette est lavée plusieurs fois dans l'eau distillée chaude, puis placée dans une atmosphère saturée d'ozone durant 6 heures.

d) La plaquette est sortie à l'air ambiant puis plongée quelques minutes dans du tetrachlorure de carbone.

e) De nouveau placée dans l'atmosphère d'ozone pendant une dizaine d'heures. Cette oxidation rend la diode beaucoup plus stable, en particulier sous vide.

f) La plaquette est de nouveau sortie à l'air ambiant, le contact électrique de la couche d'inversion étant fait 6 heures après la deuxième oxydation.

3.3. CONTACT ÉLECTRIQUE DE LA BARRIÈRE

Au moyen d'un cache de mica une mince couche d'or (quelques μ g/cm) et déposée par évaporation sous vide sur la couche d'inversion la surface de cette couche déterminant la zone utile du compteur (6) un fil d'or de 50 μ de diamètre (7) est soudé sur un petit appendice solidaire de la zone utile, soit à la laque d'argent, soit par thermo contact; l'autre extremité du fil d'or est soudée à l'indium sur le conducteur électrique (5). Dans le cas du contact à l'argent il faut attendre le séchage complet de la laque (qui peut être accéléré par le chauffage à l'air), afin d'obtenir des caractéristiques électriques stables.

Les performances atteintes par les diodes fabriquées selon cette méthode sont les suivantes:

4. Résultats

4.1. CARACTÉRISTIQUE INVERSE

Les diodes de 20 mm² ont les caractéristiques suivantes (silicium de résistivité 1.600 $\Omega \times$ cm).

0,2 μA à 40 V
0,4 μA à 90 V .

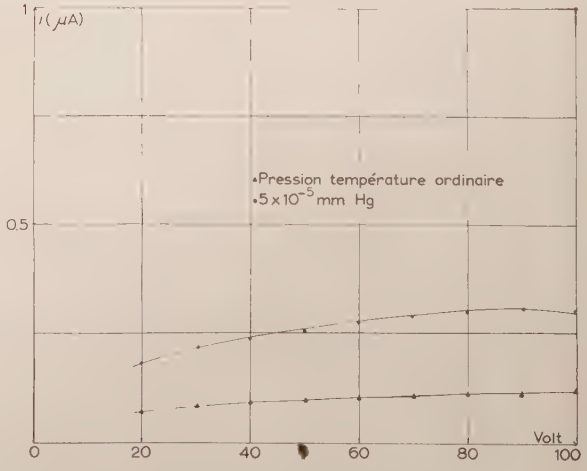

Fig. 4. Caractéristique inverse.

Les diodes de 9 mm² donnent

0.05 μA à 20 V

0.1 μA à 40 V

0.2 μA à 90 V.

Ces performances pouvent être amélierées avec silicium de plus haute résistivité.

La surface maximum réalisée est de 1 cm². Nous donnons des exemples de caractéristiques dans le figure 2 ainsi que l'influence du vide sur ces caractéristiques.

4.2 EPAISSEUR DE LA BARRIÈRE

Pour du silicium de 2.500 $\Omega \times$ cm de résistivité et une polarisation inverse de 90 V, l'épaisseur e de la barrière est

$$e = 230\,\mu\,.$$

Nous pensons augmenter cette épaisseur en utilisant du silicium plus pur et en augmentant la tension inverse de polarisation. On est limité dans cette voie par l'apparition de microclaquages. L'épaisseur de la barrière est déterminée par des mesures de capacité de la jonction (fig. 5).

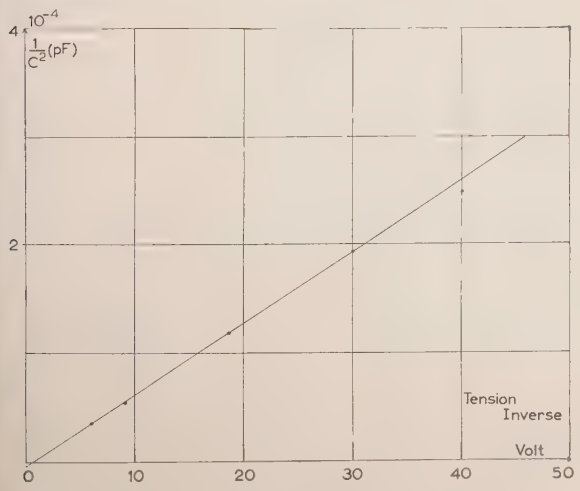

Fig. 5. Capacité de la barrière.

4.3. RÉSOLUTION

Nous donnons fig. 6 un spectre de particules α issus d'une source contenant un mélange de U^{233} et Pu^{239}, réalisé au moyen d'une de nos diodes.

Nous voyons que la largeur des pics est de 40 keV environ.

Ce spectre a été réalisé au laboratoire d'Electronique Physique du Centre d'Etudes Nucléaires de Saclay grâce à l'obligeance de Madame Koch.

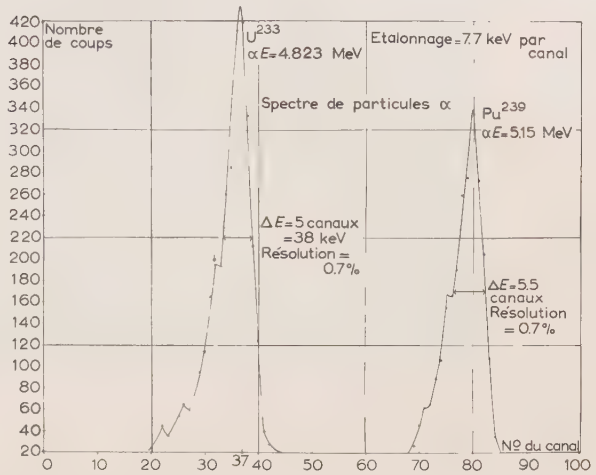

Fig. 6. Spectre de particules α.

4.4. STABILITÉ DANS LE TEMPS

A l'air: la stabilité dans le temps de ces détecteurs est très bonne lorsque les diodes sont conservées à l'air sans précaution spéciale. En quatre mois

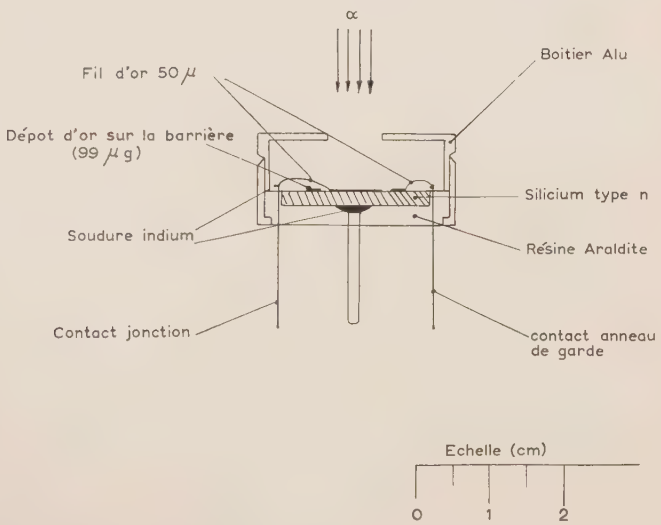

Fig. 7. Schéma de la diode à barrière de surface.

nous n'avons pas observé de variation notable des caractéristiques.

Sous vide: Ainsi qu'on peut le voir fig. 4 le courant inverse augmente lorsqu'on place la diode sous vide. Mais on atteint rapidement une valeur

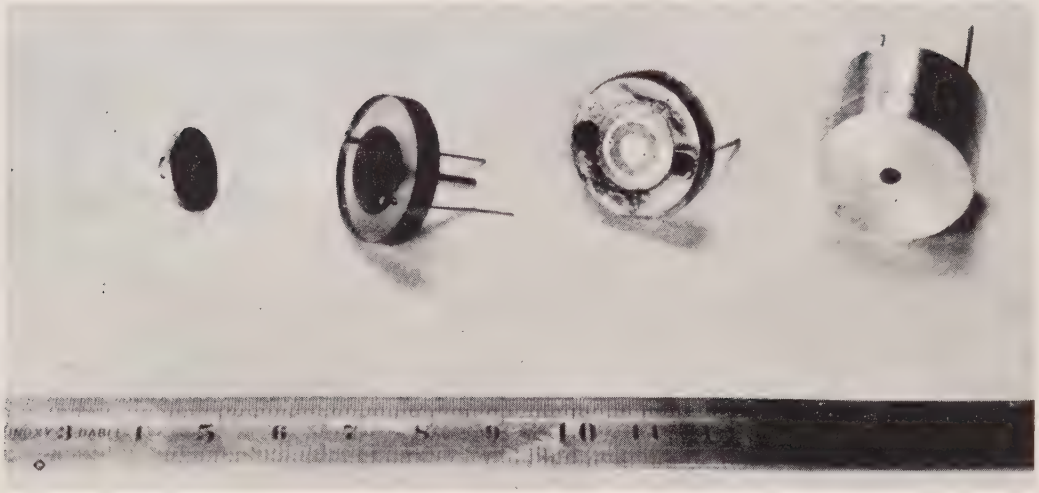

Fig. 8. Photographie de la diode à barrière de surface.

maximum qui reste ensuite très stable dans le temps. Ceci semble du à l'action de l'*ozone*.

Le schéma complet du détecteur est donné par la figure 7 et la photographie, fig. 8.

5. Utilisation du détecteur pour la spectrométrie de neutrons rapides

Ce détecteur peut être évidemment utilisé pour la spectrométrie de particules lourdes chargées quelconques.

Mais nous nous proposons avant tout de l'utiliser pour construire un spectromètre à neutrons rapides.

Description du spectromètre à neutrons rapides: voir fig. 9.

Le principe de ce spectrométre est le suivant: on utilise la réaction (n,α) sur le Li^6 (ref.[3])).

$$n + Li^6 \rightarrow He^4 + H^3 + Q$$

$$Q = 4.78 \text{ MeV}.$$

La particule α et le triton sont détectés par des diodes. Les deux impulsions sont ajoutées de manière à obtenir la somme des énergies.

On en déduit l'énergie du neutron:

$$E_n = E_\alpha + E_t - 4.78 \text{ MeV}.$$

Le schéma du spectromètre est donné fig. 9.

Le Li^6 est déposé sur une diode sous forme de FLi^6 par évaporation sous vide. L'épaisseur de la couche est d 1 μ environ. Une deuxième diode est alors appliquée sur la couche de FLi^6.

L'ensemble des 2 diodes peut être considéré comme un compteur 4π.

Ce spectromètre est actuellement en cours d'essais

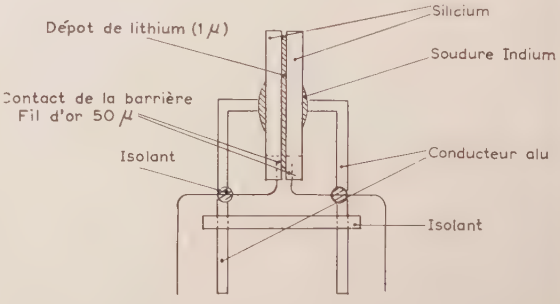

Fig. 9. Schéma du spectromètre à neutrons rapides.

(en particulier le dispositif électronique d'addition et d'amplification des impulsions).

Les premiers résultats soront publiées prochainement.

[3]) T. A. Love et R. B. Murray, Trans. I.R.E. on nuclear Science **5**, 1 (1961) 91.

NUCLEAR INSTRUMENTS AND METHODS 13 (1961) 211–214; NORTH-HOLLAND PUBLISHING CO.

THE PREPARATION OF THIN SELF SUPPORTING BORON FILMS

A. H. F. MUGGLETON and F. A. HOWE

Atomic Weapons Research Establishment, Aldermaston, Berks. England

Received 17 June 1961

A method of producing thin (20–100 $\mu g/cm^2$) self supporting films of boron by vacuum evaporation is described. The high evaporating temperature required was obtained by electron bombardment. The merits of various crucible materials are discussed and a technique for mounting the foils is described.

1. Introduction

Various techniques have been developed for making boron films suitable for use in nuclear experiments. They include

(a) vapour plating[1–3]);

(b) painting with boron in suspension[1]);

(c) settling of finely divided particles[1]);

(d) bonding amorphous powder to a suitable surface using a binding agent such as polystyrene dissolved in acetone[1]), and (e) vacuum evaporation[4–7]).

Method (a) produces good quality, uniform films by a rather hazardous and complicated technique whereas the other methods, with the exception of (e), produce comparatively thick, non-uniform films which are chemically impure and unsuitable for nuclear spectroscopy experiments[8]).

Several workers[4–7]) have made boron films by vacuum evaporation and this was the method finally selected by the authors. Due to the reactivity of boron with refractory metals at the temperatures necessary for volatilisation ($\approx 2300°C$), the use of normal resistance heating was ruled out. It was considered that satisfactory results could be obtained using refractory crucibles and two methods presented themselves (i) Radiofrequency induction heating and (ii) Electron bombardment heating.

2. R. F. Induction Heating

The R.F. induction heating method was tried initially using a carbon crucible inductively heated in a high vacuum chamber. Analysis of films produced this way showed that at least 50% of the deposit was carbon.

Tungsten, the next crucible material considered, was readily attacked by molten boron, the resulting films having approximately 3% tungsten contamination. In addition, tungsten crucibles are difficult to produce and consequently expensive.

The most satisfactory crucible material was found to be tantalum. Although the material cost is about the same as tungsten, machining is easier, the crucibles resist the molten boron to a greater extent and the resulting films contain only trace amounts of tantalum.

The induction method, outlined above, produced satisfactory results but had the following disadvantages:

(i) Discharges, which occasionally occurred due to the effusion of gas, caused severe pitting of the water cooled R. F. work coil. This pitting would eventually result in the work coil being punctured and the system flooded with water.

[1]) R. W. Dodson, A. C. Graves, L. Helmholz, D. L. Hufford, R. M. Potter and J. G. Poveletes, Chapter 1 in A. C. Graves and D. K. Froman, Miscellaneous Physical and Chemical Techniques of the Los Alamos Project (McGraw-Hill Book Co., Inc., New York).

[2]) R. Kiessling, Acta Chem. Scandinavia 2 (1948) 707.

[3]) H. I. Schlesinger, U.S. Atomic Energy Commision Report Nos MDDC 1339 and MDCC 1340.

[4]) H. M. O'Bryan, Rev. Sci. Instr. 5 (1934) 125.

[5]) J. Flinta, Vacuum 2, No. 3 (1960) 257.

[6]) J. G. Robins, A.E.R.E. Harwell (Private communication).

[7]) D. Barnes, R. B. Mackenzie and R. Aves, A.E.R.E. (Harwell) Report R/M 125.

[8]) S. Hinds and R. Middleton, A Study of (^{3}He, d) reactions leading to ^{11}C and ^{12}C, To be published in Proc. Phys. Soc.

(ii) Crucible lifetime was limited.

(iii) Inconvenient and expensive shielding was necessary to eliminate the radio frequency interference associated with this equipment.

3. The Electron Bombardment Method

To overcome the difficulties associated with the R.F. method it was decided to construct an electron bombardment apparatus. The evaporating chamber,

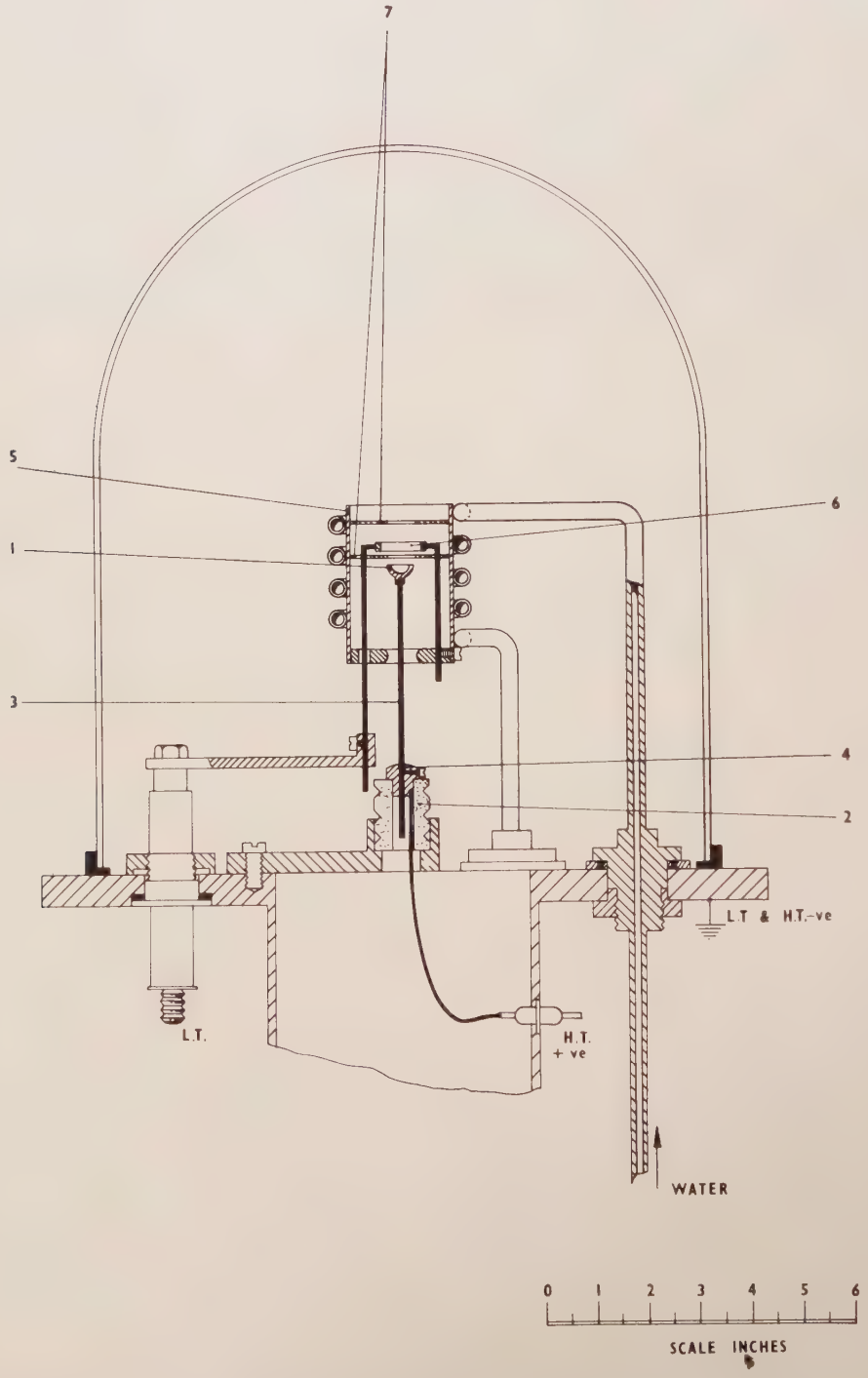

Fig. 1. Diagrammatic view of the electron bombardment apparatus. Key to figures given in the text.

shown diagrammatically in fig. 1, is mounted on an Edwards High Vacuum 6″ oil diffusion pump, suitably trapped and backed with a NGN, PSR 12 rotary pump, giving an ultimate vacuum better

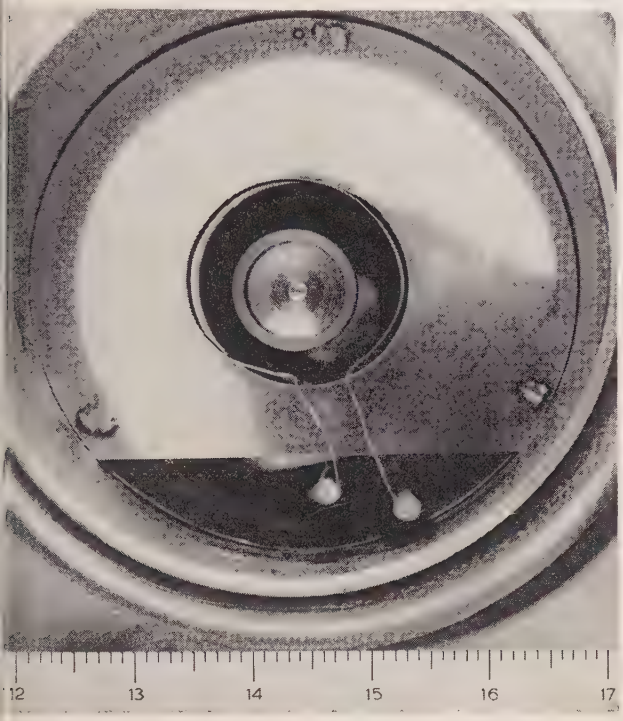

Fig. 2. Electron bombardment apparatus.

than 1×10^{-5} torr. The electron bombardment apparatus is mounted on a 14″ dia. brass plate and housed in a 12″ dia. hard glass bell jar. Tantalum crucible (1) froms the anode of a simple diode and is insulated from the baseplate by the ceramic coil former (2). Tungsten support rod (3) is a sliding fit in boss (4) thus providing height adjustment for the crucible. A water cooled heat shield (5) protects the glass bell jar and baseplate from intense heat radiation generated during evaporation. Electrons emitted from the $\frac{1}{8}'' \times 0.005''$ tantalum filament (6) are focussed on the centre of the boron charge by two molybdenum disc electrodes (7). One side of the filament support is connected directly to the water cooled shield, the other support passing through an aperture in the base of the shield to an insulated baseplate connection. Focussing of the electron beam was attainable with considerable accuracy. Variation of crucible height and filament diameter enabled a geometry to be obtained which produced a suitable voltage-current setting at the required evaporating temperature. This temperature was maintained at the centre of the boron

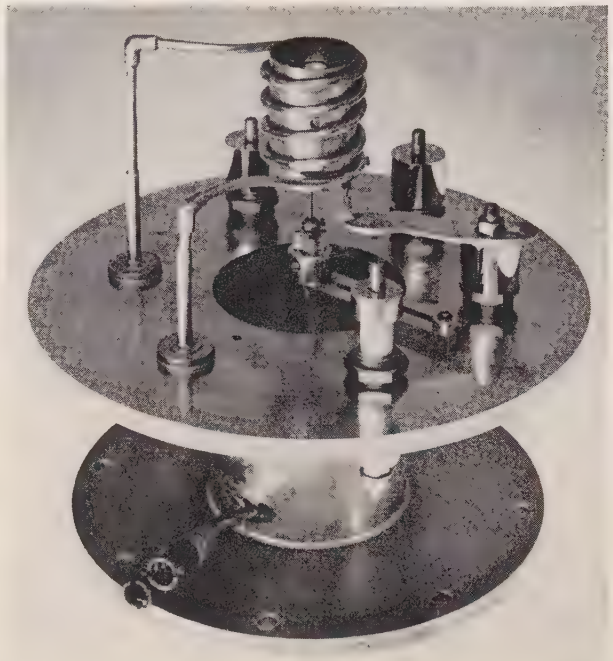

Fig. 3. Enlarged view inside the water cooled shield with the top focussing electrode removed. Showing the filament and anode assembly.

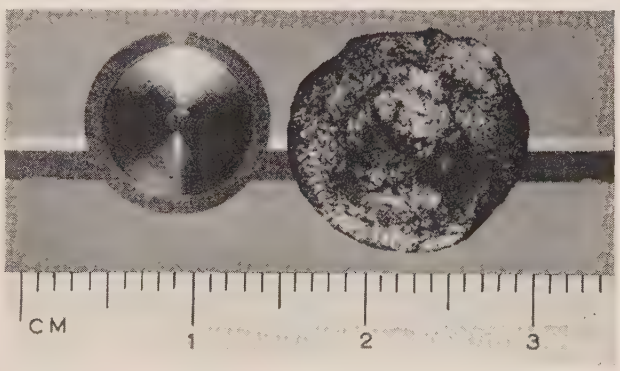

Fig. 4. Tantalum crucibles (a) new crucible; (b) crucible that has been used approximately fifty times showing the central depression caused by the focussed electron beam.

charge, a marked temperature gradient across the crucible being clearly observed. The tantalum crucible/boron interface temperature was much

lower than that of previous methods, thus minimising crucible erosion and the possibility of film contamination. Crucible life has been improved to the extent that original experimental prototypes have not been replaced.

4. General Procedure

Borosilicate microscope slides, cleaned in an isopropyl alcohol vapour degreaser, or alternatively freshly split ruby mica, were used as substrates for the evaporated boron. To facilitate subsequent stripping of the film in a water bath a spot of teepol was placed onto the exposed substrate surface and polished off vigorously with a clean selvyt cloth. The slide, together with a clean, vacuum baked, microscope cover glass slide ($1'' \times 1'' \times 0.010''$); the weight of which had been accurately determined, was mounted approximately 6 cm above the crucible. Careful handling of the cover glass reference slide with tweezers was essential for accurate film weight determination.

Having evacuated the system to a pressure of $\approx 1 \times 10^{-5}$ torr the filament temperature was raised to approximately 1500°C. After allowing the pressure to stabilize a positive voltage was applied to the anode and gradually increased to some 500 V, the filament temperature being raised to give space charge limited emission, i.e. to a point at which further increase in filament temperature produces little or no increase in anode current. The H.T. voltage was raised gradually, with occasional adjustments of filament temperature, until the crucible reached approximately 2300°C (measured with an optical pyrometer). At this temperature a satisfactory rate of evaporation was observed. Overheating caused spitting of the boron charge resulting in pinholed films. By observation of the colour change it was possible to make a reasonably accurate estimate of the weight/area of the deposit, and furthermore, by careful setting of the anode wattage, time control of the evaporation yielded reproducible results.

After allowing adequate time for cooling the system was vented to air and the calibration slide re-weighed. The weight accepted was that at a fixed time interval after venting of the system, this was necessary because of the considerable rate at which clean surfaces absorb and adsorp atomospheric gases and vapours. A gain of some 10 $\mu g/cm^2$ was found to be quite usual during the first few minutes of exposure.

If the weight of boron deposited was found to be incorrect a fresh support slide was prepared and the evaporation process repeated, using the same calibration slide and making the necessary estimated correction to the evaporation time. Attempts were made to increase the film thickness by building up layers in successive evaporations but it was found that when floating off for mounting the layers separated due to the solubility of the boron oxide interfaces.

The floatation technique described by Dearnaley[9]) was used to strip the films from their substrates.

Care was taken during this operation to avoid water creeping over the exposed boron surface before separation commenced. The target holder, which should be as thin as possible and have well polished edges to the aperture, was slid beneath the foil and raised at an angle once the film had been correctly located. Excess water was blotted from the holder with a piece of filter paper and after allowing to dry the films were stored in a dessicator until required.

5. Conclusions

High purity, self supporting boron films are best produced using the electron bombardment heating method. Crucible contamination is minimised by the use of tantalum, and suitably designed crucibles give a long working life. Carbon and tungsten were found to be unsuitable as crucible materials, the films produced in each case showed appreciable crucible contamination.

Acknowledgements

The authors would like to thank Dr. L. A. Warren for analysing the films and Mr. C. Parsons for his invaluable assistance throughout the project.

[9]) G. Dearnaley, Rev. Sci. Instr. **31** (1950) 197.

NUCLEAR INSTRUMENTS AND METHODS 13 (1961) 215–223; NORTH-HOLLAND PUBLISHING CO.

MEASUREMENTS OF INSTRUMENTAL TIME DELAY AND RESOLUTION IN A FAST COINCIDENCE SYSTEM

W. M. CURRIE, R. E. AZUMA† and G. M. LEWIS

Department of Natural Philosophy, The University, Glasgow

Received 6 July 1961

An experimental investigation has been made of the instrumental time delays and resolution of a fast coincidence system as a function of the energy liberated in the scintillators. This has been done for NaI(Tl), anthracene, plastic and liquid scintillators whose decay times, relative efficiencies and photo electron yields have also been investigated. The results serve to assess some of the errors and limitations inherent in the measurement of very short times, and give some indication of their causes

1. Introduction

There has been some discussion[1–5]) during the past ten years or so of the limitations of fast coincidence systems incorporating scintillation counters, and several efforts have been made[3,6,7]) to correlate experimental findings with theoretical predictions Unfortunately several adjustable parameters are involved, while comprehensive experimental data, particularly on instrumental time delays, are rather scarce. This work was undertaken to help fill this gap. Emphasis is placed on investigating the dependence of instrumental time delays on the energy communicated to the scintillators. These time delays are of paramount importance in many experimental investigations utilising fast coincidence units since they necessitate very restricted energy selection.

The coincidence system dealt with here uses time to pulse height conversion. In this process the output pulse from the photomultiplier cuts off the current in a limiter valve, thereby producing a positive pulse of constant amplitude at its anode. This limited pulse may be further shaped in cables and allowed to overlap a second pulse from another counter in a time to pulse height converter[8]), such as the 6BN6 valve, which charges an integrating condenser during the period of overlap. The use of a diode-discriminator coincidence unit is quite analagous[9,10]).

† Now at the Physics Dept., University of Toronto, Canada.

An alternative method involving tuned circuits and phase measurements[6]) has also been developed and some of the theoretical results derived for this technique will be adopted in the interpretation of the data. Reference should also be made to the work of Culligan and Lipman[11]) on a "zero crossing" method designed to minimise the shifts. Theoretical treatments have been given by Post and Schiff[1]) and Minton[3]), and more recently by Colombo, Gatti and Pignanelli[4]) and Gatti and Svelto[5]).

The basic relevant feature of the process depends on the accumulation of the discrete charges which cut off the limiter valve (c.f. fig. 1). Ideally, if one simplifies the electronic processes, this corresponds to the emission of Q photoelectrons at the cathode of the photomultiplier, which subsequently induce an associated step like function, at the output of the limiter. If this latter pulse overlaps an earlier ideal fast rising rectangular pulse from another

[1]) R. F. Post and L. I. Schiff, Phys. Rev. **80** (1950) 1113.
[2]) R. F. Post, Nucleonics (June 1952) 56.
[3]) G. H. Minton, J. Res. Nat. Bur. Stand. **57** (1956) 119.
[4]) S. Colombo, E. Gatti and M. Pignanelli, Nuovo Cim. **52** (1957) 1739.
[5]) E. Gatti and V. Svelto, Nucl. Instr. and Meth. **4** (1959) 189.
[6]) C. Cottini and E. Gatti, Nuovo Cim. **4**[2] (1956) 1550.
[7]) E. Bashandy, Nucl. Instr. and Meth. **6** (1960) 289.
[8]) G. C. Neilson and D. B. James, Rev. Sci. Instr. **26** (1955) 108.
[9]) Z. Bay, Phys. Rev. **83** (1951) 242.
[10]) R. E. Bell, R. L. Graham and H. E. Petch, Can. J. Phys. **30** (1952) 35.
[11]) G. Culligen and N. H. Lipman, CERN Report.

counter, only the front edge of the slowly rising pulse contributes to the instrumental time delay. Further time delay will be associated with the light collection and with the photomultiplier. In the first instance these will be neglected but will be referred to below. In a time-to-pulse-height converter of the type considered here the instrumental time delay t_c is the mean integrated charge lost to the 6BN6 derived by Colombo *et al.* for the ideal case to be, to first order,

$$\sigma^2 = \frac{Q}{3}\left(\frac{\tau}{R}\right)^2\left(1 + \frac{3}{2Q} + \frac{1}{2Q^2}\right). \qquad (2)$$

These formulae take into account only the scintillation response. Experimental deviations from these will occur because of photomultiplier transit time effects, and for a variety of other reasons such

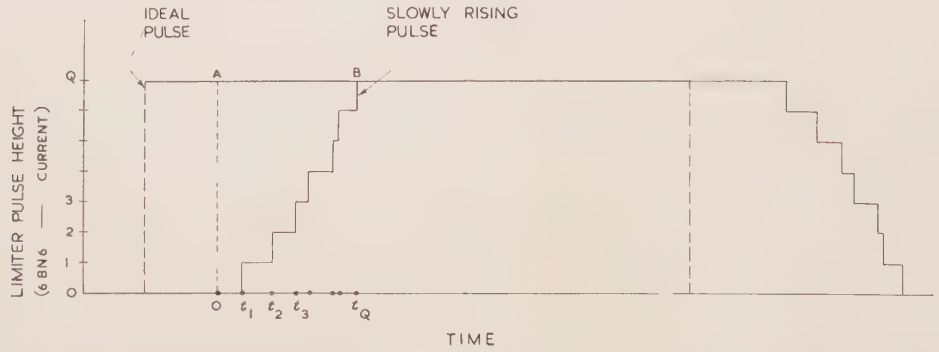

Fig. 1. Represents in simplified form the overlap between a slowly rising pulse from one counter and an ideal rectangular pulse from the other counter. The area OAB is lost due to the discrete arrival times of the electrons. Each step is associated with the liberation of 1 electronic charge at the photocathode. The area lost represents the charge which did not flow into the integrating condenser of the 6BN6 value. This gives rise to an instrumental time delay t_c. (The limiter current is assumed here to vary linearly with photomultiplier output until cut off.)

condenser divided by the maximum current in the 6BN6. Thus in fig. 1 it is the area OAB divided by the maximum current, AO, in the 6BN6 valve.

If each electron emitted by the photocathode results in a cathode flow i in the 6BN6, i.e. if the limiter and 6BN6 valve characteristics are linear, then

$$t_c = \frac{t_1 i + t_2 i + t_3 i + \cdots\cdots + t_Q i}{Qi}$$

where $t_1, t_2, \ldots, t_Q$ are the emission times of the first Q photoelectrons following a scintillation event. Thus t_c is the centroid of the charges. It can be shown on this basis, to second order, that

$$t_c = \frac{Q+1}{2}\left(\frac{\tau}{R}\right)\left(1 + \frac{Q+2}{3R}\right) \qquad (1)$$

where τ is the phosphor decay time and R is the total number of photoelectrons produced by the scintillation.

The resolution time is specified by the variance in t_c. The variance σ^2, equal to $(\overline{t^2} - \bar{t}^2)$ has been as fluctuation in photomultiplier gain and delays in light collection. To cite one instance at this stage, the instrumental time delay should be appreciably increased if the output pulse, generated by a photomultiplier from a single initial photoelectron, has a finite time spread λ. Here,

$$\lambda^2 = \int_0^\infty f(t)\,(t-a)^2 \mathrm{d}t \qquad (3)$$

where $f(t)$ is the pulse shape and a the arrival time of its centroid. The number of emitted photoelectrons then concerned in the process leading to cut-off will be greater than otherwise. The experimental consistency of the various hypotheses and other matters are referred to below.

2. Instrumentation and Procedure

The fast coincidence system used for these measurements was a time to pulse height converter of the fast-slow type first used by Neilson and James[8]) and developed by Green and Bell[12]). The present system is illustrated in fig. 2. The photomultipliers were RCA 6342A tubes operated at

[12]) R. E. Green and R. E. Bell, Nucl. Instr. 3 (1958) 127.

2300 V. The 6BN6 converter valve was run with 15 and 6 V on the anode and accelerator respectively. The single channel analysers made the selection of any desired energy range possible. The purpose of the biased amplifier was to permit magnification of the time scale, so that any selected portion of the coincidence pulse height spectrum could be expanded to cover the 150 channels of a multi-channel analyser. Calibration of the time scale was effected by adding varying lengths of 200 ohm cable (c.f. fig. 3).

The performance of the apparatus compares favourably with recent quotations[13–16]). Fig. 4 shows how the apparatus responded to self coincidences (limited pulse from one photomultiplier applied to both channels) produced by Co^{60} γ-rays. It shows also prompt coincidence curves obtained with Co^{60} γ-rays, and the annihilation radiation of Na^{22}. A full width resolution of $\approx 5 \times 10^{-10}$ sec with Co^{60} γ-rays is the lowest figure yet obtained with the present apparatus.

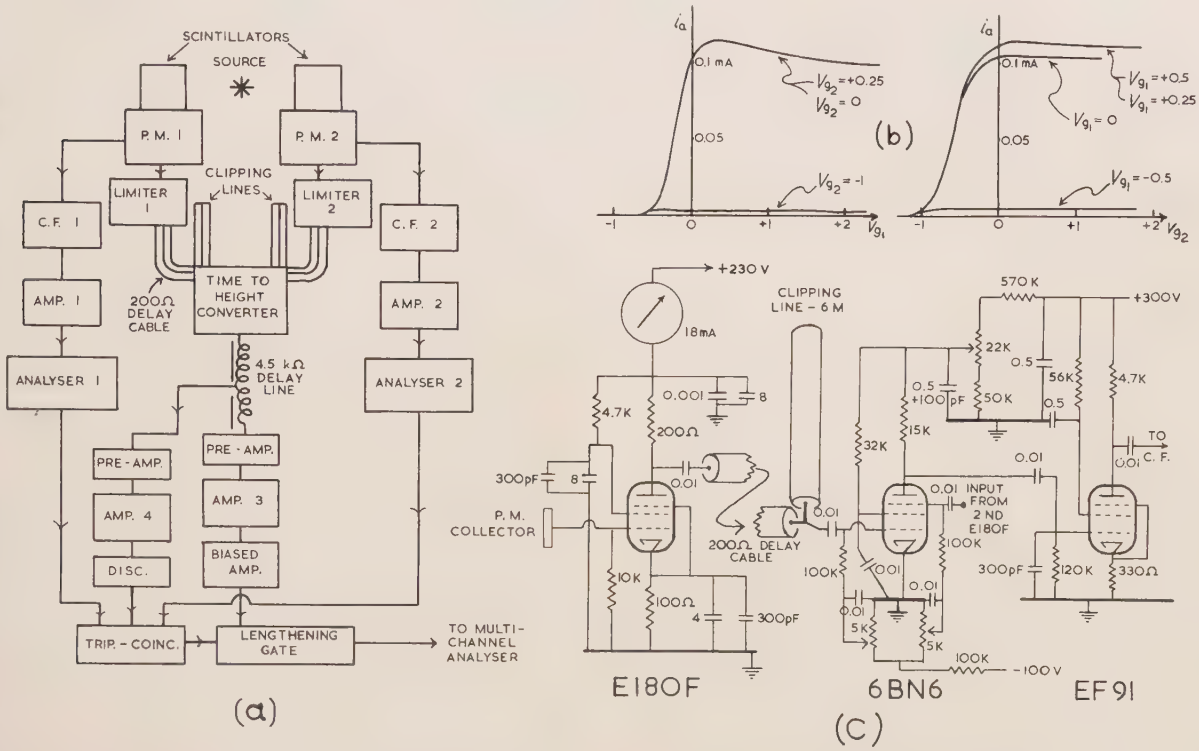

Fig. 2. (a) Block diagram of the fast coincidence system; (b) Characteristic of the 6BN6 value with 15 V on the anode and 6 V on the accelerator; (c) Details of an E180F limiter circuit and of the 6BN6 time-to-pulse-height converter.

3. Ancillary Measurements

The velocity of propagation in the 200 ohm delay cable was measured both by a standing wave method and by a time of flight (of photons) method. The two measurements gave the same result, namely $(0.90 \pm 0.01)c$ as the velocity for the cable.

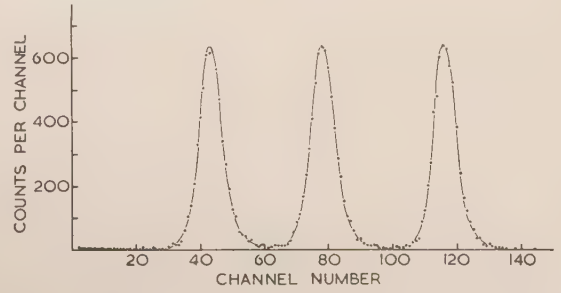

Fig. 3. Resolution curves obtained with a Co^{60} source. The separation between the peaks was produced by 50 cm of the delay cable (1.85 ns).

[13]) R. E. Bell and M. H. Jorgensen, private communication.
[14]) M. Bonitz and E. J. Berlovitch, Nucl. Instr. and Meth. **9** (1960) 13.
[15]) J. V. Kane, R. E. Pixley, R. B. Schwartz and A. Schwarzschild, Phys. Rev. **120** (1960) 162.
[16]) P. C. Simms, N. Benczer-Koller and C. S. Wu, Phys. Rev. **121** (1961) 1169.

The scintillation decay times were investigated for the samples used by a fast oscillograph method similar to that used by Phillips and Swank[17]). For

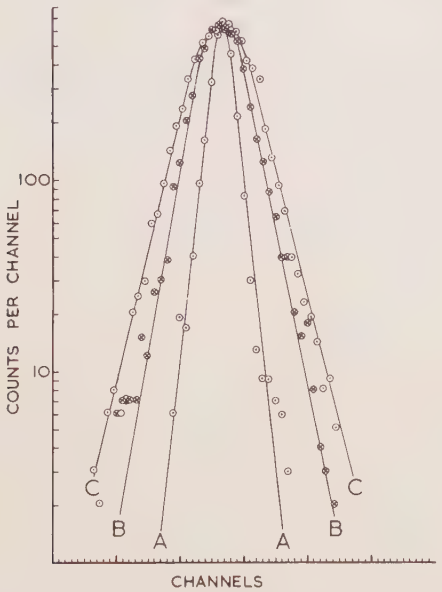

Fig. 4. Typical resolution curves obtained with energy selection illustrating the performance of the system. (A) Self coincidences (one multiplier output applied to both channels); full width resolution $= 2.7 \times 10^{-10}$ sec.; (B) Coincidences with Co^{60} prompt γ-rays; full width resolution $= 5 \times 10^{-10}$ sec; (C) Coincidences with Na^{22} annihilation radiation; full width resolution $= 5.9 \times 10^{-10}$ sec.

2.5 cm dia. $\times$ 2.5 cm NaI(Tl) the pulse shape was exponential with a decay time of $(2.34 \pm 0.12) \times 10^{-7}$ sec. The rise time was shown to be very fast, and plays no part in the work here. In the case of 1 cm^3 anthracene it was found that the decay was practically linear up to 60 nsec with an exponential tail. This did not present any difficulty in the analysis. It leads to an effective exponential decay time of (37 ± 2) nsec. No evidence of fast decay modes in NaI(Tl) or anthracene was found. With 2.5 cm diam. $\times$ 2.5 cm plastic and liquid scintillators the method indicated only that the decay times were less than 7 nsec.

The relative efficiencies of the scintillators were obtained by direct comparison. It is essential that the photoelectron yield P, per keV of dissipated energy be known with some precision, since otherwise an analysis in terms of Q and R is not very meaningful. Accordingly a preliminary effort was made to determine P. The energy resolution of a NaI(Tl)/6342A combination was studied in the range 35–280 keV. It was found that η^2, where η is defined as (full width at half height in keV)/(energy in keV), varied as the reciprocal of the energy, and that the values could be predicted if it were assumed that at least $2(\pm 15\%)$ photoelectrons were produced per keV of energy dissipated in the scintillator. Since fluctuations in light collection and other effects[18–20]) will tend to increase ηP can be expected to exceed this value of 2. It will be explained in the last section how a figure of $2.5(\pm 5\%)$ was obtained for P from the t_c shifts and σ^2 variation curves.

The results are listed in table 1. There is an error

Table 1.

Scintillator	τ (sec) (* quoted by manufacturer)	Efficiency (%) of anthracene ($\pm$ 2 %)	Photoelectrons per keV ($\pm$ 5% – c.f. fig. 7)
NaI(Tl)	$(2.34 \pm 0.12) \times 10^{-7}$	175	2.5
Anthracene	$(3.7 \pm 0.2) \times 10^{-8}$	100	1.4
Plastic Ne102	$*4 \times 10^{-9}$ $< 7 \times 10^{-9}$	35	0.5
Liquid Ne211	$*3 \times 10^{-9}$ approx. $< 7 \times 10^{-9}$	33	0.47

[17]) H. B. Phillips and R. K. Swank, Rev. Sci. Instr. **24** (1953) 611.

[18]) G. C. Kelley, P. R. Bell, R. C. Davis and N. H. Lazar, Nucleonics (April 1956) 53.

[19]) C. D. Zerby, A. Mayer and R. B. Murray, Bull. Am. Phys. Soc. **5** (1960) 417.

[20]) J. Monahan, S. Raboy and C. C. Trail, Bull. Am. Phys. Soc. **5** (1960) 104.

of 5% on the absolute value of P for NaI(Tl) but the relative values of P are believed correct to $\pm 2\%$.

4. Procedure

The position of the centroid of any resolution curve will depend on the energy selection. The change in t_c produced by a change of energy was measured for a given scintillator by observing the centroid shift of the resolution curve. The measurements of t_c were necessarily relative, since the zero value of t_c corresponds to the high energy limit and is inaccessible. Some measurements of this kind have already been made by Bashandy[7]) who treated his results in a manner different from that employed here. Also Bonitz and Berlovich[14]) have reproduced similar data but have not attempted to analyse the shifts.

For each series of measurements a plastic scintillator was used in channel 1 and the energy selected in this channel was kept fixed. The bias of the single channel analyser in channel 2 was varied systematically and resolution curves were recorded for each bias setting. The results of such a series of measurements with NaI(Tl) as the scintillator on the second counter are shown in fig. 5. The observed peaks (fig. 5) give directly the variation of t_c with energy. Furthermore the broadening of these peaks at low energies is due almost entirely to statistical fluctuations in the emission of light from the NaI(Tl), and the contribution of this variance to the total width obviously outweighs the contribution from channel 1 and from other sources.

Therefore these peaks are also adequate for obtaining the variation of σ^2 with energy. A similar procedure was followed when anthracene was used as the scintillator on the second counter. Moreover each sequence of measurements was repeated several times so as to improve the accuracy.

For the plastic and liquid scintillators the shift of the resolution curves as a function of energy was found in the same way as above. But the variation of σ^2 with energy was obtained somewhat differently as follows. Both single channel analysers were calibrated in terms of energy, and both were varied simultaneously so that the same energy range was selected in each channel. When this was done the centroid of the resolution curve did not move by more than $\pm 10^{-10}$ sec, thus indicating that the time delay in channel 1 was the same as that in channel 2. The changes in σ^2 were twice the changes which would have been produced had the energy been varied in only one channel, and a more accurate evaluation of the variation of σ^2 with energy could thus be obtained.

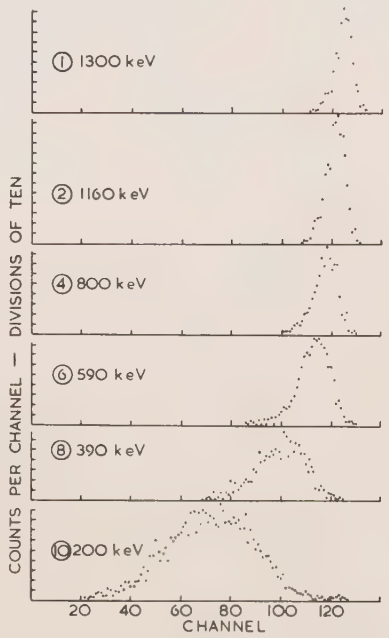

Fig. 5. Illustrating how the change of instrumental time delay, t_c, with energy was measured for a NaI(Tl) scintillator in Channel 2. The peaks were recorded for the mean energies indicated. The odd numbered peaks (only No. 1 shown) were all recorded with electrons of 1300 keV and were used as reference peaks and for stability checks. In the case of NaI(Tl) and anthracene, the variation of resolving time with energy was also obtained from such shifted peaks.

5. Results and Discussion

5.1. TIME DELAYS

The changes in time delay t_c for different energies, in NaI(Tl) and anthracene scintillators are shown in fig. 6. For each material the experimental points are measured relative to one another. The solid curve drawn through the NaI(Tl) points was calculated from eq. (1) by assuming that Q was the charge emitted at the photocathode by the liberation of 6.1 keV in the scintillator. It was then found that this figure for Q, taken in conjunction with the measured relative efficiency and decay time of

anthracene gave the theoretical curve drawn through the anthracene points in fig. 6. The zero of the time scale t_c was obtained from these theoretical considerations. However the measurements of time delay made with plastic and liquid scintillators could not be compared satisfactorily with theory in this simple way. For the quoted decay time of plastic and the measured relative efficiency the curve calculated from eq. (1) could not be made to

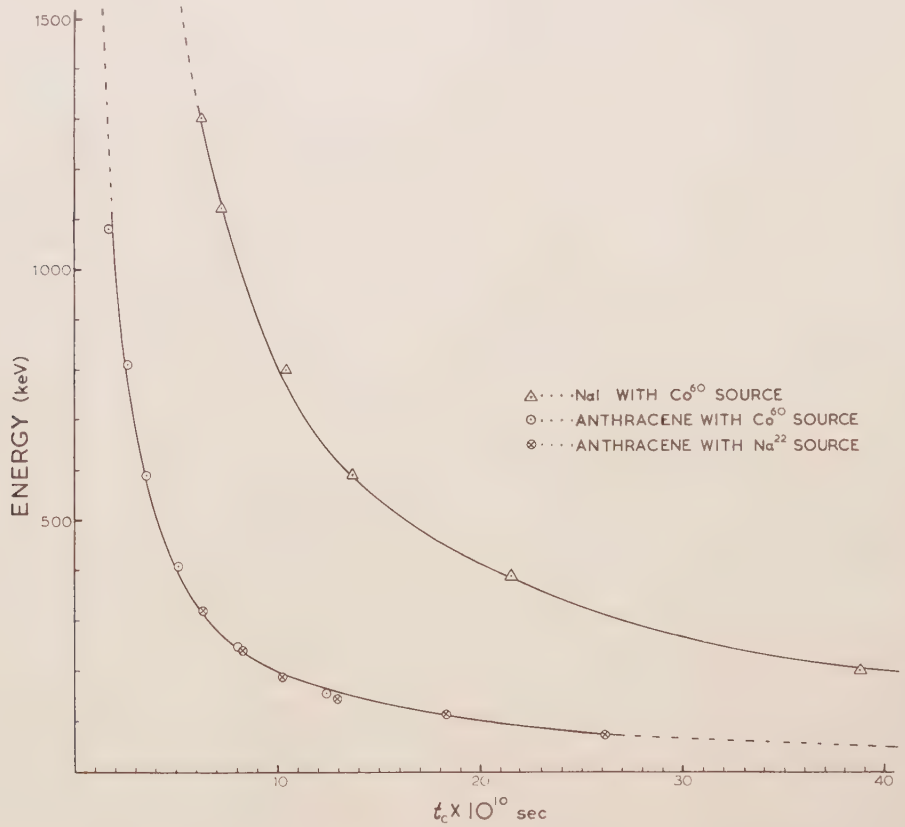

Fig. 6. Change of instrumental time delay, t_c, with energy for NaI(Tl) and anthracene scintillators. The solid curves are the theoretical curves obtained from eq. (1) with $Q = 15$ and P (number of photoelectrons/keV) = 2.5 and 1.4 for NaI(Tl) and anthracene respectively. The true zero of the t_c scale for the two curves (corresponding to the high energy limit) cannot be known experimentally. (The two experimental anthracene points at lowest energy were corrected to allow for slight non-linearity in the output of the scintillator.)

fit the experimental points. In fact the experimental points could not be fitted to a curve of this type at all. For these fast scintillators the effect of any transit time spread factor λ would be very important on the time shifts, which would be increased thereby. The fast scintillators are analysed more fully later (c.f. fig. 8).

To assess the value of P (the number of photocathode electrons per keV liberated in the scintillator) t_c^2 was plotted against σ^2 for the NaI(Tl) peaks. For, from eq. (1) and (2), to first order:

$$\sigma^2 = \frac{4}{3}\frac{Q}{(Q+1)^2}\, t_c^2. \qquad (4)$$

The plot is shown in fig. 7, where the values of σ^2 have been corrected to take account of the finite "window" widths, i.e. the variation of t_c in the energy interval selected for each point. A straight line plot was obtained and the gradient gave a figure of 15 photoelectrons for Q, and hence a figure for P of 2.5 photoelectrons per keV. A similar plot of t_c^2 against σ^2 for anthracene, for large values of t_c, showed a gradient very nearly, the same as that for NaI(Tl), confirming that Q was the same for both series of measurements. It will be noticed that

the mean line through the points does not pass through the origin. This is because of the finite contribution to σ^2 from the plastic scintillator in channel 1 and from the photomultipliers.

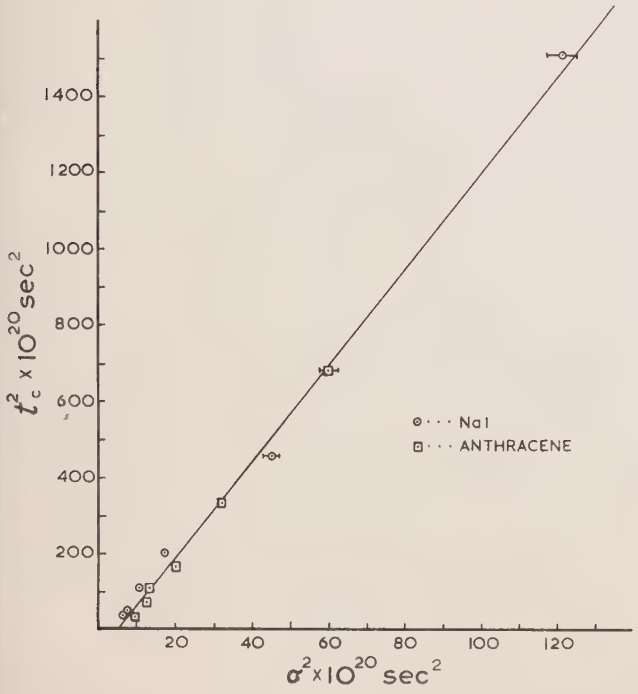

Fig. 7. t_c^2 plotted against the variance for NaI(Tl) and anthracene for large values of t_c. By the use of eq. (4) and the gradient of the mean line drawn through the points, a value of 15 was obtained for Q, showing overall consistency of interpretation for large t_c. The line does not go through the origin because of the contribution to the variance from channel 1 scintillator and the multipliers.

Returning to the fast scintillators, the results are illustrated in a different manner. Fig. 8 shows the experimental results along with the simple theoretical curve for plastic (broken curve) calculated from eq. (1) using the data of table 1. This figure should be compared directly with fig. 7 in the paper by Colombo *et al.*[4]). In that paper C designates the photoelectron equivalent of the charge required to cut off the limiter valve and it is pointed out that $C = Q$ only in the ideal case when $\lambda/\tau = 0$. In all other cases $C < Q$. This is because the limited speed of response of the multiplier (as measured by λ) to a delta function input (single photoelectron) introduces an additional delay whose energy dependence is different from that given in eq. (1). This effect is most serious when λ/τ is appreciable and when $t_c \lesssim \lambda$.†

Following Colombo *et al.* calculations have been made†† and it has been shown that the deviation of the experimental curve for plastic from the ideal curve (fig. 8) can be satisfactorily explained if it is assumed that $\lambda \approx 10^{-9}$ sec.

The data for the liquid scintillator are not quite consistent with these conclusions but liquid scintillator decay processes are known to vary with the oxygen content and the figure of 3×10^{-9} sec quoted in table 1 as the decay time could easily be slightly low for this reason.

For the slowly decaying NaI(Tl) and anthracene the value for λ just quoted would not affect the shapes of the curves given in fig. 6 within the range of energies considered. Calculations have shown that

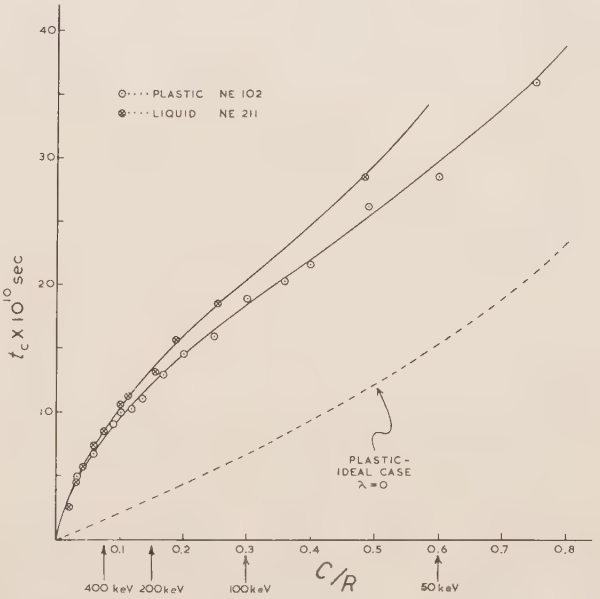

Fig. 8. Change of instrumental time delay with energy for plastic and liquid scintillators. This figure should be compared directly with fig. 7 of ref.[4]). C is the number of photoelectrons equivalent to the cut off charge. $C/R \propto 1/E$ where E is the energy liberated in the scintillator.

† When the limiter valve is cut off, by C equivalent photoelectrons, some of the information from the scintillator is still in transit in the multiplier. Hence Q, the number of actual photelectrons is greater than C by the amount which is, effectively, still in transit.

†† In the calculations it was assumed that

$$f(t) = c(e^{-\frac{1}{2}ct} - e^{-ct})$$

where $c = \sqrt{5}/\lambda$ in order to satisfy eq. (3).

the effect of λ in these cases would be merely to shift the zero of the t_c scale by about 9×10^{-10} sec. and 1.0×10^{-9} sec for NaI(Tl) and anthracene respectively. Only at very high energies would eq. (1) be seriously misleading for these scintillators.

5.2. TIME RESOLUTION

Lastly, leaving the subject of time delays, fig. 9 shows the variation with energy of the total variance of two counters equipped with plastic scintillators. It was explained in § 2 how measurements of σ^2 were made by changing the energy in both channels simultaneously by equal amounts. The results were corrected for finite "window" width by the use of fig. 8. Were eq. (3) for the variance strictly valid, the contribution of the two plastic scintillators to the total variance would be correctly given by the broken curve in fig. 9 (assuming data of table 1 and $Q = 15$). The inclusion of a second order term in eq. (2) and the effects of gain fluctuations in the photomultiplier would raise the broken curve slightly at lower energies and make it concave upwards like the experimental curve. But there would still be a substantial gap $\gtrsim 5 \times 10^{-20}$ sec^2 between the two curves. The effect of the electronics, as exhibited by fig. 4a is of only minor importance and so this contribution of $\gtrsim 5 \times 10^{-20}$ sec^2 to the total variance must be largely the result of time spread in the photomultipliers, i.e. inter-dynode fluctuations ε_{dd}^2 and photoelectron transit time fluctuations ε_{ph}^2.

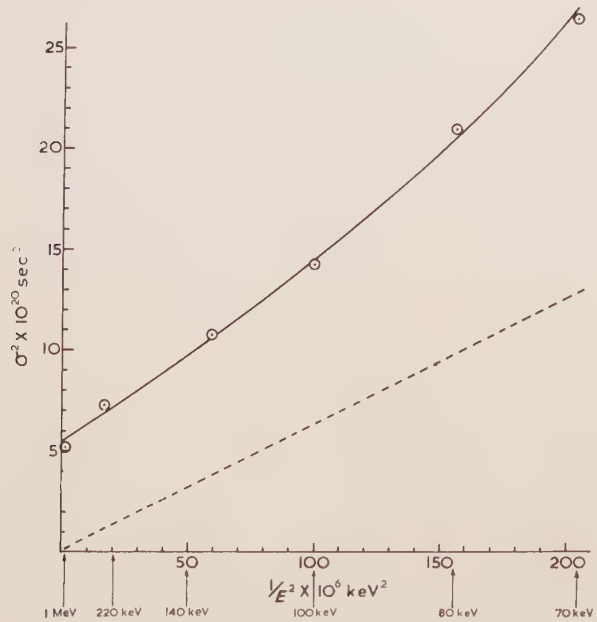

Fig. 9. A plot of the variance as a function of energy for a system of two counters with plastic scintillators. The energy "window" was changed by equal amounts in the two channels. The dotted curve shows the contribution to be expected from both scintillators on the basis of eq. (2). At high energies dominant contributions to the variance are attributable to the photomultiplier transit time variances (cf. text).

The effects of ε_{dd}^2 and ε_{ph}^2 have been considered in detail in refs.[4]) and [5]). Following ref.[5]):

$$\lambda^2 = (n - 1)\,\varepsilon_{dd}^2$$

where n is the number of dynodes. Thus for the 6342A and $\lambda \approx 10^{-9}$ sec, $\varepsilon_{dd}^2 \approx 3 \times 10^{-10}$ sec. The effect that this has on σ^2 may be simply understood if it is remembered that Q is a constant, and is equal to C, only when $\lambda = 0$. In all practical cases Q is greater than C and varies with the energy. As a result eq. (2) could be written more correctly as

$$\sigma_1^2 = \frac{Q(R)}{3}\left(\frac{\tau}{R}\right)^2 (1 + \text{small terms})\,. \qquad (5)$$

The variance ε_{ph}^2 is largely the result of time spread in the photoelectrons travelling between the photocathode and the first dynode. Ideally, if $\lambda = 0$, this will add a constant contribution ε_{ph}^2/Q to the total variance. In the non-ideal case the contribution arising from this effect can be written

$$\sigma_2^2 = \frac{\varepsilon_{ph}^2}{Q(R)}\,. \qquad (6)$$

Thus if $Q(R)$ is known $\sigma^2 = \sigma_1^2 + \sigma_2^2$ can be obtained from eqs. (5) and (6). $Q(R)$ has been obtained graphically from the curves given in ref.[5]) and it has been found that the observed curve in fig. 9 can be explained quantitatively in the range 500–70 keV if it is assumed that $\varepsilon_{ph} \approx 7 \times 10^{-10}$ sec. This is very reasonable since the maximum time delay between photoelectrons leaving the centre of the photocathode and others leaving the circumference of a circle 2.85 cm in diameter is quoted by the manufacturers of the 6342A as 1.3 nsec. For a circle 2.5 cm in diameter, as used in the present measurements, the maximum relative delay will be 1.0–1.2 nsec and the r.m.s. delay

should be about $1/\sqrt{2}$ times this, i.e. $\approx 8 \times 10^{-10}$ sec. It must be remembered that this is not quite the same thing as ε_{ph} since, strictly speaking (see ref.[5]))

$$\varepsilon_{ph}^2 = \varepsilon_{cd}^2 + \frac{\varepsilon_{dd}^2}{g-1}\left(1+\frac{2}{g}\right)$$

where ε_{cd}^2 is the cathode/first dynode variance and g is the secondary emission factor. However the second term is small and can be neglected so that ε_{ph}^2 can be almost entirely attributed to the transit time fluctuations between the photocathode and the first dynode.

Above about 500 keV only one measurement has been made, not sufficient to give the exact variation of σ^2 with $1/E^2$. From eqs. (5) and (6) it is expected that σ^2 should tend to zero at very high energies (several MeV). This would mean that the solid line in fig. 9 would not intersect the σ^2 axis at the point shown, but at a lower point determined mainly by the electronics.

In conclusion it may be stated that the observed performance characteristics of the fast coincidence system have been explained in a quantitative and detailed fashion. The theory developed in refs.[4]) and [5]) has been shown to give a correct description of these characteristics and, apart from a slight discrepancy in the case of the liquid scintillator, all the data have been shown to be internally consistent. Of special note, fig. 9 reveals that the intrinsic variance of the scintillators is of only secondary importance at all energies above ≈ 100 keV and that at 1 MeV it accounts for less than 10% of the total variance. This fact has not always been realised in the past although it has been explained here largely on the basis of known photomultiplier characteristics.

Acknowledgements

The authors would like to thank Professor P. I. Dee for his interest in the work. One of us (W.M.C.) wishes to thank the Department of Scientific and Industrial Research for a research grant.

NUCLEAR INSTRUMENTS AND METHODS 13 (1961) 224–230; NORTH-HOLLAND PUBLISHING CO.

CALCULATION OF RECOIL SPECTRA INDUCED BY FAST NEUTRON SPECTRA IN NUCLEAR EMULSIONS

HANS DECKERS

Studiecentrum voor Kernenergie, Laboratories of Mol, Belgium

Received 29 May 1961

In fast neutron spectroscopy using nuclear emulsions, the relation between the neutron spectrum and the proton spectrum is generally deduced from the properties of the neutronproton scattering. From the experiments performed in our laboratory it appears that it is advantageous to measure the spectrum of the range projected on the plane of the emulsion only, taking into account the geometry of the exposure. The present paper provides a mathematical basis for the analysis of data obtained under such conditions, in the case of complex neutron spectra range straggling in the emulsion is accounted for. Both the analytical and the Monte-Carlo method are dealt with. Finally a correlated sampling method is described which yields avery accurate calculation of the recoil spectrum induced by a fission spectrum.

1. Introduction

Hydrogen H^+ is very widely used as a neutron-charged particle "converter" for fast neutron spectrometry in nuclear emulsions[1]) and ionization chambers. In many respects the problem of analysing the data is very similar in both methods.

For neutron energies up to 10 MeV the cross section for the n–p scattering is isotropic in the center-of-mass system. This fact implies that the energy spectrum of proton recoils for perfectly monoenergetic neutrons is rectangular (in principle) from zero to an energy equal to that of the neutron. As a consequence the response of the spectrometer is not "unique" i.e. an incident neutron of one given energy can give rise to a track length or pulse height ranging from zero to that corresponding to a head-on collision. This non-uniqueness complicates the analysis when the incident neutrons are not monoenergetic.

The distributions arising from several monoenergetic neutron groups, can still be analysed by a "peeling off" technique[2]), but the problem of unraveling a complex spectrum in such situations presents considerable difficulties. An attempt at a general solution has recently been made by Maienschein at Oak Ridge[3]).

In this laboratory[4,5,6]) experimental proton spectra are analysed in the following way: the experimental proton spectrum is compared to a family of calculated proton spectra. This comparison yields best values of the parameters, which are characteristic for the neutron spectrum. The present paper describes the calculation of these recoil proton spectra as a function of given complex neutron spectra, account being taken of range straggling in the emulsion.

The quantities which are of interest for the following considerations are:

$\sigma_{np}(E)$ the scattering cross section for neutrons of energy E.

[H] the hydrogen concentration.

$N(E)$ the neutron energy spectrum, i.e. number of neutrons per cm², per sec, per energy interval (flux)

$R(E)$ the proton energy spectrum, i.e. number of protons per cm³ emulsion, per energy interval.

$R_1(l)$ the proton range spectrum.

$R_2(l_p)$ the proton projected range spectrum.

[1]) L. Cranberg and L. Rosen, Measurement of Fast Neutron Spectra, in "Nuclear Spectroscopy", Part A, edited by Fay Ayzenberg-Selove (Academic Press, New York, 1960) p. 363.

[2]) M. V. Pasechnik *et al.*, Proc. First Intern. Conf. on Peaceful Uses of Atomic Energy, Geneva 2 (1956) p. 3.

[3]) F. C. Maienschein, Private Communication to L. Cranberg and L. Rosen noted in ref.[1]).

[4]) C. Beets and H. Deckers, To be published in Proc. Third Intern. Conf. on Nuclear Photography, Moscow, 1961.

[5]) C. Beets, J. L. Campan, H. Deckers and C. P. Zaleski, Submitted for publication to J. Nucl. Energy, Part A.

[6]) C. Beets and H. Deckers, The Fission Neutron Spectrum of U^{235} (to be published).

In the experiments described in ref.[4,5,6]) it proved to be profitable to work with projected range spectra.

1.1. THE RELATION BETWEEN NEUTRON AND PROTON ENERGY SPECTRA

A quite general relation between neutron and proton energy spectra is given by

$$R(E) = \int_E^{+\infty} \sigma_{np}\,[\mathrm{H}]\,\frac{N(u)}{u}\,\mathrm{d}u \tag{1}$$

$$N(E) = -\frac{E}{[\mathrm{H}]\,\sigma_{np}\,(E)}\,\frac{\mathrm{d}}{\mathrm{d}E}\,R(E) \tag{2}$$

u is an integration variable.

This relationship supposes, that energy and momentum are conserved, and that the scattering is isotropic in the center-of-mass system. The latter condition is fulfilled up to 10 MeV.

We now derive eq. (1). In the case of neutrons having an energy between E_n and $E_n + \mathrm{d}E_n$, the isotropy condition yields the following expression for the number of recoil protons in an elementary solid angle:

$$R(E_n, \varphi^*)\,\mathrm{d}\varphi^*\,\mathrm{d}E_n = \sin\varphi^*\,\mathrm{d}\varphi^*\,\sigma_{np}\,(E_n)\,[\mathrm{H}]N(E_n)\,\mathrm{d}E_n$$

where φ^* is the c.m. angle. φ will be the laboratory angle. In the laboratory system this becomes

$$R(E_n, 2\varphi)\,\mathrm{d}\varphi\,\mathrm{d}E_n = \sin 2\varphi\,\mathrm{d}\varphi\,\sigma_{np}(E_n)\,[\mathrm{H}]N(E_n)\,\mathrm{d}E_n\,.$$

The conservation laws give

$$E_p = E_n \cos^2\varphi$$

$$\varphi = \cos^{-1}\,(E_p/E_n)^{\frac{1}{2}}$$

where E_p is the proton energy.

$R(E_p)$ is obtained by a transition from the variable φ to E_p and an integration over all neutron energies E_m, from E_p to $+\infty$:

$$R(E_p)\,\mathrm{d}E_p =$$

$$= \int_{E_n=E_p}^{+\infty} \sigma(E_n)\,[\mathrm{H}]\,\sin 2\varphi N(E_n)\,\frac{\partial(E_n, \varphi)}{\partial(E_n, E_p)}\,\mathrm{d}E_n\,\mathrm{d}E_p$$

$$= \int_{E_p}^{+\infty} \sigma(E_n)\,[\mathrm{H}]\,\frac{N(E_n)}{E_n}\,\mathrm{d}E_n\,\mathrm{d}E_p\,.$$

1.2. RESULTS OF EQ. (1) UNDER SIMPLIFIED CONDITIONS

If one takes for the neutron-proton cross section

$$\sigma_{np} = \frac{\text{const}}{E^{\frac{1}{2}}} \tag{3}$$

which is an approximation of the exact cross section (14).

Eq. (1) becomes

$$R(E) = \text{const.}\,[\mathrm{H}]\int_E^{+\infty} N(u)\,u^{-\frac{3}{2}}\,\mathrm{d}u\,. \tag{4}$$

For monoenergetic incident neutrons of energy E_0

$$N(E) = N_0\delta(E - E_0)\,,$$

where δ is the delta-function.

Eq. (4) gives the well known rectangular proton spectrum

$$R(E) = \text{const}\,[\mathrm{H}]\,N_0\int_E^{+\infty} \delta(u - E_0)\,u^{-\frac{3}{2}}\,\mathrm{d}u$$

$$\left\{\begin{array}{ll} = 0 & \text{when } E > E_0 \\ = c\,[\mathrm{H}]\,N_0\,E_0^{-\frac{3}{2}} & \text{when } E \leqq E_0 \end{array}\right\}. \tag{5}$$

For a Maxwellian spectrum with parameter T,

$$N(E) = AE^{\frac{1}{2}}\exp\,(-E/T)\,. \tag{6}$$

Eq. (4) is now converted into an exponential-integral spectrum

$$R(E) = c\,[\mathrm{H}]\,A\int_E^{+\infty} \exp\,(-u/T)\,\frac{\mathrm{d}u}{u} =$$

$$= -c\,[\mathrm{H}]\,A\,Ei\,(-E/T)\,. \tag{7}$$

1.3. COMPUTATION OF THE PROTON RANGE SPECTRUM

To obtain $R_1(l)$ from $R(E)$ a range energy relation, $l = f(E)$ is needed; one takes Barkas's relation[7]):

$$l = 0.000\,06 + 0.001\,38\,E^{\frac{3}{2}}\ \text{cm, when } E < 1\ \text{MeV} \tag{8a}$$

and

$$l = 0.001\,44 + \int_0^E \frac{\mathrm{d}\tau}{i}\ \text{cm, when } E \geqslant 1\ \text{MeV} \tag{8b}$$

with

$$i = \frac{0.5326}{\beta^2} \times [\log\,(3088\,\beta^2\gamma^2) - \beta^2 - C]\ \text{MeV/cm}.$$

Eq. (8a) can be applied up to 2 MeV, where it gives 39.7 μm instead of 40.4 μm.

The proton range spectrum $R(l)$ is obtained from eqs. (1) and (8). With the simplified σ_{np} of eq. (3) the following expression of $R_1(l)$ valid up to 2 MeV, is obtained from eqs. (4) and (8a).

$$R_1(l)\,\mathrm{d}l = R\left[\left(\frac{l - 0.000\,06}{0.001\,38}\right)^{\frac{2}{3}}\right]\left[\frac{l - 0.000\,06}{0.001\,38}\right]^{-\frac{1}{3}}\mathrm{d}l\,. \tag{9}$$

[7]) W. H. Barkas, Nuovo Cim. 7 (1958) 185.

1.4. CALCULATION OF THE PROJECTED RANGE SPECTRUM

The projection of l on the plane of the emulsion is given by

$$l_p = l \sin\theta ,$$

where θ is the angle between the normal on the plane and the track. $R_2(l_p)$ will depend on the geometry of the experiment, which determines the distribution of $\sin\theta$. The most important geometries are:

1. The beam geometry.

In this case $\sin\theta$ is given as a function of two angles

$$\sin\theta = (1 - \sin^2\alpha \sin^2\varphi)^{\frac{1}{2}}$$

α and $\sin^2\varphi$ having rectangular distributions between 0 and 2π and between 0 and 1, respectively.

2. The isotropic geometry, where no favoured direction exists for the neutrons. In this case one knows that the distribution of $\cos\theta$ is rectangular between -1 and 1.

$R_2(l_p)$ will now be calculated for an isotropic geometry.

When there is no favoured direction the number of tracks included in an angle in the interval $d\theta$ will be proportional to the solid angle

$$2\pi \sin\theta \, d\theta .$$

As a consequence $R_2(l_p)$ will then be given by

$$R_2(l_p)\, dl_p = \int_0^{\pi/2} \sin t \, R_1(l_p/\sin t) \frac{\partial(l,\theta)}{\partial(l',t)} \, dt \, dl_p$$

$$= \int_0^{\pi/2} R_1(l_p/\sin t) \, dt \, dl_p , \qquad (10)$$

where

$$t = \theta$$
$$l' = l \sin\theta .$$

1.5. THE FISSION SPECTRUM OF U^{235}

This method can be applied to the investigation of the neutrons from the fission of heavy nuclei.

It is well known[8]) that these spectra can be represented in a rather satisfactory way by a Maxwellian distribution with parameter T eq. (6)).

In order to verify this relationship for a given energy interval and to find a value for T, it is necessary to calculate $R_2(l_p,T)$ for a set of Maxwellian neutron spectra and compare these expressions with the experimental data. These particular experiments[3]) were concerned with the proton spectrum $R_2(l_p,T)$ for values of $l_p < 40\mu$ ($E < 2$ MeV). An isotropic geometry was employed[6]).

The calculation with the approximation (3) proceeds in the following way.

The given hypotheses and circumstances allow us to write, from eqs. (7) and (9)

$$R_1(l)\, dl = -\text{const. Ei}\left[-\frac{1}{T}\left(\frac{l - 0.000\,06}{0.001\,38}\right)^{\frac{2}{3}}\right]$$

$$\left(\frac{l - 0.000\,06}{0.001\,38}\right)^{-\frac{1}{3}} dl . \qquad (11)$$

Upon inserting this R_1-function into eq. (10) the spectrum $R_2(l_p)$, of the projections is found. The resulting integral can be calculated numerically for a set of T-values on a Mercury Ferranti computer.

2. The Monte-Carlo- Method

The computation of $R_2(l_p)$ for a Maxwellian fast neutron spectrum has been given as an example of the analytical method discussed in the first part of the present paper.

However, in point of actual fact, it becomes very difficult to apply this method if, in the calculation of $R_2(l_p)$, it is desired to take account of range straggling phenomena in the emulsion and of the exact energy-dependence of σ_{np}.

Furthermore, experiments with other kinds of neutron spectra and geometries can be much more difficult to treat than the experiment with U^{235} which was described in the last section.

For these reasons it appeared desirable to have another method which could take into account all these phenomena in a more straightforward way. The Monte-Carlo method is such a method.

In a Monte-Carlo calculation one follows the "history" of each of a large number, N, of particles and eventually of the progeny of each. At each "event" which is important for the destiny of the particle (e.g. an interaction with a nucleus) one forces a decision by means of a "random" number†.

† A large set of independent numbers F, belonging to a rectangular distribution between 0 and 1 exists in a computer. These numbers are referred to as "random" in this context.

[8]) J. Terrell, Phys. Rev. **113** (1959) 527.

taking into account the relative probabilities of all the possible issues.

The central limit theorem guarantees that the dispersion of the results varies as $(N)^{-\frac{1}{2}}$. However, there exist variance reducing techniques which allow smaller N-values (= machine-time). If variance reducing devices are used, the Monte-Carlo is called "sophisticated". A Monte-Carlo without variance reducing devices is called "straightforward".

In an actual experiment with nuclear emulsions, one has to limit himself to 10^3 or 10^4 events. On a comparison with these rather limited experimental results, a "straightforward" Monte-Carlo, with $N = 10^4$ to 10^5, will be sufficient.

It is also very instructive to note Monte-Carlo results for smaller N-values equal to the number of tracks measured in the emulsion, *because this gives a theoretical spectrum with statistical fluctuations similar to those in the actual experiment.*

2.1.

All the results of the first part of this paper can be expressed in Monte-Carlo language. In section 1.1 it was found that the conservation of energy and the isotropy of the n–p collision in the c.m. system were translated respectively by

$$E_p = E_n \cos^2 \varphi \tag{12}$$

and

$$P(\varphi)\,\mathrm{d}\varphi = K \sin 2\varphi\,\mathrm{d}\varphi = \tfrac{1}{2}K\mathrm{d}\,(\cos 2\varphi) =$$

$$= K\mathrm{d}\,(\cos^2\varphi) = -K\mathrm{d}\,(\sin^2\varphi)\,, \tag{13}$$

where K is a constant.

We see that $\cos^2\varphi$ has a rectangular distribution between 0 and 1 in the energy interval $0 \leqslant E_n \leqslant 10$ MeV where the collision is isotropic.

Thus for $\cos^2\varphi$ we can directly take a random number r_1, or $1 - r_1$, from the computer.

2.2.

The cross section σ_{np} may now be calculated[9]) from

$$\sigma_{np} = \tfrac{3}{4}\sigma_t + \tfrac{1}{4}\sigma_s\,, \tag{14}$$

where the triplet and singlet contributions are given by

$$\sigma_t = 4\pi\,[(a_t^{-1} - \tfrac{1}{2}r_{0t}\,k^2)^2 + k^2]^{-1}$$

$$\sigma_s = 4\pi\,[(a_s^{-1} - \tfrac{1}{2}r_{0s}\,k^2)^2 + k^2]^{-1}$$

$$k^2 = 1.206 \times 10^{-24}\,E \text{ (in MeV)}$$

$$r_{0t} = 1.70 \times 10^{-13}\text{ cm}$$

$$a_t = 5.39 \times 10^{-13}\text{ cm}$$

$$r_{0s} = 2.6 \times 10^{-13}\text{ cm}$$

$$a_n = -23.7 \times 10^{-13}\text{ cm}\,.$$

With each neutron of energy E_n is associated a proton of energy E_p provided with a statistical weight factor proportional to $\sigma_{np}(E_n)$.

2.3.

l_p can be calculated for the two geometries considered:

1. *Beam geometry*

$$l_p = l \sin\theta = l\,(1 - \sin^2\alpha \sin^2\varphi)^{\frac{1}{2}}\,,$$

where $\sin^2\varphi$ is simply $(1 - r_1)$ or r_1 of section 2.1 and where $\sin\alpha$ is given in function of a second random number by a device which is described in[10]).

2. *Isotropic geometry*

$$r = \cos\theta$$

$$l_p = l \sin\theta = l\,(1 - r^2)^{\frac{1}{2}}$$

$R_2(l_p)$ is obtained upon classifying N values of l_p.

2.4.

Protons, all having the same initial velocity, do not all have the same range. The observed ranges of individual particles from any monoenergetic source will show a substantially normal distribution about the mean range. This effect is called "range straggling".

If a calculated range l' is obtained from the range-energy relation for a recoil proton of energy E, the real range has to be chosen from the distribution:

$$P(l)\,\mathrm{d}l = \frac{1}{\sqrt{2\pi}} \exp\left[\frac{-(l-l')^2}{2s^2}\right]\mathrm{d}l\,, \tag{15}$$

[9]) J. M. Blatt and V. F. Weisskopf, Theoretical Nuclear Physics (John Wiley and Sons, New York, 1952) p. 70.

[10]) E. D. Everett and C. J. Cashwell, Monte Carlo Method for Random Walk Processes (Pergamon Press, London, 1959) p. 122.

where s is a dispersion characteristic for the emulsion and for the method employed to measure the range.

The following device[11]) is used to choose a number

$$k = \pm \frac{l - l'}{s}, \tag{16}$$

which has the distribution

$$f(k) = \sqrt{\frac{2}{\pi}} \exp(-\tfrac{1}{2}k^2) \qquad 0 \leq k \leq \infty \tag{17}$$

starting from a set of random numbers r_1 and r_2. The procedure is summarized in the following flow diagram.

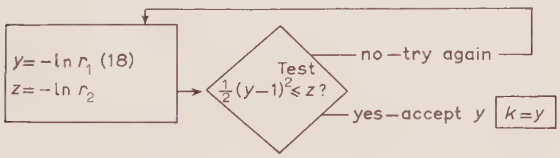

Then $l = l' \pm ks$, and the sign can be determined by the following simple device

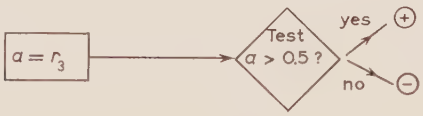

The k from the first device is really distributed according to the law[17]). Indeed, the probability of getting a given value of k is equal to the probability of picking the value y[18]), times the probability of accepting it or

$$e^{-k}\, e^{-\frac{1}{2}(k-1)^2} = e^{-\frac{1}{2}}\, e^{-\frac{1}{2}k^2}.$$

2.5.

Computation of $R_2(l_p)$ for recoil protons from a neutron beam having a deformed rectangular distribution.

The following experiment was to be analysed. A monoenergetic (1.315 MeV) proton beam from a Van de Graaff accelerator was allowed to impinge on a rather thick (60 keV) TaT-target. The neutrons from the T(p,n) He^3-reaction were recorded (by means of their recoil protons) in an Ilford L4 emulsion at 5°.

[11]) H. Kahn, Applications of Monte-Carlo, Report AECU-3259 (1954).

The following phenomena must be taken into account:

1. The energy loss of the protons in the TaT-target before causing a reaction;
2. The straggling associated with this energy loss;
3. The range straggling of the recoil protons in the emulsion.

The effect of the first two phenomena on the neutron energy spectrum is shown in fig. 1.

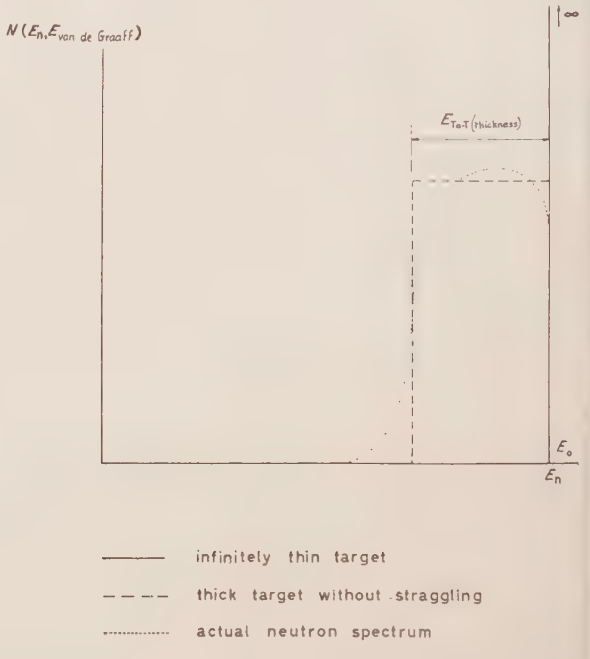

Fig. 1.
The effect of energy loss and straggling on the neutron spectrum

It may be noted, that in the actual calculation the last two phenomena have been combined into one step.

Because of the relatively low energy of the primary protons, no Landau-Symon effect has been included, furthermore σ_{np} was considered to be constant in the interval 1.315–1.255 MeV. However, no major difficulties would be associated with a generalization of the actual calculation.

In this case there is beam geometry

$$l_p = l \sin\theta \qquad \text{(see section 1.4.)}.$$

The actual calculation for one history is represented in the flos diagram of fig. 2. This is repeated N times, until sufficiently good statistics are obtained.

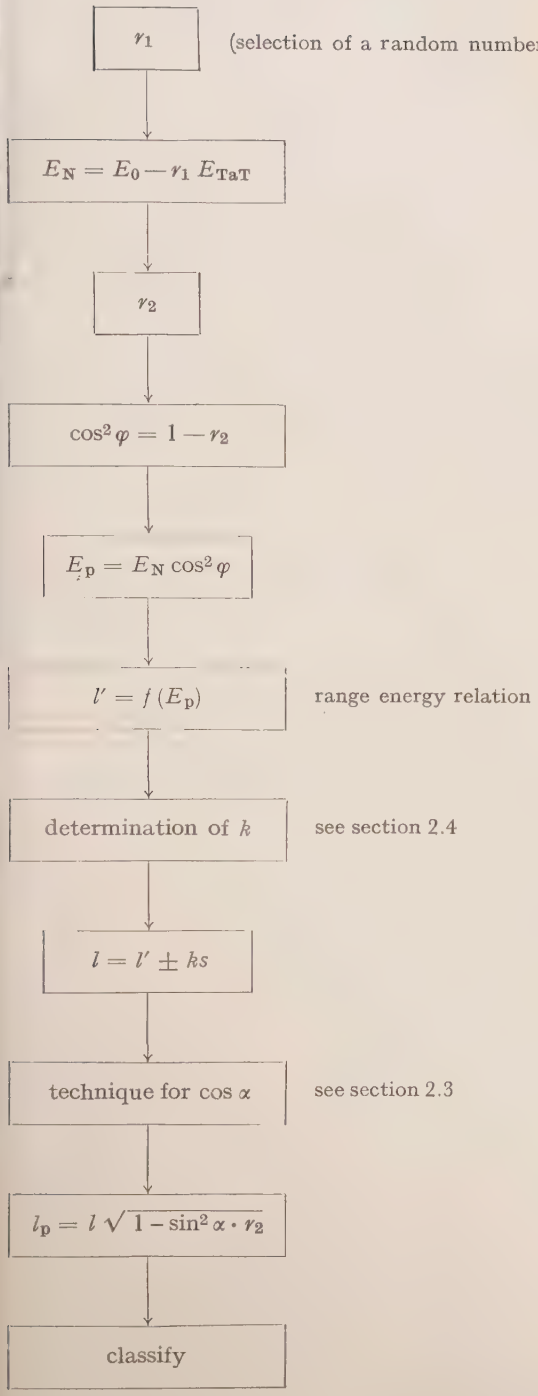

Fig. 2. The flow diagram for section 2.5.

2.6.

$R_2(l_p)$ has been calculated, for neutrons in a slab of natural uranium, from a tabulated theoretical neutron spectrum, which is to be tested for agreement with the experiment[5]).

The procedure includes the different steps described in sections 2.2, 2.3 and 2.4. A variance reducing technique is used. A very large part of the recoils are so short that they cannot be measured in the experiment. The statistics of that part of the spectrum which can be measured are favoured in the following way: below a certain neutron energy 10 times less histories are taken, each having a weight of 10. The following values of s were used successively: 0, 35 and 70 keV.

2.7.

$R_2(l_p)$) is also calculated for the fission spectrum. The method is very similar to that described in the preceding section. The sampling from distribution (6) was performed in the following way: the interval of interest $(0, 10T)$ was divided into 10 subintervals and a von Neumann sampling technique[10]) was applied in each subinterval. One single von Neuman technique would have been uneconomic for $E > 2T$ This is summarized in the following flow diagram:

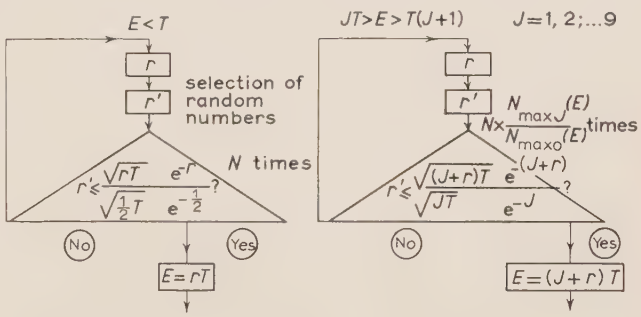

Furthermore, Russian roulette and splitting were used as variance reducing techniques.

2.8.

A very accurate estimate of $R_2(l_p)$ for fission neutrons was realized by means of correlated sampling. The calculation of 2.7 was repeated for the simplified cross section (3) anf for zero straggling, with the *same* set of random numbers. This makes both estimates highly correlated, so that the variance of their difference is very small. Very accurate values of $R_2(l_p)$ are obtained by adding this difference to the analytical results of section 1.5

3. Conculsion

A solution is found for the problem of unraveling the response of nuclear emulsions to a complex neutron spectrum. One sees that one has to make a new Monte-Carlo code and to collect new Monte-Carlo statistics for almost every new experiment. An improvement of the present method would consist in finding one single technique applicable to a large class of experimental spectra.

Acknowledgements

The author is very much indebted to Mr. Charles Beets for suggesting the problem and for his continuous encouragement.

NUCLEAR INSTRUMENTS AND METHODS **13** (1961) 231–237; NORTH-HOLLAND PUBLISHING CO.

A PROPANE BUBBLE CHAMBER WITH MECHANICAL EXPANSION

D. W. ANDERSON† and J. McKENZIE

Clarendon Laboratory, Oxford

Received 25 May 1961

A description is given of a propane bubble chamber with a sensitive volume of one litre, in which the expansion is effected by a mechanical method. A flywheel driven by a small electric motor provides a reservoir of mechanical energy, and the energy for an expansion is withdrawn through a magnetic clutch. Such an assembly is compact and readily transportable, and the recycling rate can be once per second. Information is given concerning the possible size of chamber that could be operated by this technique, using commercially available magnetic clutches.

1. Introduction

The conventional method of operating a propane bubble chamber is to use a pneumatic system. A gas supply of appropriately high pressure and large volume is not normally available, so that a special compressor must be provided, which is cumbersome and costly in comparison with the chamber itself.

Accordingly, a mechanical expansion system has been developed which allows a high repetition rate, and results in a compact and readily transportable chamber assembly.

The instantaneous power required to operate a one-litre chamber may be as high as 20 H.P., but if the repetition rate is once per second, the average power is only a fraction of a horse-power, and can be supplied by a small electric motor. In the present system a flywheel is used as a reservoir of mechanical energy, the energy being abstracted sufficiently quickly by the use of a magnetically-operated clutch.

Controlled gas pressure from a small cylinder maintains the chamber at its operating pressure, and behaves as a gas spring for recompression after an expansion.

No magnetic field was provided, since the chamber was to be exposed to protons of 80 MeV, and the charged products of any interactions would stop in the chamber, enabling the energy to be determined from the range to within a few percent. Estimates of momentum from curvature in a magnetic field of normal strength would be subject to an uncertainty of 50% as a result of multiple scattering.

† Now with G.E.C. Ltd., Stanmore, Middlesex.

2. Detailed Description

2.1. GENERAL ASSEMBLY AND EXPANSION MECHANISM

The complete assembly (fig. 1–3) is mounted on a welded steel frame ①, so that the entire mechanical unit is completely self-contained. The chamber proper ② is a 6″ cube of steel, through which a 4″ diameter hole is bored. The ends of this hole are closed by $\frac{3}{4}$″ thick plates ③ of "Armourplate" toughened glass, gasketed with rectangular cross-section lead rings ④, and held in place by bolted steel rings ⑤. Another 4″ diameter hole is bored in the bottom of the chamber to meet the first, and all edges are carefully radiused and smoothed so that no excessive turbulence is set up when the liquid flows during the expansion process. The chamber block sits on, and is bolted to a cylinder block ⑥, and between the two is a diaphragm ⑦ of 5-thou "Melinex" film, with a softened copper ring ⑧ to provide the seal. The cylinder block contains the expansion piston ⑩, sealed with "Gaco" 0-rings, and the region between the diaphragm and the piston is filled with oil ⑪, which makes an hydraulic connection between the piston and the sensitive liquid itself.

Two main heaters ㉗ of up to 750 W are clamped to the walls of the chamber block beneath asbestos sheet, and a smaller heater ㉘ of 200 W is clamped round the upper part of the cylinder block. The

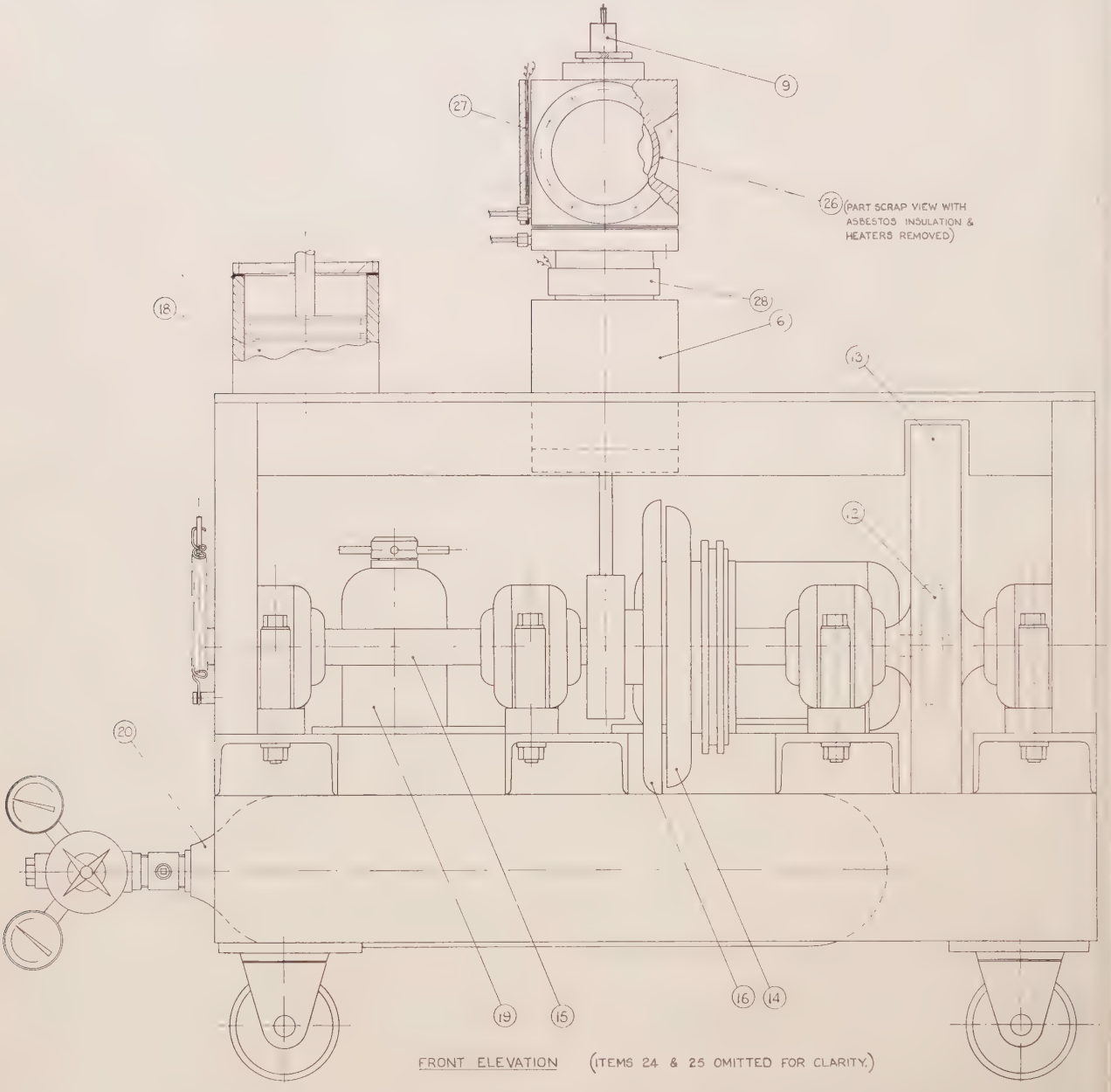

Fig. 1. General assembly of the bubble chamber—front view.

temperature is measured by means of a thermistor in the top of the chamber, and the power to the heaters is automatically adjusted to maintain the temperature constant to about 0.1°C.

A commercial transducer ⑨ is sealed into the top of the block, and enables the pressure fluctuations to be monitored. One wall of the chamber block is milled down over a region 2″ × 2″ to form a thin entry window ㉖ for the incident beam of protons.

The motor shaft carries a rubber tyred wheel ⑫ which bears on the rim of the flywheel ⑬—a disc of steel 18″ diameter and 2″ thick—and drives it at about 400 rpm. On the same shaft as the flywheel is the larger portion of the clutch ⑭, which contains the magnetising coil, fed by current through slip rings. Another coaxial shaft ⑮ carries the stator of the clutch ⑯ to which is attached the slotted link ⑰ that couples the clutch to the piston

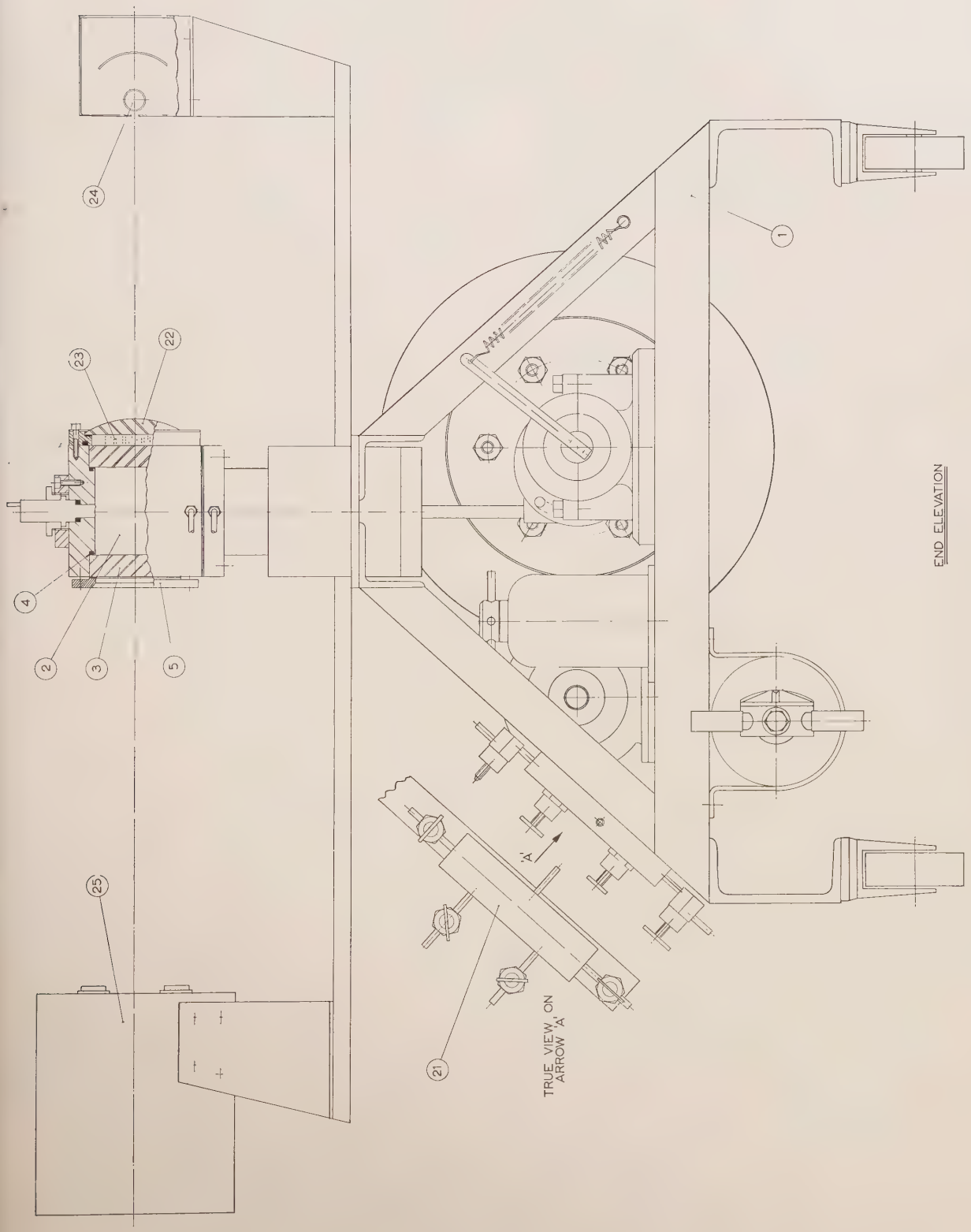

Fig. 2. General assembly of the bubble chamber—end view.

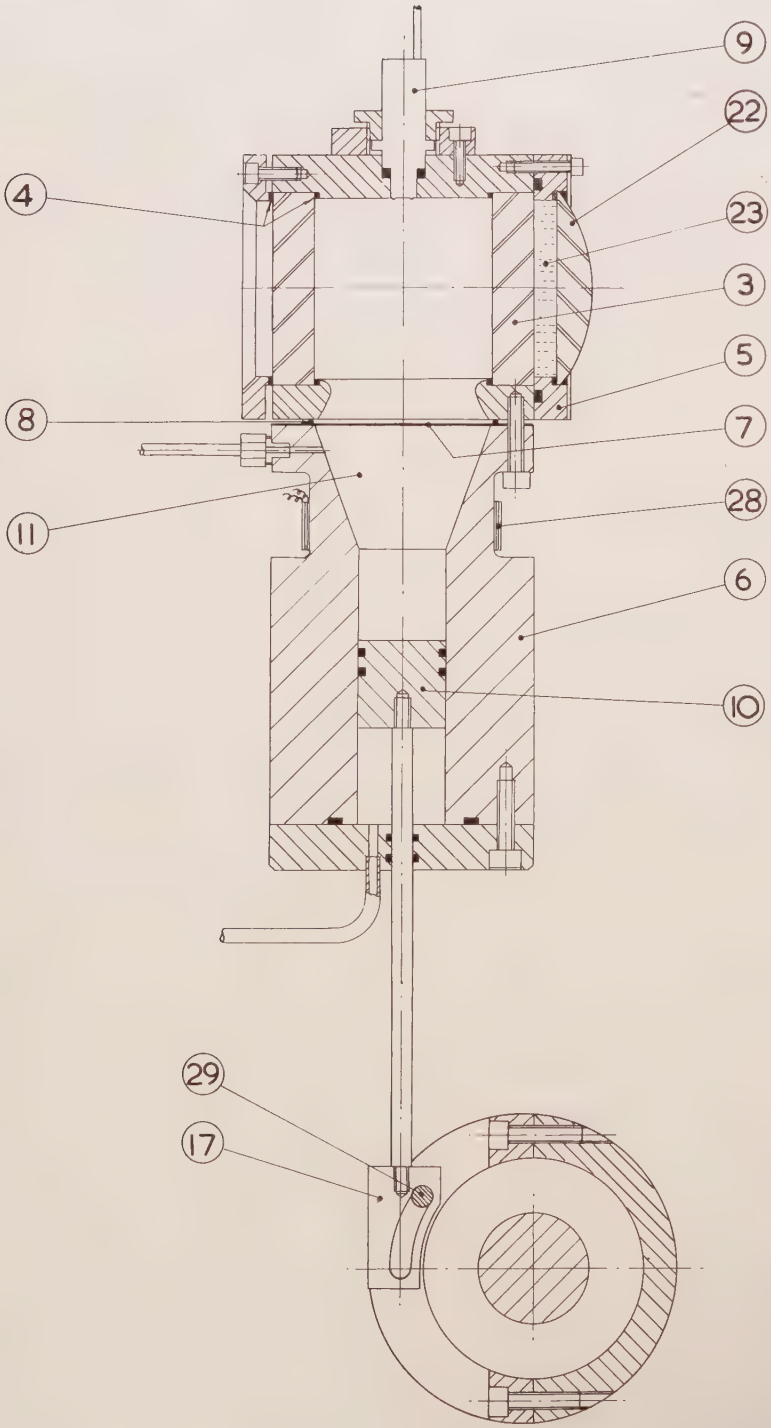

1 FRAME.
2 CHAMBER PROPER.
3 LEAD GASKETS.
4 GLASS PLATES.
5 STEEL CLAMPING RING.
6 CYLINDER BLOCK.
7 DIAPHRAM.
8 COPPER RING.
9 PRESSURE TRANSDUCER.
10 EXPANSION PISTON.
11 HYDRAULIC OIL.
12 RUBBER MOTOR WHEEL.
13 FLYWHEEL.
14 CLUTCH ROTOR.
15 HALF SHAFT.
16 CLUTCH STATOR.
17 SLOTTED LINK.
18 RESERVOIR PROPANE.
19 RESERVOIR OIL.
20 GAS CYLINDER & CONTROLLER.
21 MANIFOLD.
22 CONDENSING LENS.
23 SILICONE OIL.
24 FLASH TUBE.
25 CAMERA.
26 BEAM ENTRY WINDOW.
27 MAIN HEATER.
28 NECK HEATER.
29 DRIVING PIN.

Fig. 3. Section of the expansion mechanism.

rod. Since the clutch takes a few milliseconds to engage fully, the link is slotted to prevent the driving pin (29) from transmitting any force to the piston until after it has rotated freely in the slot, during which time the clutch builds up to full torque. After an expansion the pin is returned to the top of the slot by a spring.

Also carried on the frame is a reservoir (18) into which the propane can expand during the heating-up process, and a reservoir (19) for the hydraulic oil, to assist in the initial filling. A high-pressure cylinder and controller (20) is slung underneath the frame and the pressure can be applied via a manifold (21) to any desired part of the system.

2.2. ELECTRICAL CONTROLS

The only exacting item is the clutch switching unit. It is required to provide a square-shaped pulse of current, of amplitude 4A, and duration variable from about 20 to 100 msec. The value of 4A is the recommended current for saturating the clutch magnetically, and providing maximum pick-up torque. In more conventional applications of the clutch, this is obtained by applying 6 V to the slip rings, but owing to the considerable inductance of the coil the time constant for build-up of current is then about $\frac{1}{2}$ second—greater than the desired total duration of pulse.

To overcome this, the current is derived instead from a 200 V supply, with a 50 ohm resistor in series, so that the time constant is reduced to about 5 msec, yet the maximum current is again limited to 4 A.

The actual switching is accomplished by means of two large thyratrons capable of carrying 4 A. One, in series with the clutch coil and associated resistor is used to turn the current on, after which the other is fired, and connects a condenser (charged to -1000 V) to the anode of the first, thereby terminating the discharge and turning the current off. Conventional timing circuits with adjustable delays are used to provide the triggering signals.

2.3. OPTICAL EQUIPMENT

The dark field system of illumination is chosen to obtain maximum contrast of the bubble images. A condensing lens (22) is mounted close to one of the chamber windows, and the intervening space is filled with a transparent silicone oil (23) to minimise optical discontinuities. Rather beyond the principal focus is an FT-230 flash tube (24) which is a good approximation to a point source, so that most of the sensitive volume is illuminated by a slightly convergent beam of light. The three lenses of the triple camera (25) are outside the main beam, and thus a dark field of view is seen until there are bubbles in the chamber to scatter light from the main beam.

The *f*-number for optimum resolution depends only on the depth of chamber, and with a 10 cm depth is *f*-30. Diffraction at the lens then sets an upper limit to the attainable resolution which corresponds to about 35 bubbles per centimetre.

2.4. OPERATION

Initially, the space between the piston and diaphragm is filled with hydraulic oil, and the quantity of oil is chosen so that when the piston is in its operating position the diaphragm is bowed upwards. The oil reservoir can then be permanently disconnected. The chamber itself is filled by repeatedly evacuating and flushing with propane until all the air has been removed, and finally opening up to the propane supply. The chamber block is cooled with dry ice, and the propane distils in as a liquid.

While the liquid is being heated up to operating temperature in the region of 60°C, it undergoes a 20% expansion by volume, so the taps to the reservoir are open, and the whole system is pressurised from the gas cylinder. Thus the piston in the reservoir moves, allowing the liquid to expand without increase of pressure. Only when the operating temperature has been reached are the taps to the reservoir closed, isolating it from the system, making the chamber ready for expansions.

When only the main heaters were used, a great deal of heat was lost from the chamber downwards into the cylinder block. The result was a fairly stable state with a large vertical temperature gradient, and the chamber was sensitive only in an upper layer.

Hence the provision of the neck heater to balance the heat loss, after which the chamber was sensitive throughout its whole volume.

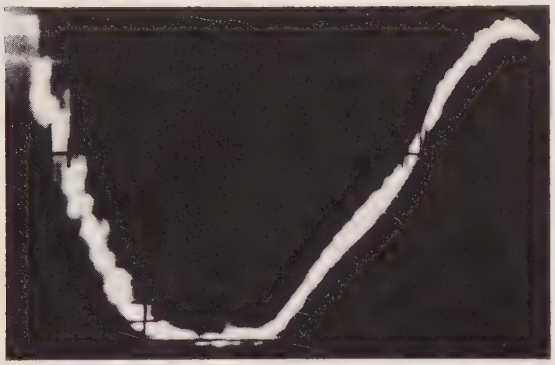

Fig. 4. Transducer record of the pressure change during an expansion.

A typical pressure trace is shown in fig. 4, in which the pressure drop takes about 5 msec and the whole cycle is completed within about 25 msec. The calibration for this trace indicated that the pressure falls by about 150 psi.

After an initiating signal, relatively long mechanical delays (of about 80 msec) ensue before the period of sensitivity, but they have proved to be reproducible to about 1 millisecond. This is less than the duration of the sensitive time, so no difficulty is experienced in operating with a pulsed accelerator.

It has been found to be important to avoid any cracks or crevices in the chamber with dimensions of about $\frac{1}{2}$ mm. For example, when the lead gaskets are new, they may leave a small crack between the glass plate and the chamber wall. If this is so, then on expanding the chamber, a sheet of boiling is observed to shoot out of the crack, and no tracks are seen. To remedy this it is sufficient to squeeze up

Fig. 5. Photograph of 80 MeV protons, showing a proton-proton collision.

the clamping rings until lead has extruded in to fill the crack.

3. Experiment

The chamber was constructed primarily as a test of the unusual method of expansion, but when it was found to work successfully it was exposed to protons of 80 MeV from the Harwell synchrocyclotron. Some 20 000 expansions have been photographed, one of which is reproduced in fig. 5, showing a proton-proton collision. Measurements have been made on a semi-automatic measuring machine at Oxford, and the results processed with a "Mercury" computer. It is necessary to make a kinematic balance for each two-pronged event, in order to determine whether the incident proton interacted with a nucleus of carbon or hydrogen in the propane. The two-pronged carbon events have been analysed in detail to give data on the $C^{12}(p,2p)B^{11}$ reaction. This experiment is particularly suited to investigation with a bubble chamber, since events occur in all spatial orientations, and it is not necessary to impose geometrical restrictions, as is the case with counter experiments. Information has been obtained on the quasi-elastic scattering of protons from carbon, and the momentum distribution of protons within the carbon nucleus, and the results will be published elsewhere.

4. Application to Larger Chambers

The magnetic clutch used on the one-litre chamber was the Warner type 1225. One larger size, type 1525, is made, and it is of interest to consider how large a chamber could be operated by the larger clutch.

With the type of mechanism described, work is done on the expansion stroke, and the recompression is achieved quasielastically. The operating pressure is about 350 psi, and the expansion ratio is 3%, so a chamber of volume V requires $350 \times 0.03\ V$ inch-lb of work, if V is in cubic inches, or 54 ft-lb if V is in litres. The work should be done within 10 milliseconds, so the power required is $5400\ V$ ft-lb/sec., which must equal the product (torque $\times$ angular velocity).

The necessary torque is plotted as a function of angular velocity for V equal to 1, 2, 3, 4 litres in

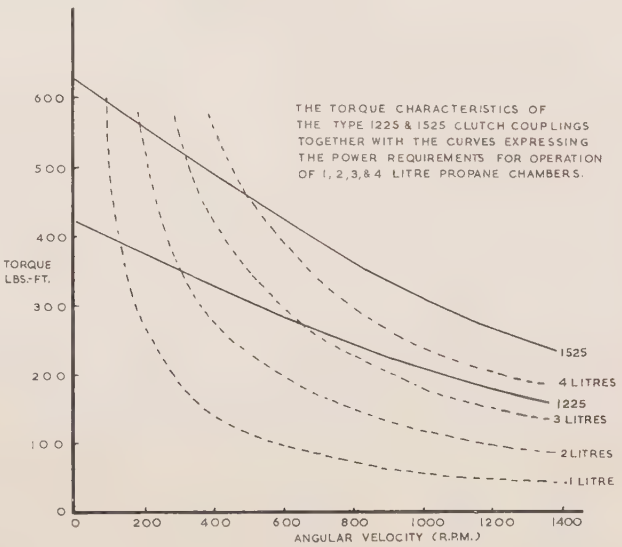

Fig. 6. The torque characteristics of the type 1225 and 1525 clutch-couplings, together with the curves expressing the power requirements for operation of 1, 2, 3 and 4 litre propane chambers.

fig. 6, together with the maker's data for torque versus angular velocity for the 1225 and 1525 types of clutch. It is seen that 4 litres is probably the largest volume of chamber that could be operated, using the type 1525 clutch.

Acknowledgments

The authors wish to thank Professor D. H. Wilkinson F.R.S. for his supervision of this work, and are grateful to the D.S.I.R. for Maintenance Awards. The project was supported by a contract from U.K.A.E.A., who also kindly made available the Harwell synchrocyclotron.

NUCLEAR INSTRUMENTS AND METHODS 13 (1961) 238–243; NORTH-HOLLAND PUBLISHING CO.

SIMULTANEOUS NUCLIDE IDENTIFICATION AND ENERGY MEASUREMENT OF NUCLEAR REACTION PRODUCTS†

CARL E. ANDERSON††, D. A. BROMLEY and M. SACHS

Yale University, New Haven, Connecticut

Received 27 May 1961

A system of particle detectors has been developed which measures the kinetic energy of nuclear reaction products and identifies their charge and mass. The method of identification is based on the Bethe-Bloch equation for the rate of energy loss of a fast heavy particle. These detectors extend this method to the identification of the isotopes of heavy reaction products such as lithium, beryllium, boron, carbon, nitrogen, and oxygen.

1. Introduction

The study of the reaction mechanisms of complex nuclei has been stimulated by the availability of intense beams of heavy ions with energies as high as 10 MeV per nucleon[1–4]). These ion beams are produced by cyclotrons and linear accelerators specifically designed to accelerate heavy ions. The early studies of these complex reactions were accomplished primarily by the use of photographic plates in which the reaction could be recorded and, by measurement of the activities, produced in targets. The intense ion beams of these accelerators have made particle counting experiments possible. A review by Zucker[5]) indicates the recent advances made in this field.

The reactions of complex nuclei produce a much larger variety of products than are found with light projectiles. Fortunately, many of these products, including those of large mass, possess enough kinetic energy to be detected by particle counters. In order to study a particular reaction, it is necessary to uniquely identify the product being observed. If both the charge and the mass of the particle can be determined, a very detailed knowledge of the reactions will be obtained. For products of low mass and charge, this unique identification is easily achieved. Preliminary results obtained Anderson *et al.*[6]) have shown that it is also possible to identify products as heavy as magnesium by their charge. Isotope identification was not achieved at that time. The apparatus has been improved and can now identify the isotopes of the reaction products as heavy as oxygen.

2. Particle Detector Systems

Several detector systems can be used to identify the reaction products. They are based on the measurement of two parameters for each particle. One system[7]) measures the particle velocity by its time of flight and the particle energy. This method has been used only in the study of fission fragments but could be extended to other reaction products. Another system, which has been used more widely[8–12]) measures the rate of energy loss of a

† This work was supported by the U.S. Atomic Energy Commission.

†† Now at The Johns Hopkins University Applied Physics Laboratory, Silver Spring, Maryland.

[1]) R. S. Livingston, Nature, **173** (1955) 54.

[2]) Guseva *et al.*, Soviet Journal of Atomic Energy, **2**, 327, Trans C.B.I.

[3]) Bolotin *et al.*, Conf. on High Energy Accelerators and Instruments, CERN (1959).

[4]) Hubbard *et al.*, The UCRL and Yale Heavy Ion Linear Acc., (to be published).

[5]) A. Zucker, Ann. Rev. Nuclear Science, **10** (1960) 27–62.

[6]) C. E. Anderson, A. Quinton, W. Knox, and R. Long, Nucl. Instr. and Meth., **6** (1960) 1.

[7]) J. C. Milton and J. S. Frazer, Phys. Rev. **111** (1958) 877.

[8]) J. C. Keck, Phys. Rev. **85** (1952) 410.

[9]) G. Igo, Clark and Eisberg, Phys. Rev. **89** (1953) 879.

[10]) G. Igo and R. M. Eisberg, Rev. Sci. Inst. **25** (1954) 450.

[11]) F. Ribe and J. D. Seagrave, Phys. Rev. **94** (1954) 934.

[12]) Wolfe, Silverman and DeWire, Rev. Sci. Inst. **26** (1955) 504.

particle, dE/dX, and its residual energy. Aschenbrenner[13]) improved this method by introducing the plotting oscilloscope to display the particle spectra. Concurrently, Grodzins[14]) was utilizing this same display technique to disentangle complicated gamma ray spectra.

The individual detectors which are useful in such systems depend primarily upon the range of the particles encountered in the experiment. Particles of short range require the use of a very thin detector to determine dE/dX in order that the residual energy be measurable. At the present time, gas counters best satisfy this requirement. Thin scintillation crystals have been used, but gas detectors are more easily made "thin". For particles of longer range, the choice of dE/dX detector is less sensitive to detector thickness; and, recently, even transmission junction detectors have been used[15]). The difficulties are transferred to the residual energy detector if the particles have long range. Silicon junction detectors are ideal for this measurement and can be obtained thick enough to stop a 40 MeV proton. For particles of still longer range, only scintillation crystals are presently suitable. Descriptions of various systems adapted to particular experiments can be found in the literature[7,16–22]).

3. Discussion

The basic relation between the two parameters measure in a dE/dX and E detector system is the Bethe-Bloch equation.

$$\frac{dE}{dX} = K\frac{MZ^2}{E},$$

where E is the initial energy, M the mass, Z the charge, and K a constant. This equation indicates that it should be relatively easy to separate reaction products by their charge, that is, into elements, since $E\,dE/dX$ is proportional to Z^2. However, to separate the products by their mass as well will be more difficult, as $E\,dE/dX$, is proportional only to the first power in M. Using this simple relation, it is evident that to separate O_{15} from O_{16} will require a dE/dX counter with a resolution of better than 5%, if we assume that the resolution of the energy detector is about 1%. The development of silicon junction detectors makes it possible to obtain 1% resolution with the energy detector, but the dE/dX detector presents a problem. The resolution in the dE/dX detector is dependent upon the small number of events leading to the production of high energy delta rays which can be lost from the detector. The theory of energy loss shows that the mean square fluctuation in energy loss Ω^2 is determined by the equation,

$$\Omega^2 = 4\pi e^4 Z_i^2\, NZ\, \Delta X,$$

where $Z_i e$ is the charge on the incident ion, NZ the number of electrons per unit volume of the stopping material, and ΔX is the path length. The resolution si given by

$$R = \frac{2.8\Omega}{\Delta E}$$

and consequently is inversely proportional to $(\Delta X)^{\frac{1}{2}}$. To obtain the resolution required to separate O^{15} from O^{16}, the detector only needs to be long enough. Of course, if the dE/dX detector is too long, the energy spread of the particles entering the energy detector will be more important than the resolution of the energy detector. Simple considerations indicate that nearly optimum conditions are obtained with an equal amount of energy lost in both detectors, i.e.,

$$\frac{\Delta E}{\Delta X} = E_R.$$

A more detailed analysis has not been made, since for heavy ions the variations of charge state with ion velocity, as well as the wide range of particle energies encountered, complicate the analysis appreciably.

[13]) F. Aschenbrenner, Phys. Rev. **98** (1955) 657.
[14]) L. Grodzins, Rev. Sci. Inst. **26** (1955) 1208.
[15]) T. H. Braid, J. L. Yntema, B. Zeidman and H. W. Broek, Bull. Amer. Phys. Soc. **6** (1961) 272.
[16]) H. W. Watters, Phys. Rev. **103** (1956) 1763.
[17]) R. H. Stokes, J. A. Northrup and K. Boyr, Rev. Scie. Instr. **29** (1958) 61.
[18]) C. D. Goodman, Phys. Rev. **110** (1958) 676.
[19]) R. H. Stokes, Rev. Sci. Inst. **29** (1958) 401.
[20]) H. E. Wegner and W. S. Hall, Phys. Rev. **119** (1960) 1654.
[21]) L. G. Kuo, M. Pertrauic and B. Turko, Nucl. Instr. and Meth. **10** (1961) 53.
[22]) E. F. Bennett, Phys. Rev. **122** (1961) 595.

4. The dE/dX Detector

The considerations discussed assume that the dE/dX detector has a negligible instrumental width. This, of course, is not the case unless care is given to the counter design. Proportional counters have been used in most of the systems described in the literature. However if high resolution, fast recovery, and long-term stability are required, an ion chamber may be used to advantage. In particular, volume through 0.00025″ Mylar windows fastened to re-entrant lucite cylinders with Eastman 910 adhesive. This construction avoids end effects in the counter and defines the active volume. The Frisch grid was made with 0.005″ diameter stainless steel wires fastened 0.031″ apart in the grid frame. The frame is constructed with one end adjustable to obtain the necessary tension in the wires to keep them straight. The collector to grid spacing is

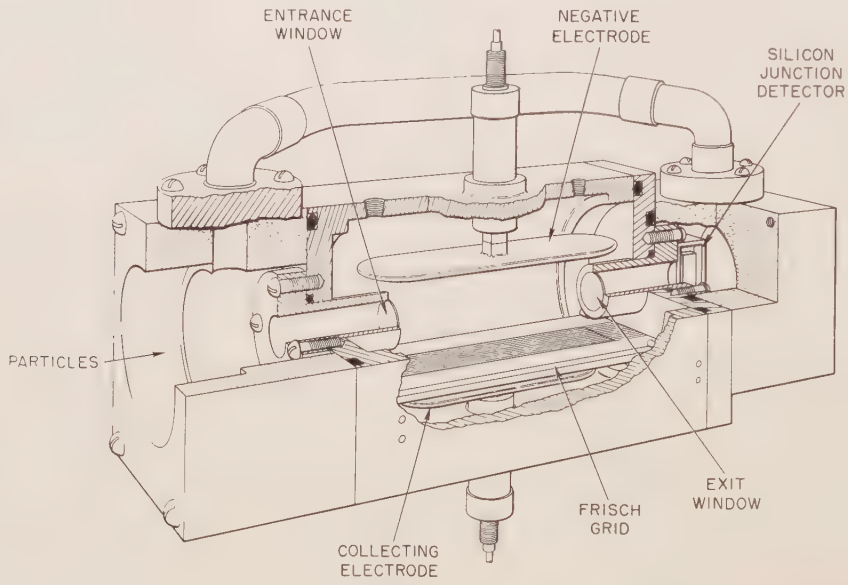

Fig. 1. Fast dE/dX Ion Chamber. The chamber is constructed from a brass block 2″ × 2″ square. The high voltage ceramic feed through insulators were obtained from The Advance Vacuum Prod. Corporation. The small pipe at the top of the drawing connects the volume in which the junction detector is located to the scattering chamber vacuum. The bias voltage and signal connections of the junction detector enter by small ceramic feed-thrus from the back wall of the detector but are not shown. The ion chamber preamplifier is mounted directly on the chamber to reduce the input capacity.

previous experience has indicated that the gas gain of a proportional counter can be effected by the high instantaneous counting rates encountered with pulsed accelerators. This effect arises from the space charge of ions left in the counter by preceding events during a beam pulse. The gas gain is also sensitive to pressure and supply voltage, but both of these parameters can be held stable.

To avoid this problem and to obtain a faster rise time for the dE/dX pulses which would yield shorter coincidence resolving times, a fast, gridded ion chamber was designed, as shown in fig. 1. A uniform field over the particle path was obtained by making the particles enter and leave the counter 0.250″, and the grid to repeller electrode spacing is 0.750″. Using the analysis by Wilkinson[23]), it can be shown that the difference in charge collector for particle paths ± 0.125″ from the midplane will be about ½%. With the given dimensions for grid, collector, and repeller spacings, as well as the grid dimensions, the analysis of Wilkinson also shows that complete electron collection will occur with equal negative and positive voltages on the repeller and collector respectively. Voltages as high as ± 4000 V have been used to obtain fast rising pulses at a detector gas pressure of 2 atmospheres.

[23]) D. H. Wilkinson, Ionization Chambers and Counters (Cambridge, 1950).

Commercially available P-10 gas [10% methane, 90% argon] was used and the pressure was kept constant by means of a Cartesian manostat. Since the detector pulses are quite small, the preamplifier was mounted as part of the detector assembly to minimize the input capacity. The full width at half maximum for 160 MeV oxygen ions losing about 20 MeV in the ion chamber was found to be approximately 4%. This is within a factor of two of the predicted resolution.

5. The Residual Energy Detector

A silicon junction detector was used to determine residual energy. Detectors from many different suppliers[24]) have been used successfully. Some detectors have their surface contact in the center of the crystal and cannot be used to detect heavy ions with relatively short ranges unless this contact is masked off. Preamplifiers have been used with these junctions but are really unnecessary in this work, as enough energy is available to give large output pulses making a simple cathode follower adequate. A very thick junction is needed in order to stop particles of low mass such as lithium. In general, the junctions used had resistivities ranging between 6000 to 10000 ohm cm. Bias voltages of over 100 V were used to obtain thick depletion layers. The resolution for a 140 MeV oxygen ion in most junction detectors was approximately 1%.

6. Electronics

The block diagrams of the electronic circuitry is shown in figs. 2 and 3. For the sake of simplicity, all impedance matching circuits are not included in the diagrams. Fig. 2 is a plotting oscilloscope. The use of 3.8 μsec clipping time amplifiers removes the need for pulse stretching. Not only can the plotting oscilloscope be used for collecting data, it has proved to be invaluable in adjusting the parameters of the pulse multiplier and for monitoring the system during long runs. Fig. 3 is a crude three dimensional analyzer which makes use of a pulse multiplier and two RIDL 400 channel analyzers. The pulse multiplier circuit is a modified copy of the one designed by R. H. Stokes[25]) and W. L. Briscoe[26]) which uses Raytheon squaring tubes QK329. The

[24]) RCA, Canada; Chalk River Laboratory, Canada; Hughes Electronics, and Solid State Radiation Corporation.
[25]) R. H. Stokes, Rev. Sci. Inst. **31** (1960) 768.
[26]) W. L. Briscoe, Rev. Sci. Inst. **29** (1958) 5.

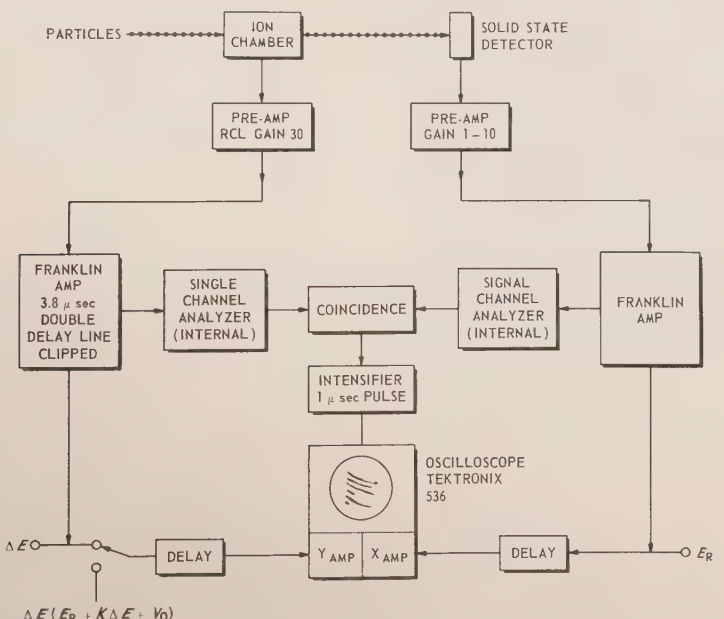

Fig. 2. Plotting oscilloscope. This is a simplified block diagram of the actual system. All impedance matching circuits have been omitted to avoid confusion. Pulse stretching circuits have not been used in order to retain the high counting rate capacity of the amplifiers.

desirability of multiplying the two parameters is easily seen by considering the energy loss equation,

$$\frac{dE}{dX} = K\frac{MZ^2}{E}.$$

Ideally, $E\,dE/dX$ should be a constant for a particular isotope. In practice, the energy measured is not the initial energy E, but the residual energy E_R. Fig. 5 is a photograph of the pulse multiplier output for the same reaction products. (See the figure legends for details.) The curvature of the lines of constant MZ^2, as shown in fig. 4, has been straightened by the present pulse multiplier, but no set of the adjustable parameters could be found that would make these straight lines horizontal. Further modifications of the multiplier are in progress, such

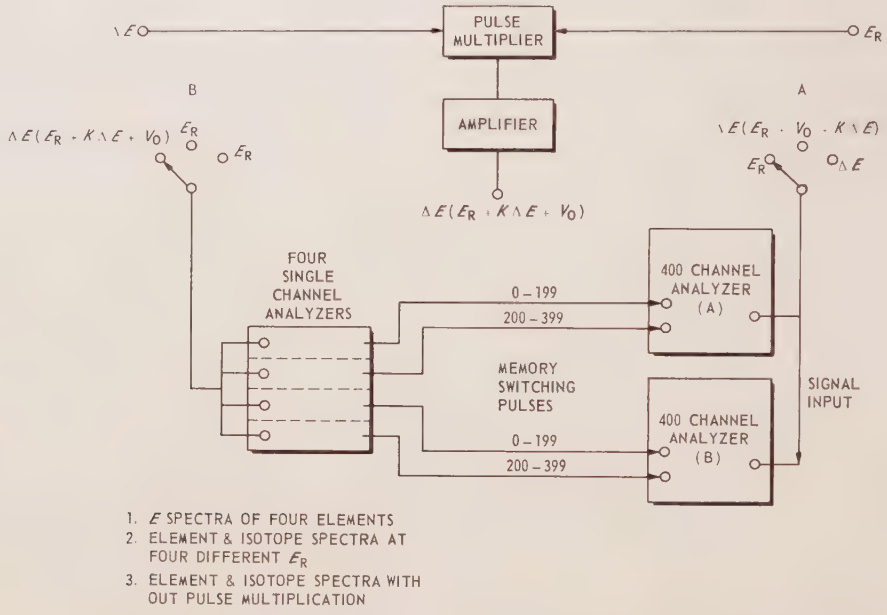

Fig. 3. XYZ Analyzer. To simplify this block diagram, only the essentials are shown. The three operating modes are chosen by the switch position. In the case of measuring the energy spectra of four elements, the single channel windows are set empirically. First the spectrum of the pulse multiplier is obtained for a limited range of E_R. The output of a pulse generator is then fed simultaneously to the multichannel analyzer and single channel analyzers. The pulse height is varied to agree with the lower or upper bounding channel of an element as shown in the recorded spectrum. The lower or upper level of the window in one of the single channel analyzers is adjusted to this pulse height value.

To obtain E, a constant pulse V_0 to account for window losses and a pulse depending on ΔE, that is $K(\Delta E)$, are added. In this application, the multiplier is used to select the elements whose energy spectra are recorded by the multi-channel analyzers. It has been used to obtain a distribution of the isotopes with constant residual energy.

7. Results

The successful operation of this equipment can be shown best by photographs taken with the plotting oscilloscope. Fig. 4 is a photograph of $\Delta E/\Delta X$ vs E_R for the reaction products from aluminum bombarded with 160 MeV oxygen ions. as adding a fraction of the E_R pulse to the multiplier pulse, which seems promising.

Even with the present multiplier, it is evident from fig. 5 that gates can be set to include all the isotopes of an element without interference from neighboring elements. This ability enables the use of the crude three-dimensional analyzer to study the oxygen on aluminum reactions, and the results will be reported elsewhere[26]). However, photographs, such as fig. 5, have already indicated the validity of the conclusions arrived at in a previous report[27]). Namely, that the great majority of the

[27]) D. A. Bromley, M. Sachs and C. E. Anderson, Bull. Amer. Phys. Soc. **6** (1961) 287.

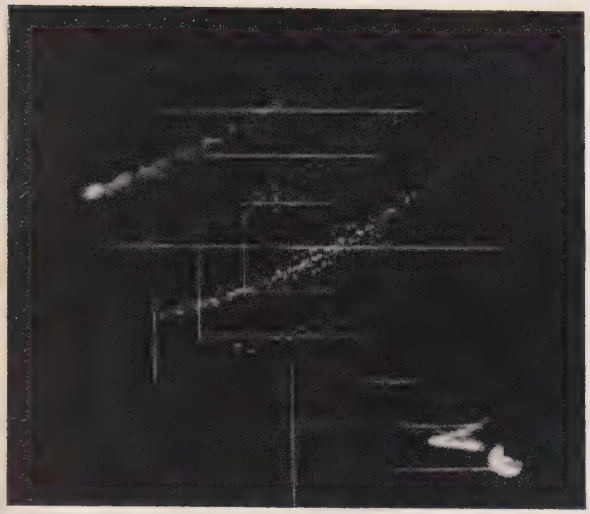

Fig. 4. Plotting oscilloscope photograph of $\Delta E/\Delta E$ vs E_R for the reaction products from aluminium bombarded by 160 MeV oxygen ions. The lines crossing the center of the graticule are the carbon isotopes. The dense core is the C^{12} line with a weaker C^{13} line above it, and a still weaker C^{11} line below it. The next group of lines belong to the nitrogen isotopes N^{14} and N^{15}.

products observed in these reactions are the stable isotopes which are not detectable by radio-chemical techniques.

8. Conclusions

The method described can be a powerful tool to separate the multitudinous reaction products and aid in understanding the reactions between complex nuclei. The limitations of the technique, at the present time, reside primarily in the data handling system.

The plotting oscilloscope is simple to use and can collect the data at rates determined by the chance occurrence of over-lapping pulses in the amplifier. The present 3.8 μsec double delay line clipped amplifiers were intended for use with CsI(Tl) crystals, which give pulses with 1.5 μsec rise time. With the present detectors, the clipping time can be shortened to increase the instantaneous counting rate allowable. Unfortunately, the photographic method lacks count capacity. More exactly, the spots quickly overlap one another, producing an uncountable smear. This prevents full realization of the resolution inherent in the energy detector. Another serious drawback is the tedious spot counting required to analyze the data.

The use of the pulse multiplier to allow the use of multichannel analyzers avoids the tedium of spot counting and does yield the desired count capacity. However, many of the reactions occurring are ignored by the need to set gates over only part of the spectrum. Further, the multichannel analyzers cannot utilize the high instantaneous counting rate capacity of the detectors.

The limitations of both methods described, as well as the obvious utility of a truly 3-dimensional pulse height analyzer, had lead to the design of such an analyzer. The Tullamore Division of the Victoreen Company has contracted to produce an analyzer with 100 channels by 200 channels with a 10^6 count capacity in each matrix location of the random access memory. When this equipment is available most of the advantages of the present detector system can be fully realized.

Fig. 5. A photograph of the multiplier output vs E_R of the same reaction. Lines of constant MZ^2 were not obtained with the multiplier. This photograph was taken for a larger number of counts to better show the separation. The uppermost line is the oxygen isotopes and are barely resolved into O^{16} and O^{15}. The next set are the nitrogen isotopes N^{15}, N^{14} with some N^{13} now showing. The next set are the carbon isotopes with a faint C^{14} line followed by C^{13} and an intense C^{12} line followed by a blur of C^{11}. Proceeding downward, the next line is B^{11}, then B^{10}, and finally Be^9 and Be^7. The lines of the light elements are turning back upon themselves because the higher energy particles are passing completely through the junction detector depletion layer.

[28]) C. E. Anderson, W. Knox, A. Quinton and G. Bach, Phys. Rev. Letters 3 (1959) 557.

NUCLEAR INSTRUMENTS AND METHODS 13 (1961) 244–246; NORTH-HOLLAND PUBLISHING CO.

AN AMPLITUDE-INSENSITIVE SYSTEM THAT DISTINGUISHES PULSES OF DIFFERENT SHAPES

T. K. ALEXANDER and F. S. GOULDING

Atomic Energy of Canada Ltd., Chalk River, Ontario, Canada

Received 27 May 1961

A method of pulse-shape discrimination is described in which the slow-to-total charge ratio is measured at a photomultiplier dynode. The ratio determination is approximately independent of amplitude over at least a 10:1 operating range.

The performance of the system as a particle discriminator selecting neutrons in a background of γ-rays is shown for stilbene and a liquid scintillation counter. The time required to determine the shape of a pulse is about 1 μs and could be less. Thus errors due to pulse pile-up at high counting rates are not serious.

The system uses a conventional amplifying system requiring only a single dynode pulse. No special photomultiplier or very fast circuits are required since the charge in the fast component is measured and no attempt is made to follow its fast rise. These features enable the system to be tested effectively with artifical pulses from a test-pulse generator.

Owen[1]) has shown that it is possible to distinguish between different particles by the shape of the light pulses that they produce in organic-phosphor scintillation counters. The method depends on there being at least two components in the light output, these components having different time-constants of decay, and the ratio between their amplitudes being dependent on dE/dx. Several circuits have been designed to make use of this effect and thus distinguish between γ-rays and neutrons[2–6]).

Ideally such a circuit should measure the ratio between slow and fast components independently of the total light emitted. In the method of pulse-shape discrimination described here the slow-to-total charge ratio is measured at a photomultiplier dynode and the ratio determination is approximately independent of amplitude over a 10:1 operating range. The method relies on integrating the input charge then twice differentiating the integrated pulse so as to produce a base-line crossover. The timing of the baseline crossover with reference to the start of the pulse is sensitive to decay components in the scintillation, but insensitive to the

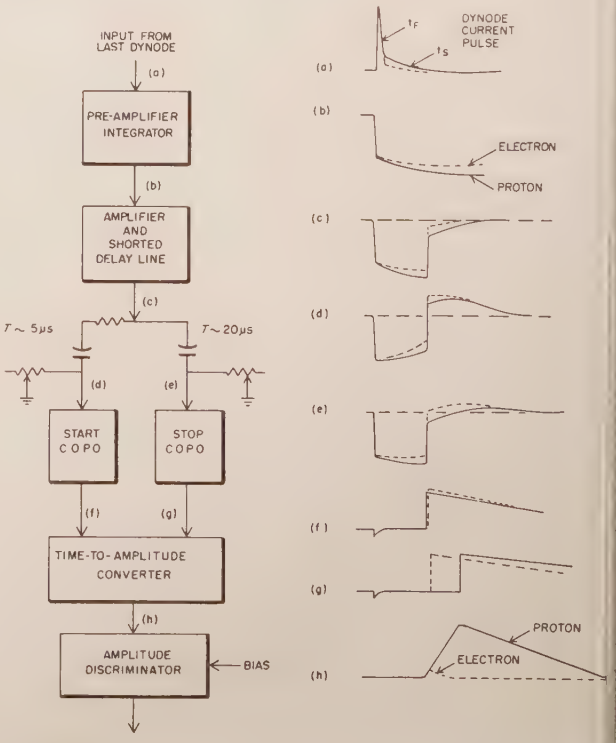

Fig. 1. Block diagram and waveforms of the pulse-shape discrimination system.

[1]) R. B. Owen, I.R.E. Trans. on Nuclear Science NS-5, N.3 (1958) 198.

[2]) R. B. Owen, Nucleonics **17**, No. 9 (1959) 92; Nucleonics **16** No. 6 (1958) 54.

[3]) F. D. Brooks, Nucl. Instr. and Meth. **4** (1959) 151.

[4]) G. C. Neilson, W. K. Dawson and F. A. Johnson, Rev. Sci. Instr. **30** No. 11 (1959) 963.

[5]) R. Bachelor *et al.*, Nucl. Instr. and Meth. **8** (1960) 146.

[6]) W. Dachnik and R. Sherr, Palmer Physical Laboratory, Princeton University, PUC 1961-25 (Jan. 20, 1961).

amplitude. Using this general principle several techniques are possible, but the one described in the following paragraphs seems to be the most convenient.

Fig. 1 shows the circuit used and the waveforms that are developed. The current pulse is integrated with a time constant much longer than the scintillation time-constants of interest. A shorted delay line is then used to differentiate the pulse producing an almost rectangular pulse $\sim 1\ \mu s$ wide. This is a conventional way of preparing a pulse for amplitude analysis and therefore a pulse equivalent to that at fig. 1(c) may be present in existing systems. The shape of the resulting pulse is analysed by feeding it to two separate channels each containing a differentiator R-C network, the time constants of the networks being different in the two channels. The time difference between the base-line crossovers of the output pulses in the two channels is then measured using the circuit described by F. S. Goulding and R. A. McNaught[7]) to detect the zero crossover time.

One channel will be called the "START" channel, and the other the "STOP" channel. The differentiating time constant preceding the START channel is made small enough so that *all* pulses cross zero during the fast part of the back-edge of the pulse [fig. 1(d)]. The time constant preceding the STOP channel is chosen so that electron-induced scintillation pulses cross zero during the fast part of the back-edge of the pulse, while pulses having larger slowly decaying components (e.g. neutrons) cross zero during the slow part of the pulse [fig. 1(e)]. Thus the time between output pulses from the START and STOP channels is small for an electron-induced scintillation pulse while it is relatively large for a proton-induced pulse. For convenience of measurement the time interval is converted to a voltage pulse in the time-to-amplitude converter. Since the time interval is measured from the back-edge of the pulse, the output of the converter is very sensitive to the relative amounts of the fast and slow components in the pulse [fig. 1(h)]. The input to the START channel is attenuated slightly to ensure that a STOP pulse occurs with every START pulse.

[7]) F. S. Goulding and R. A. McNaught, Nucl. Instr. and Meth. **8** (1960) 282.

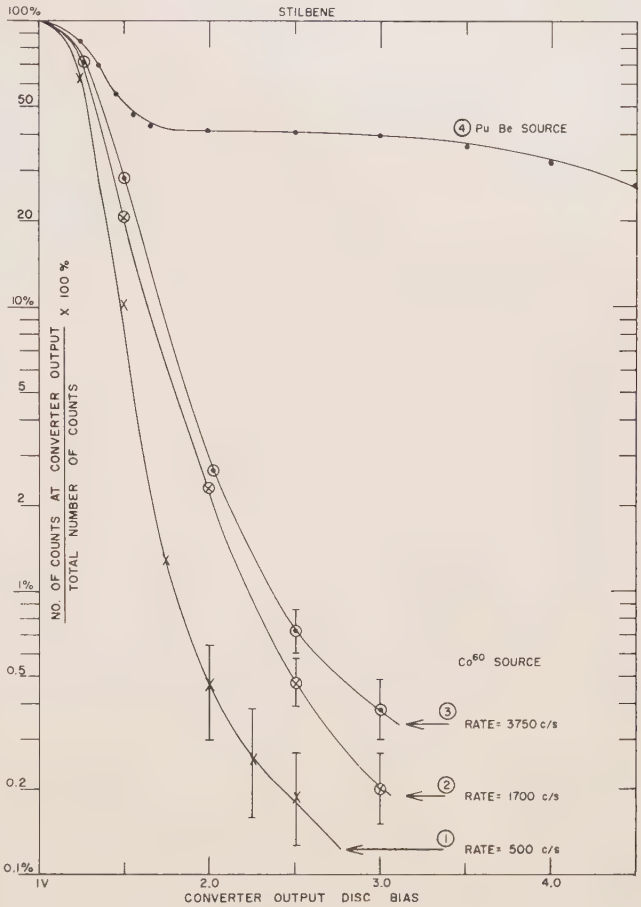

Fig. 2. Particle-discrimination performance using a stilbene scintillation counter.

Assuming that the photomultiplier current pulse is of the form $I = I_F e^{-t/\tau_F} + I_s e^{-t/\tau_s}$ and that the conditions on time constants referred to in the previous paragraph are met, the output of the converter is approximately proportional to:

$$\tau_s \ln \left\{ \frac{Q_s}{Q} \left[1 - \exp\left(\frac{-t_c}{\tau_s} \right) \right] \frac{T}{t_c} \right\} \qquad (1)$$

where

τ_s = time constant of slow component,
t_c = 2 × delay-line length,
T = time constant in the STOP channel,
$\frac{Q_s}{Q} = \frac{\text{Charge in slow component of scintillation}}{\text{Charge in fast and slow components}}$.

The response of the circuit has been measured by generating pulses containing fast and slow components with a test-pulse generator. Both τ_s and Q_s/Q were varied and the measured response was found to obey the relationship of eq. (1).

The performance of the system as a particle discriminator selecting neutrons in a background of

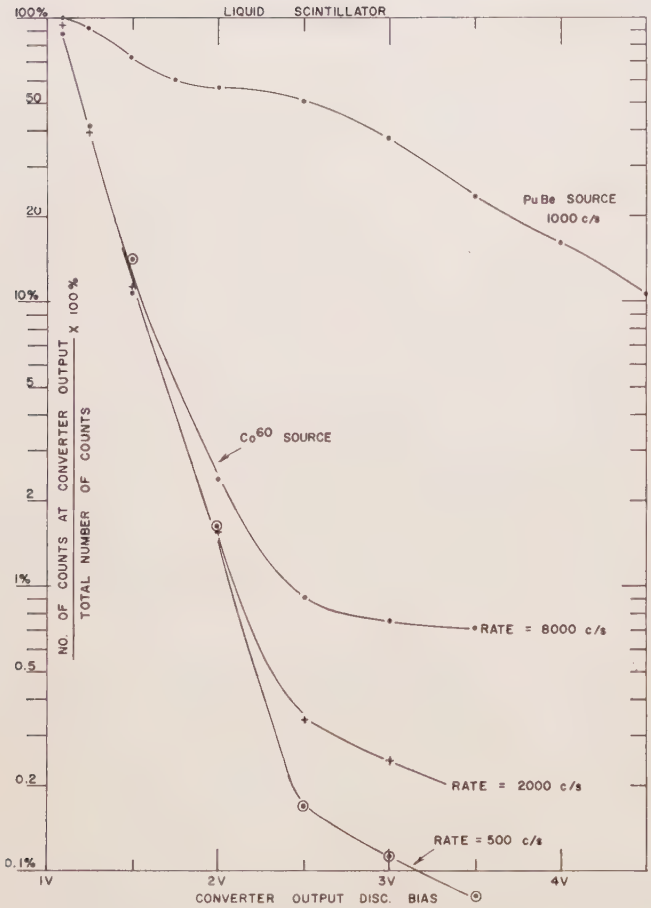

Fig. 3. Particle-discrimination performance using a liquid scintillation counter.

γ-rays was tested in the following manner. Events having an energy absorption in the scintillator equivalent to that of electrons of 300 keV or more were selected using a discriminator at (c) in fig. 1. Each time an event was detected by this discriminator, the output of the converter was examined to determine whether its amplitude exceeded a preset value determined by the bias on a second discriminator. The system would be operating perfectly if there were output from the second discriminator only for neutron events and never for γ events. The operating margin of the system could best be examined by varying the bias on the second discriminator. Bias curves were therefore obtained using γ-ray sources (Co^{60} and Radio-thorium) and also using a mixed source of neutrons and γ-rays (PuBe yielding approximately equal quantities of γ-rays and neutrons).

Fig. 2 is a set of such bias curves for a stilbene scintillation counter. The γ-ray curves are taken at several input rates to show the effect of pulse pile-up on the system. A similar set of curves for the same circuit parameters and a liquid scintillation counter is shown in fig. 3. It should be noted that a bias setting of 2.5 V in fig. 2 or 3 results in a discrimination ratio of about 200:1 against γ-rays as compared with neutrons at a counting rate of 1 kc/s. Satisfactory results were also obtained with 2.5-MeV neutrons from the D(d,n) reaction and 14-MeV neutrons from the T(d,n) reaction.

The following advantages are apparent in this method of pulse-shape discrimination:

(a) No special photomultiplier tube is required.

(b) Very fast circuits are not required since we integrate the charge in the fast component and do not attempt to follow its fast rise.

(c) The circuit can be tested effectively with artificial pulses from a test-pulse generator.

(d) A single dynode pulse is required. Both amplitude analysis and shape analysis can be performed using the same signal.

From the bias curves measured for the two scintillators and from the response of the circuit as given by equation (1), it can be estimated that the ratio Q_s/Q is less than 10% for electron-induced scintillations in agreement with Owen[1]). The large separation of the gamma-ray and neutron groups (fig. 2) for stilbene appears to be in disagreement with the accepted value of $\tau_s = 370$ ns which could mean the circuit is responding to another slower component in the pulse ($\tau_s \sim 1$ μs).

This note describes the principle of the pulse-shape discrimination circuit as applied to select one of two different types of particle. A simple extension of the principle permits detailed investigation of pulse shapes with different particle excitation conditions and has yielded interesting results which will be described fully in a later paper.

This work forms part of the research programme of Atomic Energy of Canada Ltd. to whom the authors are indebted for permission to publish this note. The assistance of G. A. Neathway in performing some of the measurements is acknowledged.

NUCLEAR INSTRUMENTS AND METHODS **13** (1961) 247–252; NORTH-HOLLAND PUBLISHING CO.

A RANDOM PULSE GENERATOR WITH PROVISION FOR EXCURSIONS

R. J. LAMDEN

United Kingdom Atomic Energy Authority, A.W.R.E., Aldermaston, Berks.

Received 28 June 1961

A generator is described which is capable of producing pulses occurring randomly in time. The mean pulse rate may be set between 10 c/s and 100 kc/s. In addition, the mean rate can be made to increase exponentially with time, and a range of time-constants between 30 ms and 10 s is provided. The output of the generator at a constant mean rate may be used for testing scalers, ratemeters, time-to-pulse-height convertors and other instruments which have to operate with randomly timed input pulses and may show defects with such pulses which are not apparent with a uniform input. The output with an excursion in the mean rate is particularly suitable for testing reactor period trip units and similar equipment.

1. Introduction

In this pulse generator, the randomly occurring pulses are generated by feeding wide-band noise to a discriminator circuit. The wide-band noise is generated by a noise diode, the heater of which is fed with direct current from a transistor series regulator. This noise is then amplified with a passband from 30 kc/s to 1.2 Mc/s and fed to a White cathode follower. At this point, the noise level is monitored. The noise is rectified by a mean level detector and the detected signal level is compared with a reference voltage. Any difference is amplified and used to control the gain of the video amplifier. In this way, the mean noise level is held very constant. The stabilised noise is also fed to a discriminator circuit and the pulses coming from this are fed to a cathode-follower and from this to the output socket. When an output at a constant mean rate is required, the discriminator operating voltage, that is, the voltage which a noise peak must reach to operate the discriminator, is fixed and is provided from a cathode-follower. By the operation of a switch, this cathode-follower can be turned into a bootstrap linear sweep generator. This makes the discriminator operating voltage vary linearly with time and, as explained in section 2, this will cause an approximately exponential increase in the discriminator operating rate. Alternatively, the discriminator operating voltage may be set by applying a voltage derived from an external source to terminals on the unit. By suitably adjusting this voltage, the pulse rate can be varied in any required way.

2. Theory

In this pulse generator, random noise originating in a noise diode is fed to a discriminator. This will be assumed to give an output pulse every time that the voltage of a noise peak exceeds the discriminator operating voltage V_c. The statistics of random noise have been worked out by S. O. Rice[1]). For Gaussian noise, which is given by a noise diode, the probability of observing at any instant a voltage between V and $V + \mathrm{d}V$ is

$$P(V)\,\mathrm{d}V = \frac{\mathrm{d}V}{\sqrt{2\pi\psi}} \exp\left(\frac{-y^2}{2\psi}\right) \qquad (1)$$

where ψ is the mean square value of V, that is

$$\psi = \overline{(V^2)}\,. \qquad (2)$$

Rice has shown that if this noise voltage has a bandwidth extending from a lower limit f_a to an upper limit f_b, the expected number of zeros per second is

$$N(0) = 2\left[\tfrac{1}{3}\frac{f_b^3 - f_a^3}{f_b - f_a}\right]^{\frac{1}{2}}. \qquad (3)$$

If $f_a \ll f_b$, as it is in the present case,

$$N(0) = 1.155 f_b \qquad (4)$$

with very little error.

[1]) S. O. Rice, Mathematical Properties of Random Noise, Bell System Tech. J. **23** (1944) 282; **24** (1944) 46.

Rice also shows that the number of maxima per second greater than V_c will be ρ, where

$$\rho = \tfrac{1}{2} \exp\left(\frac{-V_c^2}{2\psi}\right) \times N(0) \qquad (5)$$

Combining this with (4), we have

$$\rho = 0.578 f_b \exp\left(\frac{-V_c^2}{2\psi}\right) \qquad (6)$$

giving the frequency with which the discriminator triggering level is reached by the noise peaks. Fig. 1 is a graph of ρ/f_b, plotted logarithmically, against

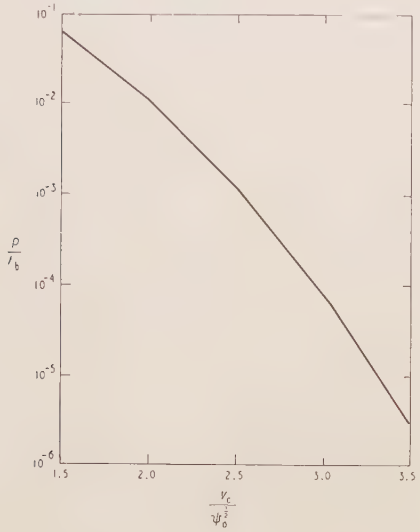

Fig. 1. Graph of $\rho/f_b = 0.578 \exp(-V_c^2/2\psi_0)$.

$V_c\psi^{-\frac{1}{2}}$. If, as in the present equipment, V_c is made to change linearly with time, from the time $t = 0$, in accordance with the equation

$$V_c = V_0 - vt \qquad (7)$$

then

$$\log_{10} \rho(t) = \log_{10} 0.578 f_b - 0.4343 \frac{(V_0 - vt)^2}{2\psi}$$

$$= \log_{10} 0.578 f_b - \frac{0.4343 V_0^2}{2\psi} + \frac{0.4343 V_0 vt}{\psi}$$

$$- \frac{0.4343}{2\psi} v^2 t^2 . \qquad (8)$$

The first two terms on the right-hand side of this equation are constant, as t varies. Provided that $\frac{1}{2}vt$ is small compared with V_0, the term in t^2 is small compared with the term in t and the variation of $\log \rho(t)$ may be taken as approximately linear. That is to say, the increase of $\rho(t)$ is approximately exponential. The accuracy of this approximation obviously depends on the maximum value of vt and therefore on the range of $\rho(t)$ in the output which is used. However, for the main application for which the excursion generator was designed, the testing of a fast excursion detector[2]), the range of $\rho(t)$ needed in any one excursion is only a small part of the range shown in fig. 1, so that the accuracy is very good.

The assumptions made in deriving this result are:

1. Low dead-time losses in the discriminator. In the present case, the dead-time is about 2.4 μs and the maximum value of ρ is 100 kc/s. The errors introduced by this assumption are small for values of ρ up to 10 kc/s or so (2.4% deadtime).

2. It is assumed in Rice's theory that the amplifier has an ideally rectangular passband. Since three nearly indentical stages of noise amplification are used, the variation of gain above the cut-off frequency will be at -18 dB/octave, so that this assumption should not lead to serious error.

3. Circuit Description

The circuit diagram of the random pulse generator is shown in fig. 2. Shot noise is generated in a noise diode V1, which is designed to operate with an anode current of 10 mA. Noise voltages developed across the load resistor R2 are fed to the amplifier stages V2, V3 and V4. These are three similar stages, with a passband from 30 kc/s to 1.2 Mc/s. The lower frequency cut-off is defined by the high-pass networks C5, R12 and C14, R21 and is made relatively high, so as to attenuate any hum voltages produced in the first stage. The gain of V3 is made adjustable by applying a negative bias voltage through the resistor R12. The direct currents to the anodes, and hence the gains of the valves V2 and V4, are stabilised by making the grids about 25 V positive, through the networks R3, R4 and R20, R21, and then using cathode resistors R8 and R24-with the relatively large value of 2.2 kΩ. These resistors are heavily by-passed, to avoid any loss of gain. The amplified noise voltage at the anode of V4 is passed to a White cathode-follower V5. The mean potential at the output of this valve is varied as

[2]) C. H. Vincent, Nucl. Instr. and Meth. **9** (1960) 181.

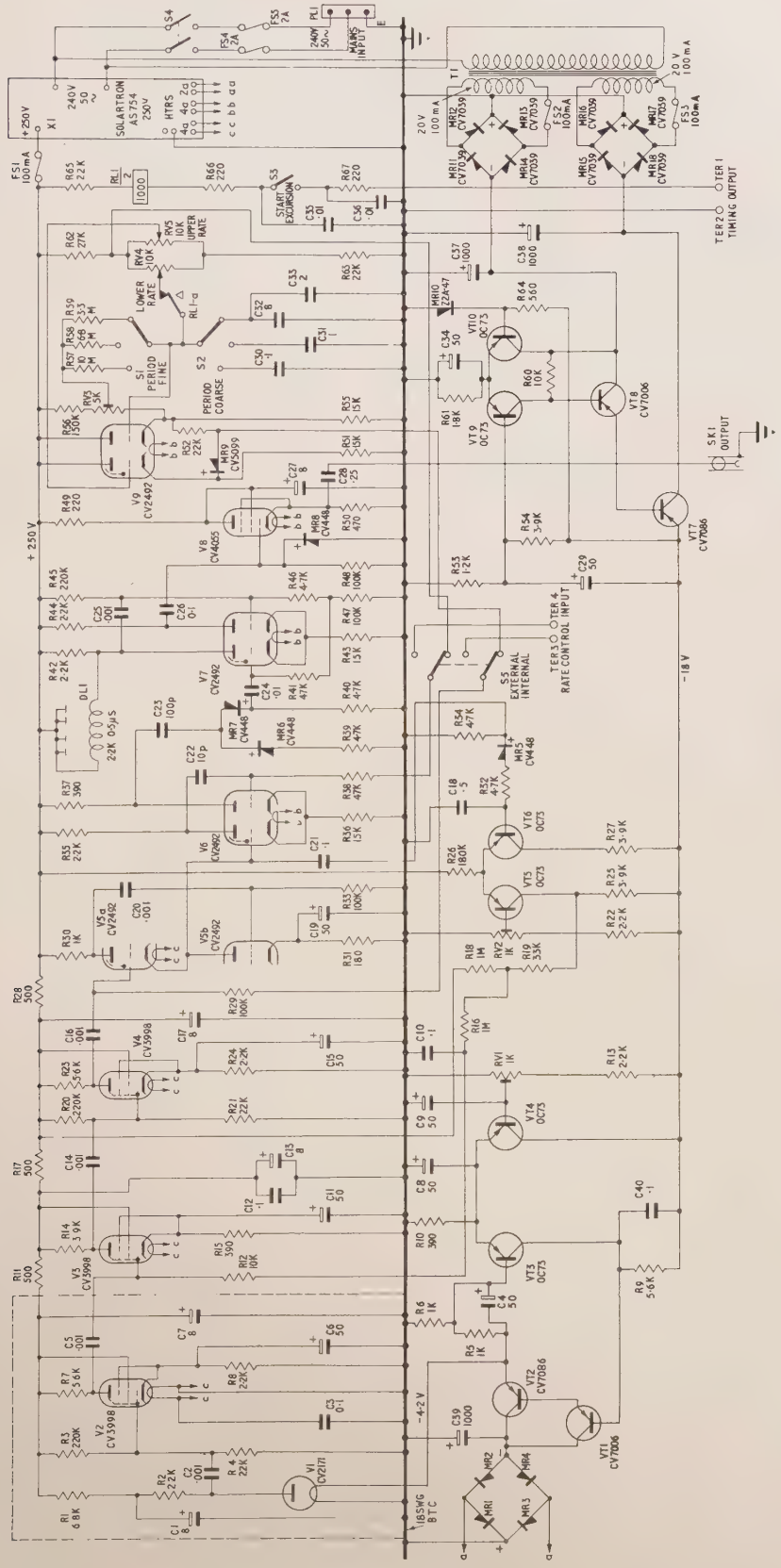

Fig. 2. Circuit diagram of random pulse generator.

required, by applying a positive voltage of about 100 V to the grid of the top triode through R29. A noise level of about 3.5 V r.m.s. is present at the output of V5, and this is fed to V6, a discriminator circuit. V6 is a Schmitt trigger circuit, the input of which is directly coupled to V5. The length of the pulse generated is defined by C22 and R38 at about 1 μs, and the effective noise voltage at which discrimination takes place can be adjusted by shifting the direct-current level of the noise voltage, controlled via R29. The positive discriminator pulses appearing across R37 are fed to the pulse-forming valve V7 through C23 and MR7. This valve is in another Schmitt trigger circuit. It generates a pulse with a duration of about 0.8 μs, defined by the delay line DL1. This pulse, which is positive and of 12V amplitude, appears at the anode of V7b. This voltage pulse is fed to V8, the output cathode-follower.

The operating voltage of the discriminator circuit V7, and thus the mean output pulse rate, is controlled by V9, and the mode of operation of this is controlled by the switch S3, START EXCURSION. With this switch in the normal open position, the relay contact RL1a connects the right-hand triode of V9 to the potentiometer RV4, LOWER RATE. The positive end of this potentiometer is connected through R38 to the discriminator valve V6. The potentiometer slider is connected through the cathode-follower V9 and through R52 and R29 to the White cathode-follower V5. Making the slider of the potentiometer more positive reduces the difference between the mean noise voltage at the input to the discriminator and the voltage at which the discriminator operates. This increases the rate of discriminator operation, and thus the output pulse rate. Fig. 3 shows the calibration of the output pulse rate ρ against the voltage (controlled by the potentiometer RV4) between the terminals of the switch S5, INTERNAL/EXTERNAL, which is here assumed to be in the INTERNAL position. This calibration is explained more fully in section 4. Suppose now that the switch S3, START EXCURSION, is closed. This opens the relay contact RL1a and turns V9b into a bootstrap linear sweep circuit. The output voltage at the junction of R52 and MR9 moves positively at a rate determined by the settings of S1, PERIOD FINE; S2 PERIOD COARSE; and the potentiometer RV3. This rise continues until the output voltage is caught by the action of the diode MR9. The voltage at which this starts to conduct is controlled by the cathode voltage of V9a, which is set by RV5, UPPER RATE.

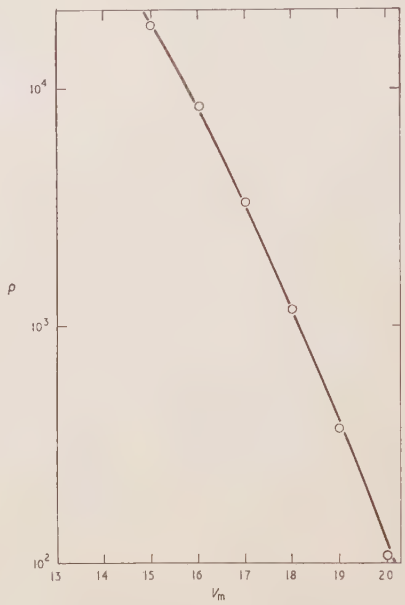

Fig. 3. The mean pulse rate ρ (in c/s) as a function of the discriminator bias voltage V_m. The value of the bias correction V_i used in calculating this theoretical curve was chosen to fit the experimentally determined points shown.

If an exponential excursion of specified period between two count rates is required, the rate of voltage change dV_c/dt needed may be calculated from the mean slope of the curve between the two corresponding points in fig. 3. The switches S1 and S2 and the potentiometer RV3 may then be set to give the required rate of rise. The rate of rise may be measured by means of an oscilloscope, or by means of a voltmeter and stop-watch, for the lower rates. In the latter case, the pointer of the voltmeter should only be timed after a sufficient interval for it to have overcome the initial inertial lag and reached a uniform speed. The potentiometer RV3 is a preset control and is normally set to a mean position which makes the engraved calibration (for period) of the switches S1 and S2 approximately correct, in accordance with the nominal values of the resistors and capacitors concerned and with the average slope of

g. 3. Alternatively, the discriminator operating oltage may be supplied from an external source. With the switch S5, INTERNAL/EXTERNAL, in he EXTERNAL position, the discriminator is onnected to terminals TER3, TER4, RATE CONTROL INPUT. The mean voltage applied to hese terminals should be about 110 V. The relatively small) voltage existing between them ontrols the output pulse rate, terminal TER4, eing the more positive. The output pulse rate can e determined for various input voltages, giving the alibration curve shown in fig. 3. From this curve, he input voltage required for any steady output ulse rate can be found. The input voltage may be erived from an external function generator and he output pulse rate may be varied in any required way.

The transistor stabilisers are operated from the ransformer T1 through the rectifier bridges MR11-MR14 and MR15-MR18. These deliver about 28 V direct-current and the bank MR11-MR14 is used to supply a stabiliser amplifier comprised of VT9 and VT10. This amplifier compares the stabiliser output voltage across R53 and R54 with the voltage across the Zener diode MR10. Any difference is amplified and fed to the base of the series transistor VT7 through the emitter-follower VT8. A well stabilised voltage of — 18 V appears at the emitter of VT7, and this is used to drive the other transistors in the unit. These are arranged in two sets, VT1-VT4, the noise diode heater regulator, and VT5 and VT6, the automatic gain control amplifier. The transistors VT1 to VT4 form a series stabiliser of the same type as VT7 to VT10. The heater voltage across R5 and R6 is compared with a voltage determined by the setting of RV1. Any difference is amplified and applied through the emitter-follower VT1 to the series transistor VT2. The valve heater requires about 300 mA at 4.2 V, and because of this the voltage supplies are obtained from the rectifier bridge MR1-MR4. This is supplied with 6.3 V r.m.s. from a heater winding on the power supply, and the output is smoothed by C39 to reduce hum, which is further reduced by the stabilising action. The potentiometer RV1 is set to give an anode current of 10 mA in the diode V1. The transistors VT5 and VT6 form an automatic gain control amplifier. The wide-band noise coming from V5 is passed through the condenser C21 to remove the direct-current component. The rectifier MR5 is a mean level rectifier, and its output is smoothed by the filter comprised of R32 and C18. This mean output is then compared with a voltage derived from the potentiometer RV2. Too large a mean noise voltage causes the amplifier output at the collector of VT5 to become more negative. This output, with its direct-current level shifted by means of R18 and R19, is smoothed by R16 and C10 and is fed back to V3 to reduce its gain, reducing the mean noise voltage. The gain of this stabilising loop is about 20 dB. The potentiometer RV2 is adjusted to give a stabilised noise level such that there is a voltage of 2 V between the base of VT6 and earth. The wide-band noise at the cathode of V5a may be seen on an oscilloscope, if a suitable screened lead or oscilloscope probe is used to prevent oscillation of the video amplifier. Lower frequency noise with an amplitude of about 3.5 V r.m.s. may be seen at the collector of VT5, when the gain control amplifier is working.

4. Experimental Results and Performance

4.1. PULSE RATE

It is of interest to compare the theoretical value of the output pulse rate given by eq. (6) with the measured values. Values for the output pulse rate were measured at various values of the discriminator voltage, which was controlled by RV4 and recorded by a voltmeter connected between the junction of R52 and MR9 and the junction of R62 and RV5. The measurements obtained are shown ringed in fig. 3. To determine ρ from eq. (6), it is necessary to know f_b, ψ and V_c. The upper frequency f_b was accurately measured with a signal generator. (The lower frequency cut-off does not make any appreciable difference to ρ.) The quantity ψ, the mean noise voltage squared, can be obtained by measuring the voltage at the junction of R32 and MR5, using a 10 kΩ series resistor to isolate the meter from video frequency components. If this voltage is V_1, it can be shown by integrating equation (1), assuming perfect rectification, that

$$V_1 = \frac{\psi^{\frac{1}{2}}}{\sqrt{2\pi}}.$$

The value of ψ was measured in this way. It was found that $V_1 = 1.34$ V, giving $\psi^{\frac{1}{2}} = 3.36$ V. The voltage measured between the junction of R52 and MR9 and the junction of R62 and RV5 differs from the voltage V_c at which the discriminator operates, because of the bias conditions of V5 and V6. If V_m is the measured voltage and the gain of the White cathode-follower V5 is taken as unity,

$$V_c = V_m - V_b \qquad (10)$$

where V_b is a constant. V_b was determined by substituting values found experimentally, and the value of $\psi^{\frac{1}{2}}$ given above, in eq. (6). It was found that $V_b = 6.0$ V. This value, and the value obtained for ψ, were substituted in eq. (6), and the result obtained is shown in fig. 3. The agreement seems very satisfactory.

4.2. STABILITY

Another factor measured was the output stability. The output pulse rate was found to vary by $\pm$ 5% for $\pm$ 20 V r.m.s. mains changes. In a twelve hour period, the output pulse rate was found to be stable to $\pm$ 3%.

4.3. TRUE RANDOMNESS

The output of a random pulse generator is truly random if there is a constant probability per unit time of an output pulse occurring. The present unit should give a good approximation to this condition at output pulse rates which are small compared with the upper limit f_b of the noise frequency band and with the reciprocal of the discriminator dead-time. Both these requirements should be met up to output rates of 10 kc/s or so. It was possible to demonstrate the randomness of the output pulses, apart from the expected dead-time effect, by displaying them on an oscilloscope with the time-base synchronised by the pulses themselves. A line of full brightness displayed the initial pulses (of constant amplitude and shape), which triggered the time-base, and this was followed by a length of undisturbed base-line to complete the expected dead-time (see fig. 4). To the right of this region, distributed uniformly along the remainder of the time-base at random, appeared lightly traced further pulses, each formed by a single sweep of the time-base. Since the conditions were adjusted so that the probability of three pulses occurring on the same sweep was small, the uniform appearance of this right-hand region of transient pulses was at least an approximate verification of the constancy of the probability outside the dead-time region.

The distribution of the number of pulses in a fixed time interval agreed accurately with a Poisson distribution in a test[3]).

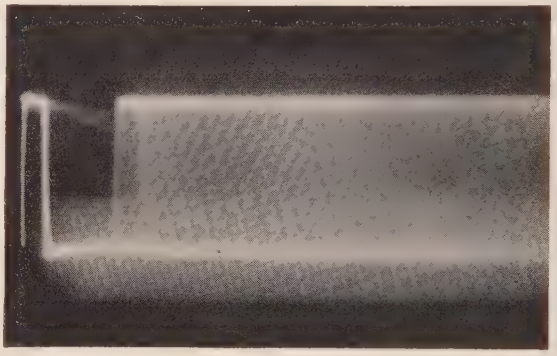

Fig. 4. Demonstration of random timing after the dead-time

4.4. OUTPUT PULSE CHARACTERISTICS

As already stated, the only type of output pulse provided by the random pulse generator is a positive one of 0.8 μs duration and 12 V amplitude. The main function of the generator is to provide the necessary randomness, together with the provision for excursions. It was therefore decided that the best way to obtain the greatest possible flexibility in use, without undesirable complication of the pulse generator, was to provide only this standard pulse, which can be modified by external equipment or used to trigger an external pulse generator, as required.

Acknowledgement

The author wishes to thank Dr. C. H. Vincent for first suggesting the instrument, and for his interest in the progress of the work.

[3]) W. G. Gore and T. Ring, A Pulse Number Sorter. An unpublished A.W.R.E. report, August, 1960.

NUCLEAR INSTRUMENTS AND METHODS 13 (1961) 253–257; NORTH-HOLLAND PUBLISHING CO.

AN INSTANTANEOUS PULSE FREQUENCY METER FOR RANDOM PULSES

K. GOPALAN and E. S. RAJAGOPAL

Department of Physics, Indian Institute of Science, Bangalore 12

Received 24 May 1961

Counting-rate meters normally used for finding pulse frequencies are sluggish in their response to any rapid change in the pulse repetition frequency (P.R.F.). An instrument is described which measures each pulse interval and provides immediately afterwards an output voltage proportional to the reciprocal of interval duration. A response to a change in the P.R.F. as rapidly as is physically possible is obtained. The instrument has wide application in low level radiation detection and in several other fields especially for rapidly varying counting-rates.

1. Introduction

Random pulse frequencies which occur for example in radiation detection, biophysical applications and other fields are usually measured with counting-rate meters which, however, are very slow in their response to any rapid change in pulse frequency[1,2,3]). Attempts to improve the transient response of the device increase the fractional probable error and reduce the sensitivity[4]).

The instrument to be described below has been developed in order to indicate the rapid changes in counting-rate, after a suitable scaling to give the necessary statistical significance, when the gamma spectrum of a radioactive source is scanned[5]); but it has applications in other fields for example, in the study of discharges of nerve-fibres and heart-beats[6,7,8]), flowrates in turbines[9]), speech analysis[10]) and in other similar situations[11,12]) where instantaneous indications of pulse frequencies are required.

The frequency range originally required to be covered by the present instrument was from 0 to 100 pulses/second. However, this range can easily be modified to accommodate higher frequencies.

2. Principle of Operation

When pulses occur randomly the most practical definition of frequency is the reciprocal of the time interval between two successive pulses.

Suppose a set of pulses A_1, A_2, A_3 . . . A_7, occur at the input and let the output of the instrument be the pulse frequency given as the output voltage

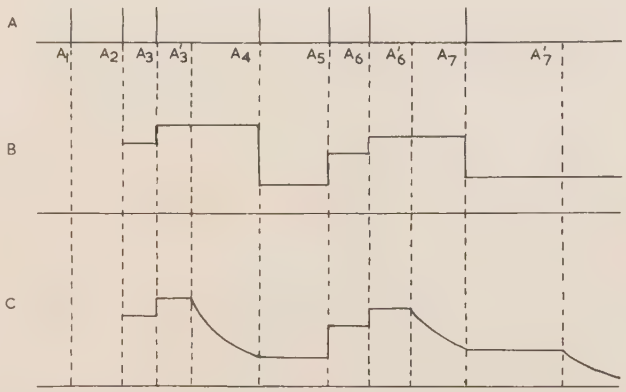

Fig. 1. Presentation of instantaneous pulse frequencies. A. Input pulses; B. Simple indication of pulse frequency; C. More refined indication used in the present instrument.

[1]) D. G. C. Luck, Frequency Modulated Radar (McGraw-Hill, N.Y., (1949) p. 90.

[2]) P. M. Fitzpatrick and K. Hazel, Rev. Sci. Instr. **30** (1959) 371.

[3]) C. H. Vincent, Nucl. Instr. and Meth. **9** (1960) 181.

[4]) W. C. Elmore and M. Sands, Electronics (McGraw-Hill, N.Y., (1949) p. 249.

[5]) E. S. Rajagopal and K. Gopalan, Proceedings of the Low Energy Nuclear Physics Symposium (February 1961), Atomic Energy Commission, Bombay p. 309.

[6]) A. M. Andrew and T. D. M. Roberts, Electronic Engng., **26** (1954) 469, 543.

[7]) A. W. Melville and J. B. Cornwall, Electronic Engng., **31** (1959) 268.

[8]) M. Manzotti, Electronic Engng., **28** (1956) 446.

[9]) T. E. Berwin, I.R.E. Trans. Electronic Computers, PGEC-9 (1960) 62.

[10]) P. G. M. Dawe and J. A. Deutsch, Electronic Engng. **27** (1955) 2.

[11]) P. A. V. Thomas, Electronic Engng. **25** (1953) 302.

[12]) E. F. MacNichol and J. A. H. Jacobs, Rev. Sci. Instr., **26** (1955) 1176.

during the succeeding interval as shown in fig. 1B. It is readily seen that a shorter interval corresponds to a larger output voltage in the succeeding interval and vice versa. This type of output has been used by Berwin and others.

A serious difficulty of this mode of operation is that if the P.R.F. falls suddenly to zero the output voltage will not reduce to zero, as it must, but will continue to indicate the value corresponding to the previous interval. For example, the pulses have stopped at A_7, but the meter continues to show the output corresponding to A_6 A_7.

This undesirable feature can be eliminated by making the output voltage at any instant determined either by the duration of the preceding pulse interval, or by the duration which the current interval has already attained, whichever is the longer. This mode of operation, which is physically the quickest possible method of finding the frequency, is illustrated in fig. 1C. If an interval is shorter than the preceding one, the higher value for the frequency is indicated soon after the interval. If an interval is longer than the preceding one, the instrument does not wait until the end of the interval before indicating a reduction in frequency. In fig. 1C the indication begins to fall away at A_3' where A_3 $A_3' = A_2$ A_3. This mode of operation has been preferred in the present case.

3. Arrangement of the Instrument

Fig. 2 shows a block diagram of the instrument. The basic timing of the pulse intervals is done by two timing units which function alternately. Each timing unit either operates to "measure" the pulse-interval by a hyperbolic charging of a capacitor in it ("operate" position of the timing unit), or it holds its capacitor charge which is a measure of the previous pulse-interval ("hold" position).

When in the operate position the timing unit charges its capacitor such that the voltage V across it is given by

$$V = V_0 - K/t \quad \text{for} \quad t \geqslant t_0 , \qquad (1)$$

where $t = 0$ is the time of arrival of the pulse which switched this timing unit on and V_0 and K are constants. The highest frequency possible is, therefore, $1/t_0$. In the present case $1/t_0 = 100$ c.p.s. as stated above. The reset control, triggered by the same pulse which switched this timing unit on, sees that the voltage on the condenser is discharged and set at $V_0 - K/t_0$ at $t = t_0$ so that the unit charges its condenser according to equation (1) afterwards. The proper switching on and off of the reset controls

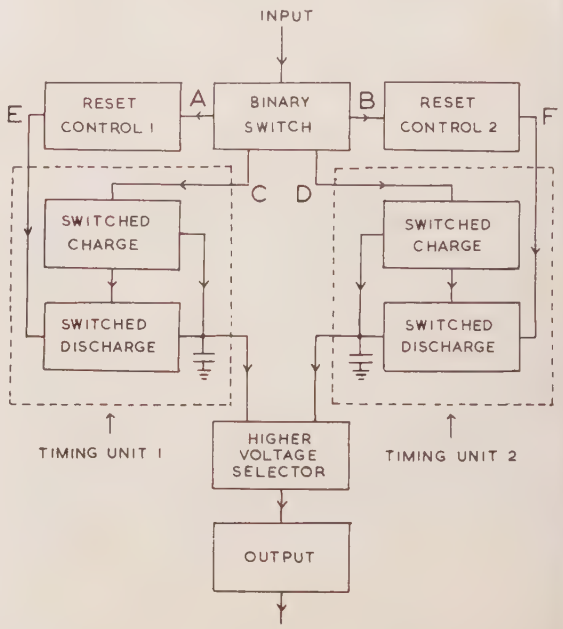

Fig. 2. Block diagram of the instrument.

and the timing units is done by the binary switch

The voltages developed across each capacitor are judged by the higher voltage selector to result in the operation of fig. 1C. If the pulses 0, 1, 2, 3 . . occur at times $t = 0$, T_1, $T_1 + T_2$, $T_1 + T_2 + T_3$ . . . ($T_2 > T_1$ and T_3 say) the voltage on the condenser of say No. 1 timing unit after $t = T_1$ is $V_0 - K/T_1$ and will be maintained so up to $T_1 + T_2$. The voltage on the timing unit No. 2 at time $t > T_1$ will be $V_0 - K/(t - T_1)$ which will be smaller than that on the unit No. 1 until $t - T_1 < T_1$ and larger than that for $t - T_1 > T_1$. Because of the action of the higher voltage selector the final output will be $V_0 - K/T_1$ during $T_1 \leqslant t \leqslant 2T_1$, $V_0 - K/(t - T_1)$ during $2T_1 \leqslant t \leqslant T_1 + T_2$ and $V_0 - K/(t - T_1 - T_2)$ during $T_1 + T_2 \leqslant t \leqslant T_1 + T_2 + T_3$. This is just the operation depicted in fig. 1C except for a change of sign which is easily removed by a simple inversion at the output stage

4. Circuit Details

The complete circuit is shown in figs. 3A, 3B and 4. V_{1A} is an amplifier for the positive input pulses of about 10 V and its output triggers the bistable

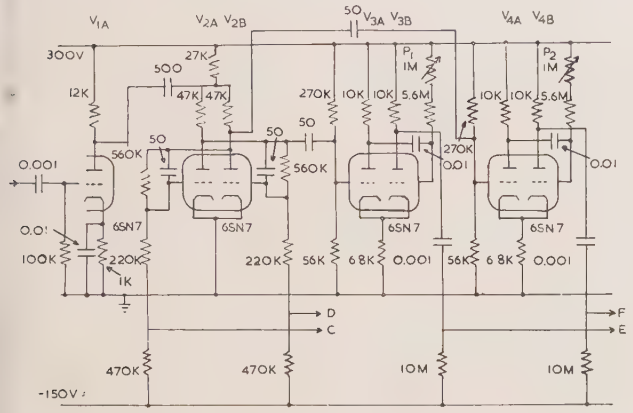

Fig. 3A.

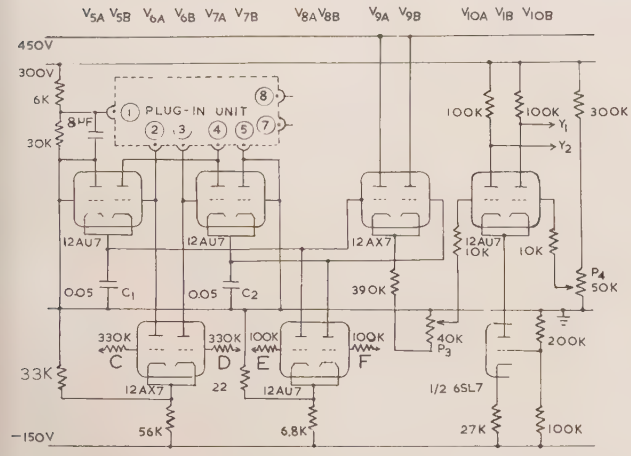

Fig. 3B.

Figs. 3A and 3B. Complete circuit diagram.

V_{1A} is $\frac{1}{2}$ 6SL7. Point C connected to V_{6A} grid, D to V_{6B} grid, E to V_{8A} grid and F to V_{8B} grid.

multivibrator V_2 (binary switch). The positive rectangular pulses from the plates A and B of V_2 trigger the identical univibrators V_3 and V_4 (reset controls 1 and 2) alternately so that positive rectangular pulses of a definite duration are made available at E and F. The delays of V_3 and V_4 are varied by the potentiometers P_1 and P_2. With the values shown, when C is at — 50 V (off polarity) D is at — 80 V (on polarity) and vice versa. The signals at E and C and those at F and D have the same on or off polarity and the polarities are changed at the arrival of the next pulse.

The high quality condensers C_1 and C_2 (0.05 μF) in the timing units are charged towards the final plate voltage 250 V of V_{5B} and V_{7A}. C_1 can be charged by the combined anode and grid currents of V_{5B} only when V_{6A} is cut off i.e C at — 80 V. For when V_{6A} conducts (with C at — 50 V) the plate voltage of V_{6A} drops down to about — 30 V cutting off V_{5B}. C_1 can be discharged only when V_{8A} conducts (during the application of the reset pulse at E). V_{5A} is connected as a diode to prevent the negative excursion of C_1 when V_{8A} discharges it. The cathode voltage of V_6 is so chosen that the section with its grid at — 80 V is cut off and that the section with its grid at — 50 V is conducting. Similarly V_8 is made non-conducting when no positive pulses occur at E or F.

The sequence of the various switching actions is now easily followed. Suppose an input pulse drives say V_{2A} nonconducting from the conducting state. The positive step produced at A triggers V_3 resulting in a positive rectangular pulse at E. Its

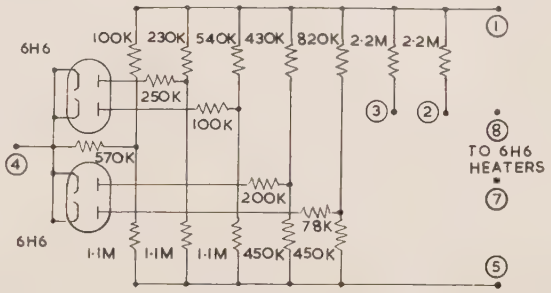

Fig. 4. Plug-in unit for a 5-diode approximation to the required hyperbolic charging law.

leading edge coincides with the input pulse (neglecting small differences due to finite rise times). Simultaneously C is driven to — 80 V and D to — 50 V. V_{6A} is cut off. Therefore V_{5B} is conducting and is ready to measure the time interval. Also V_{7A} and V_{8B} are cut off so that the voltage on C_2 is maintained at the value it had acquired just before the pulse came. But as soon as V_{5B} begins to conduct the reset pulse from E drives V_{8A} highly conducting with the result that the hang-over charge due to the last-but-one interval as well as the charge accummulating on C_1 due to the induced conduction of V_{5B} are quickly discharged. C_1

remains discharged at OV until V_3 flops back and then begins to be charged linearly towards 250 V. The diode network of fig. 4 gives such a charging current which leaves the voltage on the condenser as

$$V = 250 - 2/t \quad \text{for} \quad t \geqslant 10 \text{ msec.} \qquad (2)$$

The hyperbolic waveform of equation (2) can be realised in a number of ways[13]). Fig. 4 shows the circuit for obtaining equation (2) by the addition of six exponential segments and the design of this network is discussed in detail by Andrew and Roberts[6]). The voltage on the condenser is therefore a linear function of the reciprocal of the pulse-interval which is under way. When the next pulse comes it makes C — 50 V and D — 80 V so that V_{6B} and V_{5B} are cut off. C_1 retains the acquired voltage and C_2 begins to measure the new time interval.

According to equation (2) the voltage on a condenser in the operate state must be 50 V at 10 msec after the input pulse. This is easily secured by giving a 100 c.p.s. input to the instrument and adjusting the duration of the pulses at E and F simultaneously to give 50 V at the cathode of V_9. If C_1 and C_2 are identical the pulses at E and F must have the same duration. Any slight differences in C_1 and C_2 and in the charging tubes are approximately accommodated by a corresponding slight difference in the durations of the pulses.

The higher voltage selector is just a pair of cathode followers V_9 with a common cathode resistor. The cathode potential is determined almost entirely by the more positive grid. With a 12AX7 even when the difference in grid potentials is as small as 0.5 V the more negative grid has no effect on the output[14]).

The voltage variations at V_9 cathode constitute the output of the instrument. This is the negative of the situation in fig. 1C. Since a cathode ray tube display of frequency fluctuations is desired in the present case[5]) a fraction of this variation is applied to the direct coupled paraphase amplifier V_{10} which has a constant current source V_{1B} at its cathode for improving the linearity. The plates of V_{10A} and V_{10B} are connected to the Y-plates of a cathode ray tube. Arrangement is made for the Y-shift of the spot. Obviously other forms of presentation can be obtained if necessary.

5. Discussion

Among the many units which have been used in the past for the purpose of instantaneous random frequency indications, (as discussed in 1) only the units of Berwin[9]) and of Andrew and Roberts[6]) have performance comparable to the present instrument which additionally has a simpler circuitry than those units.

Before discussing them it is relevant here to point out the recent work of Vincent[3]) where he has effected some improvement in the transient response of counting-rate meters. But this system appears complicated and still is not as rapid as the present instrument.

Berwin's instrument gives the operation of fig. 1B only and not the more refined indication of fig. 1C. The use of two timing units is necessary for the operation of fig. 1C. The use of two separate reset controls instead of a common reset control as in the circuit of Andrew and Roberts has been preferred. This eliminates the fixed delay after the input pulse and before the common reset control (which is necessary to pin-point the correct capacitor C_1 or C_2 to be discharged by the common reset control) and the consequent voltage "pips" in the output. Moreover, one can accomodate slight variation in C_1 and C_2 and the associated charging and discharging units. The extension of the operation to higher frequencies is not also hampered by the presence of recovery times of the reset controls (since they alternately come into operation). In fact, with heavier charging and discharging currents and smaller values of C_1 and C_2 one can easily extend the frequency range to about 10^4 c.p.s.

The instrument is tested by giving inputs of 10, 20 . . . 100 c.p.s. in succession and finding the output voltage at the cathode of V_9. The voltage agrees with eq. (2) within 1% showing the excellent linearity obtained by the simple means. The detailed performance of the instrument will be communicated in a later publication.

[13]) B. Chance, V. Hughes, E. F. MacNichol, D. Sayre and F. C. Williams, M.I.T. Rad. Lab. Series, "Waveforms", Vol. 18, (McGraw-Hill, N.Y., 1949) p. 289.

[14]) P. Hariharan and M. S. Bhalla, J. Sci. Instr. **36** (1959) 192.

Acknowledgement

The author's thank Professor R. S. Krishnan for his guidance and encouragement which enabled the present work to be carried through. One of them (K.G.) thanks the Atomic Energy Department, Bombay, for the award of a Junior Research Fellowship and the other (E.S.R.) thanks the Council of Scientific & Industrial Research, New Delhi, for the award of a Senior Research Fellowship.

NUCLEAR INSTRUMENTS AND METHODS 13 (1961) 258–260; NORTH-HOLLAND PUBLISHING CO.

SPARK COUNTER AS A FAST PULSE GENERATOR

S. L. GUPTA and N. K. SAHA

Department of Physics, University of Delhi, Delhi – 6, India

Received 1 June 1961

The spark counter has been used as a fast pulse generator for testing fast coincidence circuits and its behaviour studied in detail using a Bell type of coincidence arrangement. The rise time of the spark counter pulse is estimated to be less than 4 nanosec.

1. Introduction

There is a great need of a simple type of fast pulse generator with statistical pulse frequency in nanosecond range for testing fast coincidence circuits. J. Fleury[1]) (1959) indicated that the Rosenblum sprak counter can be utilised as a nanosec pulse generator. Following the earlier works on the Rosenblum spark counter in this laboratory (Saha and Nath[2]) (1957), we have investigated the problem in detail by using a Bell, Graham and Petch[3]) type of coincidence arrangement, a brief account of which is given below.

2. The Pulse Attenuator and the Pulse Form

The counter consists of a stainless steel polished plate as cathode and 0.1 mm diameter tungsten wire as anode. The wire-plate distance is 1.4 mm. The attenuator and the pulse forming network are shown in fig. 1. The pulse attenuator consists of two parallel high impedance net works of about 2.7 MΩ and 5 pF, each coupled with a low impedance net work of 100Ω and 10 pF, the latter essentially determining the effective pulse rise time in the out put and the former limiting the quiescent corona current and fixing the RC value in accordance with the counter's own dead time ($\sim$ 50 μsec).

Output pulses are taken from either of the points S or L. The amplitude of the pulses can be varied from 0 to 50 V by varying both the capacitors C and C. A Po^{210} α-source was used for producing sparks. The number of pulses can be varied by changing the distance of the source from the counter. The counting characteristics were determined with the charging and attenuator circuit having the equivalent quenching resistance of about 1.4 MΩ and is shown in fig. 2. The plateau slope was found to be 3 per cent/100 V. The change of quiescent corona current with the applied voltage is also shown in the same figure.

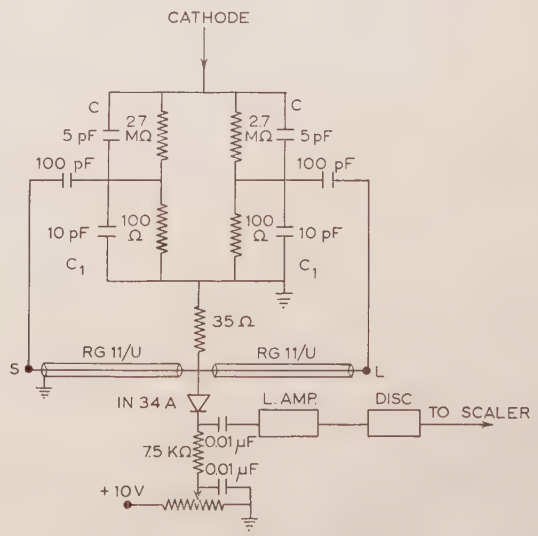

Fig. 1.
Charging and attenuator circuit with coincidence arrangement.

Fig. 3 shows a photograph of the pulse taken over a Tektronix 531 A oscilloscope with sweep speed:

[1]) J. Fleury, Proc. of the International Symposium on Nuclear Electronics (International Atomic Energy Agency, Wien, Austria, 1959) p. 259.

[2]) N. K. Saha and Narendra Nath, Nucleonics **15**, No. 6 (1957) 94.

[3]) R. E. Bell, R. L. Graham and H. E. Petch, Can. J. Phys. **30** (1952) 35.

5 div. = 20 ns. The apparent pulse rise time 20 nanosecond as seen in the photograph is limited by the rise time of the vertical amplifier of the oscilloscope. Actually the spark counter pulses here have much better rise time, as the prompt coincidence analysis shows (fig. 4).

positive time delays in terms of various lengths of RG11/U coaxial cable in the two channels of the coincidence system. The resolving time is 4 nanosecond. We therefore, conclude that the rise time of the counter pulses is better than 4 nanosecond which is in agreement with the value obtained directly over the fast oscilloscope by J. Fleury.

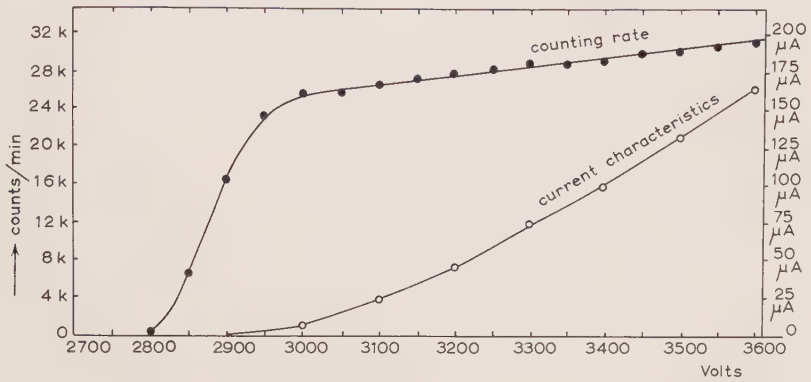

Fig. 2. Spark counter counting and quiescent corona current characteristics.

3. Coincidence Study of the Pulse Rise-Time

The pulses from the output points S and L were taken through RG 11/U 75 ohms impedance coaxial cables to a junction box with 35 ohms terminating resistor. As usual, IN34A diode discriminator, linear amplifier, and an amplitude discriminator were used to discriminate singles from the coincidences. Fig. 4 shows the prompt coincidence resolution curve obtained by introducing negative and

Fig. 5 shows another prompt coincidence resolution curve taken by replacing the 35 ohms resistor with a shorted stub of total journey time of one

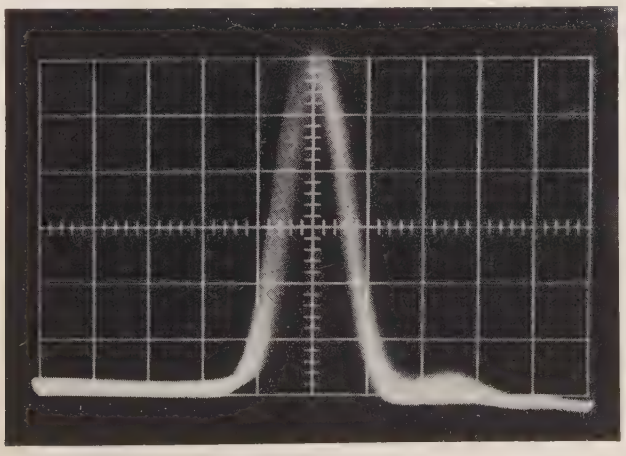

Fig. 3.

nanosecond. The resolving time obtained is about 3 nanosecond, a slight improvement over the previous case. A better resolving time can perhaps be obtained by using smaller clipping times. This was not done as the amplitude of the pulses becomes rather low.

4. Discussion

In addition, we have studied the working of the spark counter with lower values (1.1 MΩ, 0.8 MΩ, and 0.5 MΩ) of the quenching resistors. It was observed that the quiescent corona current increases considerably with decreasing quenching resistors at the same applied voltage. With 0.5 MΩ, the counting efficiency for α-particles from Po^{210} becomes extremely low. The obvious reason for this is the high intensity of the space charge sheath in the neighbourhood of the counter wire. With the quenching resistors 0.8 MΩ and 1.1 MΩ, there is a gradual and considerable improvement in the counting efficiency. In our case it has been observed that about 1.4 MΩ is the minimum value of the quenching resistor consistent with the maximum value of the corona current which can be used for normal practical working of the spark counter with Po α-particles. Furthermore, the use of the quenching resistors greater than 1.4 MΩ result in the increase of the pulse rise time. For example, with the quenching resistor of 2 MΩ we obtained a prompt coincidence resolution curve, which gave the resolving time of about 5.5 nanosecond.

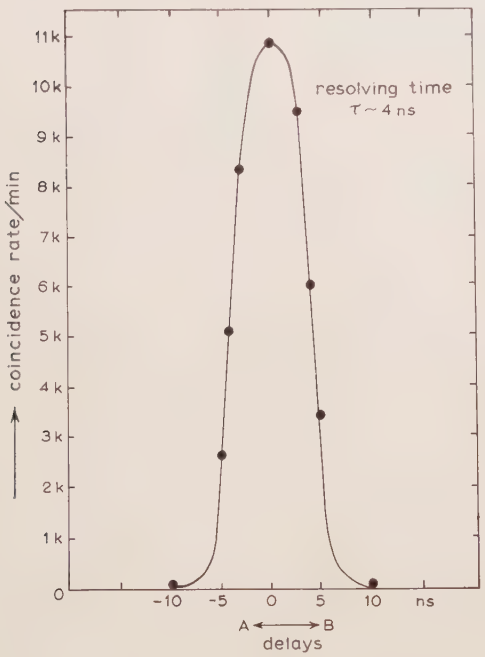

Fig. 4. Po^{210} prompt coincidence resolution curve.

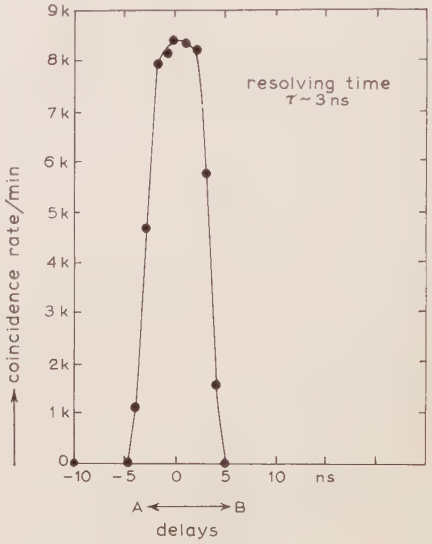

Fig. 5.
Po^{210} prompt coincidence resolution curve with shorted stub.

In the low-impedance attenuator net work, the value of the capacitors C_1 and C_1 has been chosen to be 10 pF in order to match it with the RG11/U 75 ohms impedance coaxial cable. As this value is comparable with the parasitic capacitances in the attenuator, the slightly higher values of the capacitors C_1 and C_1 would also probably give the same resolving time.

Work is in progress to determine the transit time of a number of photomultiplier tubes using these spark counter pulses.

Acknowledgements

The authors are thankful to Mr. S. C. Pancholi for helping them in measurements and many useful discussions. One of them (S.L.G.) thanks the Council of Scientific and Industrial Research, India for a fellowship.

NUCLEAR INSTRUMENTS AND METHODS **13** (1961) 261–262; NORTH-HOLLAND PUBLISHING CO.

EIN KABELVERSTÄRKER FÜR IMPULSE GROSSER AMPLITUDE

C. NOACK und W. ROETHER

Zweites Physikalisches Institut der Universität Heidelberg

Eingegangen am 28. Juli 1961

A detailed circuit is given that feeds large fast pulses into the low characteristic impedance of a cable with a gain of unity. Its output impedance is 3 Ω, its risetime less than 0,1 μsec. When working into a 150 Ω cable, the linearity is better than 1 % for positive pulses up to 120 V.

Bei kernphysikalischen Untersuchungen muß man oft schnelle Impulse großer Amplitude über ein längeres Kabel leiten; z.B. dann, wenn man ein Impulsspektrum auf einen Vielkanal-Impulshöhenanalysator geben will, der nicht unmittelbar bei der Meßapparatur steht. Um Reflexionen zu vermeiden, muß man das Kabel mit seinem Wellenwiderstand abschließen; dieser ist in der Größenordnung von 10^2 Ω. Will man also Impulse von etwa 100 V einwandfrei übertragen, so muß der Ausgang des Meßverstärkers in der Lage sein, Stromimpulse von etwa 1 A abzugeben. Im Prinzip können Kathodenfolger mit geeigneten Leistungsröhren Spitzenströme dieser Größe liefern, dabei geht jedoch die Spannungsverstärkung so stark zurück, daß eine ausreichende Linearität und Stabilität nicht mehr

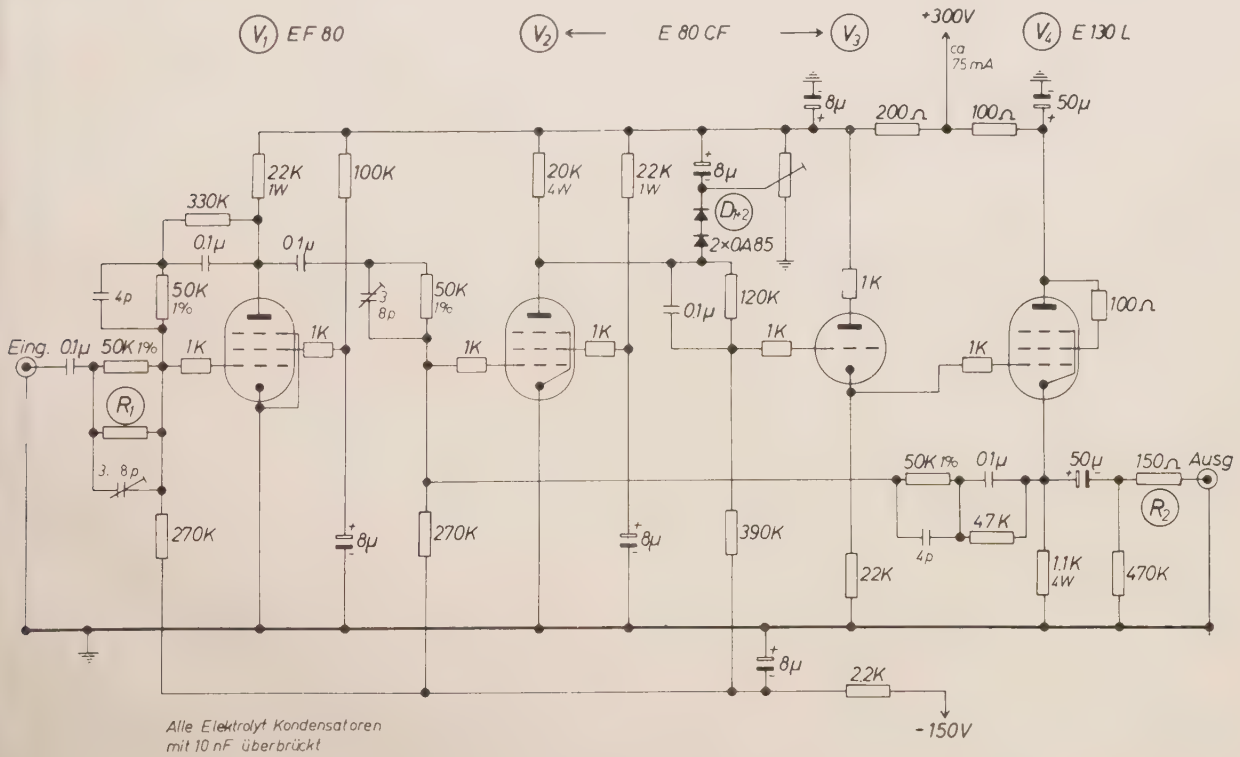

Fig. 1.

gegeben ist. Oft überträgt man deshalb die Impulse über das Kabel auf einem Niveau von nur wenigen Volt und verstärkt hinter dem Kabel nach. Dabei muß man jedoch neben dem größeren Aufwand in Kauf nehmen, daß vom Kabel aufgefangene Störungen mit verstärkt werden.

Vincent und Kaine[1]) haben kürzlich eine Schaltung angegeben, mit der sich die genannten Schwierigkeiten überwinden lassen. Sie legen den Leistungskathodenfolger, dessen Ausgang das Kabel speisen soll, in den Gegenkopplungszweig eines 1:1-Verstärkers. Die unzureichende Spannungsverstärkung des Kathodenfolgers bei Belastung durch das Kabel wird dabei durch die Verstärkungsreserve des 1:1-Verstärkers kompensiert. Diese Schaltung mit zwei parallel geschalteten E 81L als Ausgangsröhren speist Impulse von maximal 50 V in ein 100 Ω-Kabel.

Um bei allen Impulshohenanalysatoren den vollen Aussteuerungsbereich ausnützen zu können, ist es wünschenswert, grossere Impulse übertragen zu können. Figur 1 zeigt die hierzu von uns verwendete Schaltung. V_1 dient als Anodenfolger zur Phasenumkehr der positiven Eingangsimpulse; durch R_1 in der Größenordnung 1 MΩ wird die Gesamtverstärkung bei jedem Gerät möglichst genau auf 1 gebracht. Wie bei Vincent und Kaine[1]) liegt die Ausgangsröhre V_4 im Gegenkopplungszweig eines Anodenfolgers V_2, jedoch ist V_4 nicht direkt an die Anode von V_2 angekoppelt, sondern über den Kathodenfolger V_3. Dieser verhindert eine Integration der Impulse durch die Gitterkapazität der Ausgangsröhre V_4 und ermöglicht so den großen Aussteuerungsbereich. Die Dioden D_{1+2} sind nicht wesentlich für die Funktion der Schaltung, sondern gestatten, die Impulshöhen für die verschiedenen Anwendungen geeignet zu begrenzen.

Das Kabel ist durch R_2 an seinem *Eingang* abgeschlossen; so hat die (meist kapazitive) Eingangsimpedanz des nachfolgenden Geräts keinen wesentlichen Einfluß auf die Impulsform. Außerdem wird der Verstärkerausgang effektiv nur mit dem doppelten Wellenwiderstand belastet, wodurch man einen größeren Aussteuerungsbereich erhält. Das ist aus der folgenden Tabelle zu ersehen, die die wichtigsten Eigenschaften der Schaltung zusammenfaßt:

Belastung	∞	300 Ω	150 Ω	75 Ω
Linearitätsbereich bis	125 V	120 V	100 V	75 V
Max. Abweichung von der Linearität	0.5 %	0.8 %	0.8 %	1 %
Anstiegszeit ca.	40 ns	45 ns	50 ns	55 ns
Ausgangsimpedanz	3 Ω			

Geräte dieses Typs sind seit einiger Zeit in unserem Institut in Gebrauch und haben sich gut bewährt.

[1]) C. H. Vincent und D. Kaine, Electronic Engineering **32** (1960) 242.

NUCLEAR INSTRUMENTS AND METHODS 13 (1961) 263; NORTH-HOLLAND PUBLISHING CO.

LETTERS TO THE EDITOR

THE ESTIMATION OF THE RESOLVING TIME OF A COUNTING APPARATUS

G. R. MARTIN

Londonderry Laboratory for Radiochemistry, University of Durham, South Road, Durham City, England

Received 15 June 1961

Although it is now usual to arrange that the esolving time of a counting apparatus is fixed by n electronically imposed paralysis of duration letermined by circuit parameters, it is useful to ave available an independent check on this quanity. The technique which makes use of the analysis f the decay curve obtained from a radio-nuclide of vell established half-life has the virtue that it letermines the resolving time of the complete quipment, but, as usually applied, it lacks preciion, since it involves the extrapolation of the tatistically rather inaccurate "tail" of the decay urve in order to evaluate the losses at higher ounting rates.

If the apparatus is of the type in which the "dead ime" is *not* extended by the occurrence of a urther event during the recovery period, then one an write[1]):

$$N = n/(1 - n\tau) \qquad (1)$$

where n is the observed counting rate, N the "true" ate, and τ the resolving time of the apparatus. For pure radioactive substance, $N = N_0\, e^{-\lambda t}$, and (1) nay be re-written as

$$n\, e^{\lambda t} = N_0 - nN_0\tau\,.$$

A simple plot of $n\, e^{\lambda t}$ against n should then be near, and from the ratio of slope $[= N_0\,\tau]$ to ntercept $[= N_0]$, τ may immediately be evaluated. t should be noted that the linearity of this plot is sufficient indication that a law of the form of q. (1) does in fact hold over the range of counting ates examined. Furthermore, no special weight is given to the lower counting rates; indeed, the whole measurement may be carried out at rates for which the statistical accuracy is relatively high.

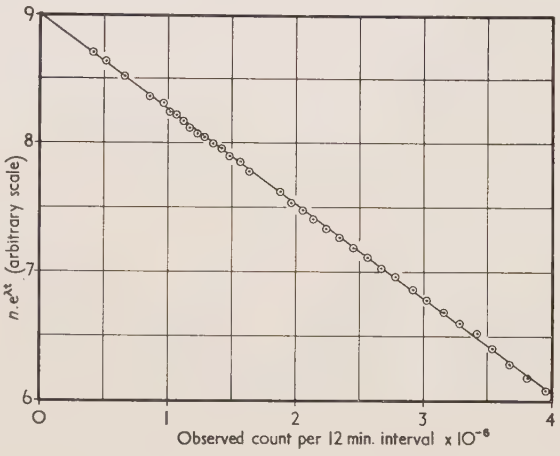

Fig. 1.

Fig 1 shows the result of applying this method to a β-proportional counter set, using the 2.576-hour ^{56}Mn as the active material; a value of 57.9 μsec is deduced for the effective "dead time" of the apparatus. ^{56}Mn may readily be prepared in a state of sufficient radiochemical purity by the reactions ^{55}Mn (n, γ) or ^{56}Fe (n,p); the short-lived activities which are also produced in the latter case decay to an insignificant level by the end of the first hour. A number of materials have half-lives known with sufficient accuracy to be useful alternative materials.

[1]) N. Hole, Ark. Mat. Ast. Fys. 33A, No. 11 (1946).

A CONSTANT INPUT IMPEDANCE PLUG-IN FOR THE TEKTRONIX 581 OSCILLOSCOPE

C. INFANTE

C.N.E.N. – Laboratori Nazionali di Frascati, Italy

Received 3 May 1961

The Tektronix 581 oscilloscope has a 100 Mc/s bandwidth and an input probe whose impedance is claimed to be 100 kΩ shunted by 10 $\mu\mu$F capacitance. Actually the probe has a tendency to ring at about 100 Mc/s, due to stray inductance effects, as stated by the manufacturer. It has often been found desirable to have an input impedance whose magnitude is frequency-independent. This has been done with the circuit to be described that has been assembled on a blank plug-in chassis. Input signals may reach the main 'scope amplifier through two ways: via condenser C or via integrating network R_1C_1 and vacuum-tube V_1: if the differentiating network made up by C and the 'scope's amplifier's input resistance (93 Ω) has a time constant equal to R_1C_1, a network with all-pass characteristics is obtained, due to the push-pull nature of the main amplifier. Inductance L and its associated resistors are added to compensate for the rise of input impedance at low frequencies due to condenser C. The unit has been designed for 125 ohm input impedance, but the values may be easily redesigned for a different impedance level. With this plug-in the oscilloscope posesses a bandwidth in excess of 100 Mc/s (about 3 nsec rise time), while the input impedance is constant within better than 3% up to at least 120 Mc. With the plug-in a slight reduction in sensitivity has been experienced (0.2 V/cm against 0.1 V/cm of the standard unit). This is due to the necessity of terminating the main amplifier on both sides. Vacuum tube V_2 terminates the amplifier at the far end.

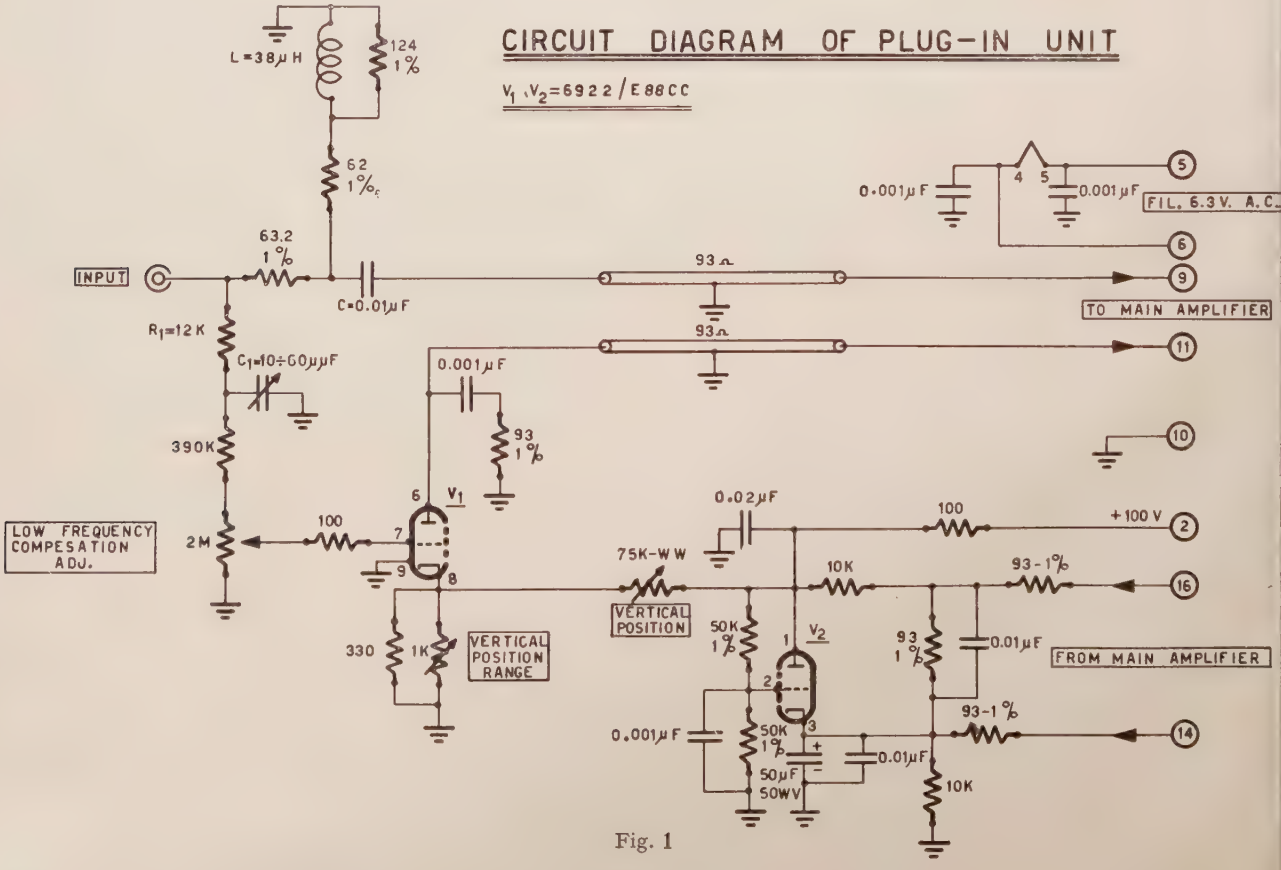

Fig. 1

NUCLEAR INSTRUMENTS AND METHODS 13 (1961) 265; NORTH-HOLLAND PUBLISHING CO.

NEWS ITEMS

CONFERENCE ON SECTOR-FOCUSED CYCLOTRONS

University of California, Los Angeles, 17–20 April 1962.

Sponsor of the conference will be the University of California. During 2–4 February 1959 an informal Conference on Sector-Focused Cyclotrons was held in Sea Island, Georgia.

The organizing and steering committee follows:

Dr. F. A. Heyn, Professor, Technical University, Delft, The Netherlands;
Dr. R. S. Livingston, Director, Electronuclear Division, ORNL;
Dr. D. L. Judd, Head, Theoretical Division, LRL, Berkeley;
Dr. K. R. MacKenzie, Professor, University of California, Los Angeles;
Dr. J. R. Richardson, Professor, University of California, Los Angeles;
Dr. B. T. Wright, Professor, University of California, Los Angeles, Chairman;

A provisional program follows:

A. Beam Dynamics and Computer Programs
Starting conditions
Mid-range
Extraction

B. Realization of Required Magnetic Fields
Including measuring techniques

C. Radiofrequency Systems

E. Operating Experience

F. Open Sessions
Design of meson producing machines
Shielding and radiation safety problems
Radiation damage
etc.

INTERNATIONAL CONFERENCE ON THE PHYSICS OF SEMICONDUCTORS

University of Exeter, 16–20 July, 1962

The Institute and Society on behalf of the International Union of Pure and Applied Physics, and the British National Committee for Physics is arranging an International Conference on The Physics of Semiconductors, which will be held at the University of Exeter from 16–20 July, 1962. The Conference is planned to follow the previous sequence of Conferences on the physics of semiconductors, which were held in Reading in 1950, Amsterdam in 1954, Garmisch in 1956, Rochester in 1958 and Prague in 1960.

Accommodation will be provided in Halls of Residence at the University. Further information regarding the Conference may be obtained from the Administration Assistant, The Institute of Physics and The Physical Society, 47, Belgrave Square, London S.W. 1.

BOOK REVIEWS

SAFE OPERATION OF CRITICAL ASSEMBLIES AND RESEARCH REACTORS, IAEA, Vienna, 1961, STI/PUB/29, Safety Series no. 4. Pp. 97. U.S. $ 1.50.

A group of reactor experts from the International Atomic Energy Agency and from some important reactor centres in the world has prepared this manual on safe operation of critical assemblies and research reactors. The Manual is published as an issue of the Agency's "Safety Series" and appears in English, French, Russian and Spanish.

After an introduction including, among other things, definitions of the therminology used, the two main chapters follow. These two chapters, dealing with critical assemblies respectively research reactors, present the details of the safety problems to be thought of in design, instrumentation, construction and operation. The radiological protection instrumentation is given a special subchapter.

The chapter on Personnel is emphasizing a very important matter, i.e. the training and the control of qualification of the personnel engaged in the operation. A special 95 hours course followed by examination is suggested for this purpose.

Administrative procedures, Safety Documents and Emergency procedures are taken up in other chapters. A selected list of references on reactor safety problems is found in the end of the manual, as well as useful examples on "reactor standing orders" and "operating instructions".

In spite of the modest Foreword by the Director General of IAEA it is believed that this manual will be used all over the world as a normalizing guide on reactor safety.

TORSTEN LINDQVIST

PROCEEDINGS OF THE INTERNATIONAL SYMPOSIUM ON POLARIZATION PHENOMENA OF NUCLEONS, BASEL, July 4–8, 1960, *Edited by* P. Huber and K. P. Meyer, Helvetica Physica Acta, Supplementum VI, 1961, Birkhäuser Verlag Basel, Pp. 436. Fr.S. 65.

The first successful nucleon polarization experiment was reported in 1951, and since then the theoretical and experimental study of nucleon polarization phenomena has been a rapidly growing field. As a consequence, as many as 52 talks were delivered at the Basel symposium on these matters last year, even though its scope was further restricted by the exclusion of high energy physics from the program.

The proceedings have been divided into four sections, a survey article forming the introduction to each section. The first section, which deals with the techniques for the production of sources and targets of polarized nuclei, should be particularly valuable. It covers about one third of the book and gives a good picture of the work going on in several laboratories to develop these new techniques, which without doubt will be most important for future polarization experiments. The introductory survey is also sufficiently general and elementary that the whole section can be read also by non-specialists. The not too speedy publication of the proceedings has, unfortunately, caused some of the reports to appear slightly out of date. In a few cases, however, the reader is brought up to the status in March 1961 by supplementary notes.

The second section reports on the generation of polarized nucleons (in particular neutrons of various energies) and deuterons by reactions. Several papers on reactions and scattering of polarized particles are collected in the third section and the fourth section deals with theories concerning polarization effects of nucleons. The last three sections are somewhat more specialized within their scopes, probably partly because the subjects treated have been recently reviewed elsewhere.

ARNE JOHANSSON

PROGRESS IN LOW TEMPERATURE PHYSICS. Volume III (1961). Editor C. J. Gorter (North-Holland Publishing Company, Amsterdam). 495 pages. Guilders 48.

After the second volume the editor did not intend to edit more books in this series. There was, however, a great demand for this type of review articles that cover the intermediate stage between original publications and advanced textbooks. Thus the third volume of "Progress in Low Temperature Physics" has now appeared and we are very grateful to the editor and the authors for this valuable contribution to the literature in the low temperature field.

The first articles treat the properties of liquid helium, such as W. F. Vinen: Vortex lines in liquid helium II, G. Careri: Helium ions in liquid helium II and M. J. Buckingham, W. M. Fairbank: The nature of the λ-transition in liquid helium. There is nowadays an increased interest in ^{3}He. The properties of liquid and solid ^{3}He are reviewed by E. R. Grilly and E. R. Hammel. Experimentalists, who want to take advantage of ^{3}He for temperatures below 1°K can gain much information from the article by K. W. Taconis about ^{3}He Cryostats.

A very interesting article by J. Bardeen and J. R. Schrieffer gives a survey of the recent developments in superconductivity. Electron resonances in metals, cyclotron resonance with non-skin damping and paramagnetic resonance, is the subject of a paper by M. YA. Azbel and I. M. Lifshitz. Volume II of this series contained an article about orientation of atomic nuclei at low temperatures. In the present volume W. J. Huiskamp and H. A. Tolhock have written another paper in this interesting field with special attention to the most recent developments. Solid state masers are treated by N. Bloembergen, and J. J. M. Beenakker gives a survey of the transport properties of hydrogenic molecules. The last article by Z. Dokoupil treats some solid-gas equilibria at low temperatures.

The editor is to be congratulated to this excellent third volume and it is hoped that a fourth volume will appear in the near future.

O. BECKMAN

. L. CHASE, *Nuclear Pulse Spectrometry* (McGraw-Hill, 1961) 21 pp., 66 s.

Books in the field of nuclear electronics have not been bundant. The edition of this monograph covering the electro-ic techniques of pulse-height and pulse-time distribution pectrometers and the amplifiers and coincidence circuits used n connection with nuclear detectors is therefore welcome.

The volume contains a little more than 200 pages. In the rst chapter a good sum-up is given of the basic physical prin-ples of detectors for electrons, γ-rays, heavy particles and eutrons. The second chapter covers linear amplifiers and here re treated different methods of pulse shaping, with a discussion f their relative merits as to signal-to noise ratios, base-line ifts and pile-up overloading. For more pertinent mathemati-al details of pulse-shaping and noise, references are given. athode followers, integrating preamplifiers and various feed-ack amplifiers, and non-overloading amplifiers are described.

In the third chapter, on single-channel pulse-height analy-ers, are discussed properties of Schmitt trigger circuits, anti-oincidence circuits for differential discriminators, window mplifiers and pulse increment analyzers. The next chapters, in good fraction of the book, treat multichannel pulse-height nalyzers of different types, and their components such a pulse retchers, analog-to-digital converters, memories of the delay-ne, the magnetic-core and the electrostatic types and their ccess systems. Not much is said about multichannel read-out ystems. After a brief chapter on photographic pulse-height nalyzers, then follows time analyzers. In these also are in-luded different coincidence circuits of the parallel and series ypes and of the differential type. Fast-slow systems, chrono-rons, time-to-pulse-height converters and multichannel time-f-flight analyzers complete the chapter. Multidimensional nalyzers is the subject of the eighth chapter and here are also reated Compton spectrometers, pair spectrometers and many-hannel multidimensional data storage using ordinary memo-ies and photographic plates. In the last chapter the calculation f counting losses is treated and ways of avoiding excessive osses such as using electrostatic temporary storage in pulsed-eam accelerator experiments, are discussed.

The book is written in a clear and lucid style and applies oth to the nuclear physicist and the electronic designer. The itter, engaged in transferring tube circuitry into semiconduc-or circuitry, could perhaps have desired to find more about ransistor circuits (although both types of circuits are discussed he emphasis is on tube circuitry).

To conclude, the book gives the reader a good picture of the lectronic techniques of pulse spectrometry and has all pos-ibilities of becoming a standard text on the subject.

P. A. TOVE

Nuclear Propulsion. Bibliographical Series No. 3. International tomic Energy Agency, Vienna, 1961. 227 pp. $ 2.00.

This bibliography contains 1528 references to literature on uclear propulsion, and will mainly be of interest to specialists in he engineering, technological and economic aspects of this field. The reference are classified under five main headings: eneral aspects of nuclear propulsion, nuclear propulsion for ircraft, rockets, marine vessels and for other forms of transport. he references under "Nuclear propulsion for marine vessels" is further broken down into five sub-headings. Under each heading the material is listed alphabetically by title, which is usually given in the original language, with a translation into either English or Russian. Short abstracts in English or Russian are included as well as an author index. N. ROBERT NILSSON

Regulations for the Safe Transport of Radioactive Materials. Safety Series No. 6. International Atomic Energy Agency, Vienna, 1961. 72 pp, $ 1.50, U.K. 9/- Stg; A.S. 31.50; NF 6,–; DM 4.80.

In preparing these regulations for the transport of radioactive materials the International Atomic Energy Agency has not only made a synthesis of the existing detailed national and international regulations but also introduced amendments suggested by recent developments in this field of rapidly increasing practical importance. The authors were aided in their task by the work of two expert panels convened to study the problem. The preliminary material was duely circulated to the member states of the Agency and to the international organizations concerned with the subject before the present document was prepared. Although the regulations are formally applicable only for the Agency's own operations it is felt that they represent an important step toward generally accepted international rules for the transportation of radioactive materials. The immediate significance of the work is of practical nature as the booklet, contains much technical information which was formerly less readily available. Graphs and tables designed to fascilitate the design of packages of fissile material safe from neutron interaction under various conditions are particularly worth mentioning.

The scientific considerations which led to the specific limits laid down in these regulations are not included in this booklet. One has to await their publication in "Notes on Certain Aspects of the Regulations" presently being printed as member No. 7 of the Agency's "Safety Series". These notes will also contain practical information on the use and meaning of the regulations. including a "layman's guide" a synoptic table, guidance on packaging, etc. A great need is being filled by the two publications. BÖRJE LARSSON

PROGRESS IN NUCLEAR ENERGY, Ser. II: Reactors, Vol. 2, Edited by H. R. McK. Hyder (Pergamon Press Oxford, 1961) 557 pp., £ 5.5.0. net.

This volume contains the edited proceedings of selected papers presented at the Second International Conference on the Peaceful Uses of Atomic Energy held at Geneva 1958. It seems perhaps as these proceedings could have been issued much earlier. However, the editor has spared no effort to collect detailed descriptions about various projects from U.S.A., Great Britain, Russia and Sweden, which collection probably has taken quite some time. The result is shown in the sixteen review papers covering such subjects as Experimental Work with Zero Energy Fast Reactors, Fast Neutron Power Reactor Studies with ZPR-III, Experience in the Use of the Physical Constants Testing Reactors, and Spert I Reactor Safety Studies.

This volume will certainly constitute a most useful and necessary reference work for those actively engaged in the design and operation of reactors.

TORSTEN LINDQVIST

Small and Medium Power Reactors, Vol. I, Conference Proceedings Vienna, 5–9 September 1960, IAEA, Vienna, 1961, STI/PUB/30. Pp. 617, US $ 9.–.

In September 1960, the International Atomic Energy Agency organized a Conference at Vienna on Small and Medium Power Reactors to review the latest developments in the technology and economics of these reactors and to discuss their role in meeting energy problems. Fifty-four papers, summarizing the latest information about power reactors and their applications, were orally presented in nine sessions.

The proceedings of this Conference are being presented in two volumes, of which this volume is the first. The content of this volume is divided in two parts, the first giving a general review of reactors systems and the second reporting on the experience in construction and operation. The contributions come mainly from the big atomic power nations as USA, USSR and United Kingdom but also Germany, France, Canada and Japan appear as contributors. The proceedings are published only in one language version, with the result that papers in Russian and French appear beside the major part of papers, that are in English. The discussions in connection with the various sessions are presented as separate chapters in the proceedings. These proceedings when completed will no doubt be of great value to scientists, engineers, reactor manufacturers and others who are interested in the development and application of nuclear power reactors.

TORSTEN LINDQVIST

H. KIEFER and R. MAUSHART, Überwachung der Radioaktivität in Abwasser und Abluft, (Teubner Verlagsgesellschaft, Stuttgart 1961).

This small monograph is intended for those who are concerned with the control of radioactivity, released in water and air at nuclear installations and laboratories. Containing up to date information on maximum permissible concentrations of radioactive nuclides as well as well-written short descriptions of the properties of relevant measuring equipment and its application, the booklet forms a good hand-book which fills a apparent gap in the German technical litterature. The foot-note bibliography is useful, although the English reader may find the list of references less complete. Nevertheless, the publication is recommended for purchase by any practising health physicist and few of the many authors in this field have succeeded in collecting so much useful information within a publication of this modest size and price.

BÖRJE LARSSON